

University of Southampton Research Repository ePrints Soton

Copyright © and Moral Rights for this thesis are retained by the author and/or other copyright owners. A copy can be downloaded for personal non-commercial research or study, without prior permission or charge. This thesis cannot be reproduced or quoted extensively from without first obtaining permission in writing from the copyright holder/s. The content must not be changed in any way or sold commercially in any format or medium without the formal permission of the copyright holders.

When referring to this work, full bibliographic details including the author, title, awarding institution and date of the thesis must be given e.g.

AUTHOR (year of submission) "Full thesis title", University of Southampton, name of the University School or Department, PhD Thesis, pagination

UNIVERSITY OF SOUTHAMPTON

FACULTY OF NATURAL AND ENVIRONMENTAL SCIENCES

Centre for Biological Sciences

**INVESTIGATION OF THE UNFOLDED PROTEIN RESPONSE AND OTHER
STRESS-RELATED RESPONSES IN DISTINCT MODELS OF
NEURODEGENERATION**

by

Matthew John Davies

Thesis for the degree of Doctor of Philosophy

February 2016

ABSTRACT

There is no cure for chronic neurodegenerative diseases and disease-modifying therapies are limited. In order to develop successful disease-modifying therapies the molecules and pathways that underpin early stages of disease, such as synapse loss, need to be better defined.

Three distinct *in vivo* mouse models of neurodegeneration have been used to investigate molecular stress response molecules and pathways. These models are the ME7 prion model, the cysteine string protein alpha (CSP α) $-/-$ model and a kainic acid model of excitotoxicity. In all cases hippocampal tissue from mice was used to investigate the neuropathology and associated stress-related pathways. The unfolded protein response (UPR) and other stress-related response molecules: immediate early genes (ATF3, c-Jun and c-Fos), activity-induced immediate early genes (Arc and Homer1a) and a cellular physiological and environmental damage stress sensor (GADD45 α) were investigated. Biochemical and immunohistochemistry analysis revealed no evidence for a robust and classic UPR in any of the three models despite neuropathological changes associated with these distinct insults being evident. However, other stress-related response molecules were induced in these models and the induction of some of these occurred at the same time/prior to synapse loss suggesting that these are early responses and potential therapeutic targets for modifying neurodegenerative disease.

Tissue analysis is confounded by cellular heterogeneity. To investigate discrete cell specific events laser capture microdissection (LCM) was used to isolate the cell bodies of dysfunctional CA3 pyramidal neurons across key stages of ME7 prion disease. Optimisation of LCM enabled enrichment of CA3 pyramidal neurons and targeted analysis of UPR molecules. mRNA analysis failed to show strong evidence for a robust induction of the UPR in these vulnerable CA3 pyramidal neurons. Total RNA has also been used for RNA sequencing to analyse differentially expressed genes and molecular pathways activated during prion disease progression. The aim of this targeted approach will be to resolve molecular targets and pathways which might mitigate the progression of chronic neurodegenerative diseases.

Table of Contents

ABSTRACT	I
TABLE OF CONTENTS.....	II
LIST OF TABLES	XII
LIST OF FIGURES	XIII
ACKNOWLEDGEMENTS.....	XIX
ABBREVIATIONS	XXII
CHAPTER 1: GENERAL INTRODUCTION	1
1.1 Chronic neurodegenerative disease	1
1.1.1 Mouse models of chronic neurodegenerative diseases.....	2
1.2 Prion diseases	4
1.2.1 The prion protein (PrP).....	6
1.2.2 PrP ^C biosynthesis	7
1.2.3 Conversion of PrP ^C to PrP ^{Sc}	10
1.3 Experimental ME7 prion disease	13
1.3.1 Hippocampal neuroanatomy.....	14
1.3.2 CA3 pyramidal neurons and their axons: the Schaffer collaterals	15
1.4 Neuropathology in ME7-animals	17
1.4.1 Behavioural deficits in ME7-animals	23
1.5 Other mouse-adapted scrapie strains	25
1.6 Cysteine string protein alpha (CSPα) knockout (-/-) model	26
1.6.1 CSP α	26
1.6.2 Deletion of CSP in flies	28
1.6.3 Deletion of CSP α in mice	29

1.6.3.1	Molecular functions of CSP α in mice	29
1.6.3.2	Molecular changes in CSP α -/- mice.....	30
1.6.3.3	Synapse loss in CSP α -/- animals.....	32
1.7	Cell stress responses	33
1.7.1	The unfolded protein response (UPR) – a cellular stress response to misfolded/ unfolded proteins	33
1.7.1.1	ER stress sensors	34
1.7.1.1.1	The integrated stress response	36
1.7.1.1.2	eIF2 α	36
1.7.1.1.3	4EBP	37
1.7.2	The UPR in acute injury	39
1.7.3	The UPR in chronic neurodegenerative disease	39
1.7.3.1	The UPR in AD.....	39
1.7.3.1.1	Sub-compartmental UPR in AD	40
1.7.3.2	The UPR in PD	41
1.7.3.3	The UPR in ALS	41
1.7.4	Other stress-related response molecules associated with homeostatic changes in neuronal function and dysfunction	43
1.7.4.1	Immediate early genes.....	43
1.7.4.1.1	ATF3.....	44
1.7.4.1.2	c-Jun	46
1.7.4.1.3	c-Fos	47
1.7.4.2	Activity-induced immediate early genes.....	47
1.7.4.2.1	Arc	47
1.7.4.2.2	Homer1a	48
1.7.4.3	Cellular physiological and environmental damage stress sensor.....	49
1.7.4.3.1	GADD45 α	49
1.8	General aims	52
CHAPTER 2: GENERAL MATERIALS AND METHODS		53
2.1	Animal husbandry	53

2.2	Stereotaxic surgery	53
2.3	Preparation of brain homogenate for intra-hippocampal injection	54
2.4	Methods of tissue collection	54
2.4.1	Perfusion.....	54
2.4.2	Whole brain extraction	54
2.4.3	Post fixation.....	54
2.4.4	Hippocampal extraction.....	55
2.5	Tissue processing	55
2.5.1	RNA extraction.....	55
2.5.2	Measurements of concentration and quality of RNA	55
2.5.3	cDNA synthesis	56
2.6	Polymerase Chain Reaction (PCR).....	56
2.6.1	Primer design.....	56
2.6.2	REDTaq PCR	60
2.6.3	Quantitative PCR (qPCR).....	61
2.6.3.1	Standard curve data preparation, normalisation and quantification.....	62
2.6.3.2	$2^{-\Delta\Delta C_T}$ calculation	63
2.6.4	Agarose gel electrophoresis.....	65
2.7	Generation of plasmids	65
2.7.1	TOPO TA cloning	66
2.7.2	Transformation into chemically competent Library Efficiency DH5 α cells	66
2.7.3	Transformant selection	66
2.7.4	Crude miniprep	67
2.7.5	Digestion of plasmids with EcoRI.....	67
2.7.6	Preparation of glycerol plasmid stock	69
2.7.7	Generation of plasmid standard curves	69
2.7.8	Sequencing of plasmids	70
2.8	HeLa cells	70

2.8.1	Maintenance of HeLa cells	70
2.8.2	Drug treatment of HeLa cells	70
2.8.3	HeLa cell extraction.....	71
2.9	Western blotting	71
2.9.1	Hippocampi extraction	71
2.9.2	Protein assay	71
2.9.3	Sample preparation	72
2.9.4	SDS-polyacrylamide gel electrophoresis (PAGE)	73
2.9.5	SDS-PAGE gel staining	74
2.9.6	Electroblotting of protein to nitrocellulose membrane.....	74
2.9.7	Antibody labelling of transferred proteins	75
2.9.8	Quantification of protein levels	76
2.10	Immunohistochemistry	81
2.10.1	Tissue preparation and sectioning	81
2.10.2	DAB staining	81
2.10.3	Quantification of positive staining	83
2.11	Immunofluorescence – HeLa cells.....	84
2.12	Statistical analysis.....	85
 CHAPTER 3: INVESTIGATION OF THE UNFOLDED PROTEIN RESPONSE AND OTHER STRESS-RELATED RESPONSES IN ME7-ANIMALS.....		86
3.1	Introduction	86
3.2	Aims	87
3.3	Specific materials and methods	89
3.3.1	qPCR.....	89
3.3.2	eIF2 α -P blocking peptide	89
3.4	Results.....	90
3.4.1	Expression of total PrP and GFAP protein and synapse integrity in ME7-animals	90

3.4.2	Expression of UPR mRNAs in ME7-animals	93
3.4.3	Expression of UPR proteins in ME7-animals	95
3.4.4	Expression of other stress-related response mRNAs in ME7-animals 104	
3.4.4.1	Expression of immediate early gene mRNAs in ME7-animals	104
3.4.4.2	Expression of activity-induced immediate early gene mRNAs in ME7-animals.....	104
3.4.4.3	mRNA expression of the cellular physiological and environmental damage stress sensor, GADD45 α , in ME7-animals.....	105
3.4.5	Expression of other stress-related response proteins in ME7-animals 107	
3.4.5.1	Western blotting.....	107
3.4.5.1.1	Expression of immediate early gene proteins in ME7-animals.....	107
3.4.5.1.2	Protein expression of the cellular physiological and environmental damage stress sensor, GADD45 α , in ME7-animals.....	107
3.4.5.2	Immunohistochemistry.....	109
3.4.5.2.1	Cell loss and vacuolation in ME7-animals.....	109
3.4.5.2.2	Expression of immediate early gene proteins in ME7-animals.....	110
3.4.5.2.3	Expression of the cellular physiological and environmental damage stress sensor, GADD45 α , in ME7-animals	118
3.5	Discussion	121
3.5.1	PrP and GFAP protein expression is increased in ME7-animals at a time when synapse loss is occurring	122
3.5.2	Limited evidence for a UPR in ME7-animals	122
3.5.2.1	Expression of UPR mRNAs.....	122
3.5.2.2	Expression of UPR proteins.....	123
3.5.3	Evidence supporting the activation of a UPR in prion disease	123
3.5.4	Evidence showing that the UPR is not activated in prion disease.....	125
3.5.4.1	High-throughput analysis shows UPR transcripts are not induced in prion disease	126
3.5.5	Other stress-related response molecules are induced in ME7-animals 127	

3.5.6	Evidence showing other stress-related response molecules are induced in prion disease	128
3.5.6.1	High-throughput analysis shows other stress-related response mRNAs are induced in prion disease.....	129
3.6	Conclusion	130
 CHAPTER 4: INVESTIGATION OF THE UNFOLDED PROTEIN RESPONSE AND OTHER STRESS-RELATED RESPONSES IN CYSTEINE STRING PROTEIN A -/- MICE		
132		
4.1	Introduction	132
4.2	Aims	133
4.3	Specific materials and methods	135
4.3.1	Breeding of CSP α mice	135
4.3.2	Genotyping of CSP α mice	135
4.3.2.1	Tissue collection.....	135
4.3.2.2	PK digestion	135
4.3.3	DNA extraction	136
4.3.4	Genomic PCR for genotyping	136
4.3.5	qPCR.....	138
4.4	Results.....	138
4.4.1	Expression of SNAP-25, SNARE-complex assembly and pre- and postsynaptic proteins in CSP α -/- animals.....	138
4.4.2	Expression of GFAP in CSP α -/- animals	142
4.4.3	Expression of UPR mRNAs in CSP α -/- animals.....	145
4.4.4	Expression of UPR proteins in CSP α -/- animals	147
4.4.5	Expression of other stress-related response mRNAs levels in CSP α -/- animals	149
4.4.5.1	Expression of immediate early gene mRNAs in CSP α -/- animals.....	149
4.4.5.2	Expression of activity-induced immediate early gene mRNAs in CSP α -/- animals	150

4.4.5.3	mRNA expression of the cellular physiological and environmental damage stress sensor, GADD45 α , in CSP α -/- animals	150
4.4.6	Expression of other stress-related response proteins in CSP α -/- animals	152
4.4.6.1	Western blotting	152
4.4.6.2	Immunohistochemistry	154
4.4.6.2.1	ATF3	154
4.4.6.2.2	c-Jun	157
4.4.6.2.3	c-Fos	157
4.4.6.2.4	Expression of the cellular physiological and environmental damage stress sensor, GADD45 α , in CSP α -/- animals	161
4.5	Discussion	163
4.5.1	SNAP-25 protein levels and SNARE-complex assembly is reduced whilst synaptic loss is not detected in CSP α -/- animals	163
4.5.2	GFAP upregulation follows SNAP-25 and SNARE-complex assembly reduction in CSP α -/- animals	164
4.5.3	CSP α -/- mice do not undergo a UPR	165
4.5.4	Other stress-related response molecules are induced in CSP α -/- animals	166
4.6	Conclusion	168
CHAPTER 5: IS THE UNFOLDED PROTEIN RESPONSE INDUCED IN A KAINIC ACID MODEL OF EXCITOTOXICITY?		169
5.1	Introduction	169
5.2	Aims	170
5.3	Specific materials and methods	172
5.3.1	KA administration	172
5.3.2	qPCR	172
5.3.3	Immunohistochemistry - mouse brain slices	172
5.3.3.1	Preparation and slicing	172

5.3.3.2	DAB staining.....	174
5.4	Results.....	175
5.4.1	Neuropathology in KA-animals	175
5.4.2	Expression of stress-related response molecules implicated in KA-induced excitotoxicity	181
5.4.2.1	Expression of the immediate early gene c-Jun.....	182
5.4.2.2	Expression of other immediate early gene mRNAs.....	185
5.4.2.3	Expression of activity-induced immediate early gene mRNAs	185
5.4.2.4	mRNA expression of the cellular physiological and environmental damage stress sensor GADD45 α	186
5.4.3	Expression of UPR mRNAs in KA-animals	188
5.4.4	Expression of UPR proteins in KA-animals.....	188
5.4.5	Expression of BiP and eIF2 α -P proteins after acute coronal mouse brain slicing	196
5.5	Discussion	198
5.5.1	The dose of KA	198
5.5.2	Stress response molecules are upregulated in KA-animals	198
5.5.3	A robust and classic UPR is not activated in KA-animals	199
5.5.4	Increased phosphorylation of eIF2 α in acute coronal mouse brain slices	201
5.6	Conclusion	202
 CHAPTER 6: LASER CAPTURE MICRODISSECTION AND TRANSCRIPT PROFILING OF THE CA3 HIPPOCAMPAL SUBFIELD IN ME7 PRION DISEASE		
		204
6.1	Introduction	204
6.2	Aims	205
6.3	Specific materials and methods.....	206
6.3.1	Tissue sectioning for LCM.....	206
6.3.2	Tissue processing for LCM	207

6.3.3	LCM of CA3.....	207
6.3.4	RNA extraction of laser microdissected CA3	208
6.3.5	qPCR.....	209
6.3.6	RNA-Seq	209
6.3.7	RNA-Seq data analysis.....	211
6.4	Results.....	212
6.4.1	The optimisation of tissue processing for LCM	212
6.4.2	Using LCM to enrich and de-enrich for mRNAs expressed in different hippocampal regions and in glial cells	213
6.4.3	The expression of UPR and other stress-related response mRNAs in laser microdissected CA3	219
6.4.4	The expression of astrocyte and microglia-associated molecules in the laser microdissected CA3 of ME7-animals.....	220
6.4.5	Expression of UPR and other stress-related response mRNAs in laser microdissected CA3 of ME7-animals	225
6.4.6	RNA-Seq analysis	227
6.5	Discussion	231
6.5.1	Optimisation of LCM	231
6.5.2	Enriching for genes expressed in the CA3 pyramidal layer and de-enriching for genes expressed outside of the CA3 pyramidal layer.....	232
6.5.3	The majority of UPR and other stress-related response mRNAs are de-enriched in laser microdissected CA3	232
6.5.4	Using LCM to investigate the molecular changes occurring in the CA3 pyramidal neurons of ME7-animals	233
6.5.5	Astrocytes and microglia infiltrate the CA3 pyramidal layer of ME7-animals	233
6.5.6	Limited evidence for a robust UPR in laser microdissected CA3 of ME7-animals	234
6.5.7	GADD45 α but not ATF3 or Homer1a mRNA, is increased in laser microdissected CA3 of ME7-animals	234
6.5.8	RNA-Seq did not resolve changes seen using qPCR	235

6.6	Conclusion	236
	CHAPTER 7: OVERVIEW AND FUTURE WORK	238
7.1	Overview	238
7.2	Future work	243
	LIST OF REFERENCES	245
Appendices	270	
	Appendix 1: Transgenic mouse models of chronic neurodegenerative diseases ...	270
	Appendix 2: Transgenic mouse models of prion disease	272
	Appendix 3: Suppliers of reagents.....	274
	Appendix 4: Example calculation of the number of plasmid copies per μl	278
	Appendix 5: Example of plasmid sequence insert.....	279
	Appendix 6: Quantification of UPR proteins in tunicamycin and PEITC treated HeLa cells	280
	Appendix 7: Immunofluorescence for ATF4 in tunicamycin treated HeLa cells .	281
	Appendix 8: PERK-P, ATF4 and CHOP protein expression in ME7-animals	282
	Appendix 9: PERK-P, ATF4 and CHOP protein expression in CSPα -/- animals	283
	Appendix 10: ATF3, c-Fos and GADD45α protein expression in the CA3b region of the hippocampus in CSPα animals.....	284
	Appendix 11: Publication	285

List of Tables

Chapter 1

Table 1.1 Prion diseases of animals.	5
Table 1.2 The etiology of different human prion diseases.....	6
Table 1.3 Examples of mouse-adapted scrapie strains with differing neuropathology and incubation times.	26

Chapter 2

Table 2.1 Sequences and positions of forward and reverse primers.	58
Table 2.2 Cycling parameters for primer pairs.	60
Table 2.3 Reagents and volumes required to make different % SDS-PAGE gels. .	74
Table 2.4 Primary antibodies used for western blotting.	77
Table 2.5 Secondary antibodies used for western blotting.....	78
Table 2.6 Primary and secondary antibodies used for immunohistochemistry.....	83

Chapter 3

Table 3.1 Expression profiles of UPR mRNAs in RML- and 301V-inoculated animals compared to ME7-animals.....	127
Table 3.2 Expression profiles of other stress-related response mRNAs in RML- and 301V-inoculated animals compared to ME7-animals.	130

Chapter 6

Table 6.1 Concentration and RIN score of RNA from laser microdissected CA3 of NBH- and ME7-animals.	211
Table 6.2 mRNAs enriched in different regions of the hippocampus.	214
Table 6.3 Read count and normalised read count for GAPDH mRNA in laser microdissected CA3 of NBH- and ME7-animals.....	228
Table 6.4 RNA-Seq vs qPCR: mean fold change of GFAP mRNA between laser microdissected CA3 of NBH- and ME7-animals.....	229
Table 6.5 RNA-Seq vs qPCR: mean fold change of CD11b mRNA in laser microdissected CA3 of NBH- and ME7-animals.....	230
Table 6.6 RNA-Seq vs qPCR: mean fold change of C1qB mRNA between laser microdissected CA3 of NBH- and ME7-animals.....	231

List of figures

Chapter 1

Figure 1.1 Genes associated with familial forms of chronic neurodegenerative diseases and ways of modelling chronic neurodegenerative diseases in mice.	4
Figure 1.2 The primary structure of mouse PrP^C and different glycosylated states.	8
Figure 1.3 The biosynthesis of PrP^C.	9
Figure 1.4 Proposed models of the conversion of PrP^C to PrP^{Sc}.	12
Figure 1.5 Coronal section through a mouse brain showing the location of hippocampus and the three main subfields of the hippocampus.	15
Figure 1.6 The hippocampal trisynaptic loop and basic structure of a CA3 pyramidal neuron.	16
Figure 1.7 Deposition of PrP^{Sc} during ME7 prion disease progression.	17
Figure 1.8 Increased microglia and hypertrophied astrocytes in ME7 prion disease.	18
Figure 1.9 Progressive loss of synaptic boutons in ME7-animals.	21
Figure 1.10 Abnormal axonal swellings and signs of local axonal degeneration in ME7-animals.	23
Figure 1.11 Timeline for the appearance of neuropathological and behavioural abnormalities in the ME7 model of prion disease.	25
Figure 1. 12 Primary structure of mouse CSPα protein.	28
Figure 1.13 A role for CSPα-Hsc70-SGT in vesicle exo- and endocytosis.	31
Figure 1.14 Timeline for the appearance of molecular deficits and synapse loss in the CSPα -/- mice.	33
Figure 1.15 UPR signalling.	38
Figure 1.16 Cellular insults leading to the induction of stress-related response molecules in neurons.	51

Chapter 2

Figure 2.1 Raw data readout from a qPCR of the GAPDH plasmid standard curve.	64
Figure 2.2 Melting curve for GAPDH.	64
Figure 2.3 Linear regression line of the GAPDH standard curve.	65
Figure 2.4 pCR 2.1 vector map, showing the position of the PCR insert and the EcoRI excision sites.	68

Figure 2.5 Digestion of potential BiP fragment containing plasmids with EcoRI, to determine the presence of the correct insert.	69
Figure 2.6 Linear regression line of a BSA standard curve.	72
Figure 2.7 SDS-PAGE gel-nitrocellulose transfer sandwich.....	75
Figure 2.8 Representative images to illustrate quantification of protein loading and normalization for calculating protein levels by western blotting. ..	80
Figure 2.9 Illustrative image processing used to quantify DAB based immunoreactivity of mouse brain sections.	84

Chapter 3

Figure 3.1 Experimental outline: investigating the UPR and other stress-related response molecules in ME7-animals.....	88
Figure 3.2 Quantification of total, di-, mono- and unglycosylated PrP and GFAP proteins in ME7-animals.	91
Figure 3.3 Immunohistochemical staining for GFAP and synaptophysin.....	92
Figure 3.4 Quantification of UPR mRNAs in ME7-animals.	94
Figure 3.5 Quantification of UPR proteins in ME7-animals.	96
Figure 3.6 Immunohistochemical staining for BiP in ME7-animals.....	97
Figure 3.7 Cross-reactivity of the two eIF2α-P antibodies with a protein of ~50 kDa in ME7-animals.	99
Figure 3.8 Expression of eIF2α-P in astrocytes of ME7-animals, as a consequence of eIF2α-P 1 antibody cross-reactivity.	100
Figure 3.9 Quantification of the phosphorylation state of total 4EBP1 protein in ME7-animals.....	102
Figure 3.10 Quantification of SIL1 mRNA in ME7-animals.	103
Figure 3.11 Quantification of immediate early gene mRNAs in ME7-animals.....	105
Figure 3.12 Quantification of activity-induced immediate early gene mRNAs in ME7-animals.....	106
Figure 3.13 Quantification of the mRNA levels of the cellular physiological and environmental damage stress sensor, GADD45α, in ME7-animals.....	106
Figure 3.14 Quantification of immediate early gene proteins and the cellular physiological and environmental damage stress sensor protein, GADD45α, in ME7-animals.	108
Figure 3.15 Haematoxylin staining of ME7-animals.	109

Figure 3.16 Immunohistochemical staining for ATF3 in ME7-animals.	112
Figure 3.17 Immunohistochemical staining for c-Jun in ME7-animals.....	114
Figure 3.18 Immunohistochemical staining for c-Fos in ME7-animals.	116
Figure 3.19 Immunohistochemical staining for GADD45 α in ME7-animals.	120

Chapter 4

Figure 4.1 Experimental outline: investigating the UPR and other stress-related response molecules in CSP α -/- animals.	134
Figure 4.2 Wildtype CSP α gene, targeting vector and position of CSP α primers.	137
Figure 4.3 Example PCR gel image used to identify the genotype of CSP α mice.	137
Figure 4.4 Quantification of CSP α , SNAP-25 proteins and SNARE-complex assembly in CSP α -/- animals.	139
Figure 4.5 Quantification of synaptophysin and PSD-95 proteins in CSP α -/ animals.	141
Figure 4.6 Quantification of GFAP to measure gliosis in CSP α -/- animals.	143
Figure 4.7 Immunohistochemical staining for GFAP in CSP α -/- animals.....	144
Figure 4.8 Quantification of UPR mRNAs in CSP α -/- animals.	146
Figure 4.9 Quantification of UPR proteins and the phosphorylation state of 4EBP1 in CSP α -/- animals.	148
Figure 4.10 Quantification of SIL1 mRNA in CSP α -/- animals.	149
Figure 4.11 Quantification of immediate early gene mRNAs in CSP α -/- animals.	150
Figure 4.12 Quantification of activity-induced mRNAs in CSP α -/- animals.....	151
Figure 4.13 Quantification of the mRNA levels of the cellular physiological and environmental damage stress sensor GADD45 α in CSP α -/ animals.	151
Figure 4.14 Quantification of immediate early gene proteins in CSP α -/- animals.	153
Figure 4.15 Immunohistochemical staining for ATF3 in CSP α -/- animals.	156
Figure 4.16 Immunohistochemical staining for c-Jun in CSP α -/- animals.....	158
Figure 4.17 Immunohistochemical staining for c-Fos in CSP α -/- animals.	160
Figure 4.18 Immunohistochemical staining for GADD45 α in CSP α -/- animals. .	162

Chapter 5

Figure 5.1 Experimental outline: investigating the UPR and other stress-related response molecules in KA-animals.	171
---	-----

Figure 5.2 Experimental outline for coronal mouse brain slicing.	174
Figure 5.3 Haematoxylin staining of hippocampal sections from KA-animals.	177
Figure 5.4 Quantification of GFAP mRNA and protein in KA-animals.	178
Figure 5.5 Immunohistochemical staining for GFAP in KA-animals.	181
Figure 5.6 Quantification of c-Jun mRNA in KA-animals.	182
Figure 5.7 Quantification of c-Jun protein in KA-animals.	183
Figure 5.8 Immunohistochemical staining for c-Jun in KA-animals.	185
Figure 5.9 Quantification of ATF3 and c-Fos immediate early gene mRNAs in KA-animals.	186
Figure 5.10 Quantification of activity-induced immediate early gene mRNAs in KA-animals.	187
Figure 5.11 Quantification of the mRNA levels of the cellular physiological and environmental damage stress sensor GADD45 in KA-animals.	187
Figure 5.12 Quantification of UPR mRNAs in KA-animals.	189
Figure 5.13 Quantification of UPR proteins in KA-animals.	190
Figure 5.14 Immunohistochemical staining for BiP in KA-animals.	193
Figure 5.15 Immunohistochemical staining for eIF2 α -P in KA-animals.	195
Figure 5.16 Quantification of BiP and eIF2 α -P proteins after acute coronal mouse brain slicing.	197

Chapter 6

Figure 6.1 Laser microdissection of the CA3 pyramidal layer.	208
Figure 6.2 Representative Agilent 2100 Bioanalyser trace.	210
Figure 6.3 Quality of RNA from laser microdissected CA3 processed by method 1 or 2.	213
Figure 6.4 Experimental outline: the expression of mRNAs in the whole hippocampus compared to laser microdissected CA3.	215
Figure 6.5 Quantification of Bok and Spock1 mRNAs in laser microdissected CA3.	217
Figure 6.6 Quantification of Dsp and Nov mRNAs in laser microdissected CA3.	218
Figure 6.7 Quantification of GFAP and synaptophysin mRNAs and levels of CD11b mRNA in laser microdissected CA3.	219
Figure 6.8 Quantification of UPR and stress-related response mRNAs in laser microdissected CA3.	220

Figure 6.9 Experimental outline: investigating transcriptional responses in laser microdissected CA3 of ME7-animals.	222
Figure 6.10 Quantification of GFAP, CD11b and C1qB mRNAs in laser microdissected CA3 of ME7-animals.	223
Figure 6.11 Immunohistochemical staining for GFAP and IBA1 in ME7-animals.	224
Figure 6.12 Quantification of UPR mRNAs in laser microdissected CA3 of ME7-animals.....	226
Figure 6.13 Quantification of other stress-related response mRNAs in laser microdissected CA3 of ME7-animals.	227

DECLARATION OF AUTHORSHIP

I, Matthew Davies, declare that this thesis and the work presented in it are my own and has been generated by me as the result of my own original research.

I confirm that:

1. This work was done wholly or mainly while in candidature for a research degree at this University;
2. Where any part of this thesis has previously been submitted for a degree or any other qualification at this University or any other institution, this has been clearly stated;
3. Where I have consulted the published work of others, this is always clearly attributed;
4. Where I have quoted from the work of others, the source is always given. With the exception of such quotations, this thesis is entirely my own work;
5. I have acknowledged all main sources of help;
6. Where the thesis is based on work done by myself jointly with others, I have made clear exactly what was done by others and what I have contributed myself;
7. None of this work has been published before submission

Signed:

Date:

Acknowledgements

Firstly, I would like to start by thanking the Gerald Kerkut Charitable Trust (GKCT) and the Medical Research Council (MRC) for providing me with this PhD studentship. A special thanks to the GKCT for also providing additional funds for experiments and for funds enabling me to attend national and international conferences to present my work.

I would like to sincerely thank my two supervisors, Professor Vincent O'Connor and Professor Hugh Perry. I am extremely grateful for your support and guidance over the last 4 years. It is safe to say I have gained a lot of scientific knowledge from you both, but I have also learnt so much more. You have both been wonderful role models and provided with me a skill set I know will enable me to go on and have a lot of success in my future endeavours. A special thanks for your belief and encouragement through the tough times. I wish you both much success for your future. From the bottom of my heart, thank you!

A special thanks to everyone in the VOC/VHP labs who I have had the pleasure of interacting with over the last 4 years. In particular to my two other 'musketees', Nico Dalliere and Jim Kearn. Thank you for sharing with me this journey and providing me with endless amounts of laughter. You both have significantly contributed to my PhD experience. I wish you both all of the very best in the future. Thanks also to Anna Crisford for mothering me and adding to the love and laughter in the lab. For the last time I must say to you.... 'did you read it'. To Nash Matinyarare, thank you for all your help, support and friendship especially through the first few months of my PhD. I hope your new career brings you much success, you deserve it.

I have to thank 3 people in particular who have been wonderful to me over these last 4 years. These 3 people have significantly contributed to my scientific skill set and knowledge and more importantly have been great friends to me. I thank Joanne Bailey, Diego Gomez and Deji Asuni for all they have done for me. Three wonderfully gifted scientists who I know will undoubtedly achieve great things. Thank you all.

Now for my wonderful friends and family. I want to start by thanking my 3 best friends, Matt Upton, Adam Sams and Nathan Sabir for their constant friendship. Thank you for understanding that I haven't always been there over the last few years and especially the

last 6 months, due to balancing both full-time work and thesis writing. Thank you for enabling me to finish the work I started and for supporting me throughout.

To my wonderful nan, grandad and uncle who I am forever indebted to. Thank you for everything you have done for me, not just in these last seven years at University but throughout my life. I regard you nan and grandad as my second mother and father and you Robert, as the brother I never had. Thank you for your unconditional love, support and guidance. I love you all.

To my two wonderful sisters, Rachel and Samantha who always have looked after their older brother. Thank you for being so understanding over the last seven years and for always being there for me. I am extremely lucky to have sisters like you both and I hope you know I will always be there for you. I love you both.

To my wonderful girlfriend who has had to deal with my ‘not-so happy’ mood over the last six months. Thank you so much for standing by me and never once complaining. Words cannot describe how wonderful you have been. I never forget things and I can promise when it’s your turn I will be right there by your side. Thank you so much for believing in me and inspiring me to be my best. I love you.

That leaves me to one last thank you. To my mum and dad, there are no words that I can find to possibly be able to describe my gratefulness to you both. Throughout my life I have been lucky enough to have had you both by my side. Never have I been pressurised into anything, I have only ever been loved and supported. There is no doubt in my mind that all my successes past, present and future are because of you. I want to thank you both for your love, support and friendship throughout this journey that I have been on. When I needed you the most you were there and you have never let me down. You both inspire me to be great and I will always aim to be the best I can. I love you both more than you will ever know. My name might be on this thesis, but without you both this wouldn’t be possible.

Mum and Dad this is for you.....

Abbreviations

-/-	Knockout
+/-	Heterozygous
+/+	Wildtype
4EBP	Eukaryotic translation initiation factor 4E (eIF4E) binding protein
6-OHDA	6-hydroxydopamine
ABC	Avidin-biotinylated horseradish peroxidase complex
ACSF	Artificial cerebrospinal fluid
AD	Alzheimer's disease
ADP	Adenosine diphosphate
ALS	Amyotrophic lateral sclerosis
AMPA	Alpha-amino-3-hydroxyl-5-methyl-4-isoxazole-propionate
ANCL	Adult-onset neuronal ceroid lipofuscinosis
AP-1	Activator protein 1
APP	Amyloid precursor protein
Arc/Arg3.1	Activity-regulated cytoskeletal protein
ATF2	Activating transcription factor 2
ATF3	Activating transcription factor 3
ATF4	Activating transcription factor 4
ATF6	Activating transcription factor 6
ATP	Adenosine triphosphate
Aβ	Amyloid- β
BCP	1-Bromo-3-chloropropane
BDA	Biotinylated dextran amine
BiP	Binding immunoglobulin protein
BSE	Bovine Spongiform Encephalopathy
bZip	Basic leucine zipper
C1q	Complement
CA1	Cornu Ammonis region 1
CA3	Cornu Ammonis region 3
cdk	Cyclin dependent kinase
CHOP	C/EBP homologous protein
CJD	Creutzfeldt-Jakob Disease
CREB	cAMP responsive element binding protein
CSP	Cysteine string protein
d	Day(s)

DAB	3,3'-Diaminobenzidine
DEPC	Diethylpyrocarbonate
DG	Dentate gyrus
D-MEM	Dulbecco's Modified Eagle Medium
DMSO	Dimethyl sulfoxide
D-PBS	Dulbecco's phosphate buffered saline (PBS)
eIF2B	Eukaryotic translation initiation factor 2B
eIF2α	Eukaryotic translation initiation factor 2 α
eIF4E	Eukaryotic translation initiation factor 4E
eIF4F	Eukaryotic translation initiation factor 4F
ER	Endoplasmic reticulum
ERAD	ER-associated protein degradation
FBS	Fetal bovine serum
FTDP-17	Frontotemporal dementia and Parkinsonism linked to chromosome 17
FUS	Fused in Sarcoma
GADD34	Growth arrest and DNA-damage inducible protein 34
GADD45α	Growth arrest and DNA damage-inducible protein 45 α
GCN2	General non-derepressible 2
GDP	Guanosine diphosphate
GFAP	Glial fibrillary acidic protein
GPI	Glycosylphosphatidylinositol
GSK-3β	Glycogen synthase kinase 3
GTP	Guanosine triphosphate
H₂O₂	Hydrogen peroxide
HCl	Hydrochloric acid
hr	Hour(s)
HRI	Haem regulated inhibitor
Hsc70	Heat shock cognate 70 kDa protein
i.p.	Intraperitoneal
IRE1	Inositol-requiring enzyme 1
ISR	Integrated stress response
JNK	c-Jun N-terminal kinase
KA	Kainic acid
kb	Kilobase
LB	Luria broth
LCM	Laser capture microdissection

LRRK2	Leucine-rich repeat kinase 2
LTP	Long term potentiation
MAPK	Mitogen activated protein kinase
min	Minute(s)
MPTP	1-methyl-4-phenyl-1,2,3,6-tetrahydropyridine
mTOR	Mammalian target of rapamycin
Mw	Molecular weight
NBH	Normal brain homogenate
NGS	Next generation sequencing
NIMR	National Institute for Medical Research
NMDA	N-methyl D-aspartic acid
NMJ	Neuromuscular junction
OCT	Optimal temperature compound
P	Postnatal day
PAGE	Polyacrylamide gel electrophoresis
PBS	Phosphate buffered saline
PCNA	Proliferating cell nuclear antigen
PCR	Polymerase chain reaction
PD	Parkinson's disease
PDI	Protein disulfide isomerase
PEITC	Phenethyl isothiocyanate
PERK	Protein kinase-like ER kinase
PFA	Paraformaldehyde
PINK1	PTEN induced putative kinase 1
PK	Proteinase K
PKR	RNA-dependent protein kinase
PMSF	Phenylmethanesulfonyl fluoride
PrP	Prion protein
PrP^C	Cellular prion protein
PrP^{Sc}	Scrapie prion protein
PSD	Post-synaptic density
PV	Parvalbumin
qPCR	Quantitative polymerase chain reaction (PCR)
RGC	Retinal ganglion cell
RIN	RNA integrity number
RML	Rocky mountain laboratory

RNA-Seq	RNA sequencing
rRNA	Ribosomal RNA
s	Second(s)
S1P	Site 1 protease
S2P	Site 2 protease
SGT	Small glutamine-rich tetratricopeptide repeat (TRP)-containing protein
shRNA	Small-hairpin RNA
siRNA	Small interfering RNA
SOD1	Superoxide dismutase 1
SRP	Signal recognition particle
TBE	Tris/Borate/EDTA
TBI	Traumatic brain injury
TBS	Tris buffered saline
TDP-43	TAR DNA-binding protein 43
Tg	Transgenic
TRP	Tetratricopeptide repeat
UPR	Unfolded protein response
UTR	Untranslated region
UV	Ultraviolet
vCJD	Variant Creutzfeldt-Jakob Disease
Vst	Variance stabilising transformation
w.p.i.	Weeks post-inoculation
WHO	World Health Organisation

Chapter 1: General introduction

1.1 Chronic neurodegenerative disease

At present there are no cures for chronic neurodegenerative diseases and therapeutics are limited (Verity and Mallucci, 2011). The main risk factor for chronic neurodegenerative diseases is advancing age (Saxena and Caroni, 2011) and with a rising age in the general population, the incidence of such diseases is increasing (Ridley and Baker, 1998). The World Health Organisation (WHO) has predicted that by 2040, chronic neurodegenerative diseases will be the second leading cause of death in the developed world (Verity and Mallucci, 2011). Therefore, a big challenge is to develop disease modifying therapies which can slow the progression of these diseases.

Examples of chronic neurodegenerative diseases include Alzheimer's disease (AD), Parkinson's disease (PD), amyotrophic lateral sclerosis (ALS)/motoneuron disease and prion disease. These diseases have distinct clinical, biochemical and pathological features and clinical symptoms of disease are a result of these (Halliday and Mallucci, 2015, Pievani et al., 2014). Despite this, there are numerous similarities between these diseases including the initial aggregation and deposition of disease-specific misfolded protein(s), which is followed by synaptic dysfunction and loss (Halliday and Mallucci, 2015, Matus et al., 2008, Saxena and Caroni, 2011, Stefani and Dobson, 2003). Irreversible neuronal loss follows synaptic loss and is a late-event in chronic neurodegenerative diseases (Mallucci, 2009).

AD is the most common chronic neurodegenerative disease and is associated with memory loss and cognitive impairment (Götz and Ittner, 2008). Pathological accumulations of extracellular amyloid plaques and intracellular neurofibrillary tangles are characteristic of AD. The amyloid plaques are composed of amyloid- β (A β) peptides generated from the cleavage of the amyloid precursor protein (APP). Neurofibrillary tangles are composed of hyperphosphorylated tau protein (Götz and Ittner, 2008).

PD is largely a movement disorder associated with a loss of dopaminergic neurons (Lin and Farrer, 2014, Skovronsky et al., 2006). PD is characterised by intracellular deposits called Lewy bodies and Lewy neurites which contain aggregated α -synuclein (Bezard et al., 2013, Luk et al., 2012b, Spillantini et al., 1997). ALS is associated with a loss of

upper and lower motoneurons, which results in muscle weakness, paralysis and death (Joyce et al., 2011).

1.1.1 Mouse models of chronic neurodegenerative diseases

To investigate disease processes, animal models of chronic neurodegenerative diseases have been used with the hope of translating findings in these models into humans. These models go some way to capturing aspects of chronic neurodegenerative diseases and are useful for trying to unpick molecular and cellular processes leading to synapse dysfunction, loss and subsequently neurodegeneration (Verity and Mallucci, 2011).

Chronic neurodegenerative diseases have sporadic and familial etiologies. Mutations in genes associated with the generation of, and/or the disease-specific misfolded protein have been exploited and used to create transgenic (Tg) mouse models to investigate the evolution of disease pathology (Götz and Ittner, 2008). Figure 1.1a lists common genes which are mutated in chronic neurodegenerative diseases. The mutations associated with different Tg mouse models of AD, PD and ALS discussed in this thesis are shown in appendix 1.

Tg mouse models of AD can have mutations in the APP gene and in PSEN1 and PSEN2 (encoding presenilin 1 and 2 – which are part of a proteolytic complex known as γ -secretase which cleaves APP to generate A β peptides) (Götz and Ittner, 2008). No mutations in the tau gene (*MAPT*) have been associated with familial AD, although mutations in *MAPT* have been found in some patients with frontotemporal dementia and Parkinsonism linked to chromosome 17 (FTDP-17) (Spillantini et al., 1998). Mutations in *MAPT* have been used to generate mouse models of tauopathies (Goedert, 2004, Götz and Ittner, 2008, Hutton et al., 1998, Poorkaj et al., 1998).

Familial forms of PD are associated with mutations in a number of different genes (Figure 1.1a). Mutations in *SCNA* (which encodes α -synuclein) and the gene leucine-rich repeat kinase 2 (*LRRK2*) are used to model PD (Dawson et al., 2010). Three other PD-associated genes: PTEN induced putative kinase 1 (*PINK1*); *PARK2* (parkin) and DJ-1 are autosomal recessive genes and knock-down of these genes have been used to model PD (Dawson et al., 2010). Neurotoxins which cause dopaminergic neuronal death have also been used to model PD: this includes the neurotoxins 6-hydroxydopamine (6-OHDA) and 1-methyl-4-phenyl-1,2,3,6-tetrahydropyridine

(MPTP) (Bezard et al., 2013). Mouse models of PD have also been created by injection of viral vectors containing genes with mutations in disease causing proteins, in to the brains of mice (Bezard et al., 2013).

The majority of ALS cases are sporadic, although around 10% have a genetic or familial component (Jiang et al., 2014). Numerous mutations have been associated with familial ALS, including mutations in *SOD1* encoding superoxide dismutase 1 (SOD1), *TARDBP* encoding TAR DNA-binding protein 43 (TDP-43) and *FUS* encoding the RNA-binding protein Fused in Sarcoma (FUS) (Joyce et al., 2011, Liscic and Breljak, 2011).

Genetic prion disease can be modelled using Tg mice overexpressing the mutant prion gene. Tg mouse models of prion disease are shown in appendix 2. Intracerebral inoculation of wildtype non-Tg mice with brain homogenate containing the prion disease-associated protein (section 1.2.1) is used to model infectious prion disease. Peripheral routes of inoculation can also be used to study prion disease, although incubation times are normally longer (Watts and Prusiner, 2014). Tg mice (expressing multiple copies of the prion gene) inoculated with brain homogenate containing the disease-associated protein have a greatly accelerated disease progression compared to non-Tg wildtype mice (Moreno et al., 2012, Watts and Prusiner, 2014). Tg prion mice without any mutations can also develop spontaneous prion disease (Watts and Prusiner, 2014).

Although the majority of mouse models of AD, PD and ALS are from Tg mice which overexpress mutant human or mouse disease-associated genes, some models are created by the overexpression of wildtype human genes (Götz et al., 1995, Xu et al., 2010). In addition, brain homogenates from mouse models of AD and PD (containing aggregated disease-associated protein) or *in vitro* generated synthetic protein aggregates have been inoculated into the brains of Tg mice (Polymenidou and Cleveland, 2012). This has been shown to lead to protein aggregation, spreading of the protein aggregates and neurodegeneration in these models. Although most of these ‘transmission’ studies have been performed on Tg mice, inoculation of wildtype non-Tg mice with synthetic A β ₁₋₄₂ oligomers and α -synuclein fibrils has been shown to lead to neurodegeneration (Baleriola et al., 2014, Luk et al., 2012a).

Figure 1.1b depicts different ways of using mice to model chronic neurodegenerative disease.

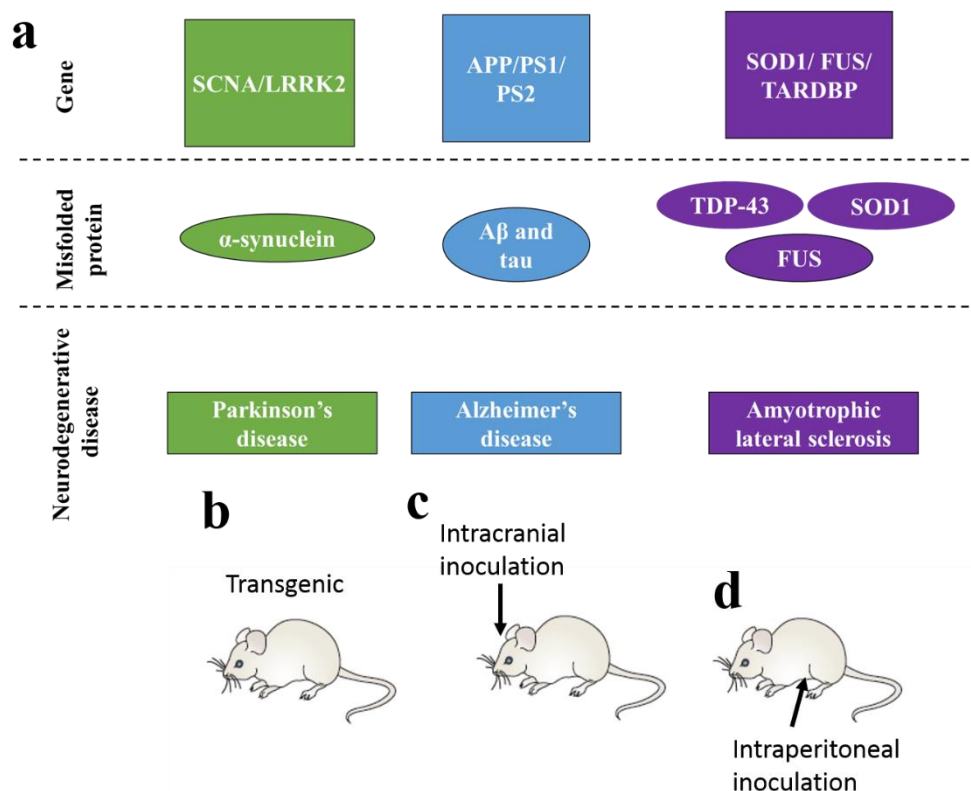


Figure 1.1 Genes associated with familial forms of chronic neurodegenerative diseases and ways of modelling chronic neurodegenerative diseases in mice.

Mutations in the genes shown in (a) are associated with different chronic neurodegenerative diseases. The pathological misfolded protein(s) associated with these diseases is shown. Mouse models of chronic neurodegenerative diseases can be created using transgenic mice, expressing one or more mutations in the human or mouse genes shown in (b). In addition, intracranial (c) and intraperitoneal injection (d) of aggregated disease-associated protein either from homogenate extracted from mice or made *in vitro* can be used to model chronic neurodegenerative disease. Neurotoxins and viral vectors containing genes with mutations in disease causing proteins have also been injected into mice and used to model Parkinson's disease. Figure (a) adapted from Pievani et al., 2014.

1.2 Prion diseases

Prion diseases are a class of rare and fatal chronic neurodegenerative diseases (Prusiner, 1991). They affect both animals (e.g. Bovine Spongiform Encephalopathy (BSE) in cattle) (Table 1.1) and humans (e.g. Creutzfeldt-Jakob Disease (CJD) and Kuru) and have an etiology that is sporadic, inherited and infectious (Table 1.2) (Watts and

Prusiner, 2014). In humans they effect on average only one person per million per annum (Torres et al., 2014). Prion disease is characterised by vacuolation of the grey matter (spongiform degeneration), reactive gliosis, microglial cell activation and neuronal cell death (Cunningham et al., 2003, Fraser, 1993). The disease rapidly progresses and culminates in death after a few months of clinical symptoms (Heiseke et al., 2010). These symptoms can include dementia, ataxia, disordered movement, insomnia and psychiatric disturbances (Hetz et al., 2007, Taylor et al., 2002).

An important feature of prion diseases is the ability of the disease to be transmitted between organisms (Gajdusek et al., 1966, Gajdusek et al., 1967, Gibbs et al., 1968). In humans iatrogenic CJD has been reported due to the transmission of prion-containing material in human growth hormone, dura mater grafts and from blood transfusions of donors (Brown et al., 2000, Ironside, 2012). The BSE epidemic led to the emergence of human variant CJD (vCJD), which is believed to be caused by the consumption of infected beef products from cattle (Hill et al., 1997, Prusiner, 1996, Will et al., 1996).

Prion disease	Animal
Scrapie	Sheep and goats
Transmissible Mink Encephalopathy (TME)	Mink
Chronic Wasting Disease (CWD)	Mule deer and Rocky Mountain elk
Bovine Spongiform Encephalopathy (BSE)	Cattle
Feline Spongiform Encephalopathy (FSE)	Domestic cats and wild cats

Table 1.1 Prion diseases of animals.

Table adapted from Ridley and Baker, 1998.

Etiology	Prion disease
Sporadic	Creutzfeldt-Jakob disease (CJD) Fatal insomnia
Inherited	Familial CJD
	Gerstmann-Sträussler-Scheinker syndrome (GSS)
	Fatal familial insomnia
Infectious	Kuru
	Iatrogenic CJD
	Variant CJD (vCJD)

Table 1.2 The etiology of different human prion diseases.

Table adapted from Ridley and Baker, 1998.

1.2.1 The prion protein (PrP)

In an attempt to define the basis of infectious prion disease, Alper and co-workers demonstrated that ionizing and UV irradiation which destroys nucleic acid did not destroy the infectious material in scrapie which could be transmitted between organisms (Alper et al., 1967). Subsequent work in identifying this agent, employed the use of Syrian golden hamsters to assay scrapie infectivity in different fractions and established that a protein was the causative agent of the disease (Bolton et al., 1982, Prusiner, 1982). This led to the ‘protein-only hypothesis’ (which proposes that prion disease is caused by a disease-associated protein) and the term ‘PrP’ was introduced to describe the proteinaceous infectious agent that is resistant to most of the procedures that destroy viruses and viroids (Prusiner, 1982).

The proteinase K (PK) resistant polypeptide purified from hamster brains infected with scrapie and absent from uninfected brains, has a molecular weight of approximately 27-30 kDa and is denoted PrP²⁷⁻³⁰ (Bolton et al., 1982, Prusiner, 1982). It was revealed that levels of PrP mRNA remained unaltered during the course of scrapie infection, this led to the discovery that PrP was encoded by a normal chromosomal gene; ‘*Prnp*’ (Chesebro et al., 1985, Oesch et al., 1985). Mutations in this gene have been linked to familial forms of prion disease (Hsiao et al., 1989) and used to create Tg models of prion disease (section 1.1.1). The product of the *Prnp* gene was identified as a protease sensitive protein of 33-35 kDa, named PrP^C (cellular isoform of PrP) (Meyer et al., 1986, Oesch et al., 1985). Numerous functions have been assigned to PrP^C (Campana et

al., 2005) including copper and/or zinc binding and metabolism (Brown, 2001a, Watt and Hooper, 2003) and in the maintenance of normal synaptic homeostasis (Collinge et al., 1994, Mallucci et al., 2002) The infectious prion, denoted as PrP^{Sc} (Sc standing for scrapie), encoded by the same host gene as PrP^C (Basler et al., 1986), is a conformationally altered partially protease-resistant isoform of the normal cellular protein (Aguzzi and Heikenwalder, 2006, McKinley et al., 1983, Verity and Mallucci, 2011).

1.2.2 PrP^C biosynthesis

The primary structure of mouse PrP^C is shown in Figure 1.2a. During the translation of PrP^C, a signal peptide sequence at the amino terminus of PrP^C emerges from the ribosome. This signal sequence is recognised and captured by a signal recognition particle (SRP). The binding of SRP to the signal sequence slows down the rate of protein synthesis and targets the SRP-peptide-ribosome-mRNA complex to the ER, where SRP binds to a heterodimeric SRP receptor (Guerriero and Brodsky, 2012) (Figure 1.3). Following this, SRP is released and translation ensues with the insertion of the emerging immature PrP^C polypeptide into the translocation pore of the ER and subsequently the ER lumen (Guerriero and Brodsky, 2012).

In the ER, PrP^C is subjected to numerous post-translational modifications (Figure 1.3). This includes the cleavage of the signal sequence by a signal peptidase (Linden et al., 2008), the folding of PrP^C by ER chaperones, the formation of a single disulfide bond between two cysteine residues and the addition of a glycosylphosphatidylinositol (GPI) anchor at the carboxylic terminus (which enables its association with lipid membranes) (Linden et al., 2008). In addition, PrP^C can be glycosylated at two asparagine residues (Asn180 and Asn190 in mice) in the ER. PrP^C can therefore exist in either an unglycosylated, monoglycosylated or diglycosylated form (Figure 1.2b).

PrP^C is transported from the ER to the Golgi apparatus where the core glycan structure formed in the ER is further elaborated (Abid and Soto, 2006, Guerriero and Brodsky, 2012). Finally, PrP^C is transported to the cell surface where it is attached by its GPI anchor (Caughey et al., 1989, Cohen et al., 1994). PrP^C is enriched in detergent resistant membranes (Aguzzi and Heikenwalder, 2006) and expressed on neurons and astrocytes (Brown, 2001b, Moser et al., 1995). At the plasma membrane PrP^C can be internalised

via endocytosis and either recycled back to the plasma membrane or degraded by the lysosome (Harris, 2003).

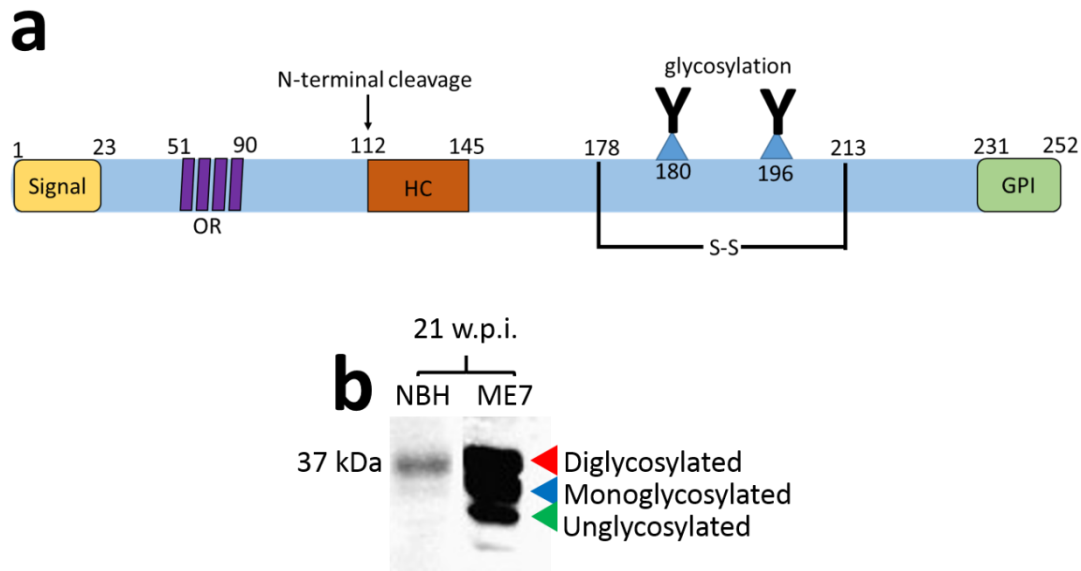


Figure 1.2 The primary structure of mouse PrP^c and different glycosylated states.

A signal sequence for ER targeting is present at the N-terminus. This is followed by the octapeptide repeats (OR), thought to bind copper atoms and a hydrophobic core (HC). The N-terminal cleavage point indicates where the protein is endogenously cleaved. The disulfide bond (s-s) as well as the glycosylation sites are shown. The protein is anchored to cell membranes by a glycosylphosphatidylinositol (GPI) anchor. Numbers denote the position of the relative amino acids. Figure a is adapted from Brown, 2001b. Western blot of total PrP in NBH and ME7 samples at 21 weeks postinoculation (w.p.i.). The three bands detected represent the different glycosylated forms of PrP: di-, mono- and unglycosylated. Figure b adapted from Gray et al., 2009.

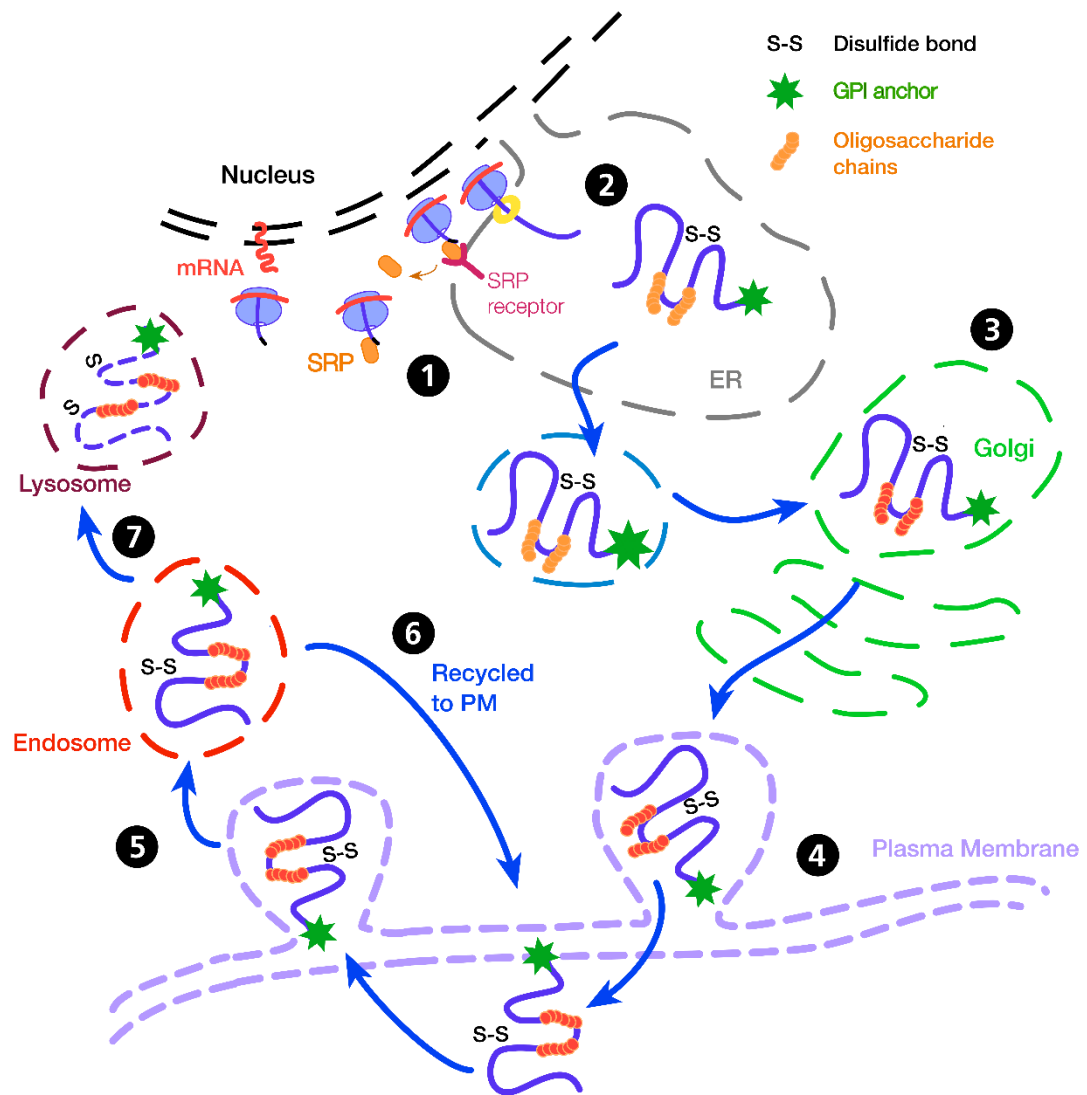


Figure 1.3 The biosynthesis of PrP^C.

PrP^C mRNA is trafficked from the nucleus into the cytoplasm. In the cytoplasm translation of PrP^C occurs. The emergence of a signal peptide from the PrP^C protein is detected by a signal recognition particle (SRP) which binds to the signal sequence (1). SRP slows down the rate of PrP^C translation and targets the SRP-polypeptide-ribosome-mRNA complex to the ER by the binding of SRP to an SRP receptor. After this SRP is released and translation continues, with the immature PrP^C polypeptide being translated through the ER translocation pore and into the ER lumen, where the signal sequence is cleaved. Inside the ER lumen the PrP^C protein is subjected to a number of posttranslational modifications including the correct folding of the protein, the formation of a disulfide bond, glycosylation and the addition of a glycosylphosphatidylinositol anchor (GPI) to the carboxyl terminus of the protein (2). The protein is then trafficked to the Golgi apparatus where the core glycan structure of PrP^C is further modified (3),

before being transported to the plasma membrane where PrP^C attaches via its GPI anchor (4). PrP^C can be internalised via endocytosis (5) and either recycled back to the plasma membrane (6) or targeted for degradation by the lysosome (7).

1.2.3 Conversion of PrP^C to PrP^{Sc}

PrP^{Sc} has the exact same amino acid sequence as PrP^C (Prusiner, 1996, Prusiner, 1998). The main difference between these two proteins is a post-translational conformational change. In contrast to PrP^C which has a high α -helical content (42% α -helix and 3% β -sheet), PrP^{Sc} has a much greater β -sheet content and a reduced α -helical content (43% β -sheet and 30% α -helix) (Pan et al., 1993).

During prion disease, infectious PrP^{Sc} converts PrP^C into PrP^{Sc} by refolding its α -helices into β -sheets (Pan et al., 1993). Infectivity in prion disease has found to be correlated with oligomeric forms of PrP^{Sc} as opposed to monomeric forms. In a study by Silveira et al 2005, PrP^{Sc} consisting of 14-28 molecules (300-600 kDa) was found to be the most infectious (Silveira et al., 2005). The conversion process is thought to occur at the cell surface and in endosomal/lysosomal compartments (Borchelt et al., 1992, Caughey and Raymond, 1991, Caughey et al., 1991) and both astrocytes and neurons can convert PrP^C to PrP^{Sc} (Radford and Mallucci, 2010). As PrP^C is converted to PrP^{Sc}, PrP^C continues to be produced by translation without a change in transcription and is used as a substrate for further conversion. Genetic forms of prion disease are thought to occur because the mutant PrP^C molecules misfold into a PrP^{Sc}-like form, whilst sporadic prion diseases are thought to be due to spontaneous misfolding of PrP^C (Senatore et al., 2013).

The full molecular sequence of events which occurs when PrP^C is converted into PrP^{Sc} is still not completely known, however, numerous models have been suggested to explain the conversion process (Figure 1.4). The template-assisted model proposes that normally the spontaneous conversion of PrP^C into PrP^{Sc} is prevented. However, in the presence of monomeric PrP^{Sc} and an additional conversion factor (referred to as Protein X) (Prusiner, 1996, Telling et al., 1995), PrP^{Sc} binds to an intermediate form of PrP to form a heterodimer. The intermediate PrP protein is then converted by PrP^{Sc} into a homodimer of PrP^{Sc} (Abid and Soto, 2006). The PrP^{Sc} homodimer can then further oligomerise or fragment and assist in the further conversion of PrP^C to PrP^{Sc}.

The seeded nucleation model proposes that monomeric PrP^{Sc} exists in a dynamic equilibrium with PrP^{C} , with the equilibrium normally being heavily sifted towards PrP^{C} (Abid and Soto, 2006, Aguzzi and Polymenidou, 2004). Monomeric PrP^{Sc} therefore represents a minor fraction of the total PrP levels and is relatively unstable. It only becomes stabilised when forming an oligomer. In the presence of infectious PrP^{Sc} , a PrP^{Sc} oligomeric seed is slowly formed (Abid and Soto, 2006). This oligomeric seed acts to recruit and stabilise further monomeric PrP^{Sc} into a growing structure which can fragment, creating additional nuclei to recruit more PrP^{Sc} monomers (Abid and Soto, 2006, Aguzzi and Polymenidou, 2004).

Finally, the nucleated-assisted model proposes that in the presence of a conversion factor PrP^{C} forms an unfolded intermediate referred to as PrP^* (Abid and Soto, 2006). This intermediate is converted to PrP^{Sc} when recruited into a PrP^{Sc} oligomer. Oligomeric PrP^{Sc} can then be used to further recruit and convert PrP^* into PrP^{Sc} .

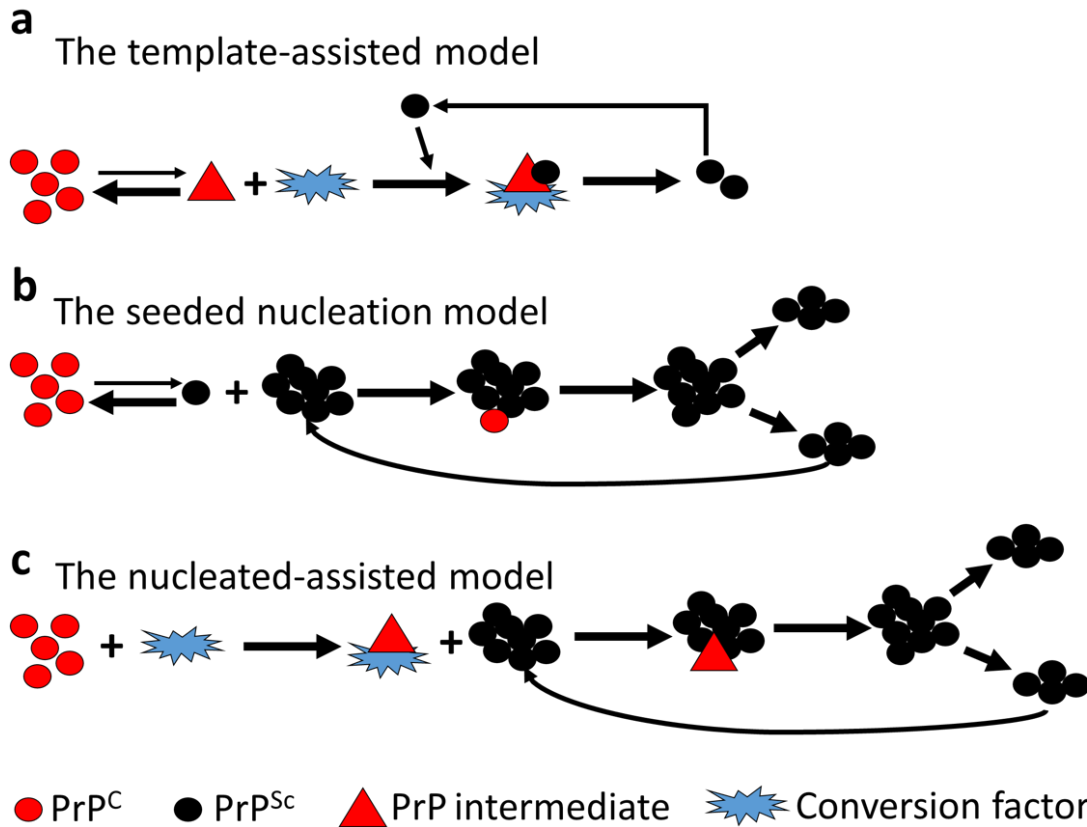


Figure 1.4 Proposed models of the conversion of PrP^C to PrP^{Sc}.

The template-assisted model proposes normally the formation of PrP^C is favoured over a PrP intermediate. However, in prion disease, in the presence of a conversion factor, PrP^{Sc} binds to a PrP intermediate forming a heterodimer. PrP^{Sc} converts the PrP intermediate into PrP^{Sc}, therefore forming a homodimer of PrP^{Sc}. This can oligomerise and fragment to enable further conversion (a). The seeded nucleation model proposes that PrP^C and PrP^{Sc} exist in a dynamic reversible equilibrium. Normally the formation of PrP^C is favoured, however, in the presence of PrP^{Sc}, a PrP^{Sc} seed is slowly formed, which can recruit more PrP^{Sc} molecules. This aggregated PrP^{Sc} oligomer can fragment into smaller oligomers which can seed further PrP^{Sc} formation (b). The nucleated-assisted model proposes that an intermediate protein referred to as PrP* is generated from the interaction of PrP^C with a conversion factor. In prion disease PrP* would be incorporated into an oligomer of PrP^{Sc} and converted into PrP^{Sc}. Oligomers of PrP^{Sc} can fragment and act as seeds for further conversion of PrP* into PrP^{Sc}. Figure adapted from Abid and Soto, 2006.

The conversion of PrP^C to PrP^{Sc} is needed to develop clinical prion disease. Knockout mice lacking PrP^C (Prnp^{0/0} mice) are relatively normal (Büeler et al., 1992, Manson et al., 1994) and resistant to prion disease (Büeler et al., 1993). However, some defects in

synaptic function are seen in these knockout animals (Colling et al., 1996, Collinge et al., 1994, Mallucci et al., 2002, Manson et al., 1995).

In addition, preventing the conversion process of PrP^C to PrP^{Sc} has been shown to be neuroprotective. Removal of the GPI anchor from PrP^C did not result in clinical signs of prion disease even though conversion of PrP^C to PrP^{Sc} could still occur (Chesebro et al., 2005). Cre recombinase deletion of PrP^C after challenge with PrP^{Sc} reversed spongiform degeneration, prevented neuronal loss and progression to clinical stages of disease (Mallucci et al., 2003). A more recent paper has shown that mice with Cre recombinase deletion of PrP^C do ultimately succumb to prion disease when inoculated with PrP^{Sc}, although this is significantly delayed compared to wildtype mice (Mirabile et al., 2015). RNAi knockdown of PrP via lentiviral small-hairpin RNA (shRNA), prevented the onset of behavioural deficits and neuronal loss and prolonged survival in these mice (White et al., 2008). These effects were seen despite the accumulation of extra-neuronal PrP^{Sc}. However, in another study, PrP^{Sc} generated by astrocytes expressing PrP^C was sufficient to cause neurodegenerative changes even though PrP^C was not neuronally expressed (Jeffrey et al., 2004).

1.3 Experimental ME7 prion disease

Scrapie is a prion disease of sheep and goats (Table 1.1). The successful transmission of scrapie to mice in 1961 provided an infectious *in vivo* laboratory model that could be used to study the neuropathology of prion disease (Chandler, 1961).

ME7 prion disease is initiated in our laboratory by the bilateral injection of 1 µl (10% w/v) of the ME7 strain of murine modified scrapie or normal brain homogenate (NBH) (control) into the dorsal hippocampus of C57BL/6J mice. NBH-animals refers to animals injected with NBH and ME7-animals refers to animals injected with ME7 scrapie. The hippocampus was studied because the ME7 strain particularly affects the hippocampus and hippocampal neuroanatomy, electrophysiology and function is well known (Betmouni et al., 1996). In addition, the vulnerability of one subset of hippocampal neurons, CA3 pyramidal neurons (section 1.3.2), is well studied in the ME7 prion disease model.

1.3.1 Hippocampal neuroanatomy

The hippocampus is a region of the brain involved in learning and memory and memory loss is seen in chronic neurodegenerative diseases which present with dementia (Halliday and Mallucci, 2015). The hippocampus has a well-defined synaptic circuitry that can be used to study the neurobiological basis of behavioural changes and inter-neuronal communication (Andersen et al., 2006). A mouse brain coronal section is shown in Figure 1.5 illustrating the location of the hippocampus within a section of the mouse brain. The three main anatomically distinct subfields of the hippocampus are known as the dentate gyrus (DG), the Cornu Ammonis region 3 (CA3) and the Cornu Ammonis region 1 (CA1) (Andersen et al., 2006). These three regions form what is known as the trisynaptic loop, a circuit of excitatory synaptic connections within the hippocampus. The first synaptic connection is formed between the entorhinal cortex and the granule neurons of the dentate gyrus (synapse 1) via the perforant pathway (Figure 1.6a). The granule neurons (cell bodies located in the granule cell layer of the DG) of the DG then relay information via their axons, known as mossy fibres, to the pyramidal neurons of the CA3 region (synapse 2). CA3 pyramidal neurons project their axons, known as Schaffer collaterals to the pyramidal neurons of the CA1 region (synapse 3). CA1 pyramidal neurons then project axons to the subiculum and entorhinal cortex (Andersen et al., 2006). The cell bodies of both the CA3 and CA1 pyramidal neurons are located within the pyramidal layer of the CA3 and CA1 regions.

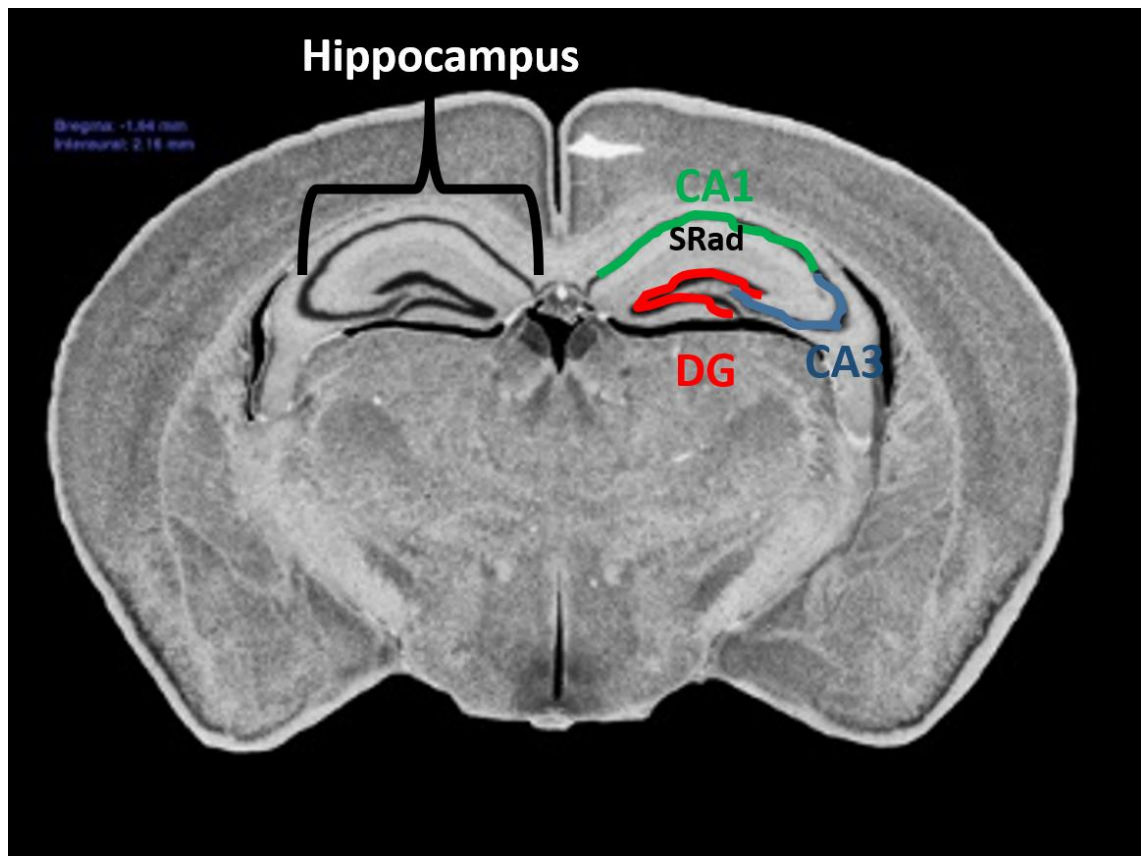


Figure 1.5 Coronal section through a mouse brain showing the location of hippocampus and the three main subfields of the hippocampus.

Image acquired from Mouse Brain Library, http://www.mbl.org/atlas170/atlas170_frame.html, section number 20. Accessed on 29th June 2015. CA1, Cornu Ammonis region 1; CA3, Cornu Ammonis region 3; DG, dentate gyrus and SRad, stratum radiatum.

1.3.2 CA3 pyramidal neurons and their axons: the Schaffer collaterals

The pyramidal neurons of the CA3 receive input from the granule neurons of the DG and provide the main excitatory input to CA1 neurons, via their Schaffer collateral axons. In addition, CA3 neurons can form recurrent connections with other CA3 neurons and some CA3 neurons can send projections back to the DG (Wittner et al., 2007). CA3 neurons can also send projections to these regions in the hippocampus on the contralateral side.

Extensive Schaffer collateral axons branch off from the principle CA3 neurons axon (Wittner et al., 2007) (Figure 1.6b). Along the length of the Schaffer collateral axons are numerous presynaptic boutons (referred to as '*en-passant*') which are separated by

segments of axonal shaft (Ishizuka et al., 1990). These presynaptic boutons synapse onto the dendrites of the CA1 pyramidal neurons in the stratum radiatum (a laminar region of the hippocampus) (Li et al., 1994). Biocytin labelling of CA3 pyramidal neurons in the hippocampus of rats has revealed that each neuron forms ~30,000-60,000 synapses (Li et al., 1994).

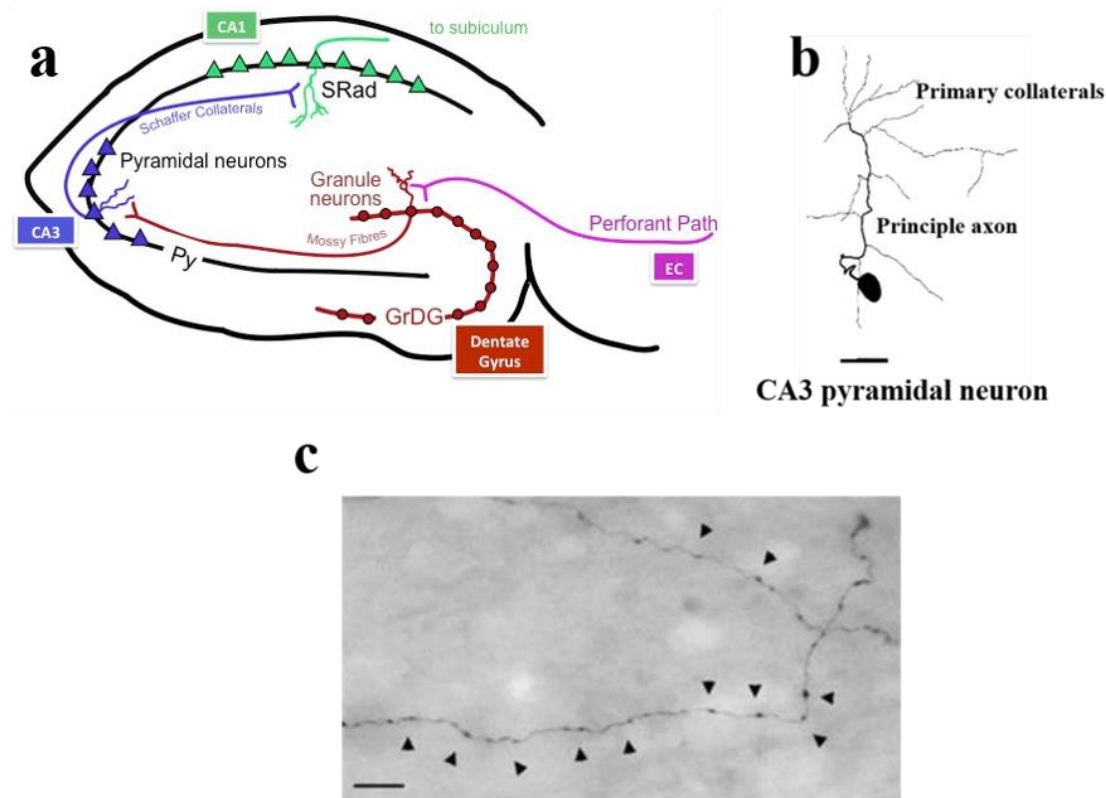


Figure 1.6 The hippocampal trisynaptic loop and basic structure of a CA3 pyramidal neuron.

Simplified diagram of the trisynaptic loop in the hippocampus (a). The entorhinal cortex (EC) provides synaptic input to the granule neurons of the DG, via the perforant pathway. The pyramidal neurons of the CA3 region receive input from the granule neurons of the dentate gyrus via their mossy fibre axons. CA3 pyramidal neurons project via their Schaffer collateral axons to CA1 pyramidal neurons where they synapse in the stratum radiatum of the hippocampus. CA1 pyramidal neurons send axonal projections to the subiculum and EC (not shown). The basic morphology of a reconstructed CA3 pyramidal neuron (b). A principle axon emanates from the cell body, from which numerous axon collaterals branch off. Additional collaterals (not shown) will branch off of these primary collaterals. (c) Light micrograph shows that along the length of the collaterals are *en-passant* synaptic boutons (black arrowheads) which synapse onto the postsynaptic dendrites of CA1 pyramidal neurons. Scale bar on

image b is 100 μm and scale bar on image c is 10 μm . Image b taken from Li et al., 1994 and image c taken from Wittner et al., 2007. CA1, Cornu Ammonis region 1; CA3, Cornu Ammonis region 3; DG, dentate gyrus; GrDG, granule cell layer of the DG; Py, pyramidal layer of CA3 and CA1 and SRad, stratum radiatum.

1.4 Neuropathology in ME7-animals

This ME7 model has a disease duration of ~21 weeks post-inoculation (w.p.i.), clinical signs appear at around ~20 w.p.i. and include reduction in mobility, hunched posture, poor coat condition, ataxia and weight loss (Combrinck et al., 2002, Guenther et al., 2001). There are no scrapie symptoms or pathology seen in NBH-animals (Cunningham et al., 2003, Gray et al., 2009).

Deposits of PrP^{Sc} appear in the DG region from 8 w.p.i. and spread to the other subfields of the hippocampus as disease progresses (Figure 1.7) (Gray et al., 2009). At end-stage disease PrP^{Sc} is also found in the thalamus, medial and lateral septal regions and entorhinal cortex (Cunningham et al., 2003, Gray et al., 2009). In ME7 prion disease from 8 w.p.i. the appearance of hypertrophied glial fibrillary acidic protein (GFAP) expressing astrocytes and increased numbers of activated microglia can be seen (Figure 1.8) (Betmouni et al., 1996, Cunningham et al., 2003).

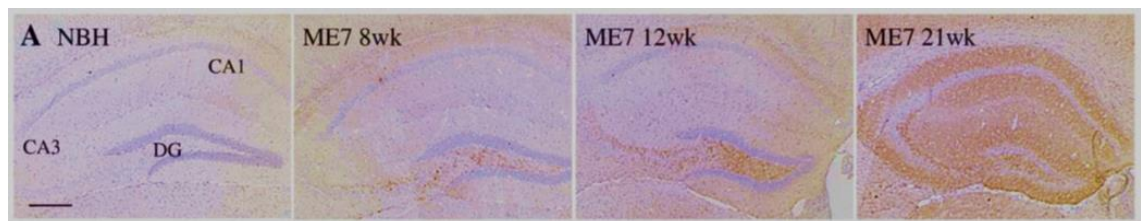


Figure 1.7 Deposition of PrP^{Sc} during ME7 prion disease progression.

Coronal hippocampal sections of control (NBH) and ME7 infected animals stained for heat and formic acid resistant PrP^{Sc} aggregates, using the PrP antibody 6H4 antibody. PrP^{Sc} accumulation and deposition, increased in a time dependent fashion first appearing in the DG at 8 weeks and then spreading to CA3 and CA1, with deposits throughout the entire hippocampus come week 21. Scale bar 200 μm . Image taken from Gray et al., 2009. CA1, Cornu Ammonis region 1; CA3, Cornu Ammonis region 3 and DG, dentate gyrus.

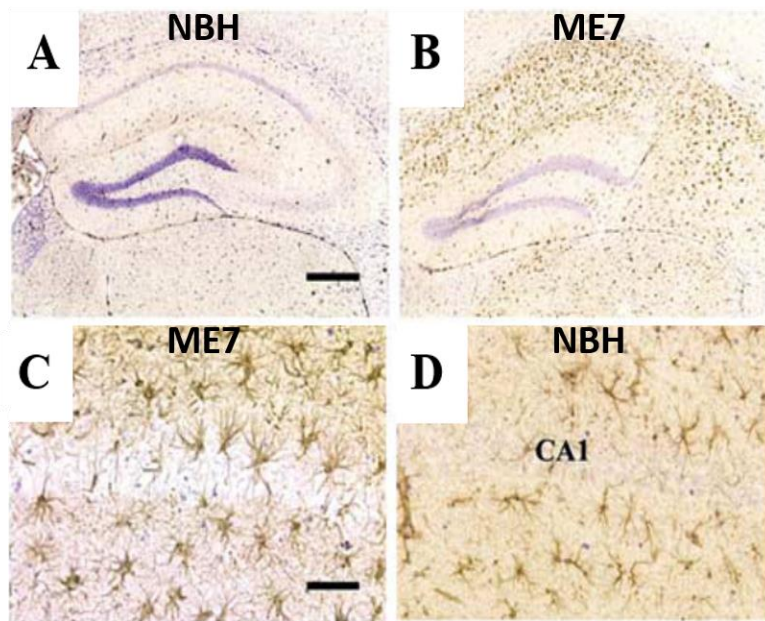


Figure 1.8 Increased microglia and hypertrophied astrocytes in ME7 prion disease.

Immunohistochemistry staining for CD68 shows increased numbers of microglia in ME7-animals (B) compared to NBH-animals (A). Immunohistochemistry staining for GFAP shows hypertrophy of astrocytes in ME7-animals (C) compared to NBH-animals (D). Staining was performed at 13 w.p.i. Scale bar, 200 μ m (A, B), 70 μ m (C, D). Image taken from Cunningham et al., 2003.

Electron microscopy in the stratum radiatum of C57BL/FaBtDk \times VM/Dk mice inoculated with ME7 revealed that synaptic loss is an early event in ME7 prion disease and precedes neuronal loss (Jeffrey et al., 2000). Synaptic loss has been studied in wildtype C57BL/6J mice inoculated with ME7 in our laboratory. From 12 w.p.i. presynaptic loss is seen in the stratum radiatum of the hippocampus. A combination of immunohistochemistry and western blotting has revealed disrupted staining for a number of presynaptic proteins such as the presynaptic vesicle protein synaptophysin (Cunningham et al., 2003, Gray et al., 2009). In contrast, postsynaptic proteins such as postsynaptic density protein 95 (PSD-95), showed less disruption and levels of these remain largely unaltered during disease progression (Gray et al., 2009). Although PrP^{Sc} deposits are seen in ME7-animals from 8 w.p.i., no deposits are detected in the stratum radiatum at the time of synaptic loss, which suggests that deposits of PrP^{Sc} do not correlate with synaptic loss (Cunningham et al., 2003).

Electron microscopy has revealed a significant loss of glutamatergic, asymmetric synapses from the stratum radiatum of ME7-animals from 12 w.p.i. (Sisková et al., 2009). During this synaptic degeneration visualised as darkening of the presynaptic element and loss of intracellular specialisations the postsynaptic membrane was shown to curve around and envelop the degenerating presynaptic compartment (Sisková et al., 2009, Sisková et al., 2010). As disease progressed from 12 to 21 w.p.i. an increasing number of post-synaptic densities (PSDs) lacked contact with a presynaptic specialisation. The degeneration of these synapses appears to be a neuron autonomous event since glial cell processes were not seen directly associated with the degenerating synapse or interposed between the pre- and post-synaptic elements (Sisková et al., 2009).

Recently biotinylated dextran amine (BDA) tracing of hippocampal CA3 neurons *in vivo* has provided additional insight into the process of synapse loss (Al-Malki, 2012). From 13 w.p.i., synaptic boutons are progressively lost along the length of the Schaffer collateral axons of ME7-animals (Al-Malki, 2012) (Figure 1.9). The synaptic boutons which remain intact appear hypertrophied.

Abnormal axonal swellings can also be seen from 13 w.p.i. along the Schaffer collateral axons (Figure 1.10), signifying that the axonal compartment of CA3 pyramidal neurons is also dysfunctional. A reduction in the number of axons in the stratum radiatum and signs of local axonal degeneration were also seen in ME7-animals from 13 w.p.i. (Figure 1.10). In support of this, axonal terminal degeneration has been shown to occur in mice on a different genetic background and inoculated with ME7 (Jeffrey et al., 2000) and at around a similar time long term potentiation (LTP) – a form of synaptic plasticity was impaired (Chiti et al., 2006, Johnston et al., 1998).

As well as synaptic and axonal changes, a loss of apical dendritic spines, a reduction in dendritic arborization and length can also be seen in CA3 pyramidal neurons of ME7-animals from 13 w.p.i. Dendritic spine loss has also been shown to occur on CA1 pyramidal neurons of C57BL/6J×VM/Dk mice (Belichenko et al., 2000). Like the swellings seen on axons, dendritic swellings are also seen on the apical dendrites of CA3 neurons (Al-Malki, 2012) and on dendrites of CA1 pyramidal neurons (Belichenko et al., 2000). Synaptic, axonal and dendritic alteration precede changes in the CA3 cell soma, which is reduced in size from 16 w.p.i. (Al-Malki, 2012) earlier than what has

previously been reported (Gray et al., 2009). The distinct pyramidal shape of the CA3 neurons is disrupted and they adopt a more rounded cell soma. Similar to neurons, BDA labelled astrocytes showed signs of degeneration in ME7-animals (Al-Malki, 2012). This demonstrates that both neurons and astrocytes are susceptible to ME7 prion disease.

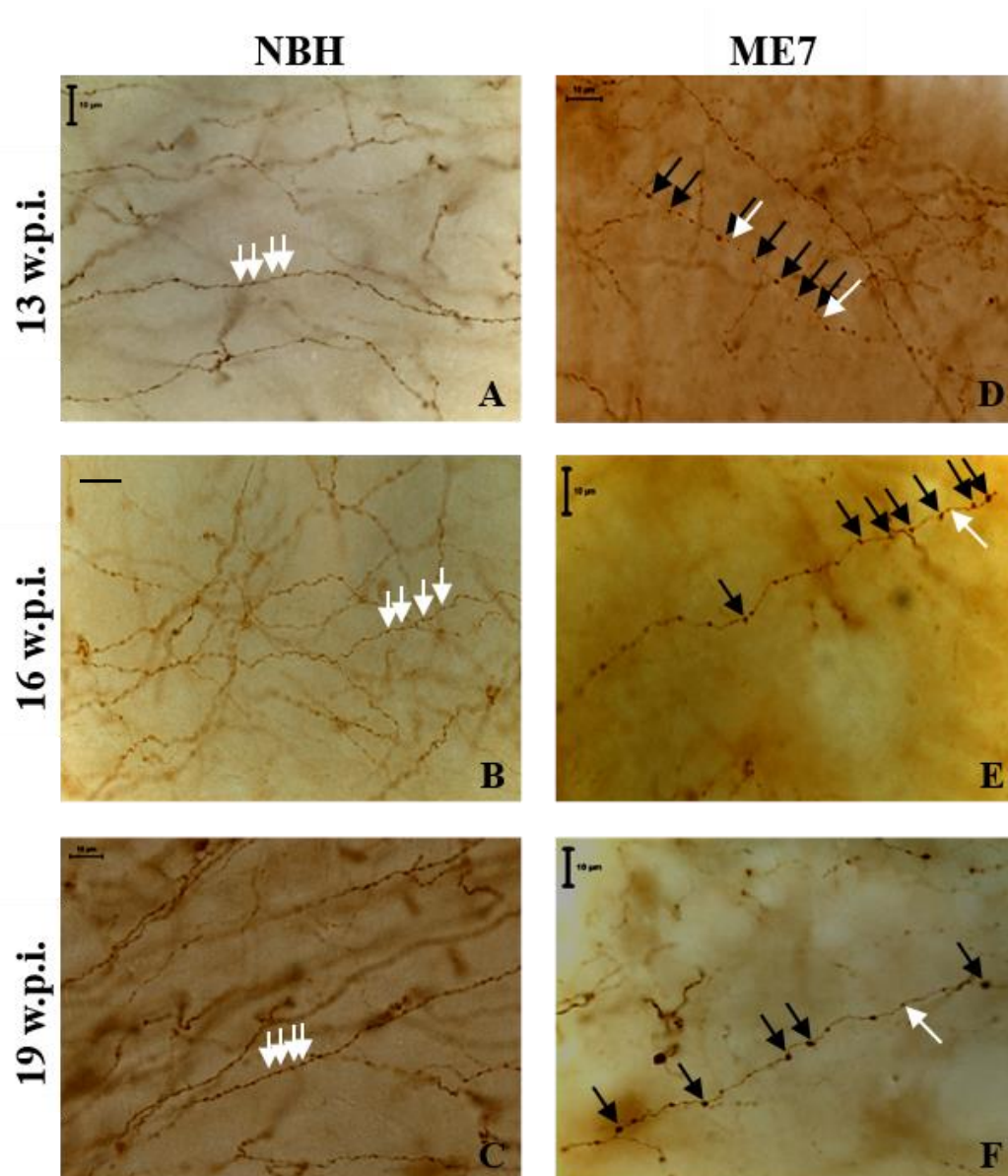
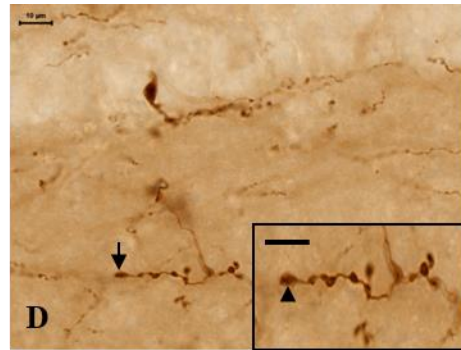
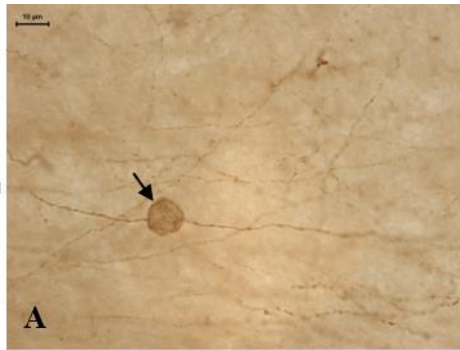


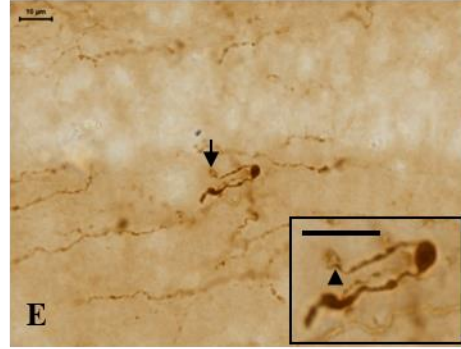
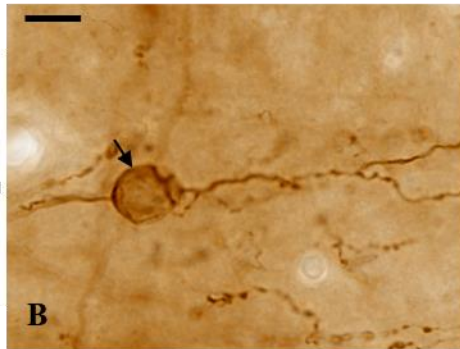
Figure 1.9 Progressive loss of synaptic boutons in ME7-animals.

Synaptic boutons along the length of the CA3 Schaffer collateral axons are progressively lost from 13 w.p.i. in ME7-animals. NBH-animals (left panel) show an even distribution of synaptic boutons (white arrows) along the length of the Schaffer collateral axons (A-C). In ME7-animals (right panel) there is a progressive loss of synaptic boutons along the length of the axon. Synaptic boutons that remain intact appear hypertrophied (black arrows) and are separated by increased distances of axonal shaft. White arrows are representative of normal synaptic boutons. Scale bars, 10 μm. w.p.i., weeks post-inoculation. Image taken from Al-Malki, 2012.

13 w.p.i.



16 w.p.i.



19 w.p.i.

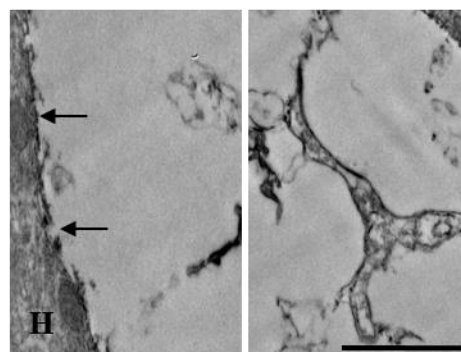
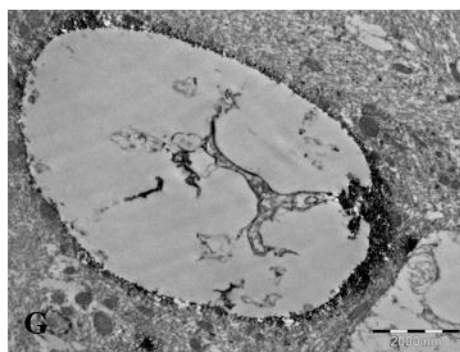
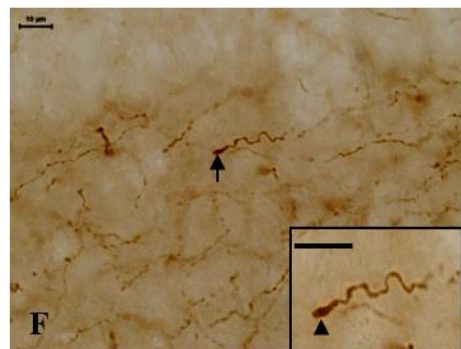
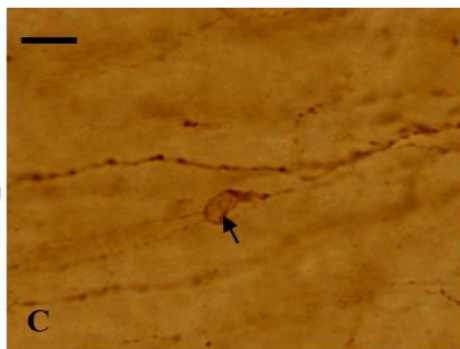


Figure 1.10 Abnormal axonal swellings and signs of local axonal degeneration in ME7-animals.

The appearance of abnormal axonal swellings ($\geq 2.20 \mu\text{m}$) (black arrows) can be seen on CA3 Schaffer collateral axons of ME7-animals from 13 w.p.i. (A-C). Features of local axonal degeneration can be seen from 13 w.p.i., in which axons appear thicker and end in swollen bouton-like structures (black arrows and arrowheads in the insets) (D-F). Axonal swellings and signs of axonal degeneration are not seen in NBH-animals. Electron micrograph of an axonal swelling labelled with BDA tracer (G-H). (G) The majority of the axonal swelling is empty with only residual indistinct structures seen. (H) High magnification electron micrograph showing disruption of the axonal border (arrows) and distorted/degenerated membrane within the swelling. Scale bars, $10 \mu\text{m}$ except for (G and H) where scale bars are $2 \mu\text{m}$. w.p.i., weeks post-inoculation. Image taken from Al-Malki.

Despite early changes in synaptic, axonal and dendritic compartments and the cell soma, neuronal loss is not seen in ME7-animals until late-stage disease (~ 18 w.p.i.), when there is a significant loss of CA1 pyramidal cells (40%) (Cunningham et al., 2003). Neuronal loss is also a late event in C57BL/FaBtDk \times VM/Dk mice (Jeffrey et al., 2000). In a Tg model of inherited prion disease (TgPG14-A3^{+/-}) deletion of the pro-apoptotic protein Bax prevented neuronal loss, but neurological symptoms were not altered suggesting that early changes in the other neuronal compartments such as the synapses are key pathological causes of neuronal dysfunction in prion disease (Chiesa et al., 2005).

1.4.1 Behavioural deficits in ME7-animals

Behavioural tests have been performed on prion diseased mice and these provide a non-invasive means of determining disease progression (Cunningham et al., 2003, Perry and O'Connor, 2010). Numerous different behavioural tasks have been used in ME7-animals and some of these are briefly described below.

Burrowing is a test of species-typical behaviour reliant on an intact dorsal hippocampus (Deacon et al., 2002). In this test, plastic cylindrical tubes filled with food pellets are raised above the ground. The amount of food pellets displaced or burrowed in a given time is measured (Cunningham et al., 2003, Guenther et al., 2001).

Nest construction also requires an intact dorsal hippocampus and is a test of species typical behaviour (Cunningham et al., 2003, Deacon et al., 2002). Nests made using a cotton square (nesting material) are scored using a defined scale based on how well the nests are assembled (Cunningham et al., 2003, Guenther et al., 2001). Glucose consumption, a test of appetitive behaviour, was assessed by filling plastic bottles with glucose solution. The amount of glucose solution consumed by the mice was recorded (Cunningham et al., 2003, Guenther et al., 2001). Open field is a test of activity and is measured by placing a mouse in a square box and measuring the distance the mouse travels in a set period of time (Cunningham et al., 2003, Guenther et al., 2001).

The onset of cognitive impairments in prion diseased mice has been assessed using learning and memory tests: a spontaneous alternation T-maze task (Guenther et al., 2001), Y-maze alternation task (Cunningham et al., 2009) and delayed response learning task (Deacon et al., 2005) and all of these tasks require an intact dorsal hippocampus. In the T-maze task the mouse is placed in the maze (at the base of the T) and at the start can only enter one arm of the T. After confinement in this arm for a short period of time the mouse is placed back at the base of the T. The mice then has the option to enter both arms of the T. The tests is repeated 5 times per mouse. The percentage of times they enter the alternate arm to the one they first enter is recorded and is a measure of spatial learning and memory.

Strength and co-ordination can be assessed by different tasks. The inverted screen test is commonly used to monitor strength (Guenther et al., 2001). A mouse is placed on a square wire mesh and inverted 180°. The time taken to fall off of the wire mesh within a set time period is recorded. Horizontal bar is a test used to assess strength and co-ordination (Guenther et al., 2001). A horizontal metal bar is held by two wooden supports. A mouse is placed onto the centre of this bar. Mice are then monitored for how long it takes them to fall off or if they can reach either of the wooden supports.

Injection of ME7 into the hippocampus of mice leads to significant impairments in burrowing, nest construction, glucose consumption and an increase in open field activity in ME7-animals (Cunningham et al., 2003) (Figure 1.11) These behavioural changes occur before deficits in cognition (from 16 w.p.i.) (Cunningham et al., 2009, Deacon et al., 2005, Guenther et al., 2001) and long before deficits in strength and motor

coordination (from 18 w.p.i.) (Cunningham et al., 2009, Guenther et al., 2001). In the ME7 prion model synaptic loss correlates with the onset of deficits in behavioural tasks and these deficits are seen before neuronal loss and clinical signs.

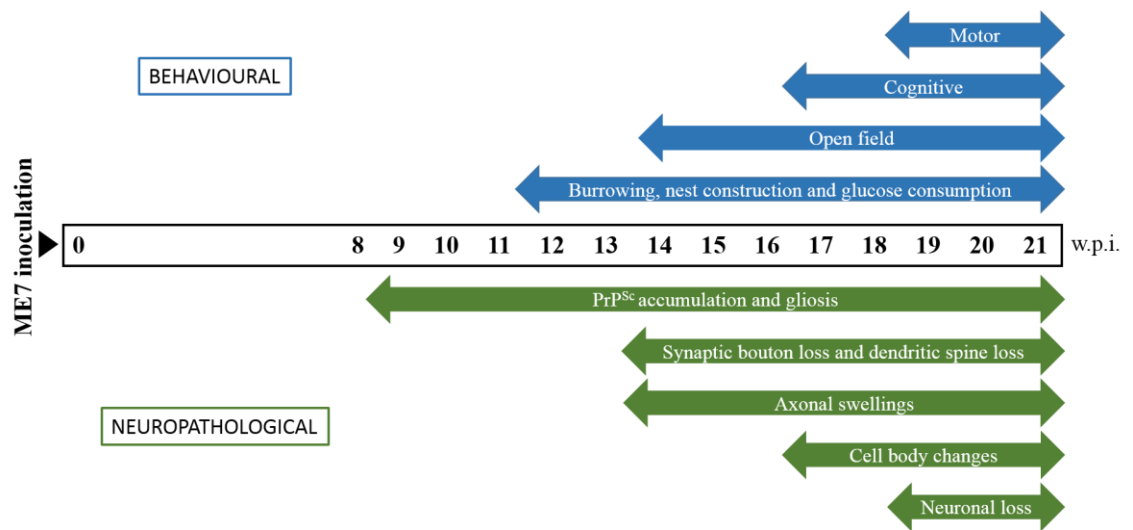


Figure 1.11 Timeline for the appearance of neuropathological and behavioural abnormalities in the ME7 model of prion disease.

The first neuropathological changes occur at around 8 w.p.i. after intra-hippocampal injection of the ME7 agent. These changes are characterised by the accumulation and deposition of PrP^{Sc} and the appearance of hypertrophied astrocytes and the increased number of microglia. Synaptic loss, dendritic spine loss and axonal swellings are detectable from 12 w.p.i. on the CA3 pyramidal neurons. A decrease in the size of the CA3 cell body area and change in the shape of the cell soma is visible from 16 w.p.i. CA1 neuronal loss occurs ≥ 18 w.p.i. The first signs of behavioural impairments and deficits are seen just after 11 w.p.i. Around this time impairments in burrowing, nest construction and glucose consumption are seen in ME7-animals. Shortly after this (~13 w.p.i.) mice become hyperactive (open field). Cognitive deficits are seen from 16 w.p.i. and this is shortly followed by motor impairments (strength and coordination) from 18 w.p.i. Clinical symptoms (not shown on the diagram) can be seen from 18 w.p.i. w.p.i., weeks post-inoculation.

1.5 Other mouse-adapted scrapie strains

In addition to the ME7 strain, other mouse-adapted strains of scrapie prions exist. These strains each have different rates of disease progression and their own pattern of lesion profiles affecting different anatomical brain regions (Bruce et al., 1991, Verity and Mallucci, 2011). The different neuropathologies seen with different prion strains are

thought to be a result of an interaction between different conformations of PrP^{Sc} as well as the effects of the mouse background used (Bruce et al., 1991, Safar et al., 1998, Ye et al., 2004). Table 1.3 shows the main areas of pathology and different incubation times for different scrapie prion strains injected into C57BL/6J mice. The Rocky Mountain laboratory (RML) strain is the most closely associated with ME7 in terms of behavioural deficits and pathology. RML-animals, like ME7-animals have CA3 presynaptic degeneration, deficits in behavioural tasks including burrowing and memory-based tasks, and neuronal loss in the CA1 (Moreno et al., 2012).

Strain	Areas of pathology	Incubation period (days)
ME7	Vacuolation in the CA1 region (hippocampus), thalamus and cortex (Cunningham et al., 2003).	~171 (Bruce et al., 1991).
22L	Vacuolation in region of Purkinje cells (cerebellum) (Sisková et al., 2013).	~148 (Bruce et al., 1991).
79A	Vacuolation primarily in white matter (Hilton et al., 2013).	~158 (Bruce et al., 1991).
RML	Vacuolation in the CA1 region (hippocampus), vacuolation in thalamus, midbrain and pons (Moreno et al., 2012, Siso et al., 2002).	~154 (Moreno et al., 2012).*

Table 1.3 Examples of mouse-adapted scrapie strains with differing neuropathology and incubation times.

Incubation time defined as the period between injection and time for which clinical signs are observed for a period of 3 weeks. * Interval between injection and appearance of clinical signs.

1.6 Cysteine string protein alpha (CSP α) knockout (-/-) model

1.6.1 CSP α

CSP was originally discovered in *Drosophila* (Zinsmaier et al., 1990) and later in described in mammals (Mastrogiacomo and Gundersen, 1995). CSP α is one of three

mammalian CSP isoforms, CSP β and CSP γ being the other two. Originally CSP α was thought to be the only isoform expressed in the brain (Fernández-Chacón et al., 2004), however, recently CSP β has also been shown to be expressed in the brains of mice (Gundersen et al., 2010). CSP α is a 34 kDa protein expressed on synaptic vesicles (Braun and Scheller, 1995, Braun et al., 1996, Mastrogiacomio and Gundersen, 1995, Mastrogiacomio et al., 1994).

CSP α contains an N-terminal J-domain (conserved tripeptide of histidine, proline and aspartic acid), a string of cysteine residues which form the cysteine string domain are palmitoylated, enabling membrane attachment (Chamberlain and Burgoyne, 1998, Chamberlain and Burgoyne, 2000, Fernández-Chacón et al., 2004, Swayne et al., 2006, Zinsmaier et al., 1990) (Figure 1.12). CSP α assembles with the chaperone heat shock cognate 70 kDa protein (Hsc70) via its J-domain and with a small glutamine-rich tetratricopeptide repeat (TRP)-containing protein (SGT) via its C-terminal domain to form an active chaperone complex (Sharma et al., 2011, Tobaben et al., 2001). This complex is responsible for stimulating the ATPase activity of Hsc70 (Braun et al., 1996, Chamberlain and Burgoyne, 1997a), and is assembled in the presence of adenosine diphosphate (ADP) and disassembles when adenosine triphosphate (ATP) is present (Tobaben et al., 2001).

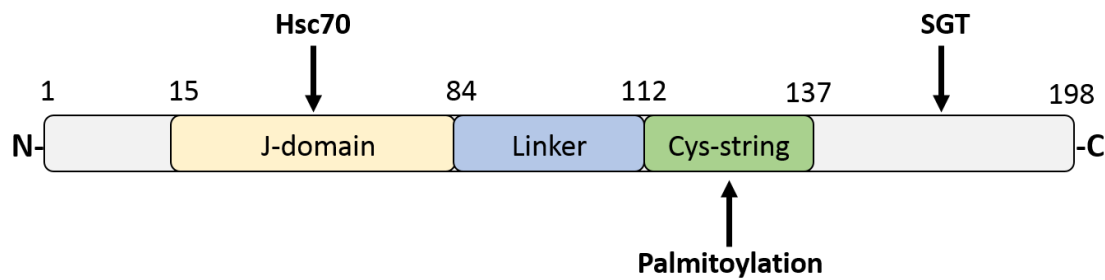


Figure 1.12 Primary structure of mouse CSP α protein.

CSP α protein contains an N-terminal J-domain, a linker region and a string of cysteine amino acids (Cys-string) which are palmitoylated, enabling the attachment of CSP α to the plasma membrane of synaptic vesicles. The binding sites for Hsc70 and SGT are shown. Numbers denote the relative position of amino acids. Figure adapted from Evans et al., 2003.

1.6.2 Deletion of CSP in flies

Most flies which have the CSP gene deleted die during development, with only a small number surviving to adulthood (Zinsmaier et al., 1994). The ones that do survive have a temperature-sensitive phenotype, characterised by impairments in synaptic transmission, paralysis and early death (Zinsmaier et al., 1994). In *Drosophila* larvae there is a reduced stimulus-evoked neurotransmitter release at the permissive temperature (22°C) and complete failure of stimulus-evoked release at the non-permissive temperature (30°C) at neuromuscular junction (NMJ) synapses (Umbach et al., 1994). This disruption is independent of spontaneous release events and indicates that the basis of the temperature-sensitive phenotype is a disruption in excitatory-secretion coupling (Umbach et al., 1994). The temperature-sensitive effects of CSP deletion was suggestive that CSP may be involved in chaperoning a protein at the synapse which enables vesicle fusion and exocytosis. At high temperatures this protein conformation might be destabilised therefore leading to failure of stimulus-evoked transmitter release (Broadie, 1995). This theory was extended when CSP was shown to bind and stabilise denatured firefly luciferase protein, therefore, showing that CSP does have general chaperone capabilities (Chamberlain and Burgoyne, 1997b).

1.6.3 Deletion of CSP α in mice

Deletion of the CSP α gene in mice also results in a neurodegenerative phenotype, characterised by astrogliosis with synaptic and neuronal loss (Sharma et al., 2012a). CSP α $-/-$ mice are normal at birth in comparison to wildtype ($+/+$) and heterozygous ($+/-$) mice but develop a progressive muscle weakness and sensorimotor deficit between 2 to 4 weeks of age (Fernández-Chacón et al., 2004). At postnatal day (P) 15 these mice stop gaining weight, become lethargic at day P30 and begin to die in the second postnatal month (Fernández-Chacón et al., 2004). None survive beyond three months of age (Fernández-Chacón et al., 2004). There is however no obvious difference between CSP α $+/+$ and CSP α $+/-$ mice, except for a slight impairment in open field activity of CSP α $+/-$ mice up to an age of P40 (Fernández-Chacón et al., 2004). This suggests that reduced levels ($\sim 50\%$) of CSP α is not sufficient to cause a neurodegenerative phenotype in the CSP α $+/-$ mice. However, mutations in the human CSP α gene cause autosomal-dominant adult-onset neuronal ceroid lipofuscinosis (ANCL), a neurodegenerative disorder caused by the accumulation of misfolded protein (lipofuscin) in the lysosomes (Noskova et al., 2011).

Levels of CSP α protein have been shown to be downregulated in human frontal cortex, hippocampus and superior temporal gyrus from AD patients (Tiwari et al., 2015, Zhang et al., 2012). In comparison, levels of CSP α have been shown to be upregulated in the cerebellum which is protected from degeneration in post-mortem AD tissue (Tiwari et al., 2015). Interestingly, CSP α is reduced in ME7-animals at 21 w.p.i. (Gray et al., 2009).

1.6.3.1 Molecular functions of CSP α in mice

CSP α has been proposed to serve numerous functions in the presynaptic compartment. These functions include chaperoning of the SNARE protein SNAP-25 (Sharma et al., 2011), regulation of dynamin 1 polymerization (Zhang et al., 2012) and controlling excitability of neurons via reducing the density of calcium-dependent K $^{+}$ (BK) channels at the presynapse (Kyle et al., 2013).

1.6.3.2 Molecular changes in CSP α -/- mice

The CSP α -Hsc70-SGT chaperone complex has been shown to bind directly to SNAP-25 and facilitate SNARE-complex formation (Sharma et al., 2011) (Figure 1.13). In CSP α -/- mice levels of SNAP-25 are reduced, as are the levels of presynaptic SNARE complexes composed of SNAP-25 and the other two SNARE proteins, syntaxin and synaptobrevin (Chandra et al., 2005, Sharma et al., 2011). The reduction in SNAP-25 and SNARE-complex is seen from P5 in CSP α -/- animals. SNARE-complex assembly has also been shown to be reduced in tissue from human AD and PD patients (Sharma et al., 2012b).

When CSP α is deleted, SNAP-25 has been suggested to be more likely to misfold at the synapse inhibiting the formation of SNARE-complexes (Sharma et al., 2011), as a result of the change in conformation, SNAP-25 is ubiquitinated and degraded by the proteasome (Sharma et al., 2011). SNARE-proteins are highly reactive and an excess of syntaxin and synaptobrevin relative to SNAP-25 in CSP α -/- mice has been proposed to lead to nerve terminal damage which culminates in neurodegeneration (Sharma et al., 2012a). Inhibiting the proteasome increases the levels of SNAP-25 and SNARE-complexes in CSP α -/- mice and this has been shown to alleviate the neurodegenerative phenotype and increase lifespan in these mice (Sharma et al., 2012b).

Knockdown of SNAP-25 in CSP α -/- mice exacerbates their phenotype and decreases lifespan, whereas increasing the levels of SNAP-25 can actually rescue their phenotype. This neuroprotective effect was associated with increased SNARE-complex formation, synapse and neuronal number (Sharma et al., 2012a).

In addition, the Tg overexpression of α -synuclein in CSP α -/- mice has been shown to reverse the neurodegenerative phenotype caused by loss of CSP α , whereas deletion of endogenous α -synuclein exacerbates the CSP α -/- phenotype (Chandra et al., 2005). The Tg overexpression of α -synuclein increased lifespan, reversed weight loss, motor impairment and associated neuropathology seen in CSP -/- mice (Chandra et al., 2005). There was an increase in SNARE-complex formation, however, SNAP-25 levels in CSP α -/- mice were not reversed by α -synuclein expression (Chandra et al., 2005). This suggests that the effects of α -synuclein are downstream of SNAP-25. In conjunction, neurons which lack α -synuclein are not rescued which imply that α -synuclein acts cell autonomously (Chandra et al., 2005).

Although SNAP-25 levels are reduced in CSP α $-/-$ animals (Chandra et al., 2005, Sharma et al., 2011), this alone is not sufficient to cause neurodegeneration since SNAP-25 $+/-$ mice which also have a similar reduction in SNAP-25, are phenotypically normal and indistinguishable from SNAP-25 $+/+$ mice (Washbourne et al., 2002). This suggests other proteins are involved. Zhang et al., performed a screen for CSP α client proteins and showed that both SNAP-25 and dynamin 1 bind to CSP α and are CSP α clients (Zhang et al., 2012). Similar to SNAP-25, levels of dynamin-1 were reduced in CSP α $-/-$ animals. CSP α was shown to regulate the polymerisation of the GTPase dynamin 1 suggesting that CSP α is vital for both exocytosis and endocytosis. In addition, an endocytosis defect has been shown since there is a failure to recycle vesicles during prolonged stimulation in CSP α $-/-$ mice (Rozas et al., 2012). Electron microscopy has shown features that resembled impaired vesicle recycling in motor nerve terminal of CSP α $-/-$ mice (Rozas et al., 2012).

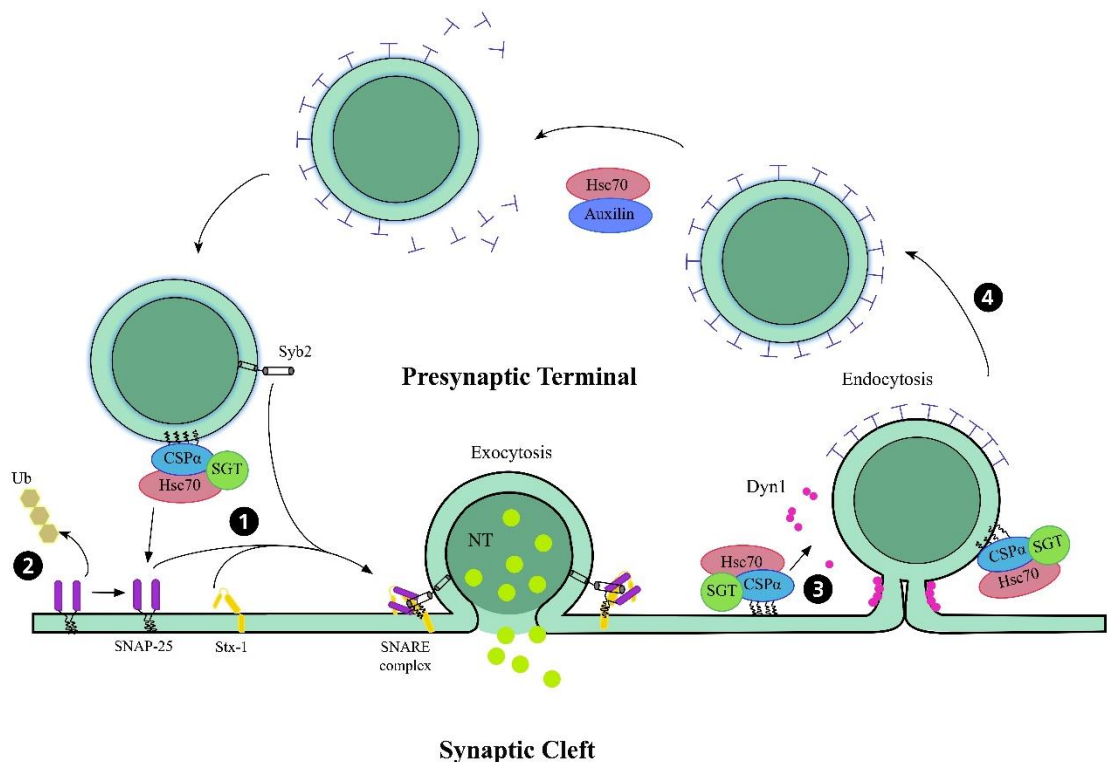


Figure 1.13 A role for CSP α -Hsc70-SGT in vesicle exo- and endocytosis.

The CSP α -Hsc70-SGT complex chaperones the SNARE protein SNAP-25 enabling SNARE-complex formation and vesicle exocytosis (1). In the absence of CSP α , SNAP-25 is ubiquitinated and degraded by the proteasome (2) and SNARE-complex assembly is reduced. CSP α -Hsc70-SGT also promotes dynamin 1 polymerisation,

enabling vesicle endocytosis (3). Endocytosed vesicles are recycled for further rounds of exocytosis (4). Figure adapted from Zhang et al., 2012. Auxilin and Hsc70 regulate clathrin uncoating. Dyn1, dynamin 1; NT, neurotransmitter; Stn, syntaxin; Syb2, synaptobrevin and Ub, ubiquitin.

1.6.3.3 Synapse loss in CSP α $-/-$ animals

In CSP α $-/-$ mice there is use-dependent degeneration of synapses, with highly active synapses such as the neuromuscular junction, photoreceptor ribbon synapses and Calyx of Held being the most affected (Fernández-Chacón et al., 2004, García-Junco-Clemente et al., 2010, Schmitz et al., 2006) (Figure 1.14). The photoreceptor ribbon synapses are one of the first to be lost in CSP α $-/-$ animals and this occurs from P14 (Schmitz et al., 2006). Ultrastructural changes and synaptic transmission defects can be seen in the NMJ from P14, which coincides with behavioural abnormalities (Fernández-Chacón et al., 2004). From P20 there are synaptic transmission impairments in the Calyx of Held and synaptic degeneration from P25 (Fernández-Chacón et al., 2004). In the hippocampus of CSP α $-/-$ mice there is a selective degeneration of highly active parvalbumin positive (PV+) synaptotagmin 2 expressing GABAergic interneurons, which typically have high action potential frequencies (up to 200 Hz) (Csicsvari et al., 1999, Ylinen et al., 1995). The synaptic terminals of less active neurons such as the glutamatergic pyramidal neurons, which typically have an action potential frequency of 1 Hz (Csicsvari et al., 1999, Frerking et al., 2005) do not undergo degeneration *in vivo* (García-Junco-Clemente et al., 2010). Synaptophysin staining in hippocampal neuronal cultures has demonstrated a 28% loss of synapses from 21 days *in vitro* (Zhang et al., 2012). Fewer synaptic vesicles are also seen in synapses of CSP α $-/-$ animals *in vivo* (Zhang et al., 2012).

This suggests that neurons with higher synaptic activity and hence more dependent on CSP α for SNARE-complex formation and synaptic vesicle recycling, have an increased vulnerability to synaptic degeneration. This subtype selectivity in the CSP α $-/-$ model is paralleled by studies in ALS which show selective vulnerability of a group of fast-fatigable NMJ synapses (Frey et al., 2000).

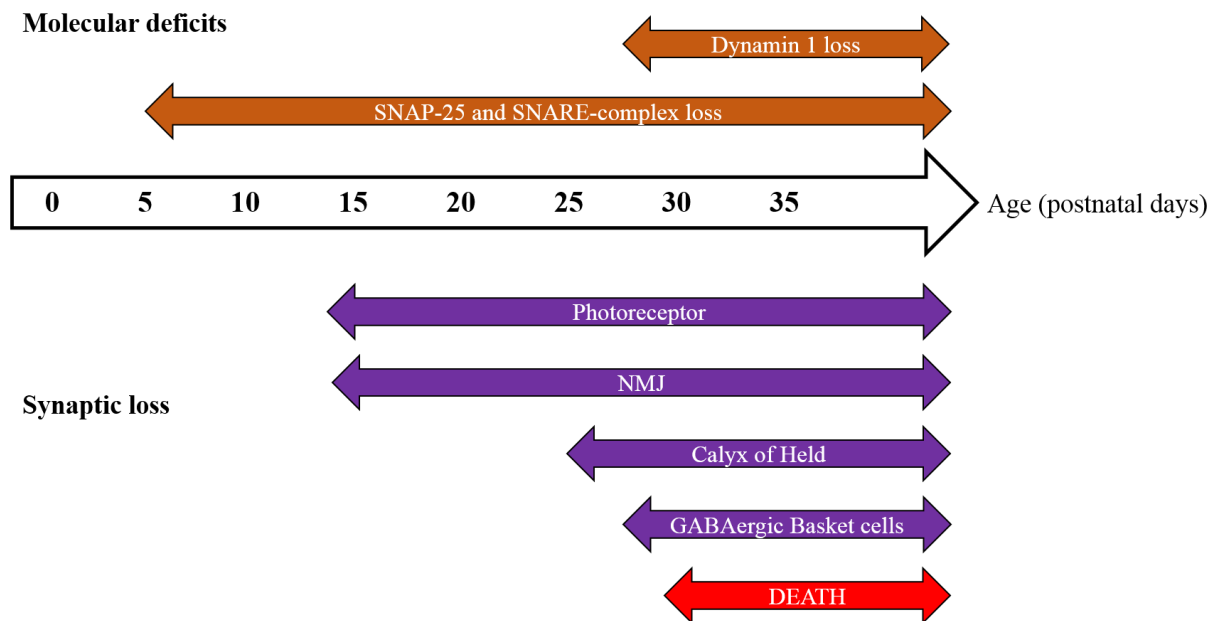


Figure 1.14 Timeline for the appearance of molecular deficits and synapse loss in the CSPα -/- mice.

SNAP-25 and SNARE-complexes are reduced from P5 in CSPα -/- animals. Following this at P28, levels of dynamin 1 are reduced. Different neurons have different susceptibilities to CSPα loss. The photoreceptor ribbon synapses and NMJ synapses are the first to be lost from P14. This is followed by synapse loss at the Calyx of Held (P25) and parvalbumin synaptotagmin 2 expressing GABAergic basket cells (P28). CSPα -/- animals begin to die from ~P30. NMJ, neuromuscular junction and P, postnatal days.

1.7 Cell stress responses

When the normal homeostasis of a cell is perturbed, molecular response pathways are activated to try to combat this stress and to re-establish cell homeostasis. The following section describes the cellular stress responses associated with protein misfolding. Other stress-related response molecules, which are independent of this response but nonetheless are indicative of cellular dysfunction, are also discussed.

1.7.1 The unfolded protein response (UPR) – a cellular stress response to misfolded/ unfolded proteins

The ER is responsible for the synthesis, folding, modification and transport of secretory proteins as well as acting as a calcium store (Paschen and Frandsen, 2001). Within the

ER there are numerous chaperones which catalyse the correct folding of proteins that are required for normal cell function (Torres et al., 2014). When misfolded proteins accumulate and/or calcium homeostasis in the ER is disturbed, ER stress ensues (Lindholm et al., 2006).

‘ER stress’ is defined as an imbalance between the demands of the cell for the functioning of the ER and the ability of the ER to cope with the increasing disturbance in homeostasis (Nunziante et al., 2011, Ron and Walter, 2007). ER stress is activated to try to restore the functioning of the ER and to remove any misfolded and potentially harmful proteins, thereby facilitating protein homeostasis.

The UPR is an adaptive, highly conserved response triggered in the ER (also involving the Golgi apparatus and nucleus) under stressful conditions (Kaufman, 1999, Ron and Walter, 2007, Zhao and Ackerman, 2006). It aims to restore the homeostasis by suppressing general protein translation and by increasing the transcription of chaperones and other proteins involved in the refolding of misfolded proteins (Paschen and Mengesdorf, 2005, Ron and Walter, 2007). In addition, it also activates a process known as ER-associated protein degradation (ERAD) which is responsible for retrotranslocating misfolded proteins from the ER to the cytosol where they are polyubiquitinated and degraded by the proteasome (Meusser et al., 2005, Saxena and Caroni, 2011).

1.7.1.1 ER stress sensors

There are three transmembrane sensors of ER stress; inositol-requiring enzyme 1 (IRE1), double-stranded RNA-activated protein kinase-like ER kinase (PERK) and activating transcription factor 6 (ATF6) (Matus et al., 2011, Paschen and Mengesdorf, 2005) (Figure 1.15). Normally these sensors are kept inactive by the ER chaperone binding immunoglobulin protein (BiP) (Kanekura et al., 2009, Paschen and Mengesdorf, 2005, Zhao and Ackerman, 2006). When the UPR is activated BiP dissociates from these sensors to refold damaged proteins (Kanekura et al., 2009, Paschen and Mengesdorf, 2005). Loss of bound BiP leads to oligomerisation, autophosphorylation and activation of the two kinases IRE1 and PERK (Kanekura et al., 2009, Paschen and Mengesdorf, 2005). However, binding of the unfolded/misfolded proteins directly to the stress sensors has been suggested as a possible route that may lead to their activation (Ron and Walter, 2007).

IRE1 has a luminal domain for stress sensing and a cytosolic kinase and endonuclease domain (Rutkowski and Kaufman, 2007, Saxena and Caroni, 2011). Its endonuclease activity leads to the splicing of a 26 base intron from the mRNA of the transcription factor XBP-1, which promotes the transcription of genes involved in the UPR and ERAD (Ron and Walter, 2007, Zhao and Ackerman, 2006). Spliced XBP-1 results in a frame-shift of the coding sequence, resulting in the formation of a 54 kDa protein as opposed to a protein of 34 kDa (Paschen and Mengesdorf, 2005). When PERK is activated it phosphorylates the eukaryotic translation initiation factor 2 α (eIF2 α) at Ser51, leading to the inhibition of the initiation step of global translation (Kanekura et al., 2009, Paschen and Mengesdorf, 2005, Saxena and Caroni, 2011). However, some mRNA species which contain an upstream non-coding open reading frame in their 5' untranslated region (UTR) (Kaufman, 1999, Schröder and Kaufman, 2005) are still translated (Saxena and Caroni, 2011). Activating transcription factor 4 (ATF4) is one of these mRNA species and it acts as a transcription factor, stimulating UPR/ERAD gene expression (Lu et al., 2004). The growth arrest and DNA-damage inducible protein 34 (GADD34) is a phosphatase which dephosphorylates eIF2 α -P and is induced in response to ER stress (Novoa et al., 2001). This protein promotes recovery of translation after inhibition by eIF2 α -P. Under conditions of ER stress, ATF6 translocates from the ER (where it normally resides) to the Golgi where it is cleaved by the two proteases; site 1 protease (S1P) and site 2 protease (S2P) (Ye et al., 2000) into a cytosolic fragment which can migrate to the nucleus and enhance transcription of UPR and ERAD genes (Rutkowski and Kaufman, 2007, Saxena and Caroni, 2011, Zhao and Ackerman, 2006).

Molecules involved in the UPR which are upregulated by ER stress sensors include chaperone proteins such as BiP, calreticulin, calnexin and protein disulfide isomerase (PDI) (Saxena and Caroni, 2011). Two other mechanisms selective in the ER have been proposed to help deal with stress. The first is the degradation of ER-associated mRNAs by IRE1 (Hollien and Weissman, 2006) and the second is the inhibition of ER translocation, a process referred to as pre-emptive quality control (Kang et al., 2006).

If the UPR is unsuccessful in restoring ER homeostasis, prolonged and severe ER stress may lead to apoptosis (Tabas and Ron, 2011). In this scenario, multiple pathways can lead to cell death. The ER localised caspase, caspase 12 in rodents and its homolog caspase 4 in humans, have both been implicated (Hitomi et al., 2004, Nakagawa et al., 2000). In addition, IRE1 activates the c-Jun N-terminal kinase (JNK) pathway which

can lead to caspase activation and the inhibition of anti-apoptotic proteins (Doyle et al., 2011, Urano et al., 2000). The C/EBP homologous protein (CHOP) pathway is another such pro-apoptotic pathway activated by ATF4, ATF6 and XBP1 (Oyadomari and Mori, 2003) under conditions of prolonged ER stress. Activation of CHOP induces cell death by promoting protein synthesis and oxidation (Marciniak et al., 2004, Oyadomari and Mori, 2003).

1.7.1.1.1 The integrated stress response

The phosphorylation of eIF2 α is a process that inhibits translation and aims to preserve energy as the cell activates molecular programmes to deal with the cellular stress (Ron and Walter, 2007, Wek et al., 2006). Phosphorylation of eIF2 α is driven by PERK activation under conditions of ER stress; however, three other eIF2 α kinases also exist in mammals which are activated by distinct stress conditions (Wek et al., 2006). These kinases all lead to the phosphorylation of eIF2 α and are collectively referred to as the integrated stress response (ISR) (Sidrauski et al., 2013). The other three kinases are RNA-dependent protein kinase (PKR), general control non-derepressible 2 (GCN2) and haem regulated inhibitor (HRI). PERK (discussed above) is activated by the accumulation of misfolded/unfolded protein in the ER, PKR is activated in response to viral infection, GCN2 is activated in response to amino acid starvation and UV light and HRI is activated in response to haem deficiency (Sidrauski et al., 2013).

1.7.1.1.2 eIF2 α

eIF2 is composed of three subunits: α , β and γ . eIF2 forms the ternary complex by binding to guanosine triphosphate (GTP) and the initiator Met-tRNA (Sidrauski et al., 2013). The 43S pre-initiation complex is then formed by the ternary complex associating with the 40S ribosomal subunit (Sidrauski et al., 2013). The pre-initiation complex scans the mRNA to find the initiating AUG codon for translation to commence. Once complete GTP which is bound to eIF2, is hydrolysed to guanosine diphosphate (GDP) and eIF2 is released from the ribosome (Jiang et al., 2004). GDP-eIF2 is recycled back to GTP-eIF2 by the guanine nucleotide exchange factor, eukaryotic translation initiation factor 2 B (eIF2B) (Jiang et al., 2004).

Under conditions of stress the eIF2 α kinases phosphorylate the α subunit of eIF2 which inhibits eIF2B (Hinnebusch and Lorsch, 2012, Ron and Walter, 2007). This prevents

recycling of eIF2 from a GDP bound state to a GTP bound state (Wek et al., 2006), therefore preventing the formation of ternary complex and drastically reducing the levels of global translation (Ron and Walter, 2007). eIF2 occurs in excess of eIF2B, thus inhibition of translation can occur when only a fraction of eIF2 α is phosphorylated (Hinnebusch and Lorsch, 2012).

1.7.1.1.3 4EBP

Translation can also be controlled by eukaryotic translation initiator factor 4E (eIF4E) binding proteins (4EBP) and this like eIF2 α is controlled by phosphorylation (Sonenberg and Hinnebusch, 2009). The eukaryotic translation initiation factor 4F (eIF4F) is a complex of proteins involved in the recognition of the 5' cap of mRNA, a process required for the cap-dependent translation. Hypophosphorylation of 4EBP leads to cap-dependent translation inhibition by binding to the eIF4E protein and preventing the formation of the eIF4F complex, whereas phosphorylation increases translation by removing this inhibition (Sonenberg and Hinnebusch, 2009). The mammalian target of rapamycin (mTOR) is a kinase which phosphorylates 4EBP (Sonenberg and Hinnebusch, 2009). Inhibiting mTOR signalling by the drug rapamycin has been suggested to be a potential therapeutic approach for treating chronic neurodegenerative diseases (Bove et al., 2011).

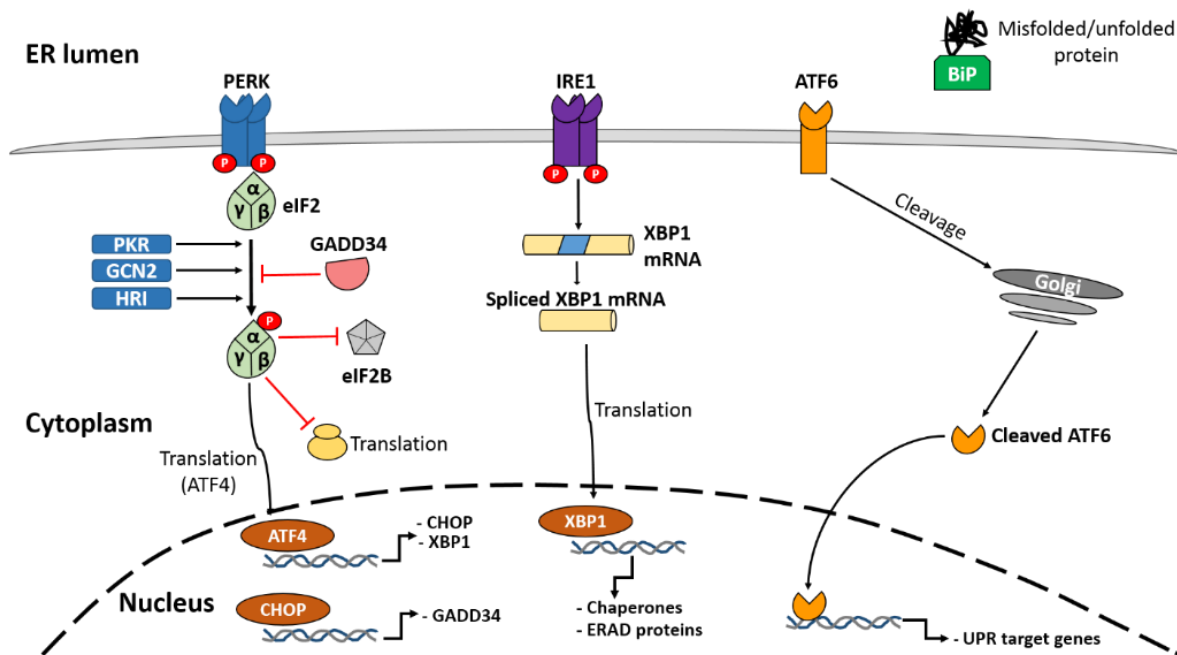


Figure 1.15 UPR signalling.

In normal non-stressful states the ER chaperone BiP is bound to the three ER sensors (ATF6, PERK and IRE1), resulting in their inactivity. When ER stress occurs due to the build-up of unfolded/misfolded protein, BiP dissociates from the sensors to try to refold any misfolded proteins. Dissociation of BiP and/or activation by the presence of unfolded/misfolded protein leads to the dimerization, autophosphorylation and activation of PERK and IRE1. Activated PERK leads to the phosphorylation of eIF2 α . The three other eIF2 α kinases, PKR, GCN2 and HRI can also phosphorylate eIF2 α . Phosphorylation of eIF2 α inhibits eIF2B. As a result global protein synthesis is greatly reduced. Some mRNA species, including ATF4, are still translated. ATF4 translocates to the nucleus where it stimulates expression of ER stress response genes (CHOP and XBP1). CHOP is translated and drives the expression of GADD34, an eIF2 α phosphatase which drives dephosphorylation of eIF2 α -P. Activated IRE1 leads to the splicing of a 26 base intron from the coding region of XBP1 resulting in the formation of a 54 kDa protein that translocates to the nucleus and stimulates expression of genes involved in the UPR (ER chaperones and ERAD proteins). Under conditions of ER stress ATF6 translocates to the Golgi, where it is cleaved by two site specific proteases, S1P and S2P, into an active cytosolic fragment, which can then translocate to the nucleus and induce the expression of UPR target genes.

1.7.2 The UPR in acute injury

ER stress has been shown to occur in acute brain conditions such as ischemia (Lindholm et al., 2006, Paschen and Frandsen, 2001). Accumulation of protein aggregates within the ER after ischemia suggests an impairment of ER function (Hu et al., 2000). In cerebral ischemia the UPR sensor PERK is activated and eIF2 α -P is increased (Kumar et al., 2001), as is IRE1, resulting in the processing of XBP-1 mRNA (Paschen et al., 2003). In conjunction, CHOP and ATF4 (Hayashi et al., 2005) and BiP, spliced XBP-1 and CHOP (Tajiri et al., 2004) are upregulated after ischemia. In ischemia, upon CHOP activation, apoptotic pathways are induced, however in CHOP $-/-$ mice, apoptosis is reduced demonstrating an important role for ER stress in mediating apoptosis in ischemia (Tajiri et al., 2004). In addition, activation of caspase-12 has been shown to occur in a rat model of traumatic brain injury (TBI) (Larner et al., 2004), consistent with ER stress mediated cell death (Hitomi et al., 2004, Nakagawa et al., 2000).

ER stress is also activated in acute lesions *in vivo*. Axotomized retinal ganglion cells (RGCs) show signs of ER stress (Hu et al., 2012). Levels of CHOP were upregulated and there was a modest increase in BiP and spliced XBP1 in these cells (Hu et al., 2012). There was an increase in RGCs survival in CHOP $-/-$ mice subjected to optic nerve crush in comparison to $+/+$ mice, implicating ER stress induced apoptosis as a key mechanism of cell death in acute injury (Hu et al., 2012).

1.7.3 The UPR in chronic neurodegenerative disease

1.7.3.1 The UPR in AD

There is some evidence to suggest that the UPR is activated in chronic neurodegenerative diseases. Levels of BiP have been shown to be upregulated specifically in the neurons of the temporal cortex and hippocampus of AD patients (Hoozemans et al., 2005). In addition, eIF2 α -P, PERK-P and IRE1-P have been shown to be increased in the brains of AD patients (Chang et al., 2002, Hoozemans et al., 2009, Ma et al., 2013, O'Connor et al., 2008). ATF4 mRNA and protein was found to be expressed in the axons in the brains of AD patients and these ATF4 positive processes were found close to amyloid plaques (Baleriola et al., 2014). PERK-P and IRE1-P has also been shown to be upregulated in tissue from patients with frontotemporal

dementias with tau-P pathology (Nijholt et al., 2012). However, other studies have suggested that there is no change/a decrease in levels of BiP between AD patients and age-matched controls (Katayama et al., 1999, Sato et al., 2000).

In a Tg mouse model of AD (Tg6799 (5XFAD)), PERK-P and eIF2 α -P was increased (Devi and Ohno, 2014). Genetic reduction of PERK reduced phosphorylation of PERK and eIF2 α and this led to a reduction in A β deposits, a rescue in memory deficits and to the prevention of neurodegeneration (Devi and Ohno, 2014). In another Tg mouse model (APP^{swe}/PS1 Δ E9), genetic deletion of PERK was also shown to decrease eIF2 α -P (Ma et al., 2013). This deletion led to a reduction in amyloidogenesis and mitigated the associated deficits in protein synthesis, synaptic plasticity and spatial memory (Ma et al., 2013). Deletion of GCN2 also decreased deficits in synaptic plasticity and spatial memory, but had no effect on the basal phosphorylation of eIF2 α (Ma et al., 2013). PKR^{-/-} mice or mice in which PKR activity had been blocked also enhanced learning and memory (Zhu et al., 2011).

In a Tg mouse model of tauopathy (rTg4510), there was increased PERK-P (Abisambra et al., 2013). In this model soluble tau also impaired the ERAD process. Depleting the levels of tau led to a reduction in PERK-P (Abisambra et al., 2013), suggesting that tau activates the UPR and drives the phosphorylation of PERK. More recently, a selective activation of the PERK-eIF2 α arm of the UPR has been shown to be activated in the hippocampi of rTg4510 mice, expressing high levels of mutant tau (Radford et al., 2015). This was associated with the sustained repression of general translation in these mice, at the same time as synaptic protein levels were reduced and neuronal loss in the hippocampus was detected (Radford et al., 2015). In this model the activation of PERK was linked to tau mediated phosphorylation, driven by glycogen synthase kinase-3 (GSK-3 β), which phosphorylates tau (Radford et al., 2015). Reducing the levels of tau led to reduced levels of eIF2 α -P and ATF4, thus implicating mutant tau as an activator of the UPR (Radford et al., 2015).

1.7.3.1.1 Sub-compartmental UPR in AD

Injection of A β ₁₋₄₂ oligomers into the hippocampal DG of wildtype mice causes a loss of forebrain neurons which project to the DG. These oligomers were shown to cause local axonal synthesis of ATF4 protein via eIF2 α -P and retrograde spreading of pathology to the cell body resulting in forebrain neuronal cell death via CHOP induction. Inhibiting

the translation of ATF4 via small interfering RNA (siRNA) knockdown of ATF4 prevented the decrease in basal forebrain cholinergic neurons. In addition, oligomeric A β ₁₋₄₂ has been shown to induce ER stress (increased eIF2 α -P) (Yoon et al., 2012), and ER stress can activate JNK3 (a brain-specific JNK isoform), which facilitates the processing of APP, by the two enzymes β - and γ -secretase (Götz and Ittner, 2008, Yoon et al., 2012). JNK3 activity is increased in both human AD patients and in a Tg AD mouse model (Tg6799 (5XFAD)) (Yoon et al., 2012). Deletion of JNK3 in Tg AD mice, led to a reduction in A β ₁₋₄₂ levels and plaque load. Its deletion also increased the number of neurons and improved cognition, thus highlighting ER stress and specifically JNK3 as a key player in AD pathology and a promising therapeutic target for AD.

1.7.3.2 The UPR in PD

Increased PERK-P and eIF2 α -P have been shown to be present in post-mortem brains of patients with PD (Hoozemans et al., 2007). ER stress and cell death have been shown to be activated in a Tg mouse model of PD (G2-3). In this model there is an upregulation of UPR molecules, including BiP and splicing of XBP1, however, levels of eIF2 α -P remained unchanged (Colla et al., 2012a). Induction of UPR molecules coincided with increased levels of aggregated α -synuclein associated with the ER/microsomes (Colla et al., 2012a, Colla et al., 2012b). In addition, mutant human α -synuclein has been shown to bind BiP *in vivo* in Tg mice (SYN120) with truncated human α -synuclein (Bellucci et al., 2011). This model was associated with increased BiP and ATF4 compared to wildtype mice (Bellucci et al., 2011). In conjunction, the ER stress resulted in increased cleavage of caspase 12 and the accumulation of polyubiquitin (Colla et al., 2012a).

Interestingly, the PD associated gene PARK2 seems to confer protection against ER stress and UPR mediated cell death due to its ubiquitin-protein ligase activity - which supports the degradation of misfolded proteins relieving the burden on the ER (Imai et al., 2000).

1.7.3.3 The UPR in ALS

Evidence for UPR activation has been reported in sporadic human ALS with a number of UPR molecules including ATF6, PERK and IRE1 induced (Atkin et al., 2008). In a Tg mouse model of ALS (SOD1 (G93A)), ER stress was shown to occur early and prior to synapse and axonal loss (Saxena et al., 2009). This longitudinal *in vivo* analysis

identified motoneurons which are either selectively vulnerable (fast fatigable) or resistant (fast fatigue-resistant and slow) to ALS (Saxena et al., 2009). In this mouse model ubiquitin signals in both vulnerable and resistant motoneurons were shown to increase (Saxena et al., 2009). However, an upregulation of ATF4, eIF2 α -P and BiP and downregulation of ubiquitin-proteasome-related genes occurred selectively in vulnerable motoneurons, which coincides with activation of microglia, ~20 days before the earliest signs of denervation (Saxena et al., 2009). Resistant motoneurons underwent a similar pattern of events but with a delay. Enhancement of ER stress by peripheral nerve crush exacerbated disease (Saxena et al., 2009).

Tg ALS mice (SOD1, G85R) mice with haploinsufficient PERK, have an accelerated disease onset, with increased SOD1 aggregation, earlier activation of the UPR (increased CHOP and BiP) and apoptotic pathways and reduced lifespan (Wang et al., 2011). However, mutant SOD1 mice with deletion of central nervous system XBP1 were more resistant to ALS and showed reduced levels of aggregated SOD1, due to its increased clearance by macroautophagy (Hetz et al., 2009). Therefore, different UPR pathways seem to provide alternative disease outcomes. Determining the outcome for each pathway is essential if therapeutics are to be designed to either inhibit or activate the UPR.

SIL1 is an adenine nucleotide exchange factor for BiP (Zhao et al., 2005). It binds to BiP when BiP is bound to ADP and catalyses the release of BiP from substrate binding (Chung et al., 2002). SIL1 is highly expressed in those motoneurons which are resistant to ER stress and ALS pathology (Filezac de L'Etang et al., 2015) and in contrast SIL1 is not robustly expressed in motoneurons which are prone to ER stress and motoneuron degeneration (Filezac de L'Etang et al., 2015). SIL1 is protective against ER stress as reduction in SIL1 causes enhanced ER stress and accelerates ALS pathology in Tg ALS mice (human SOD1, G93A). Conversely, enhancement of SIL1 levels was neuroprotective, delaying axon loss and increasing survival in these ALS mice (Filezac de L'Etang et al., 2015). SIL1 levels were reduced in another Tg mouse model of ALS (TDP-43, A315T) (Filezac de L'Etang et al., 2015). In the spinal cord from human ALS patients, a number of motoneurons show increased SIL1 expression, similar to what is seen in the disease-resistant motoneurons of Tg ALS SOD1 mice (Filezac de L'Etang et al., 2015).

Details of how the UPR may be implicated in prion disease is discussed in chapter 3.

1.7.4 Other stress-related response molecules associated with homeostatic changes in neuronal function and dysfunction

1.7.4.1 Immediate early genes

Early work using seizure-inducing models was used to identify transcriptional changes in neurons subjected to acute stress (Cole et al., 1990, Vendrell et al., 1993). The identified genes have emerged as responses which have been shown to be engaged during the evolution of neurodegenerative diseases. The earliest changes in gene expression in response to seizure-inducing stimuli involves the immediate early gene transcription factors (Hughes et al., 1999). Including activating transcription factor 3 (ATF3), c-Jun and c-Fos, these transcription factors are normally expressed at low levels, but are rapidly induced in response to diverse stimuli, including synaptic, neurotransmitter and growth factor stimulation (Hughes et al., 1999, Tzingounis and Nicoll, 2006).

c-Jun, c-Fos and ATF3 are members of the Jun, Fos and ATF/cAMP responsive element binding (CREB) family of transcription factors, respectively. These transcription factors form what is known as the activator protein 1 (AP-1), a dimeric protein composed of Jun, Fos and ATF family members which regulates gene transcription (Meng and Xia, 2011, Vesely et al., 2009). c-Jun, c-Fos and ATF3 along with other Jun, Fos, ATF/CREB family members and other proteins are part of a large superfamily of transcription factors known as basic leucine zipper proteins (bZIP) (Hunt et al., 2012, Meng and Xia, 2011, Miller, 2009). The UPR associated proteins and transcription factors, ATF4, CHOP, ATF6 and XBP-1 are also bZIP proteins (Chinenov and Kerppola, 2001, Miller, 2009, Wek et al., 2006). bZIP proteins are characterised by a basic region and a leucine zipper region. The basic region (positively charged) of these proteins enables binding to negatively charged (phosphate groups) DNA sequences in the promoter and enhancer region of target genes which regulates gene transcription, whilst the leucine zipper region (a sequence of heptad repeats of leucine amino acids) enables homo- and heterodimerisation with other bZIP family proteins (Hunt et al., 2012). Dimerisation occurs because the leucine zipper region of two bZIP proteins forms parallel coiled-coil α helices which wrap around each other (Miller, 2009).

Different bZip protein families (i.e. Jun, Fos and ATF/CREB) have different DNA binding affinities and sequence specificities (Meng and Xia, 2011, Miller, 2009). For example, c-Jun and c-Fos transcription factors bind AP-1 sites with the DNA sequence TGA(C/G)TCA (Chinenov and Kerppola, 2001), whilst ATF3 binds to the ATF/CRE DNA sequence (TGACGTCA). However, cross-family heterodimerisation results in an increased number of DNA sequences recognised by bZIP proteins (Miller, 2009). For example, when ATF3 forms a heterodimer with c-Jun it can bind to AP-1 sites (Miller, 2009). Because of the different combination of dimers formed from bZIP proteins and hence DNA sequences recognised, a large number of different genes can be activated or repressed by this superfamily of transcription factors (Meng and Xia, 2011).

1.7.4.1.1 ATF3

As discussed above, ATF3 is a member of the ATF/CREB protein family of transcription factors (Hai and Hartman, 2001). ATF3 represses transcription of target genes by acting as a homodimer (Ahlgren et al., 2014, Zhang et al., 2011), but can activate transcription when it heterodimerizes with other transcription factors such as c-Jun (section 1.7.4.1.2) (Hai and Curran, 1991, Hunt et al., 2012). Activation of transcription by heterodimerization has been shown to lead to cell death, whereas transcriptional repression has been shown to be neuroprotective (Song et al., 2008, Zhang et al., 2011). Because of this, both pro-survival and pro-death functions have been assigned to ATF3 (see review (Hunt et al., 2012)).

ATF3 is expressed at low levels in unstressed cells, including neurons, but is highly upregulated following diverse stressful stimuli or injury (Hai and Hartman, 2001, Hai et al., 1999, Hunt et al., 2012, Moore and Goldberg, 2011). ATF3 can be induced by mitogen-activated protein kinases (MAPK) including JNK and P38 (Hunt et al., 2012). JNK activates c-Jun and P38 activates activating transcription factor 2 (ATF2) and the induction of both of these molecules can in turn drive ATF3 expression (Hunt et al., 2012). Axonal injury has been shown to lead to the activation and retrograde transport of JNK to the cell body where it induces a cell body response, which is a molecular programme including the induction of ATF3 (Lindwall and Kanje, 2005). ATF3 is also induced by ER stress via the eIF2 α -P-ATF4 arm of the UPR (Hunt et al., 2012, Jiang et al., 2004). Signalling via the N-methyl D-aspartic acid (NMDA) receptor can also lead to the induction of ATF3 via calcium and CREB signalling (Hunt et al., 2012, Zhang et

al., 2009). Activation of ATF3 by synaptic signalling through NMDA-Ca²⁺-CREB has been shown to have neuroprotective role and in this context ATF3 has been described as an ‘activity-regulated inhibitor of death’ gene (Ahlgren et al., 2014, Zhang et al., 2009). Once induced ATF3 can repress its own expression, thus tightly regulating the levels of ATF3 (Wolfgang et al., 2000).

Because ATF3 is induced in response to a wide variety of stimuli it has been suggested to be a general marker of cell stress and dysfunction (Francis et al., 2004, Hai and Hartman, 2001). ATF3 has been shown to be induced following peripheral (Tsujino et al., 2000) and central axotomy (Song et al., 2008).

ATF3 has also been implicated in the context of neurodegenerative disease. Dendritic swellings (or beadings), are early hallmarks of neuronal injury and these have been observed on the CA3 pyramidal neurons of ME7-animals (section 1.4). In a model of excitotoxicity, dendritic beading and neuronal cell death was seen (Ahlgren et al., 2014). ATF3 was shown to protect against dendritic beading and increase neuronal network activity, whereas, knockdown of ATF3 exacerbated dendritic beading (Ahlgren et al., 2014). Similarly, overexpression of ATF3 has also been shown to be neuroprotective and protect against cell death in an *in vivo* kainic acid mouse model of excitotoxicity (Francis et al., 2004) and to reduce brain damage following a mouse stroke model *in vivo* (Zhang et al., 2011).

In a Tg mouse model of ALS (SOD1, G93A), ATF3 is highly induced in the cell bodies of vulnerable motoneurons prior to synapse and axonal loss (Saxena et al., 2009). The induction of ATF3 was not seen in resistant motoneurons until later during the disease time course. Induction of ATF3 was seen at the same time as UPR molecules were upregulated, however, ATF3 displayed one of the greatest levels of induction. ATF3 has been shown to be induced in ALS models by other research groups and this has led to the suggestion that ATF3 induction might be an early disease-specific marker, which ultimately marks neurons which are to succumb to synapse, axonal and cell body degeneration (Malaspina et al., 2010, Saxena et al., 2009, Vlug et al., 2005). These studies suggest ATF3 is a key stress-related molecule which is induced in response to cell stress and injury and a molecule whose manipulation might be useful for delaying disease progression.

1.7.4.1.2 c-Jun

c-Jun can form homo- and heterodimers with other transcription factors and expression can be induced by numerous stimuli and pathways (Herdegen and Leah, 1998). c-Jun is highly induced by neuronal injury (Herdegen and Leah, 1998) and widely known as a molecule induced during the cell body response reaction following axotomy (Herdegen and Leah, 1998, Herdegen et al., 1997). The induction of c-Jun has been associated with both pro-death and pro-survival and regenerative responses (Herdegen et al., 1997, Park et al., 2011, Raivich and Behrens, 2006, Song et al., 2008).

Post-translational modification of c-Jun via its phosphorylation by JNK proteins, enhances the trans-activation potential of c-Jun (Herdegen and Leah, 1998). In an AD Tg mouse model (TgCRND8) inhibition of JNK signalling has been shown to be neuroprotective reversing synaptic transmission impairments and rescuing memory deficits (Sclip et al., 2011). The phosphorylation of JNK and c-Jun has been shown to be induced in human AD hippocampal tissue (Thakur et al., 2007, Zhu et al., 2001) and found in association with aggregated tau (Pearson et al., 2006). c-Jun-P is increased in motoneurons in a Tg mouse model of ALS (SOD1, G93A) concomitantly with ATF3 and CHOP (Vlug et al., 2005). c-Jun has also been found to be induced in AD human brains in association with DNA damaged neurons (Anderson et al., 1996).

In a Tg ALS mouse model (SOD1, G93A), c-Jun expression was shown to be reduced in motoneurons, due to motoneuron degeneration, but increased in neurons of the brainstem and spinal cord (Jaarsma et al., 1996). Similarly, in human ALS spinal cord tissue, c-Jun expression was induced (Virgo and de Belleruche, 1995). In an infectious prion disease mouse model using the RML strain, c-Jun was shown to be downregulated in CA1 neurons at early stages of disease, however, at end-stage disease c-Jun was upregulated in RML-animals (Majer et al., 2012).

The association of c-Jun with models of neurodegeneration and human tissue from neurodegenerative disease patients has led to the suggestion that c-Jun might be a cellular response to neuronal stress in neurodegenerative disease (Virgo and de Belleruche, 1995).

1.7.4.1.3 c-Fos

c-Fos, like ATF3 and c-Jun is rapidly induced in neurons in response to numerous stimuli, including excitotoxicity, mechanical and ischaemic brain injury (Herrera and Robertson, 1996, Hughes et al., 1999). However, unlike ATF3 and c-Jun, c-Fos can only heterodimerise with members of the Jun family and cannot form homodimers (Jochum et al., 2001).

In vitro exposure of a hippocampal cell line to A β led to the induction of c-Fos, which was associated with reduced cell viability and inhibition of c-Fos expression by anti-sense oligonucleotides increased cell viability (Gillardon et al., 1996). c-Fos and c-Jun immunoreactivity has been detected in neurons and astrocytes of human AD brains (Zhang et al., 1992). A quantitative analysis of c-Fos immunoreactivity in the hippocampus of human AD brains showed that c-Fos expression was increased in the CA3 region (Marcus et al., 1998). In the same study, c-Jun immunoreactivity was also increased in the CA3 and also CA1 (Marcus et al., 1998). Most relevant to this thesis, in an infectious prion disease mouse model using the RML strain, c-Fos was shown to be induced in CA1 neurons of RML-animals at the mid-stages of disease progression, before neuronal loss was seen in the hippocampus (Majer et al., 2012).

1.7.4.2 Activity-induced immediate early genes

Synaptic and neuronal dysfunction/degeneration can cause changes associated with neuronal activity (García-Junco-Clemente et al., 2010, Majer et al., 2012, Terry et al., 1991). Increased neuronal activity can induce the expression of two other immediate early genes, the activity-regulated cytoskeletal gene (Arc or Arg3.1) and Homer1a. These are referred to as effector IEGs and as the name implies are involved in ‘effecting’ or modifying the growth, morphology or function of cells (Guzowski, 2002, Tzingounis and Nicoll, 2006).

1.7.4.2.1 Arc

Arc is a neuronally expressed molecule whose mRNA is rapidly induced in response to increased neuronal activity (Kerrigan and Randall, 2013, Link et al., 1995, Lyford et al., 1995) and Arc mRNA is induced by the activation of NMDA receptors and voltage-gated calcium channels (Tzingounis and Nicoll, 2006). In response to activity,

Arc mRNA is trafficked to activated dendritic post-synaptic compartments where it is translated (Steward et al., 1998, Vazdarjanova et al., 2006). In combination with two other proteins, endophilin 3 and dynamin 2, Arc regulates synaptic plasticity by promoting the endocytosis of the glutamate receptor alpha-amino-3-hydroxyl-5-methyl-4-isoxadole-propionate (AMPA), leading to a reduction in neuronal excitation and synaptic strength (Chowdhury et al., 2006, Kerrigan and Randall, 2013, Shepherd et al., 2006). As a modulator of synaptic plasticity, Arc is important for learning and memory and long-term memory deficits have been shown in Arc *-/-* mice (Plath et al., 2006). In addition, blocking Arc expression by anti-sense oligonucleotides leads to impaired long-term memory consolidation in rats (Guzowski et al., 2000).

Arc is increased in post-mortem brains tissue from AD patients (Wu et al., 2011) and synthetic A β has been shown to lead to the induction of Arc in hippocampal neurons (Lacor et al., 2004). In Tg AD mouse models (Tg6799 (5XFAD), APP/Lo, APP^{*swe*}/PS1 Δ E9) Arc expression is increased in the hippocampus (Grinevich et al., 2009, Perez-Cruz et al., 2011, Wu et al., 2011). In a Tg AD mouse model (APP^{*swe*}/PS1 Δ E9) in which Arc is deleted, levels of A β molecules and plaques were reduced (Wu et al., 2011).

1.7.4.2.2 Homer1a

Homer1a is normally expressed at low levels but is rapidly induced in response to increased neuronal activity. The induction of Homer1a leads to group 1 metabotropic glutamate receptor signalling, independent of agonist binding (Hu et al., 2010). It does this by disrupting the crosslinking action of constitutively expressed forms of other Homer molecules (Homer1b/c) (Brakeman et al., 1997, Tu et al., 1998). Signalling via these metabotropic glutamate receptors leads to a reduction in the expression of cell surface AMPA receptors (Hu et al., 2010). Both Arc and Homer1a thus contribute to synaptic scaling in response to increased neuronal activity.

In an AD Tg mouse model (APP^{*swe*}/PS1M146L), reduced expression of Homer1a and Arc was shown at a time when cognitive dysfunction occurs (Dickey et al., 2003). This was associated with A β plaques since in regions where there were no plaques this decrease in expression was not seen. In an infectious RML prion disease model, the

levels of Arc and Homer1a have been shown to be induced in CA1 neurons at relatively early stages of disease (Majer et al., 2012).

1.7.4.3 Cellular physiological and environmental damage stress sensor

1.7.4.3.1 GADD45 α

The growth arrest and DNA damage-inducible protein 45 α (GADD45 α) is a member of the GADD family of proteins which also includes GADD34 and CHOP (also known as GADD153). GADD45 α is part of the GADD45 subfamily which also includes GADD45 β and γ . These GADD45 proteins are induced by a number of different cellular stressors (both physiological and environmental) including DNA-damaging agents and nutritional deprivation (Fornace et al., 1988, Fornace et al., 1992, Moskalev et al., 2012, Rosemary Siafakas and Richardson, 2009). GADD45 has been suggested to have an array of functions including cell cycle arrest (preventing the replication of damaged DNA), DNA repair and genomic stability regulation and its induction has been associated with both apoptosis and cell survival (Gupta et al., 2005, Lin et al., 2011, Sheikh et al., 2000).

The diverse stimuli which lead to an induction of GADD45, has led to the suggestion that GADD45 is a stress sensor of environmental and physiological stress (Liebermann and Hoffman, 2008). The extent of cellular damage is thought to determine cellular fate i.e. death or survival, and this is thought to be mediated by the interaction of GADD45 with different proteins (Liebermann and Hoffman, 2008).

The protective effects of GADD45 are brought about by its role in DNA excision repair through its interaction with the DNA repair protein, proliferating cell nuclear antigen (PCNA) (Moskalev et al., 2012, Smith et al., 1994, Smith et al., 2000) and by causing cell cycle arrest (G1 and G2/M) via the interaction with the cell cycle proteins, cyclin dependent kinase (cdk1/cdc2) and cyclin B1. GADD45 protein disrupts the association of the cdc2/cyclin B1 complex and inhibits cdc2 kinase activity, ultimately leading to G2/M cell cycle arrest (Liebermann and Hoffman, 2008, Moskalev et al., 2012, Vairapandi et al., 2002, Wang et al., 1999, Zhan et al., 1999). In addition, GADD45 has also been shown to interact with the cyclin dependent kinase inhibitor p21, leading to G1 cell cycle arrest (Liebermann and Hoffman, 2008, Vairapandi et al., 1996). In

contrast, the prodeath effects of GADD45 are brought about by p38 and JNK kinase pathway activation (Liebermann and Hoffman, 2008).

GADD45 has been shown to be induced in the brains of post-mortem AD patients (Torp et al., 1998) and GADD45 has been shown to be increased in a human cell line exposed to A β (Santiard-Baron et al., 1999). c-Jun and c-Fos were also increased in this cell line in response to A β (Santiard-Baron et al., 1999). Similar to ATF3, GADD45 was induced in the cell bodies of vulnerable motoneurons in a Tg mouse model of ALS (SOD1, G93A), prior to synapse and axonal loss (Saxena et al., 2009).

In this thesis, only the expression of GADD45 α was analysed. GADD45 α can be induced by the tumour suppressor protein p53 (Kastan et al., 1992) and like ATF3 has been shown to be induced by ATF4 (Jiang et al., 2007). Unlike the other stress-related molecules discussed above GADD45 α is ubiquitously expressed (Befort et al., 2003). GADD45 α has been shown to be induced by axotomy and has been shown to co-localise with ATF3 and c-Jun (Befort et al., 2003). Optic nerve crush leads to the upregulation of UPR molecules including BiP, CHOP and spliced XBP1 in retinal ganglion cells (Hu et al., 2012). This induction occurred at the same time as when GADD45 α was also induced (Hu et al., 2012).

Figure 1.16 shows common cellular insults which lead to the induction of stress-related response mRNAs.

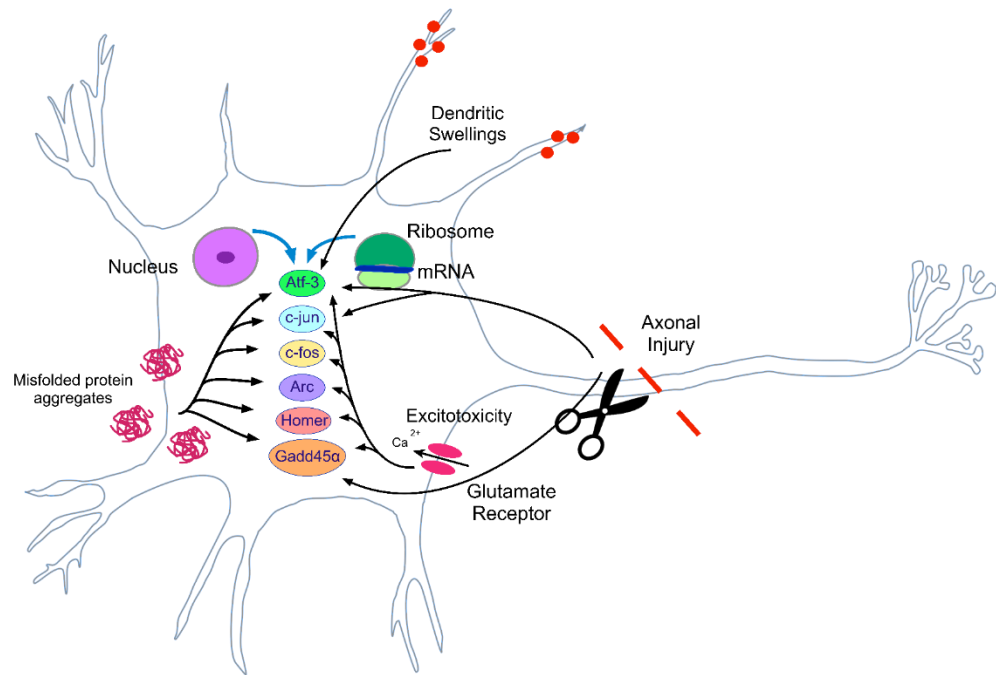


Figure 1.16 Cellular insults leading to the induction of stress-related response molecules in neurons.

The immediate early genes: ATF3; c-Jun and c-Fos, the activity-induced immediate early genes: Arc and Homer1a and the cellular physiological and environmental damage stress sensor GADD45 α can be activated by different cellular insults. These insults include axonal injury caused by axotomy or nerve crush, dendritic injury due to dendritic swellings, excitotoxicity and misfolded protein aggregates. The molecules induced by these insults are shown by solid black arrows.

1.8 General aims

Stress-response pathways are activated by different cellular insults, including protein misfolding. The UPR and other stress-related response molecules, discussed in the general introduction, have been implicated in human and animal models of chronic neurodegenerative diseases. At present there are no therapies which can successfully delay the progression of human chronic neurodegenerative diseases. Identifying pathways and molecules (such as those above) which could be targeted for therapeutic intervention is needed. The main aim of this thesis was to investigate whether the UPR and other stress-related response molecules (including immediate early genes, activity-induced immediate early genes and a cellular physiological and environmental damage stress sensor) are activated in the hippocampus of mice in different models of neurodegeneration. In particular, these pathways and molecules were investigated in:

- The ME7 prion mouse model (chapter 3). This murine prion disease model is a well characterised laboratory model of a protein misfolding disease with chronic neurodegeneration. Using this model, prion disease can be induced in wildtype mice without the need for Tg overexpression of a particular protein. The time course of disease is well established as are cellular and molecular pathology and behavioural changes.
- The CSP α $-/-$ mouse model (chapter 4). This model is associated with synaptic protein misfolding and neurodegeneration. It is induced by the genetic deletion of CSP α which leads to well-established phenotypical changes and death from ~P30.
- In order to show that stress response molecules and pathways are expressed in the injured brain, two models of acute brain injury were investigated (chapter 5). Mice were injected with kainic acid as a model of excitotoxicity mimicking aspects of acute brain injury in stroke and traumatic brain injury. Acute mouse brain slicing was used as a simple, highly reproducible model of acute traumatic brain injury.

In chapter 6, these pathways and molecules were investigated specifically in the vulnerable CA3 pyramidal neurons of ME7-animals by using laser capture microdissection (LCM).

Chapter 2: General materials and methods

The suppliers of all reagents used in this thesis can be found in appendix 3.

2.1 Animal husbandry

C57BL/6J female mice (Charles River Laboratories) were bred in-house and were caged in groups of 10. Mice were housed according to Home Office regulations, at an ambient room temperature of 21 ± 2 °C and on a standard 12 hour:12 hour light-dark cycle. Food (RM-1, Special Diet Services) and water were provided *ad libitum*.

2.2 Stereotaxic surgery

All procedures were carried out under a UK Home Office license and in accordance with the Animals (Scientific Procedures) Act, 1986 (license number = 30/3056). Female C57BL/6J mice, aged between 9-13 weeks (18-26 g) were used for experiments. Anaesthetic was made up of 1 ml ketamine, 0.5 ml xylazine (Rumpon) and 8.5 ml sterile saline (0.9% (w/v) NaCl), mixed and stored at 4 °C away from direct light. Each mouse was anaesthetised with 0.1 ml/10 g of a ketamine/xylazine mix intra-peritoneally (i.p.). Lidocaine was applied to the ears and lacrilube to the eyes of the mice after the animals were anaesthetised and prior to performing surgery. Upon loss of the pedal reflex mice were mounted on a stereotaxic frame (David Kopf Instruments). An incision was made in the scalp and connective tissue removed and the skull exposed. Burr holes were drilled with a no.5 tungsten carbide burr (Dentsply Ltd), on either side of the midline using the stereotaxic coordinates for the dorsal hippocampus relative to bregma; -2.0 mm (anterior-posterior), ± 1.7 mm (bilateral), to expose the surface of the cortex. Injections were made using a 10 μ l Hamilton syringe (Sigma-Aldrich) -1.6 mm deep into the hippocampus. The mice were slowly injected with 1 μ l of NBH or ME7 brain homogenate (section 2.3). After injection the syringe was left in place for 1-2 minutes (min) and then carefully withdrawn. The scalp was sutured (sutures from Ethicon) and the mouse placed in a heated recovery chamber set at 32 °C. Once the mice had regained a righting reflex they were re-housed in separate groups of NBH- and ME7-animals.

2.3 Preparation of brain homogenate for intra-hippocampal injection

NBH and ME7 homogenates used in this thesis were generated by previous laboratory members prior to this work being undertaken.

A brain from a normal C57BL/6J mouse or from a mouse terminally infected with the ME7 scrapie agent was cut up into small pieces and then homogenised in sterile saline (10% w/v) with a Kontes pellet pestle motor (Sigma-Aldrich). The homogenate was passed through successively smaller gauge needles attached to a disposable syringe before dispensing into 40 µl aliquots and storing at -80 °C, until required. Each aliquot was freeze-thawed only once.

2.4 Methods of tissue collection

2.4.1 Perfusion

Mice were terminally anaesthetised with sodium pentobarbital. Once the pedal reflex had disappeared, the mice were pinned ventral side up and the thoracic cavity was opened to expose the heart. A butterfly needle (27-gauge, Venisystems, Eire) was inserted into the left ventricle of the heart and the right atrium was cut. The mice were perfused with heparinised saline (0.9% (w/v) NaCl containing 5000U/L heparin) until the perfusate ran clear. For histology mice were perfusion-fixed with 10% neutral buffered formalin.

2.4.2 Whole brain extraction

The brains of mice were exposed by cutting away the skin on the forehead and then peeling the skull away from the brain. The brain was then carefully removed and used for either hippocampal extraction (section 2.4.4) or post-fixed (section 2.4.3).

2.4.3 Post fixation

The formalin-fixed mouse brains were post-fixed in 10% neutral buffered formalin for 2-3 days (d) at 4 °C. The brains were dehydrated through increasing ethanol concentrations (70% (×2), 80% (×1), 90% (×1) and 100% (×3), each for 2 hr). A

Leica-TP 1020 tissue processor (Leica) was subsequently used to immerse brains in HistoClear for 8 hr and then in paraffin wax at 60 °C for 4 hr. Finally brains were orientated, embedded in fresh wax and allowed to cool before the wax blocks were stored at room temperature in an air tight container.

2.4.4 Hippocampal extraction

The cerebellum was removed from the brain and the cortices were separated from each other at the midline. The midbrain was then removed to reveal the underlying hippocampus. Incisions were made at the ends of the hippocampus, enabling it to be rolled away from the cortex and white matter. The isolated hippocampal tissue was placed into 1.5 ml sterile Eppendorfs and immediately frozen on dry ice. Tissue was stored at -80 °C until required.

2.5 Tissue processing

2.5.1 RNA extraction

Precautions were taken to avoid contamination with RNases when performing RNA extraction procedures. The benches, pipettes and Kontes pellet pestle motor were treated with RNaseZap solution according to the manufacturer's instructions. Plastic pellet pestles were autoclaved at 121 °C and pipette tips were certified free of RNases.

RNA extraction was carried out by homogenising in 1 ml Trizol (≥ 10 volumes per mass of tissue) in a 1.5 ml tube using a pellet pestle motor. 0.2 ml of 1-Bromo-3-chloropropane (BCP) was added and the homogenate was centrifuged at 4 °C for 5 min at $12,000 \times g$. The upper aqueous phase was transferred to a new tube and total RNA was purified using the Qiagen RNeasy minikit (Qiagen) according to the manufacturer's instructions. The RNA was eluted from Qiagen columns after recommended wash steps using 30 μ l RNase free water. RNA was sub-aliquoted into 5 μ l aliquots and stored at -80 °C until required.

2.5.2 Measurements of concentration and quality of RNA

Total RNA (section 2.5.1) was analysed using a NanoDrop spectrophotometer (Thermo Fischer Scientific) to determine the concentration and quality of the RNA. Typical RNA

yields were 200-500 ng/μl. All the RNA used in this thesis exhibited an absorbance maximum at 260 nm and A260:A280 and A260:A230 values of ~2.00.

2.5.3 cDNA synthesis

Total RNA (section 2.5.1) was reverse transcribed into cDNA using the iScript Select cDNA Synthesis Kit, according to the manufacturer's instructions and was incubated in 0.2 ml tubes as follows:

Total	20 μl
5× iScript Select Reaction Mix	4 μl
Oligo (dT) ₂₀ Primer	2 μl
iScript Reverse Transcriptase	1 μl
Nuclease-free water	Variable
RNA sample (200 ng total RNA)	Variable

The reactions were incubated on a thermocycler (GeneAmp PCR System 9700, Applied Biosystems) under the following conditions:

90 min	42 °C
5 min	85 °C
Hold	4 °C

The resulting cDNA product was subject to long-term storage at -20 °C.

2.6 Polymerase Chain Reaction (PCR)

2.6.1 Primer design

Forward and reverse oligonucleotide primer sequences (Table 2.1) were designed to be used for both conventional PCR and for quantitative PCR (section 2.6.3). Primers were designed using the following criteria: 18-24 bases in length, melting temperature between 54 °C-66 °C, amplicon size between 70-450 bases, a GC% between 40-70%, at least one GC clamp, avoiding runs of three or more Cs orGs at the 3' end of primers and no more than 4 di-nucleotide repeats. Primers were designed using the Oligonucleotide Analyser; (www.idtdna.com/analyzer/Applications/OligoAnalyzer/), to ensure there were no hairpin structures or self/hetero-primer dimerization. The primers

were compared against Ensembl BLAST to ensure specificity of the primers for the gene of interest. The primers were selected to span either an exon-exon junction and/or be separated by an intron to ensure amplification of cDNA as opposed to genomic DNA. In circumstances when this was not possible, a control where the reverse transcriptase enzyme was omitted from the cDNA synthesis reaction was performed. Forward and reverse primers were accepted if their melting temperatures were within 4 °C of each other.

In the PCR, an annealing temperature of approximately 3 °C below the lowest melting temperature for the primers in cognate pairs was used. The extension time was calculated, with the rule of one min per kilobase (kb). Amplicon sizes ≤ 350 were given an extension time of 30 seconds (s), whilst amplicon sizes 350-1 kb were given an extension time of 60 s. All of the reactions had a cycle number of 35. Table 2.2 lists the cycling parameters for the primer pairs used. Primers were ordered from Eurofins (Germany).

Gene	Primer sequence 5'-3'		Primer length (bp)	Primer position
Arc	Fwd	5-AGAATGACACCAGGTCTCA-3	19	Fwd primer spans junction of exons 2 and 3 Rev primer targets exon 3
	Rev	5-CTCTGCCTTGAAAGTGTCTT-3	20	
ATF3	Fwd	5-TGCCATCGGATGTCCCTCTGCG-3	21	Fwd primer targets exon 2
	Rev	5-GTGGGCCGGTGCAGGTTGAG-3	20	Rev primer targets exon 4
ATF4	Fwd	5-CCCTTCGACCAGTCGGGTTTGG-3	22	Fwd primer targets exon 2
	Rev	5-AAGGCATCCTCCTTGCCGGTG-3	21	Rev primer spans junction of exons 2 and 3
BiP	Fwd	5-GGACCACCTATTCCTGCGTCG-3	21	Fwd primer spans junction of exons 2 and 2 Rev primer targets exon 3
	Rev	5-CCAAGTGCCTCCGATGAGGC-3	20	
Bok	Fwd	5-CTTTTGC GCGCCGGCCTCTC-3	20	Fwd primer targets exon 2
	Rev	5-ACCTTGCCCCATGTGATACCTGC-3	23	Rev primer spans junction of exons 3 and 4
C1qB	Fwd	5-CCAGGGATAAAGGGGAGAA-3	20	Fwd primer targets exon 2
	Rev	5-TTCTGTGTAGCCCCGTAGTC-3	20	Rev primer targets exon 3
CD11b	Fwd	5-GCTATTTGTTTCGGCTCCAACCTG-3	23	Fwd primer targets exon 5
	Rev	5-ATGTGATCTTGGGCTAGGGTTTC-3	23	Rev primer targets exon 7
c-Fos	Fwd	5-GGGACAGCCTTTCCTACTAC-3	20	Fwd primer targets exon 1
	Rev	5-AAAGTTGGCACTAGAGACGG-3	20	Rev primer targets exon 2
CHOP	Fwd	5-TCCCCAGGAAACGAAGAGGAAG-3	22	Fwd primer spans junction of exons 3 and 4 Rev primer targets exon 4
	Rev	5-TCATGCGTTGCTTCCCAGGC-3	20	

c-Jun	Fwd	5-TGAAGCCAAGGGTACACAAG-3	20	Fwd primer targets exon 1
	Rev	5-AAAGTCCATCGTTCTGGTCG-3	20	Rev primer targets exon 1
Dsp	Fwd	5-CAGCAAGTGGTACGTGACGG-3	20	Fwd primer targets exon 12
	Rev	5-TGTCTCATCGTTTTTCAGCTTGG-3	22	Rev primer spans junction of exons 13 and 14
eIF2α	Fwd	5-CTGTTCCAGAGGACTGCCTG-3	23	Fwd primer targets exon 4
	Rev	5-AGATAGATGGGTCTGAGACTG-3	19	Rev primer spans junction of exons 4 and 5
GADD34	Fwd	5-CCTAAGCTGCCCCCTTCGACTGC-3	22	Fwd primer targets exon 2
	Rev	5-CAGCGAAGTGACCTTCCGAGC-3	22	Rev primer spans junction of exons 2 and 3
GADD45α	Fwd	5-GATGGACACGGTGGGCGATG-3	20	Fwd primer targets exon 2
	Rev	5-CGGGGTCTACGTTGAGCAGC-3	20	Rev primer spans junction of exons 2 and 3
GAPDH	Fwd	5-TGAACGGGAAGCTCACTGG-3	19	Fwd primer targets exon 5
	Rev	5-TCCACCACCCTGTTGCTGTA-3	20	Rev primer targets exon 7
GFAP	Fwd	5-TTTCTCCAACCTCCAGATCC-3	20	Fwd primer targets exon 7
	Rev	5-CCGCATCTCCACAGTCTTTA-3	20	Rev primer targets exon 8
Homer1a	Fwd	5-GGCAAACACTGTTTATGGACTGG-3	23	Fwd primer targets exon 3
	Rev	5-GTAATTCAGTCAACTTGAGCAACC-3	24	Rev primer targets exon 5
Nov	Fwd	5-ACTGGCATTGTCATGGTTCC-3	20	Fwd primer spans junction of exons 2 and 3
	Rev	5-GGCACTGCGACTTTTCTCGG-3	20	Rev primer targets exon 3
SIL1	Fwd	5-CAGGAGAAGAGTGCGAAGGTAC-3	22	Fwd primer targets exon 9
	Rev	5-GGGATGAATCCTGGGTCAACTC-3	22	Rev primer targets exon 10
Spliced XBP-1	Fwd	5-CCTGAGCCCGGAGGAGAA-3	18	Fwd primer targets exon 1
	Rev	5-TGCACCTGCTGCGGACTC-3	18	Rev primer spans spliced intron
Spock1	Fwd	5-CCTCTCTTCAACTCGTGCGACTC-3	21	Fwd primer targets exon 9
	Rev	5-TCCTCTTCGCAGCTTACAGTGCC-3	21	Rev primer spans junction of exons 11 and 12
Synaptophysin	Fwd	5-GAGAACAACAAAGGGCCAAT-3	20	Fwd primer targets exon 4
	Rev	5-GCACATAGGCATCTCCTTGA-3	20	Rev primer targets exon 5

Table 2.1 Sequences and positions of forward and reverse primers.

Primers were designed using NCBI-Primer blast according to the set of criteria outlined in section 2.6.1. bp, base pairs; Fwd, forward and Rev, reverse.

Primer	T _M (°C)	Amplicon size (bp)	T _A (°C)	Extension time (s)
Arc Fwd	54.5	140	55	30
Arc Rev	55.3			
ATF3 Fwd	63.7	293	62	30
ATF3 Rev	65.5			
ATF4 Fwd	65.8	179	63	30
ATF4 Rev	63.7			
BiP Fwd	63.7	203	62	30
BiP Rev	63.5			
Bok Fwd	65.5	245	64	30
Bok Rev	64.2			
C1qB Fwd	66.0	177	62	30
C1qB Rev	61.7			
CD11b Fwd	62.4	275	59	30
CD11b Rev	60.6			
c-Fos Fwd	59.4	110	57	30
c-Fos Rev	57.3			
CHOP Fwd	62.1	238	61	30
CHOP Rev	61.4			
c-Jun Fwd	57.3	175	57	30
c-Jun Rev	57.3			
Dsp Fwd	61.4	249	60	30
Dsp Rev	58.4			
eIF2 α Fwd	61.4	100	60	30
eIF2 α Rev	60.3			
GADD34 Fwd	65.8	106	63	30
GADD34 Rev	63.9			
GADD45 α Fwd	63.5	110	61	30
GADD45 α Rev	63.5			
GAPDH Fwd	58.8	307	58	30
GAPDH Rev	59.4			
GFAP Fwd	62.9	100	61	30
GFAP Rev	62.8			
Homer1a Fwd	60.6	442	59	60
Homer1a Rev	59.3			
Nov Fwd	57.3	197	57	30
Nov Rev	61.4			
SIL1 Fwd	62.1	112	60	30
SIL1 Rev	62.1			
Spliced XBP-1 Fwd	60.5	313	58	30
Spliced XBP-1 Rev	60.5			
Spock1 Fwd	61.8	290	57	30

Spock1 Rev	59.8			
Synaptophysin Fwd	62.8	150	61	30
Synaptophysin Rev	62.8			

Table 2.2 Cycling parameters for primer pairs.

bp, base pairs; Fwd, forward; Rev, reverse and s, seconds.

2.6.2 REDTaq PCR

REDTaq ReadyMix PCR Reaction Mix was used according to the manufacturer's instructions for individual reactions:

Total	25 μ l
REDTaq ReadyMix PCR Reaction Mix	12.5 μ l
Nuclease-free water	9.5 μ l
Forward primer (10 μ M)	1 μ l
Reverse primer (10 μ M)	1 μ l
Template cDNA	1 μ l

The reaction was incubated (GeneAmp PCR System 9700, Applied Biosystems, UK) under the following cycling conditions. Conditions in **bold** were adjusted in order to optimise the conditions for the specific primer pair used, as shown in Table 2.2.

Initial denaturation	94 °C	2 min	} 35 cycles
Denaturation	94 °C	40 s	
Annealing	62 °C	30 s	
Extension	72 °C	30 s	
Final Extension	72 °C	10 mi	
Hold	4 °C	∞	

PCR products were stored at -20 °C long-term. They were separated by agarose gel electrophoresis (section 2.6.4).

2.6.3 Quantitative PCR (qPCR)

qPCR was performed using iQ SYBR Green Supermix or iTaq Universal SYBR Green Supermix, according to the manufacturer's instructions. Detection of PCR products was monitored by measuring the increase in fluorescence, which was caused by the binding of SYBR Green dye to double stranded DNA. qPCR reactions were scaled down to 25 μ l reactions:

Total	25 μ l
SYBR Green Supermix	12.5 μ l
Nuclease-free water	9.5 μl
Forward primer (10 μ M)	1 μ l
Reverse primer (10 μ M)	1 μ l
Template cDNA (200 ng total RNA)	1 μl

Volumes in **bold** were in some instances adjusted for low copy number transcripts, such as ATF3 where the volume of template cDNA was 3 μ l instead of 1 μ l. Reactions were dispensed into a 96-well plate (Bio-Rad) and all reactions were performed in duplicate to ensure accuracy in pipetting.

The reaction was incubated in a Chromo 4 DNA Engine thermocycler (Bio-Rad), running Opticon Monitor v3.1 software, under the following cycling conditions (conditions in **bold** were adjusted for the specific primer pair used, as shown in Table 2.2):

Initial denaturation	94 °C	10 min (iQ SYBR Green) 30 s (iTaq Universal SYBR Green)	} 35 cycles
Denaturation	94 °C	1 min (iQ SYBR Green) 15 s (iTaq Universal SYBR Green)	
Annealing	62 °C	30 s	
Extension	72 °C	30 s	
Final Extension	72 °C	10 min	
Hold	4 °C	∞	

PCR products were stored at 4 °C short-term and -20 °C long-term. They were separated by agarose gel electrophoresis (section 2.6.4).

Standard curves were produced for most genes (section 2.7.8), using 10^{15} - 10^8 plasmids/ μ l (section 2.7). For genes for which plasmid standard curves were not generated, either a cDNA serial dilution standard curve was made from total RNA extracted from the hippocampi of a naive C57BL/6J mouse or the $2^{-\Delta\Delta C_T}$ method was used to calculate fold change between control and treatment samples. A cDNA serial dilution curve was constructed from 5-fold serial dilutions as follows: neat cDNA (800 ng total RNA input), 1:5, 1:25 and 1:125 dilutions in nuclease-free water. Both plasmid and cDNA standards were run in duplicate and the spacing between the standard dilutions should be even as shown in Figure 2.1. A melting curve was run for each qPCR reaction, this is because SYBR green detects all double-stranded DNA, including contaminating DNA and primer dimers. A single peak on the melting curve between 85 °C-90 °C indicates that only the desired product was detected and amplified (Figure 2.2).

cDNA samples were quantified relatively by comparison to a standard curve or using the $2^{-\Delta\Delta C_T}$ method. The C_T number is the cycle number at which the fluorescence crosses the threshold (usually set at 0.010) (background fluorescence) and indicates the amount of mRNA of the gene of interest. The lower the C_T numbers the higher the amount of mRNA in the original sample and vice versa.

2.6.3.1 Standard curve data preparation, normalisation and quantification

If the C_T value for a sample was lower than the C_T value of the least concentrated plasmid or cDNA standard, then the sample was deemed to be below the limit for accurate quantification. Such samples were not included in any further analysis.

GraphPad Prism (GraphPad Software, Inc) was used to plot the log of the number of plasmids/ μ l or cDNA dilution against the C_T value for each standard. A linear regression line was fitted and the R^2 number and the equation for the line ($y=mx+c$) was calculated. Standard curves were accepted if the $R^2 \geq 0.95$ (Figure 2.3). From this the average C_T number for each duplicate was calculated and was used to rearrange the equation of the standard curve regression line ($AU = (C_T - c)/m$) generated for each set of standards, to determine the arbitrary units for each sample. The data for each sample

was then transformed to find the power, 10^{AU} . Data for each sample was then normalised by dividing the power of the particular gene by the power of the housekeeping gene GAPDH for each sample. After the data was transformed and normalised to GAPDH, graphs were then plotted of fold change between control and treated samples.

2.6.3.2 $2^{-\Delta\Delta CT}$ calculation

Fold change was calculated using the $2^{-\Delta\Delta CT}$ method. Samples were normalised to GAPDH using the following equation: average CT of sample - average CT of housekeeping gene for that sample = ΔCT . The following equation is then used: power, $2^{(\Delta CT \text{ control sample} - \Delta CT \text{ treated sample})} = 2^{-\Delta\Delta CT}$ (normalised fold change between control and treated samples). Graphs of fold change between control and treated samples were created from this.

Efficiencies of qPCR reactions in which the $2^{-\Delta\Delta CT}$ method was employed to calculate relative expression of genes can be found in the materials and methods section of chapters 3-6. Efficiency was calculated from opticon monitor software in which the mean fluorescence of each sample was determined 1 and 2 cycles after the set threshold. A perfect doubling of product gives a reaction efficiency of 100%. Reaction efficiencies are expressed as a percentage.

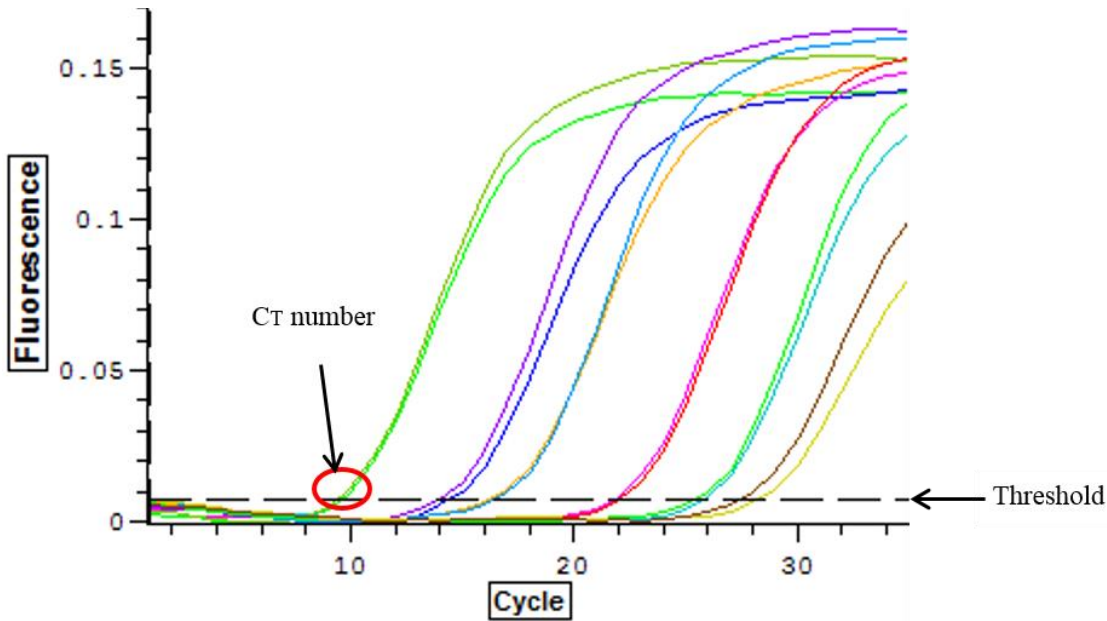


Figure 2.1 Raw data readout from a qPCR of the GAPDH plasmid standard curve.

The dashed line refers to the threshold and the CT number (red circle) is the cycle number at which the fluorescence crosses this threshold. The readout shows that duplicate samples overlap and there is equal spacing between the samples, indicating successful serial dilution of the plasmid standards. The curves from left to right represent the plasmid numbers; 1×10^{14} , 1×10^{13} , 1×10^{12} , 1×10^{11} , 1×10^{10} and 1×10^9 plasmids/ μ l.

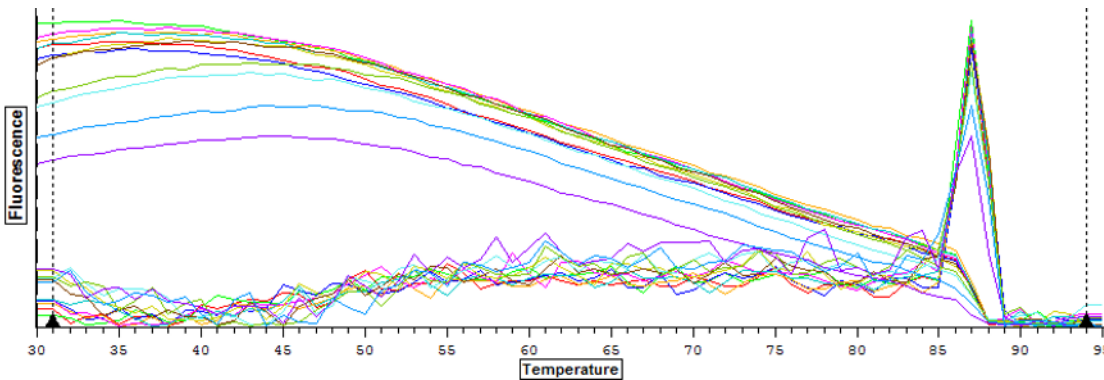


Figure 2.2 Melting curve for GAPDH.

The single peak suggests that there was no contaminating DNA or primer dimers, which if present would have produced an additional separate peak.

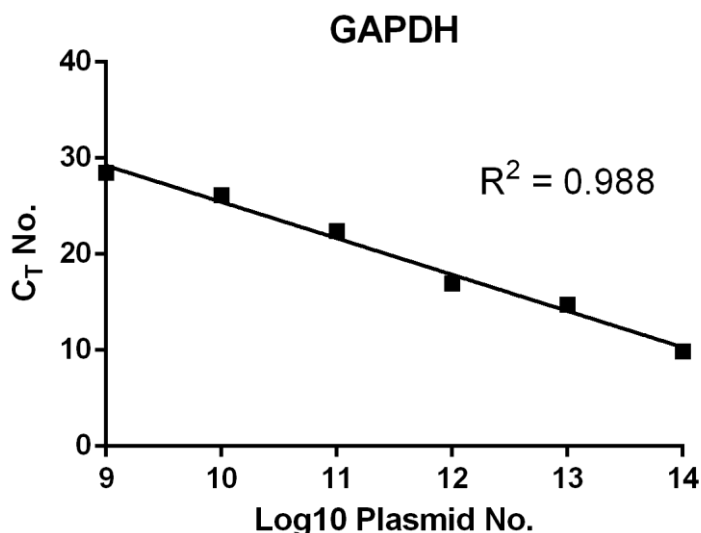


Figure 2.3 Linear regression line of the GAPDH standard curve.

Plasmid dilutions (10^{14} - 10^9 plasmids/ μ l) were used to generate a standard curve, by plotting the average C_T number of duplicates against the log₁₀ of the plasmid number. A linear regression line was fitted and the R^2 value calculated. $R^2 \geq 0.95$ indicates a reliable standard curve.

2.6.4 Agarose gel electrophoresis

Agarose gels were made by dissolving agarose in 120 ml Tris/Borate/EDTA (TBE) buffer to produce either a 1%, 2% or 3% gel. The agarose-TBE solution was heated in a microwave until molten and was allowed to cool for a few minutes before the addition of GelRed stain (1:10000). The solution was then poured into a casting mould (VWR) and allowed to set for 20-30 min. After this time, TBE buffer was added to the electrophoresis chamber. 5 μ l of a DNA ladder was added to the first well. Samples were mixed with 5 \times DNA loading buffer to obtain a 1 \times final concentration and 12 μ l of each sample was subsequently added to the other wells. 1% gels were run at 80-100V for 1 hr, whilst 2% and 3% gels were run at 70V for 2 hr. DNA bands were visualised using the G:BOX (Syngene) imager.

2.7 Generation of plasmids

Hippocampal cDNA was used as a template to amplify fragments of the indicated genes (section 2.7.8) by PCR (section 2.6.2). The PCR products were cloned directly into a

pCR 2.1 vector (Figure 2.4) and transformed into chemically competent Library Efficiency DH5 α cells. Crude miniprep (section 2.7.4) and EcoRI (section 2.7.5) digestion was then used to isolate the plasmid and determine if it contained the gene of interest. The plasmid was then sent for sequencing (section 2.7.8) prior to making plasmid standard curves.

2.7.1 TOPO TA cloning

The TOPO TA cloning kit requires PCR products with A-overhangs and was used according to the manufactures instructions in a 6 μ l reaction:

Fresh PCR product	0.5-4 μ l
Salt solution	1 μ l
Water	Up to 5 μ l
pCR 2.1 TOPO vector	1 μ l

The reaction was mixed gently and placed at room temperature for 5 min, after which it was returned to ice.

2.7.2 Transformation into chemically competent Library Efficiency DH5 α cells

2 μ l of the TOPO cloning reaction was added to one vial (200 μ l) of Library Efficiency DH5 α cells, mixed gently and incubated on ice for 30 min. The cells were then heat shocked for 30 s at 42 °C and then immediately placed back on ice. 250 μ l of room temperature S.O.C medium was added to each vial. The vials were then incubated at 37 °C for 1 hr shaking at 200 rpm. 10 and 50 μ l of each transformation was streaked out onto pre-warmed Luria broth (LB) agar plates containing 50 μ g/ml Kanamycin and 40 μ l of 40 mg/ml X-gal. The plates were incubated overnight at 37 °C.

2.7.3 Transformant selection

2-6 white colonies were picked from transformant plates, spotted onto a back-up plate and used to initiate overnight cultures in 4 ml LB medium containing 50 μ g/ml kanamycin with shaking at 37 °C.

2.7.4 Crude miniprep

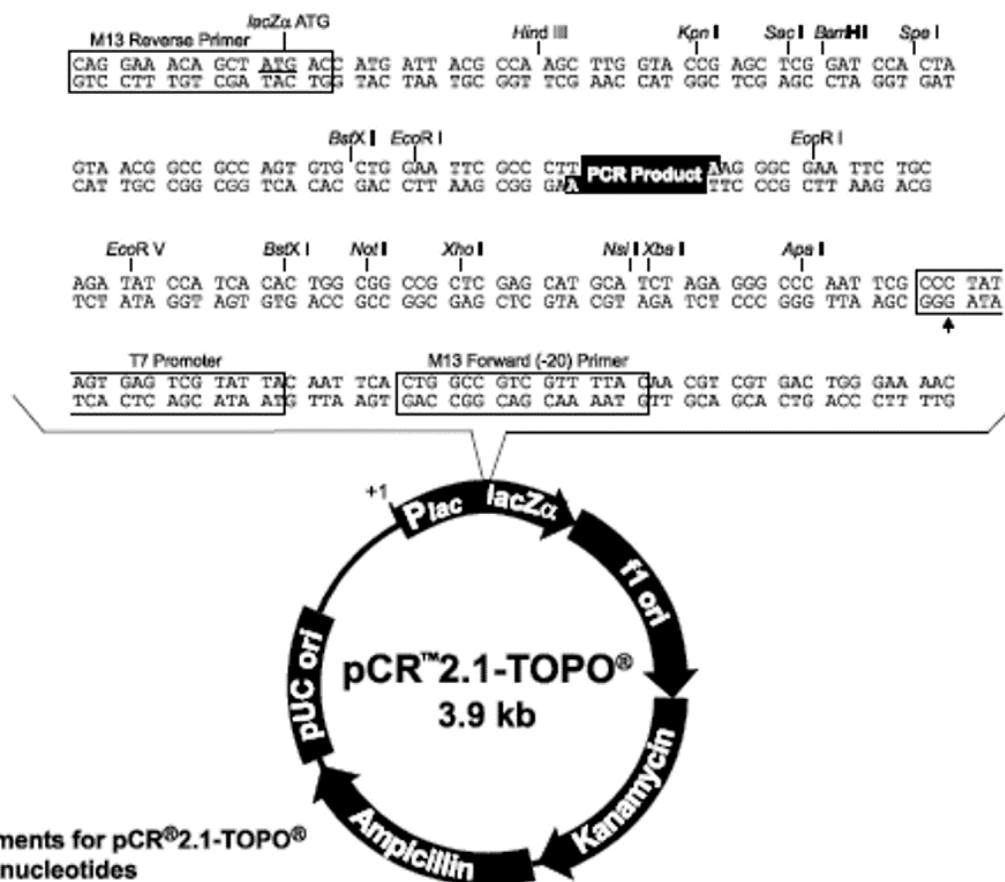
1.5 ml of overnight culture was centrifuged at 13,000 rpm for 1 min. The bacterial pellet was resuspended in 100 μ l buffer P1. 200 μ l buffer P2 was then added and the reaction was mixed gently by inverting five times. 150 μ l buffer P3 was added and the reaction again was inverted 5 times. The reaction was then centrifuged at 13,000 rpm for 5 min. 900 μ l 100% ethanol was added to a clean 1.5 ml Eppendorf and 450 μ l of the supernatant was added to the ethanol before centrifugation at 13,000 rpm for 5 min. The supernatant was discarded and the pellet was washed with 100 μ l 70% ethanol. This was followed by centrifugation at 13,000 rpm for 5 min. The ethanol was removed from the pellet and the pellet was left to air dry for one hour. The plasmid DNA pellet was resuspended in 20 μ l nuclease-free water.

2.7.5 Digestion of plasmids with EcoRI

The plasmid was digested with the restriction enzyme EcoRI, to determine if the gene of interest was present in the plasmid. 10 μ l digestion reactions were set up as follows:

EcoRI	1 μ l
Bovine serum albumin (BSA)	0.1 μ l
10 \times Buffer H	1 μ l
DNA (from miniprep)	2 μ l
Nuclease-free water	5.9 μ l

The digestions were incubated at 37 °C for 2 hr. Digested plasmids were separated by agarose gel electrophoresis (section 2.6.4) to determine the presence of the correct insert (Figure 2.5). Control reactions, lacking the EcoRI enzyme were used to show the size of the undigested circular plasmid. A plasmid only digest lacking the insert was also used as a control to show the size of the linear digested plasmid.



Comments for pCR®2.1-TOPO®
3931 nucleotides

LacZα fragment: bases 1-547
 M13 reverse priming site: bases 205-221
 Multiple cloning site: bases 234-357
 T7 promoter/priming site: bases 364-383
 M13 Forward (-20) priming site: bases 391-406
 f1 origin: bases 548-985
 Kanamycin resistance ORF: bases 1319-2113
 Ampicillin resistance ORF: bases 2131-2991
 pUC origin: bases 3136-3809

Figure 2.4 pCR 2.1 vector map, showing the position of the PCR insert and the EcoRI excision sites.

Image taken from http://tools.invitrogen.com/content/sfs/manuals/topota_man.pdf
 accessed on 18th June 2012.

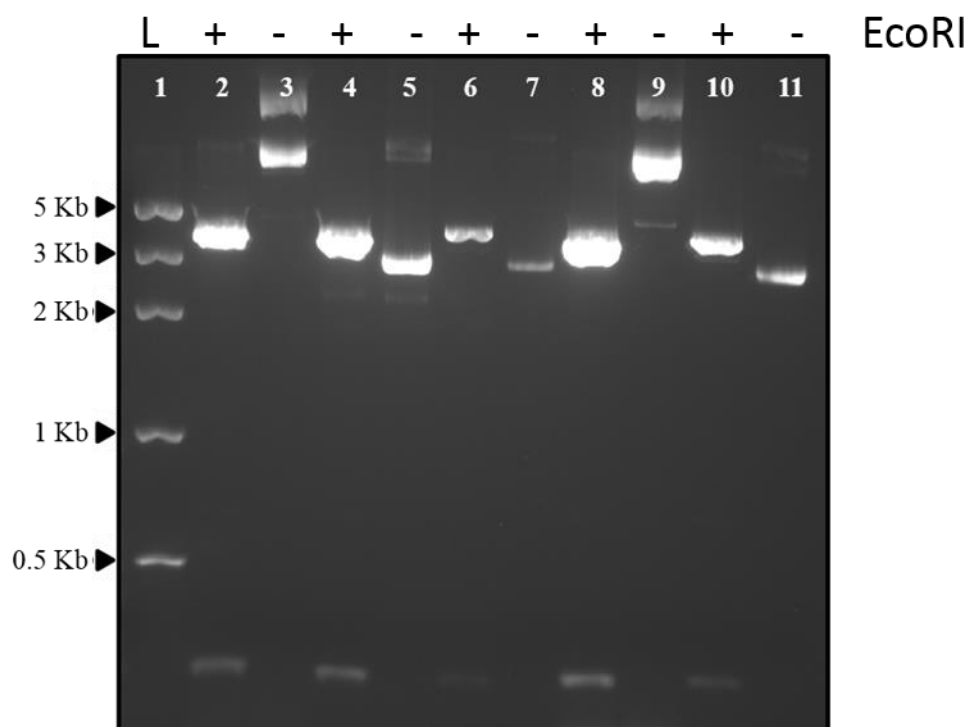


Figure 2.5 Digestion of potential BiP fragment containing plasmids with EcoRI, to determine the presence of the correct insert.

BiP cDNA was amplified using indicated primers (Table 2.1) and the reaction cloned into pCR 2.1 vector. Plasmids digested with EcoRI (+) (lanes 2, 4, 6, 8 and 10) contained the 203 bp insert which correspond to the expected size of the BiP amplicon. The size of the plasmids from reactions lacking EcoRI (-), are shown in lanes 3, 5, 7, 9 and 11. L indicates the DNA ladder.

2.7.6 Preparation of glycerol plasmid stock

Once a plasmid with the correct insert had been identified by restriction digest (section 2.7.5), the corresponding colony from the back up plates was inoculated into 1-2 ml LB medium containing 50 µg/ml kanamycin. This was incubated overnight at 37 °C, shaking at 200 rpm. 0.85 ml of the culture was added to 0.15 ml sterile glycerol in a cryovial, mixed well to give a 15% (v/v) glycerol stock which was stored at -80 °C.

2.7.7 Generation of plasmid standard curves

The concentration of the plasmids obtained from the crude minipreps (section 2.7.4) was found by using the NanoDrop spectrophotometer and this was used to calculate the

number of plasmids/ μ l (appendix 4). The plasmids were then diluted with nuclease-free water to achieve 10^{15} - 10^8 plasmids per μ l.

2.7.8 Sequencing of plasmids

Each plasmid was sent sequenced by the Sanger sequencing method using a commercial vendor (Eurofins, Germany). Chromatograms were analysed and sequences were then aligned with the data base sequence to authenticate sequence was as predicted (appendix 5). Plasmids were created for the following genes: ATF3, ATF4, BiP, CHOP, eIF2 α , GADD34, GADD45 α , and spliced XBP-1.

2.8 HeLa cells

2.8.1 Maintenance of HeLa cells

HeLa (cervical cancer) cells were maintained, prepared and kindly provided by Dr Mark Coldwell and Dr Joanne Cowan. HeLa cell preparation was done in a tissue culture room with gamma sterilised materials. HeLa cells were maintained in Dulbecco's Modified Eagle Medium (D-MEM) with 10 % (v/v) heat-inactivated fetal bovine serum (FBS) in a 37 °C incubator containing 5% CO₂.

2.8.2 Drug treatment of HeLa cells

Tunicamycin was dissolved in 100% sterile dimethyl sulfoxide (DMSO) to obtain a stock concentration of 2 mg/ml and this was stored at 4 °C, until required. A 10 mM stock of phenethyl isothiocyanate (PEITC) was made by adding 1.49 μ l PEITC to 1 ml 100% DMSO.

HeLa cells were seeded on 6 cm plates at a density of 1×10^5 cells per plate. 24 hr later cells were left untreated or treated with DMSO (0.1%), tunicamycin (2 μ g/ml) or PEITC (20 μ M). Tunicamycin was applied for 6 hr and PEITC was applied for 1 hr. Tunicamycin was used as a positive control for the induction of a classic UPR. PEITC was used as a positive control for the phosphorylation of the α subunit of eIF2.

2.8.3 HeLa cell extraction

Following drug treatment, plates containing the cells were placed on ice and the media were aspirated off. The cells were washed with Dulbecco's phosphate buffered saline (PBS) (D-PBS, 4 °C) and this was then aspirated off. D-PBS was added again and cells were scraped into 1.5 ml Eppendorfs and centrifuged for 5 min at $2500 \times g$ (4 °C). The D-PBS was then aspirated off and the cell pellet resuspended in 100 μ l M-PER reagent (supplemented with Halt protease and phosphatase inhibitor cocktail). After vortexing, the Eppendorfs were placed into chilled (4 °C) 50 ml falcon tubes and rotated end-on-end for 10 min at 4 °C. After a final centrifugation for 15 min at $14,000 \times g$ (room temperature), the extracted HeLa cells were placed into a new 1.5 ml Eppendorf and rapidly frozen on dry ice. Extracted HeLa cells were stored at -20 °C until required.

2.9 Western blotting

2.9.1 Hippocampi extraction

Hippocampi approximately 30-40 mg total weight were removed as described in section 2.4.4 and homogenised in 5 volumes (w/v) of RNase-free PBS supplemented with Halt protease and phosphatase inhibitor cocktail using a Kontes pellet pestle. Half of the homogenate was taken for RNA extraction (section 2.5.1) and the rest used for protein extraction for western blotting. Homogenates used for western blotting were combined with an equal volume of $2\times$ HEPES (40 mM)/ NaCl (250 mM) buffer (pH 7.4) containing 4% (w/v) SDS supplemented with Halt protease and phosphatase inhibitor. Samples were boiled at 95 °C for 5 min, except for western blotting for SNARE-complexes when this step was omitted. The samples were then centrifuged at 14,000 rpm for 10 min at room temperature and the supernatant was transferred to a fresh Eppendorf. SDS hippocampal extracts were stored at -20 °C until needed.

2.9.2 Protein assay

Protein concentration was measured using either the Bio-Rad D_c protein assay kit or the Pierce BCA Protein Assay Kit, according to the manufacturer's instructions. For the Bio-Rad kit a protein standard curve was produced using dilutions from a BSA stock in double-distilled H₂O (10 mg/ml). Final concentrations of 2.5 mg/ml, 2 mg/ml, 1.5

mg/ml, 1 mg/ml, 0.5 mg/ml and 0.25 mg/ml, diluted in the same buffer as the homogenate samples (section 2.9.1). Protein absorbance was measured using a FLOUstar OPTIMA (BMG LABTECH) machine and assessed using OPTIMA data analysis software and raw data was exported to Microsoft Excel (Microsoft) and then GraphPad Prism. The linearity of the standard curves was determined by fitting a linear regression line and calculating the R^2 value. Standard curves were only accepted if the $R^2 \geq 0.95$ (Figure 2.6). The concentrations of each sample were then interpolated from the standard curve. For reliable measurements of protein concentrations, samples must be within the linear range of the standard curve.

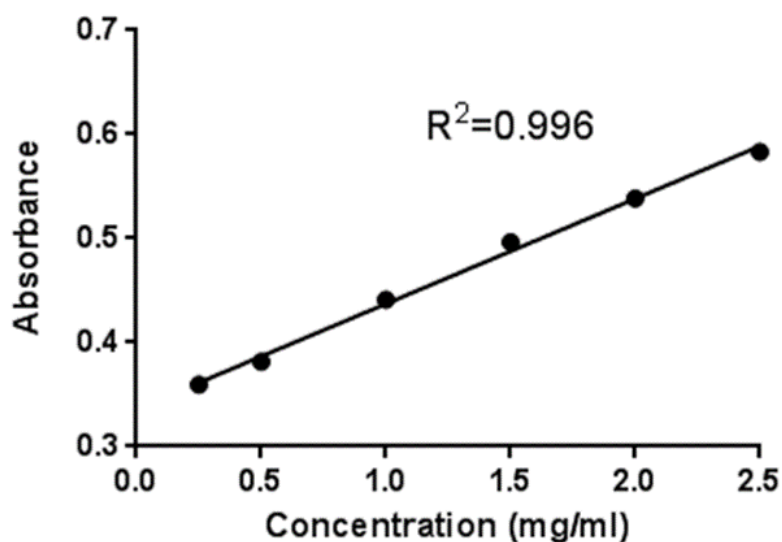


Figure 2.6 Linear regression line of a BSA standard curve.

Dilutions of BSA were used to produce a standard curve, by plotting the absorbance against the concentration of BSA. A linear regression line was fitted and the R^2 value calculated. $R^2 \geq 0.95$ indicates a reliable standard curve.

2.9.3 Sample preparation

After the concentration of each sample had been determined (section 2.9.2), samples were diluted to 2.5 $\mu\text{g}/\mu\text{l}$ using the same buffer used to homogenise and re-extract the homogenate (section 2.9.1). After this a final concentration of 2 $\mu\text{g}/\mu\text{l}$ was achieved for each sample by the addition of 5 \times sample buffer (312.5 mM tris pH 6.8, 10% (v/v)

SDS, 50% (v/v) glycerol, 25% (v/v) β -mercaptoethanol and 0.005% (v/v) bromophenol blue dye).

2.9.4 SDS-polyacrylamide gel electrophoresis (PAGE)

SDS-PAGE gels were made from resolving and stock stacking solutions (Table 2.3). The stock stacking solution was made of 15 ml 30% (v/v) acrylamide/Bis-acrylamide (29:1), 37.5 ml 0.25 M tris pH 6.8, 1 ml 10% (v/v) SDS and made up to 100 ml with double distilled water (ddH₂O). Front (short plate) and back (spacer plate) plates (1.5 mm) (Bio-Rad) were both cleaned with 70% ethanol and then assembled into a casting frame (Bio-Rad). ~7 ml of resolving gel solution was poured between the two glass plates. The resolving gel was then overlaid with water. Once the resolving gel had set (~20 min), the water was removed. ~3 ml of the stacking solution was then poured on top of the resolving gel. A 10 well 1.5 mm comb was inserted into the stacking gel. Once the stacking gel had set (~20 min) the gel cassette sandwich (i.e. the gel in between the two plates) could be removed from the casting frame and placed into a gel tank (Bio-Rad) containing 1 \times Laemmli buffer (25 mM tris, 192 mM glycine and 1% SDS). Samples were routinely boiled at 95 °C for 5 min (except for western blots for SNARE-complexes), before being vortexed and centrifuged at 14,000 rpm for 1 min at room temperature. 10-50 μ g of protein was loaded into individual wells and resolved next to a 5 μ l of Page Ruler Plus Prestained Protein ladder. The gels were run until the bromophenol blue dye front had run off the gel and the protein ladder was sufficiently separated.

% Gels	Stacker solution volume	30 % Acrylamide/ Bis-acrylamide (29:1)	3 M Tris (pH 8.8)	10% APS	10% SDS	ddH ₂ O	TEMED
15		5 ml	1.25 ml	50 μl	100 μl	Up to 10 mls	10 μl
12.5		4.2 ml	1.25 ml	50 μl	100 μl		10 μl
10		3.3 ml	1.25 ml	50 μl	100 μl		10 μl
7.5		2.5 ml	1.25 ml	50 μl	100 μl		10 μl
Stacking Gel	5 ml of stock stacking solution			50 μl			10 μl

Table 2.3 Reagents and volumes required to make different % SDS-PAGE gels.

APS, ammonium persulphate; ddH₂O, double distilled water and TEMED, N, N, N' N'-tetramethylethylenediamine.

2.9.5 SDS-PAGE gel staining

SDS-PAGE gels were incubated with gentle rocking in the following solutions. Gels were removed and first placed into fixing solution (7% (v/v) glacial acetic acid, 40% (v/v) methanol and 53% (v/v) ddH₂O) for 1 hr before being transferred to brilliant blue G-colloidal stain overnight. Subsequently, gels were placed in destain solution (10% (v/v) glacial acetic acid, 25% (v/v) methanol and 65% (v/v) ddH₂O) for 1 min and then washed with 25% methanol three times (1 min/wash), before being placed back in 25% methanol until the protein bands were clearly resolved. Gels were then scanned using an Odyssey Infrared Imaging Scanner (LI-COR) at 700 nm and analysed using Image Studio software (LI-COR). Signal intensity values for total protein in each sample was calculated as described in section 2.9.8.

2.9.6 Electroblothing of protein to nitrocellulose membrane

Sponges (Bio-rad), Whatman filter paper and nitrocellulose membrane (Bio-Rad) were immersed into transfer buffer (10% (v/v) 10 \times Laemmli buffer, 20% (v/v) methanol and 70% (v/v) ddH₂O) for 10 min. The SDS-PAGE gel was then sandwiched between filter paper and nitrocellulose membrane (Figure 2.7). Once secure this sandwich was placed

into a tank containing transfer buffer. Protein samples were transferred from the acrylamide gel to the nitrocellulose membrane at 30V for ~17 hr (overnight) at 4 °C. The transfer buffer was circulated during the overnight transfer using a stir bar and placing the blotting tank on magnetic stirrer.

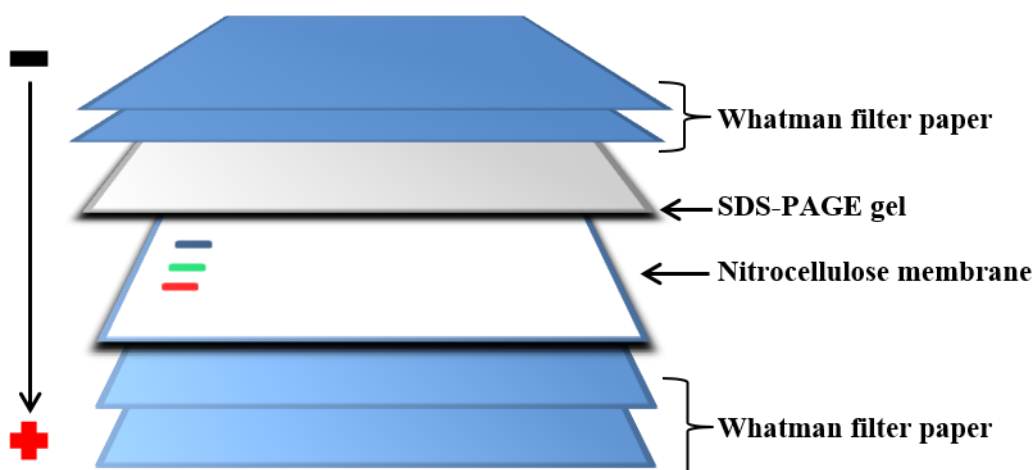


Figure 2.7 SDS-PAGE gel-nitrocellulose transfer sandwich.

This consisted of a sponge (not shown), 2× Whatman filter paper, a nitrocellulose membrane, SDS-PAGE gel, 2× Whatman filter paper and another sponge (not shown). The sandwich was then placed between plastic cassettes and inserted into the transfer tank. The sandwich was placed in the tank in an orientation which meant that the nitrocellulose membrane was closest to the anode (+). This is because the proteins will migrate from the cathode (-) to the anode (+) (arrow shows direction of protein migration). The transfer was done at 30V overnight at 4° C, with stirring.

2.9.7 Antibody labelling of transferred proteins

The nitrocellulose membranes which contained the transferred proteins were removed from this sandwich cut into strips and incubated in blocking solution (5% (w/v) dried skimmed milk, 1× TBS, 0.1% (v/v) Tween-20) for 1 hr, with gentle rocking. Membranes were then washed three times (5 min/wash) in wash buffer (1× TBS, 0.1% (v/v) Tween-20). They were then incubated with the appropriate primary antibody (Table 2.4) in indicated primary antibody solution (5% (w/v) BSA, 1× TBS, 0.1% (v/v) Tween-20). Subsequently, the membranes were washed three times (5 min/wash) in wash buffer and then incubated with the appropriate fluorescent secondary antibody

(Table 2.5) at a dilution of 1:10000 in secondary antibody solution (5% (w/v) dried skimmed milk, 1× TBS, 0.1% (v/v) Tween-20), for 1 hr at room temperature. The membranes were then washed three times (5 min/wash) in wash solution. They were scanned with an Odyssey Infrared Imaging Scanner at the appropriate wavelength (700 nm and/or 800 nm) using Image Studio software.

2.9.8 Quantification of protein levels

Quantification of total protein and the intensity of immunolabelling was done using fluorescent image studio software. A rectangle box was drawn around each visualised area of interest or immunolabelled protein and a signal intensity was calculated (Figure 2.8). Signal intensity for each sample was then normalised to total protein loading. To do this, intensity values for each sample from a SDS-PAGE stained gel (section 2.9.5) were determined. The sample with the highest intensity signal was assigned a value of 1 and all other samples were calculated as a fraction of this. Protein intensity of antibody labelled bands was then divided by total protein intensity for each sample, therefore accounting for variations in protein loading.

Primary Antibody	Supplier	Species	Dilution	Predicted MW (kDa)	Incubation conditions
4E-BP1 (53H11)	Cell Signalling Technology Catalogue no: 9644	Rabbit (monoclonal)	1:1000	15-20	Overnight at 4 °C
ATF3 (H-90)	Santa Cruz Biotech Catalogue no: sc-22798	Rabbit (polyclonal)	1:1000	21	Overnight at 4 °C
ATF4 (D4B8)	Cell Signalling Technology Catalogue no: 11815	Rabbit (monoclonal)	1:1000	48	Overnight at 4 °C
BiP (C50B12)	Cell Signalling Technology Catalogue no: 3177	Rabbit (monoclonal)	1:1000	78	Overnight at 4 °C
c-Fos	Abcam Catalogue no: ab7963	Rabbit (polyclonal)	1:1000	70	Overnight at 4 °C
c-Jun (60A8)	Cell Signalling Technology Catalogue no: 9165	Rabbit (monoclonal)	1:1000	43	Overnight at 4 °C
CHOP (9C8)	Thermo Scientific	Mouse (monoclonal)	1:1000	31	Overnight at 4 °C

	Catalogue no: MA1-250				
CSP α	Abcam Catalogue no: ab79346	Rabbit (polyclonal)	1:1000	35	Overnight at 4 °C
eIF2 α 1	Cell Signalling Technology Catalogue no: 9722	Rabbit (polyclonal)	1:1000	38	Overnight at 4 °C
eIF2 α 2 (D7D3)	Cell Signalling Technology Catalogue no: 5324	Rabbit (monoclonal)	1:1000	38	Overnight at 4 °C
GADD45 α (D17E8)	Cell Signalling Technology Catalogue no: 4632	Rabbit (monoclonal)	1:1000	22	Overnight at 4 °C
eIF2 α -P 1 (Ser51)	Cell Signalling Technology Catalogue no: 9721	Rabbit (polyclonal)	1:1000	38	Overnight at 4 °C
eIF2 α -P 2 (Ser51) (D9G8)	Cell Signalling Technology Catalogue no: 3398	Rabbit (monoclonal)	1:1000	38	Overnight at 4 °C
GFAP	Dako Catalogue no: Z0334	Rabbit (polyclonal)	1:5000	50	1 hr room temperature
PERK (33E10)	Cell Signalling Technology Catalogue no: 3192	Rabbit (monoclonal)	1:1000	140	Overnight at 4 °C
PERK-P (Thr980) (16F8)	Cell Signalling Technology Catalogue no: 3179	Rabbit (monoclonal)	1:1000	140	Overnight at 4 °C
PrP (6H4)	Prionics Catalogue no: 01-010	Mouse (monoclonal)	1:5000	25-35	1 hr room temperature
PSD-95 (6G6-1C9)	Millipore Catalogue no: MAB1596	Mouse (monoclonal)	1:1000	95	Overnight at 4 °C
SNAP-25	Abcam Catalogue no: ab41455	Rabbit (polyclonal)	1:1000	25	Overnight at 4 °C
Synaptophysin (SY38)	Abcam Catalogue no: ab8049	Mouse (monoclonal)	1:1000	38	Overnight at 4 °C

Table 2.4 Primary antibodies used for western blotting.

Secondary Antibody	Supplier	Species	Dilution	Incubations conditions
Goat anti-Mouse 680	LI-COR Catalogue no: 926-68020	Goat (polyclonal)	1:10000	1 hr room temperature
Goat anti-Mouse 800	LI-COR Catalogue no: 926-32210	Goat (polyclonal)	1:10000	1 hr room temperature
Goat anti-Rabbit 680	LI-COR Catalogue no: 926-68021	Goat (polyclonal)	1:10000	1 hr room temperature
Goat anti-Rabbit 800	LI-COR Catalogue no: 926-3211	Goat (polyclonal)	1:10000	1 hr room temperature

Table 2.5 Secondary antibodies used for western blotting.

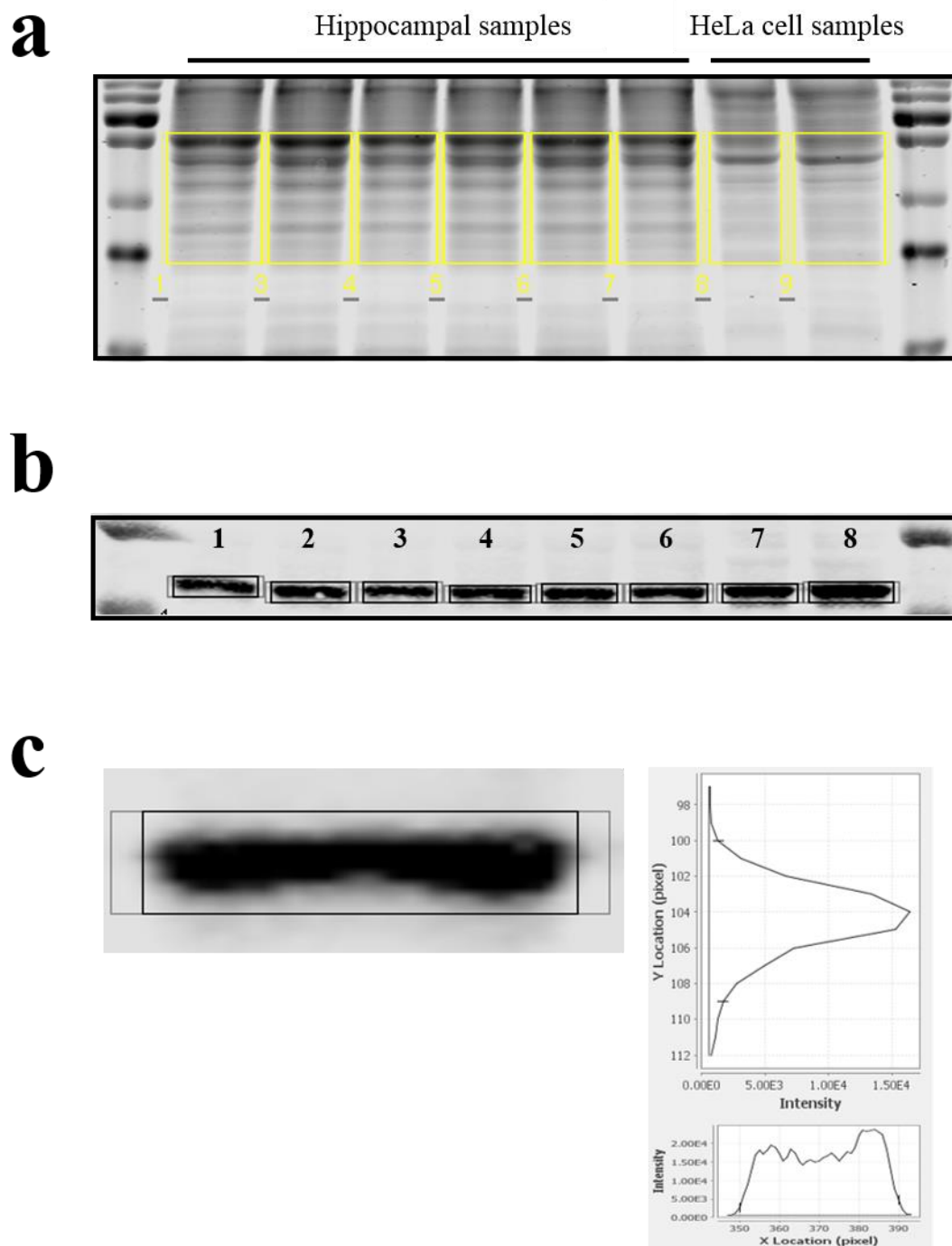


Figure 2.8 Representative images to illustrate quantification of protein loading and normalization for calculating protein levels by western blotting.

Representative Coomassie stained gel of 30 μ g protein from hippocampal and HeLa cell samples (a). Identical boxes were drawn around common protein bands within each lane to calculate total protein signal intensity for each sample and calculate relative protein load. The signal intensities for a particular protein (in this example for eIF2 α) are determined by drawing a box around the band of interest (b). Zoomed

image of the specific protein band in lane 6 from image B (c). The image shows that the full band has been included in the box and therefore quantified. Local background is detected by the two boxes either side of the main box in which the protein band is in. Image Studio software calculates the background intensity and subtracts this from the total intensity, to give a signal intensity value for the specific band only. Signal intensity profiles (horizontal and vertical) for the band are shown.

2.10 Immunohistochemistry

2.10.1 Tissue preparation and sectioning

Brains which had been fixed and embedded in wax (section 2.4.3) were sectioned using a microtome (Leica). Sections were cut until the hippocampus became visible, at which point 10 µm serial sections of the hippocampus were cut and collected. The sections were left to float on a water bath at 52 °C, until the wax had expanded. Sections were transferred to Superfrost Plus glass slides (Fisher Scientific) and placed in an incubator at 37 °C to dry. Sections were then stored at room temperature.

2.10.2 DAB staining

Sections were dewaxed by incubating them in an oven at 60 °C for 30 min. The sections were then rinsed twice in xylene, each for 10 min, before rehydration through decreasing ethanol concentrations: 100% (×2); 95% (×1); 80% (×1) and 70% (×1), for 5 min each. Sections were washed in PBS, before blocking endogenous peroxidase activity by incubating them in 1% hydrogen peroxide (H₂O₂) diluted in methanol for 15 min at room temperature. Sections were placed in 10 mM citrate buffer pH 6 (1.92 g citric acid, 1 L ddH₂O, pH 6.0) and microwaved on full power for 5 min. They were transferred to cool distilled water for 5 min, before re-microwaving them in citrate buffer for 3 min and then cooling them again by placing them in cold tap water. A hydrophobic barrier pen (ImmEdge, Vector Labs) was used to draw around each section to allow individual sections to be incubated in 100 µl of solution. Sections were blocked in blocking solution (5% (v/v) serum, 1× PBS, 0.05% (v/v) Tween-20) for 1 hr at room temperature in a humid chamber. Sections were then incubated with the indicated primary antibody (Table 2.6) in 100 µl antibody solution (0.25% (v/v) serum, 0.01% (v/v) triton X-100, 1× PBS), overnight at 4 °C. Negative controls were sections covered

with 100 µl primary antibody solution lacking the primary antibody. Sections were washed in wash buffer (1× PBS, 0.05% (v/v) Tween-20), twice (5 min/wash) and then incubated with the appropriate secondary antibody (Table 2.6) made in antibody solution for 1 hr at room temperature in a humid chamber. The avidin-biotinylated horseradish peroxidase complex (ABC) was made by adding 2 drops of reagent A (avidin) and 2 drops of reagent B (biotinylated horseradish peroxidase) to 5 ml of PBS-0.1% (v/v) Tween-20. This was vortexed and left to stand at room temperature for 30 min. Sections were incubated with ABC for 30 min at room temperature in a humid chamber and washed in wash buffer, twice (5 min/wash) and then were developed in 3,3'-Diaminobenzidine (DAB) solution (5 ml DAB (25 mg/ml), 250 ml phosphate buffer (0.1 M, pH 7.4)), containing 0.0015% (v/v) H₂O₂ for 30 s. Sections were placed in PBS to halt the reaction. If the sections required extended exposure time they were placed back into DAB and visually scored for staining. Sections were then washed twice in PBS (5 min/wash) and counterstained with Harris haematoxylin for 5 s. Sections were placed into tap water to wash off excess stain and were continually rinsed with tap water until the water remained clear. Sections were placed in 1% HCl-70% ethanol for 2 s and then rinsed with tap water for 2 min to differentiate the haematoxylin stain. Sections were dehydrated through an increasing series of ethanol concentrations: 70% (×1); 80% (×1); 95% (×1); 100% (×2) for 5 min. This was followed by two xylene 10 min rinses. Mounting medium was used to cover slip sections and these were left to dry overnight in a fume hood.

Images from stained sections were taken using a Leica microscope (Leica DM5000B), with Leica QWin software for image capture. Representative images from different regions of the hippocampus were captured at different magnifications using the same microscope settings at each magnification.

Antibody	Supplier	Species	Dilution
Alexa Fluor 555 anti-rabbit*	Invitrogen (molecular probes) Catalogue no: A-21428	Goat (polyclonal)	1:500
ATF3 (H-90)	Santa Cruz Biotech Catalogue no: sc-22798	Rabbit (polyclonal)	1:100
ATF4* (D4B8)	Cell Signalling Technology Catalogue no: 11815	Rabbit (monoclonal)	1:200
Biotinylated Goat anti-Mouse	Vector Labs Catalogue no: BA-9200	Goat	1:200
Biotinylated Goat anti-Rabbit	Vector Labs Catalogue no: BA-9200	Goat	1:200
BiP (C50B12)	Cell Signalling Technology Catalogue no: 3177	Rabbit (monoclonal)	1:200
c-Fos	Abcam Catalogue no: ab7963	Rabbit (polyclonal)	1:200
c-Jun (60A8)	Cell Signalling Technology Catalogue no: 9165	Rabbit (monoclonal)	1:400
eIF2 α -P 2 (Ser51) (D9G8)	Cell Signalling Technology Catalogue no: 3398	Rabbit (monoclonal)	1:100
GADD45 α	Merck Millipore Catalogue no: 07-1230	Rabbit (polyclonal)	1:1000
GFAP	Dako Catalogue no: Z0334	Rabbit (polyclonal)	1:1000
Synaptophysin (SY38)	Abcam Catalogue no: ab8049	Mouse (monoclonal)	1:100

Table 2.6 Primary and secondary antibodies used for immunohistochemistry.

*used for immunofluorescence.

2.10.3 Quantification of positive staining

Only images captured at 20 \times magnification were used for quantification. Images were saved as TIFF files and were opened up in ImageJ software (National Institute of Health). In ImageJ, images were converted to 8-bit images (gray scale). One image for each staining performed was chosen based on clear and qualitative positive staining. The images were thresholded in ImageJ so that only positive staining (dark brown) was detected. This threshold was then used for all subsequent images which had been simultaneously stained and processed for detection of the same antigen. This ensured all images were thresholded to the same extent and this prevented biasing the quantification of images. The free-hand tool on ImageJ was used to draw around the particular region of interest which was to be quantified (Figure 2.9). This was either the entire DG, CA3 or CA1 region or the granule cell layer of the DG or the pyramidal layer of CA3 or

CA1. The analysis tool was used to measure the staining intensity as a % area of positive staining. The fold change of the % area of positive staining between control and treatment was used for statistical analysis and graphical depiction.

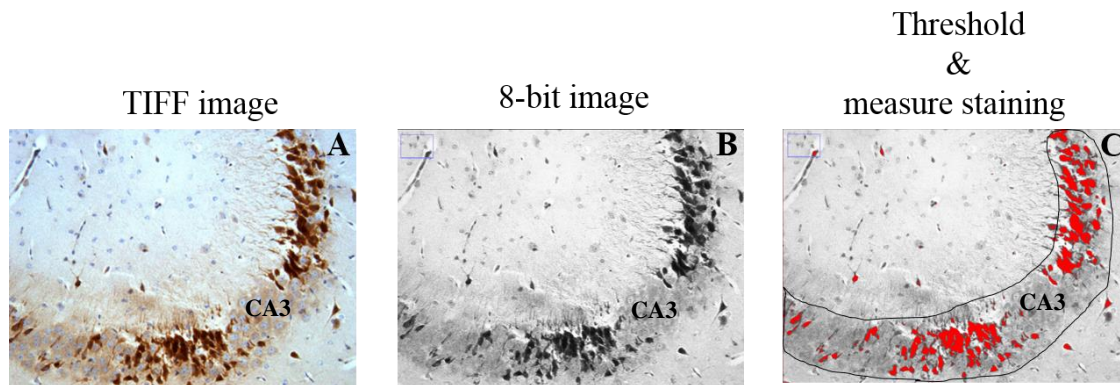


Figure 2.9 Illustrative image processing used to quantify DAB based immunoreactivity of mouse brain sections.

In this example a mouse brain section was stained for ATF3 and developed with DAB before 20 \times magnification images were captured and imported into ImageJ. The image was turned into an 8-bit image and was thresholded so that only positive staining was detected (red). The region of interest under investigation was drawn around (black line) and was used to measure the signal intensity as the % area of positive staining. The scale bar (100 μ m) is indicated under image C. CA3, Cornu Ammonis region 3.

2.11 Immunofluorescence – HeLa cells

HeLa cells used for immunofluorescence were kindly provided by Dr Noel Wortham. HeLa cells were placed on coverslips in a 12-well plate. The HeLa cells had been fixed with 4% paraformaldehyde (PFA) in 1 \times PBS and were then washed three times (5 min/wash) with PBS.

HeLa cells were incubated with 50 mM NH_4Cl in 1 \times PBS for 5 min and then incubated in 0.1% (v/v) Triton X-100 in 1 \times PBS for 5 min. HeLa cells were incubated with blocking solution (10% (v/v) serum, 1 \times TBS, 0.05% (v/v) Tween-20) for 1 hr. HeLa cells were then incubated with ATF4 primary antibody (Table 2.6) in blocking solution overnight at 4 $^{\circ}\text{C}$. HeLa cells used as negative controls were incubated in blocking solution lacking the primary antibody. The following morning HeLa cells were washed three times (5 min/wash) with TBS and then incubated in blocking solution containing the secondary antibody (Table 2.6) and Hoechst (1:1500) for 30 min in the dark. HeLa

cells were then washed three times (5 min/wash) with TBS and mounted (with the coverslips) on Superfrost Plus glass slides using Mowiol mount mix (12 ml glycerol, 12 ml 200 mM Tris HCl (pH 8.5), 2.4 g Mowiol-488). Slides were left to dry overnight in a fume hood.

Images were acquired with the same microscope and software as in section 2.10.2. Images were captured at different magnifications using the same microscope settings at each magnification.

2.12 Statistical analysis

Data was imported into GraphPad Prism. GraphPad Prism software was used for the production of graphs and statistical testing. Statistical tests used in this thesis include: repeated measures two-way ANOVA with Bonferroni post-analysis; one way ANOVA with Bonferroni post-analysis and Unpaired Student's *t*-test, two-tails. The statistical test used for the analysis of data sets is highlighted in the figure legends in chapters 3-6. A *P* value of ≤ 0.05 was taken as statistically significant. Statistical testing was not performed for datasets when one or more treatments had an $n = \leq 2$, unless otherwise stated.

Chapter 3: Investigation of the unfolded protein response and other stress-related responses in ME7-animals

3.1 Introduction

Prion diseases can be sporadic, inherited or transmitted (Fraser, 1993). The infectious capacity of prion diseases has been successfully exploited to develop animal models of prion disease (Chandler, 1961). These models have clear temporal progression and display key pathological features seen in human chronic neurodegenerative diseases (Verity and Mallucci, 2011). The predictable manner in which disease progresses makes these models ideal for investigating and defining cellular and molecular changes associated with chronic neurodegeneration in a longitudinal manner *in vivo*.

The ME7 prion model has been used to gain insights into chronic neurodegenerative disease pathogenesis. In our laboratory the ME7 model disease is initiated by bilateral intrahippocampal injection of ME7-infected brain homogenate. Previous observations using the ME7 model have found that synaptic loss in the stratum radiatum of the hippocampus is one of the earliest events occurring at ~13 w.p.i., long before any signs of neuronal loss (Cunningham et al., 2003, Gray et al., 2009, Sisková et al., 2009). In particular, the pre-synaptic compartment is selectively vulnerable. The topology of this synaptic loss has been made clearer by BDA tracing of CA3 pyramidal neurons. Using BDA tracing, synaptic bouton loss and the appearance of abnormal axonal swellings can be seen along the Schaffer collateral axons of CA3 pyramidal neurons in the hippocampus of ME7-animals from 13 w.p.i. (Al-Malki, 2012). This is reinforced by the observation that, concomitant with synapse loss and the appearance of abnormal axonal swellings, there is a reduction in dendritic spines, density of dendritic branching and length of dendrites of the CA3 pyramidal neurons in ME7-animals (Al-Malki, 2012). Similarly, swellings can be seen on the dendrites and morphological changes in the shape of the cell body are apparent in ME7-animals from 16 w.p.i.

BDA tracing of CA3 pyramidal neurons in ME7-animals suggests important structural changes to neuronal compartments during the course of prion disease progression. However, the molecular events leading to and associated with these morphological

alterations are not well defined. An important conceptual advance has come from a Tg mouse model of ALS (SOD1, G93A), in which morphological dysfunction is mapped onto a progressive time course (Saxena et al., 2009). The high degree of predictability of morphological changes seen in this model enables a detailed analysis of molecular events which can be analysed at distinct time-points and correlated with structural changes (Saxena et al., 2009). This revealed a transient induction of UPR and other stress-related response molecules early on in the vulnerable motoneurons of SOD1 (G93A) mice (Saxena et al., 2009). The induction of UPR molecules was shown to be a key determinant leading to full-blown motoneuron disease (Saxena et al., 2009). More recent studies in another mouse model of infectious prion disease, published after initiating this work, has highlighted the sustained activation of the UPR in neurons during prion disease progression (Moreno et al., 2013, Moreno et al., 2012). Both the ALS and prion studies highlighted above show that key molecular events might be important and provide a correlate to the morphological changes seen during disease progression in the ME7 model.

In this chapter, the ME7 prion model has been used to investigate whether UPR and other stress-related response molecules are activated and correlate with the morphological alterations seen in ME7-animals (Al-Malki, 2012). A greater understanding of the ‘molecular players’ in chronic neurodegenerative disease will enable better targeted therapeutic approaches which may slow or even arrest disease progression.

3.2 Aims

In this chapter the aim was to investigate the molecular responses associated with the onset and progression of chronic neurodegeneration, in the ME7 prion disease mouse model, with a particular focus on the UPR. Other stress-related response molecules (immediate early genes, activity-induced immediate early genes and a cellular physiological and environmental damage stress sensor) were investigated in ME7-animals. Tissue from control (NBH) and ME7-animals was taken across a time course, spanning early-, middle- and late-stages of disease. Hippocampal tissue was used for quantitative western blotting and qPCR and whole brain tissue sections (containing the hippocampus) was collected for immunohistochemistry. These techniques were used to:

- Quantify the expression of UPR and other stress-related response mRNAs
- Quantify the expression of UPR and other stress-related response proteins
- Investigate where in the hippocampus these molecules are expressed

The experimental outline for this study is shown in Figure 3.1.

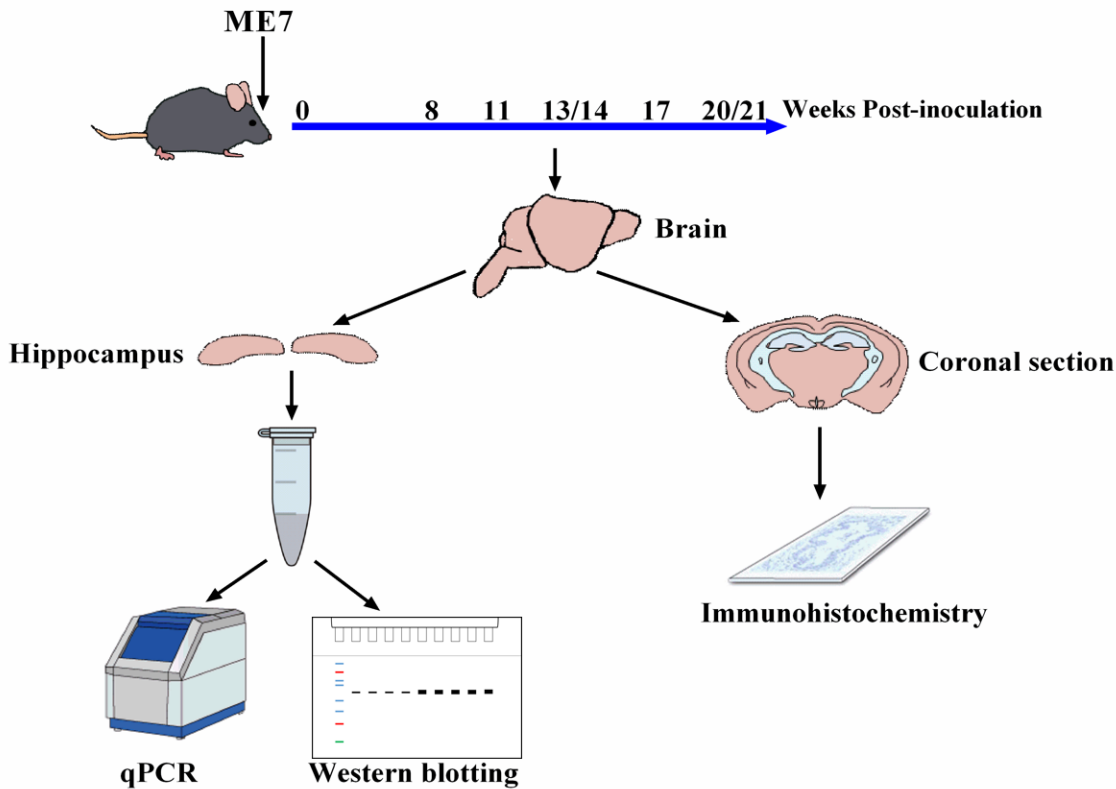


Figure 3.1 Experimental outline: investigating the UPR and other stress-related response molecules in ME7-animals.

C57BL/6J female mice were injected with 1 μ l of NBH or ME7 brain homogenate bilaterally into the dorsal hippocampus. Mice were killed at different time points (8-20 w.p.i) after inoculation. The brain was removed and used for hippocampal dissection. The dissected hippocampus was homogenised and the homogenate split into two aliquots. One aliquot was used to isolate RNA and perform qPCR and the other to isolate protein and to perform quantitative western blotting. Coronal sections were cut from NBH- and ME7-animals at 13 and 21 w.p.i. and used for immunohistochemistry. NB Tissue from NBH- and ME7-animals at 20 w.p.i. and used for western blotting was processed prior to tissue from NBH- and ME7-animals at 8-17 w.p.i. w.p.i., weeks post-inoculation.

3.3 Specific materials and methods

3.3.1 qPCR

mRNA expression was calculated as described (section 2.6.3.1), with the exception of SIL1 and Homer1a mRNA, which was calculated using the $2^{-\Delta\Delta C_T}$ method (section 2.6.3.2). SIL1 had a qPCR efficiency of 30.63% whilst GAPDH (used to normalise SIL1 expression) had a qPCR efficiency of 91.44%. Homer1a had a qPCR efficiency of 82.34% and GAPDH (used to normalise Homer1a expression) had a qPCR efficiency of 91.55%.

3.3.2 eIF2 α -P blocking peptide

Western blotting was performed as in section 2.9. Prior to incubation of the nitrocellulose membrane with primary antibody, the eIF2 α -P antibody was incubated with an equal volume of eIF2 α -P blocking peptide (Cell Signalling Technology) for 30 min in primary antibody solution (section 2.9.7). After this time, nitrocellulose membranes were incubated with the primary antibody solution containing the primary antibody and blocking peptide. Subsequent steps were the same as in 2.9.7.

Immunohistochemistry was performed as in section 2.10. Prior to incubation of the coronal brain sections with the primary antibody, the eIF2 α -P 1 antibody was incubated with twice the volume of the eIF2 α -P blocking peptide for 30 min in primary antibody solution (section 2.10.2). After this time, coronal brain sections were incubated with the primary antibody solution containing the primary antibody and blocking peptide. Subsequent steps were the same as in section 2.10.2.

3.4 Results

3.4.1 Expression of total PrP and GFAP protein and synapse integrity in ME7-animals

Tissue taken during disease progression was analysed by quantitative western blotting which revealed that the levels of total PrP progressively increased in the hippocampus of ME7-animals from 14 w.p.i. (Figure 3.2a and b). This increase is directly related to the proportion that is PK resistant (PrP^{Sc}) (Gray et al., 2009). The three forms (di-, mono- and unglycosylated) of total PrP were quantified. Diglycosylated PrP remained unchanged between NBH- and ME7-animals between 8-17 w.p.i., but at 20 w.p.i. levels were increased in ME7-animals (Figure 3.2c). Unlike diglycosylated PrP, levels of mono- and unglycosylated PrP progressively increased in ME7-animals from 14 w.p.i (Figure 3.2a, d and e).

Quantitative western blotting for GFAP, revealed that GFAP progressively increased in ME7-animals from 14 w.p.i. (Figure 3.2a and f). GFAP cleavage products could be seen in ME7-animals from 14 w.p.i. (Figure 3.2a), in agreement with a previous observation (Gray et al., 2006).

Immunohistochemical staining also showed that the levels of GFAP were progressively increased in ME7-animals from 13 w.p.i. (Figure 3.3 A-D). In ME7-hippocampi, GFAP+ astrocytes appear hypertrophied and had more elaborate processes compared to NBH-animals (Figure 3.3 E-F). In addition, there was an increased infiltration of GFAP+ astrocytes into the neuronal layers of the hippocampus in ME7-animals. Infiltration of hypertrophied astrocytes into the pyramidal layer of CA3 is shown in Figure 3.3 E-F. Immunohistochemical staining for the presynaptic protein synaptophysin, revealed reduced and disorganised staining in the stratum radiatum of the hippocampus in ME7-animals from 13 w.p.i. (Figure 3.3 G-H). Staining within this region became further reduced and disorganised as disease progressed (Figure 3.3 I-J).

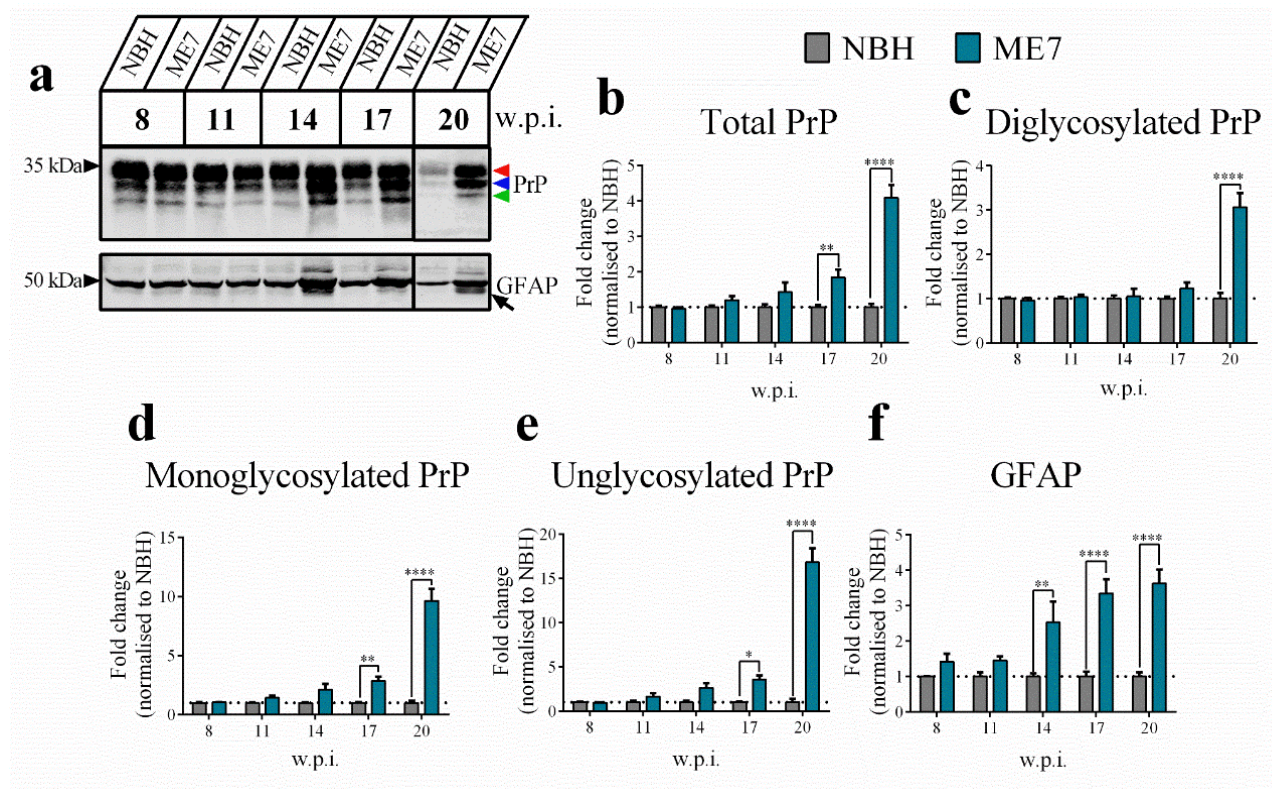


Figure 3.2 Quantification of total, di-, mono- and unglycosylated PrP and GFAP proteins in ME7-animals.

Representative western blots (a) and related quantification for total (b), di- (c), mono- (d) and unglycosylated PrP (e) and GFAP (f) in SDS extracted hippocampi from NBH- and ME7-animals killed at different time-points (8-20 w.p.i.). Coloured arrowheads in (a) mark di- (red), mono- (blue) and unglycosylated PrP (green). The black arrow highlights GFAP cleavage products seen in ME7-animals from 14 w.p.i. Data in graphs represents mean \pm SEM of the protein expression values from $n = 4$ animals per condition and time-point. Statistical test = repeated measures two-way ANOVA with Bonferroni post-analysis. Statistical significance relative to NBH: * $P \leq 0.05$, ** $P \leq 0.01$, and **** $P \leq 0.0001$. w.p.i., weeks post-inoculation.

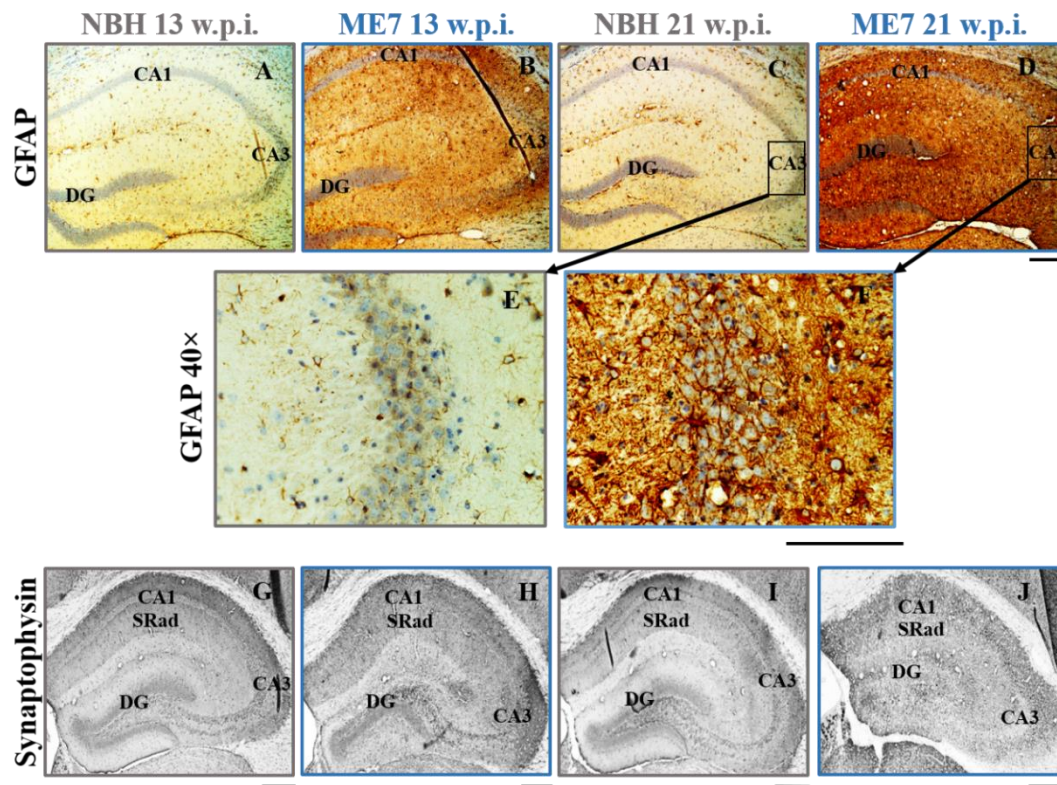


Figure 3.3 Immunohistochemical staining for GFAP and synaptophysin in ME7-animals.

Representative immunohistochemical staining for GFAP (A-F) and synaptophysin (G-J) in the hippocampus of NBH- and ME7-animals killed at 13 and 21 w.p.i. Magnified images of GFAP staining in NBH- and ME7-animals at 21 w.p.i. is shown (E-F). Scale bar for GFAP images is indicated under image D (200 μ m), scale bar for 40 \times GFAP images is located under image F (50 μ m) and scale bars for synaptophysin images are indicated under each of the images (300 μ m). $n = 3$ animals per condition and time-point. CA1, Cornu Ammonis region 1; CA3, Cornu Ammonis region 3; DG, dentate gyrus; SRad, stratum radiatum and w.p.i., weeks post-inoculation. Staining performed by masters student, Matthew Cooper.

3.4.2 Expression of UPR mRNAs in ME7-animals

A number of signatures can be used to resolve the UPR even in complex tissue such as the hippocampus. The levels of UPR mRNAs were assessed from distinct time-points of ME7 prion disease by qPCR. A number of mRNAs were selected based on their known ability to be induced under conditions of ER stress. mRNA levels of spliced XBP-1 and ATF4 were unchanged between NBH- and ME7-animals across the disease time course (Figure 3.4b and e). mRNA levels of GADD34 also remained largely unchanged between NBH- and ME7-animals, except for at 14 w.p.i. when levels of GADD34 were significantly increased in ME7-animals relative to NBH-animals (Figure 3.4c).

mRNA levels of BiP were unchanged between NBH- and ME7-animals between 8-17 w.p.i., but were significantly increased in ME7-animals at 20 w.p.i. (Figure 3.4a). Similarly, mRNA levels of CHOP were unchanged between NBH- and ME7-animals between 8-17 w.p.i., although CHOP mRNA levels were significantly increased in ME7-animals at 20 w.p.i. (Figure 3.4d).

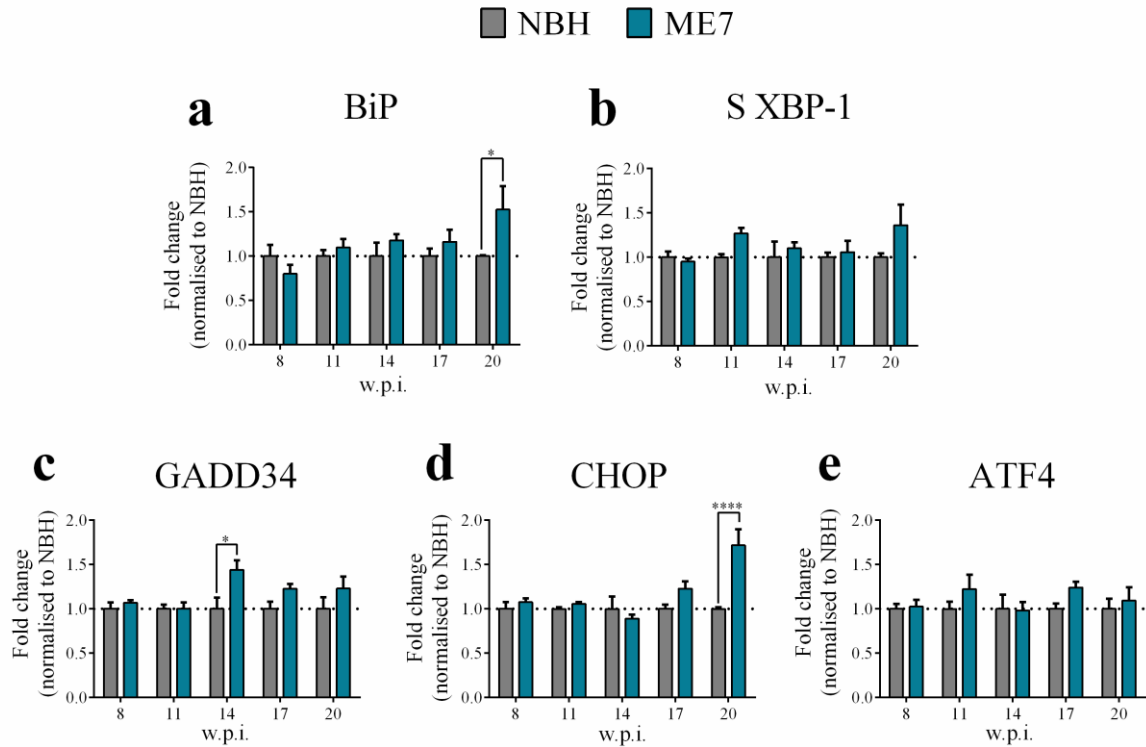


Figure 3.4 Quantification of UPR mRNAs in ME7-animals.

qPCR analysis for BiP (a), spliced XBP-1 (b), GADD34 (c), CHOP (d) and ATF4 (e) mRNAs in hippocampal homogenates from NBH- and ME7-animals killed at different time points (8-20 w.p.i.). Data in graphs represents normalised mean \pm SEM of the mRNA expression values (done in duplicate) from $n = 4$ animals per condition and time-point. Statistical test = repeated measures two-way ANOVA with Bonferroni post-analysis. Statistical significance relative to NBH: * $P \leq 0.05$, ** $P \leq 0.01$, and **** $P \leq 0.0001$. S, spliced and w.p.i., weeks post-inoculation.

3.4.3 Expression of UPR proteins in ME7-animals

Induction of the UPR proteins: BiP, eIF2 α -P, ATF4 and CHOP was confirmed by quantitative western blotting of HeLa cells treated with either tunicamycin or PEITC (appendix 6). Immunofluorescence staining also showed an induction of ATF4 protein in HeLa cells treated with tunicamycin (appendix 7). This shows that the reagents used are able to detect changes in these UPR proteins and provide a readout for a UPR. They also set a benchmark for the fold change typically seen under activation of a classic UPR. Immunoreactivity of the UPR proteins PERK-P, ATF4 and CHOP could not be detected in SDS extracted hippocampi from NBH- and ME7-animals (appendix 8). ATF4 immunoreactivity could also not be detected by immunohistochemistry (data not shown). BiP and eIF2 α -P protein were therefore used as the two main readouts of a UPR response at the protein level in ME7-animals.

Following the analysis of the expression of UPR mRNAs, levels of UPR proteins was investigated by quantitative western blotting for BiP and eIF2 α -P. Levels of BiP protein remained unchanged between NBH- and ME7-animals across disease progression (Figure 3. 5a-b). In addition, qualitative immunohistochemical staining for BiP revealed no distinct changes in BiP expression between NBH- and ME7-animals in the DG, CA3 and CA1 regions of the hippocampus at 13 and 21 w.p.i. (Figure 3.6).

Levels of eIF2 α -P (expected Mw: 38 kDa) were determined using two different eIF2 α -P antibodies (Table 2.4). Using both antibodies, the levels of eIF2 α -P did not change in ME7-animals at any stage during disease progression (Figure 3.5a, c and d). Quantification of the western blot shows that at 20 w.p.i. the ratio of eIF2 α -P:eIF2 α is reduced in ME7-animals compared to NBH-animals (Figure 3.5d). At 20 w.p.i. the eIF2 α -P band at 38 kDa appears as a double band when using the eIF2 α -P 1 antibody (Figure 3.5a). For this time-point both bands were quantified as eIF2 α -P immunoreactivity.

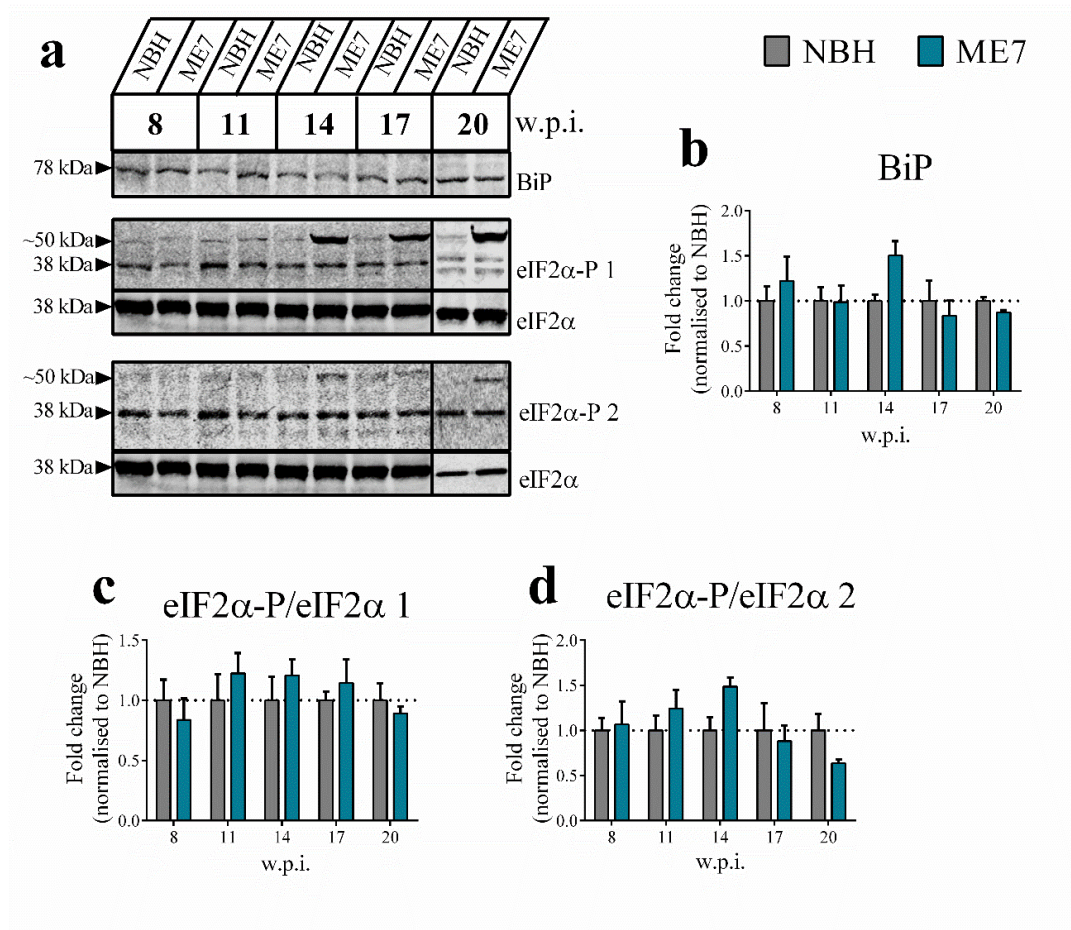


Figure 3.5 Quantification of UPR proteins in ME7-animals.

Representative western blotting (a) and related quantification for BiP (b), and eIF2α-P (Ser51) (c and d) in SDS extracted hippocampi from NBH- and ME7-animals killed at different time points (8-20 w.p.i.). Two different eIF2α-P antibodies were used to probe for eIF2α-P, denoted as 1 and 2. Data in graphs represents mean \pm SEM of the protein expression values from $n = 4$ animals per condition and time-point, except NBH- and ME7-animals at 20 w.p.i., where $n = 3$. Statistical test = repeated measures two-way ANOVA with Bonferroni post-analysis (8-17 w.p.i.) and unpaired Student's t -test, two-tails (20 w.p.i.). w.p.i., weeks post-inoculation.

BiP

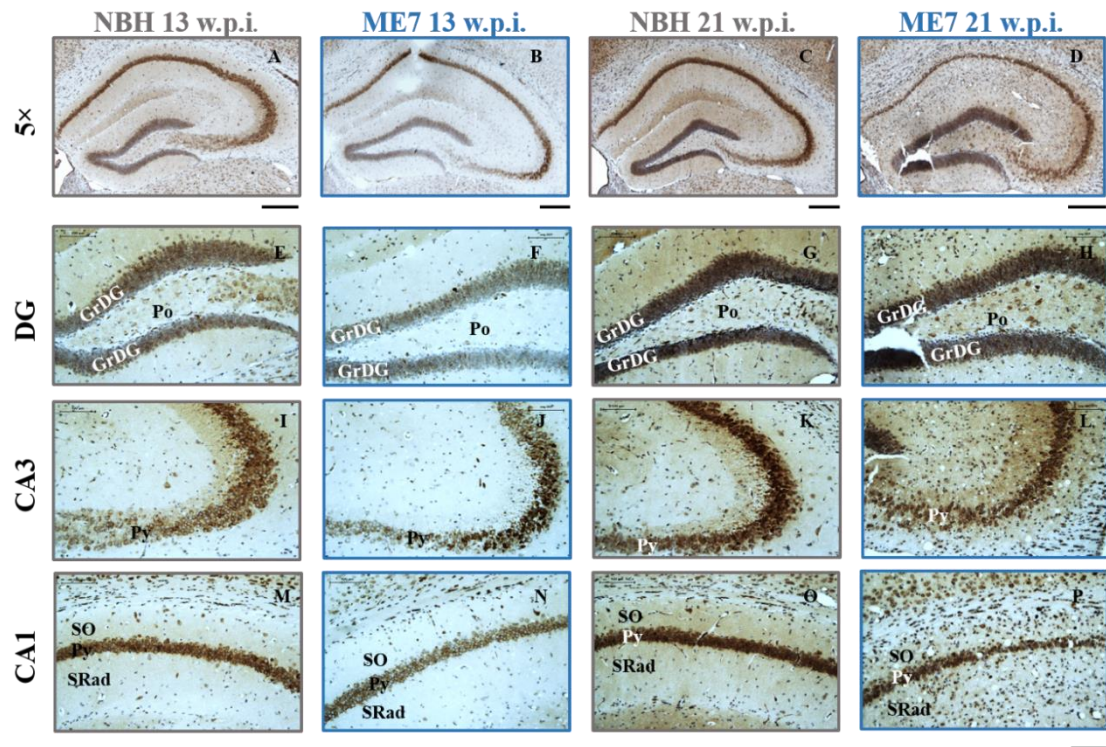


Figure 3.6 Immunohistochemical staining for BiP in ME7-animals.

Representative immunohistochemical staining for BiP in different regions of the hippocampus. Immunohistochemical staining was performed on NBH- and ME7-animals killed at 13 and 21 w.p.i. Scale bars for 5× images are indicated under each of the images (300 μm) and the scale bar for DG, CA3 and CA1 images is indicated under image P (100 μm). $n = 3$ animals per condition and time-point. CA1, Cornu Ammonis region 1; CA3, Cornu Ammonis region 3; DG, dentate gyrus; GrDG, granule cell layer of the DG; Po, polymorphic layer; Py, pyramidal layer; SO, stratum oriens; SRad, stratum radiatum and w.p.i., weeks post-inoculation. Staining performed by masters student, Matthew Cooper.

An additional band at ~50 kDa can be seen selectively from 14 w.p.i. in SDS extracted hippocampi from ME7-animal, when using the eIF2 α -P antibodies (Figure 3.5a). This band is more intense when using the eIF2 α -P 1 antibody. A band of similar size can also be seen in SDS extracted hippocampi from ME7-animals at end-stage disease, when run on an SDS-PAGE gel and coomassie stained (Figure 3.7a). A band with a molecular weight (Mw) corresponding to the additional immunoreactivity has been previously excised and subjected to *in situ* trypsin digestion and then analysed by liquid chromatography-mass spectrometry (Gray et al., 2006). This proteomic analysis identified the protein as a lower Mw cleaved fragment of GFAP (Gray et al., 2006).

SDS extracted hippocampi from NBH- and ME7-animals was western blotted for eIF2 α -P using both antibodies (1 and 2) in the presence or absence of an eIF2 α -P blocking peptide. This was done in parallel with HeLa cells which had been treated with DMSO (control) or PEITC (Cavell, 2012, Yeomans, 2013). PEITC treated HeLa cells acted as a positive control for this experiment. Levels of eIF2 α -P (38 kDa) are faint in both NBH- and ME7-animals, using both eIF2 α -P antibodies (Figure 3.7b and c). However, as expected levels of eIF2 α -P are increased in PEITC treated HeLa cells compared to DMSO treated HeLa cells (Figure 3.7b and c). The additional band at ~50 kDa is induced in ME7-animals using both eIF2 α -P antibodies, although this is more prominent when using the eIF2 α -P 1 antibody (Figure 3.7b and c). Incubation of the nitrocellulose membranes with the eIF2 α -P 1 or 2 antibody, which had been pre-treated with the eIF2 α -P blocking peptide, resulted in the eIF2 α -P at 38 kDa disappearing in all the samples (Figure 3.7b and c). The band at ~50 kDa seen in ME7-animals using the eIF2 α -P antibodies was reduced to a comparable immunoreactivity seen when using secondary antibody only as a control (Figure 3.7b, c and d).

The immunoreactive band at ~50 kDa seen when using the eIF2 α -P antibodies is approximately the same size as the GFAP protein (Figure 3.7d). The additional band at ~50 kDa seen using the eIF2 α -P antibodies could be present because of a cross-reactivity of the eIF2 α -P antibodies with GFAP or a GFAP cleavage product, which are both selectively induced in ME7-animals from 14 w.p.i. (Figure 3.2a). Immunohistochemical staining for eIF2 α -P (using the eIF2 α -P 1 antibody) in NBH- and ME7-animals at 21 w.p.i. shows that astrocytes are distinctly labelled in the ME7-animals, supporting the idea that the eIF2 α -P 1 antibody cross reacts with GFAP or a GFAP cleavage product (Figure 3.8 A-E). Incubation of the eIF2 α -P 1 antibody

with the eIF2 α -P blocking peptide prior to exposure to the mouse brain sections eliminated all staining including that seen in astrocytes (Figure 3. 8 F-I). Caution must therefore be aired when interpreting western blot or immunohistochemistry data using this eIF2 α -P antibody, in disease models where astrogliosis is a prominent feature.

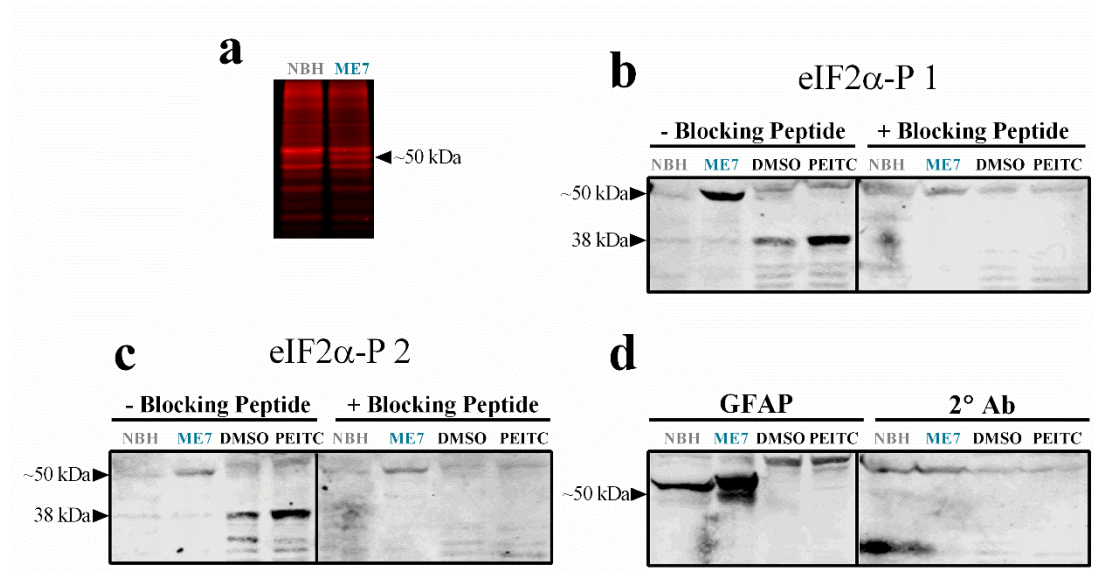


Figure 3.7 Cross-reactivity of the two eIF2 α -P antibodies with a protein of ~50 kDa in ME7-animals.

Coomassie stain of SDS extracted hippocampi from NBH- and ME7-animals sacrificed at 20 w.p.i. (a). Western blotting for eIF2 α -P (Ser51) (b and c) and GFAP (d) in the same NBH- and ME7-animals as (a) and from HeLa cells treated with DMSO or PEITC (+ve control). Two different eIF2 α -P antibodies were used to probe for eIF2 α -P, denoted as 1 and 2. Western blots for eIF2 α -P were performed in the absence or presence of an eIF2 α -P blocking peptide. A secondary antibody only control was used to highlight background immunoreactivity (d). $n = 1$ animal or HeLa cell preparation per condition. +ve, positive and w.p.i., weeks post-inoculation.

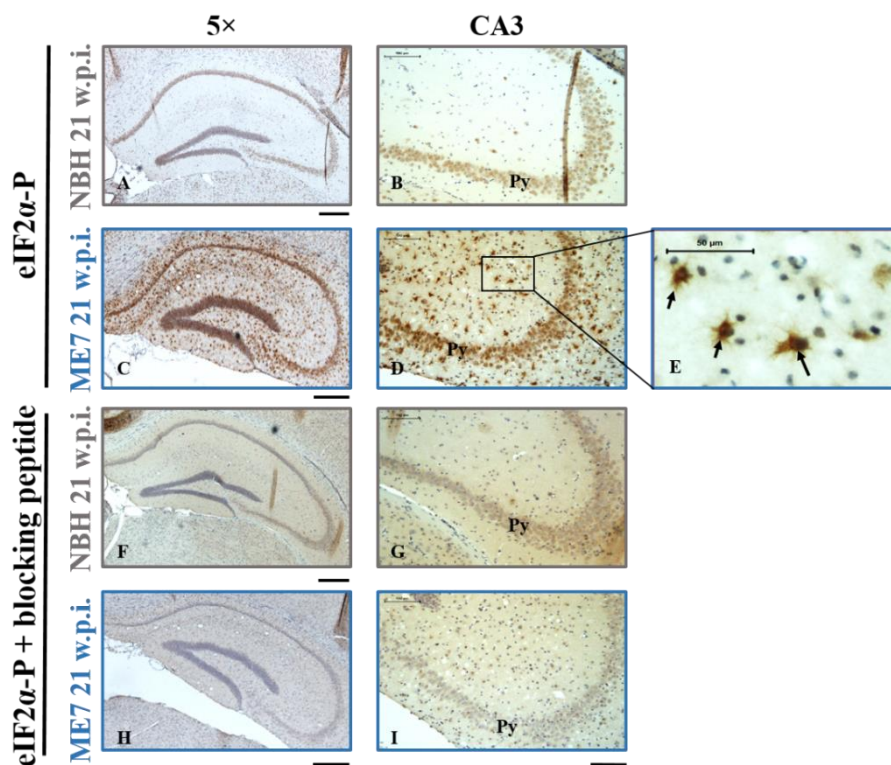


Figure 3.8 Expression of eIF2 α -P in astrocytes of ME7-animals, as a consequence of eIF2 α -P 1 antibody cross-reactivity.

Immunohistochemical staining for eIF2 α -P (Ser51) in a NBH- and ME7-animal at 21 w.p.i., using the eIF2 α -P 1 antibody in the absence (A-E) or presence (F-I) of an eIF2 α -P blocking peptide. Magnified image (E) shows labelled astrocytes. Scale bars for 5x images (300 μ m) are indicated under each of the images, scale bar for CA3 images (100 μ m) is indicated under image I and scale bar for magnified image (E) (50 μ m) is shown on image. CA3, Cornu Ammonis region 3; Py, pyramidal layer and w.p.i., weeks post-inoculation. Staining performed by master's student, Matthew Cooper.

Although the levels of eIF2 α -P did not change between NBH- and ME7-animals, the phosphorylation state of 4EBP1 was investigated as an additional readout and partial indicator of how translationally active cells of the hippocampus are (Figure 3. 9a, b and c). The three bands of total 4EBP1 represent different phosphorylation states. The upper hyperphosphorylated (Thr37, Thr46, Ser65 and Thr70) form of 4EBP1 (upper band) would not be bound to the translational protein eIF4E, whereas the phosphorylated (Thr37 and Thr46) form of 4EBP1 (middle band) and hypophosphorylated form of 4EBP1 (lower band) would be bound to eIF4E (section 1.7.1.1.3). Therefore, a lower ratio of hyperphosphorylated: phosphorylated/hypophosphorylated 4EBP1 would partially suggest lower levels of translation. Ratios of the hyperphosphorylated: phosphorylated/hypophosphorylated 4EBP1 revealed no significant change in the phosphorylation status of 4EBP1 between NBH- and ME7-animals across disease progression (Figure 3.9a, b and c). This result supports the evidence that suggests that cells in the hippocampus are still translationally active.

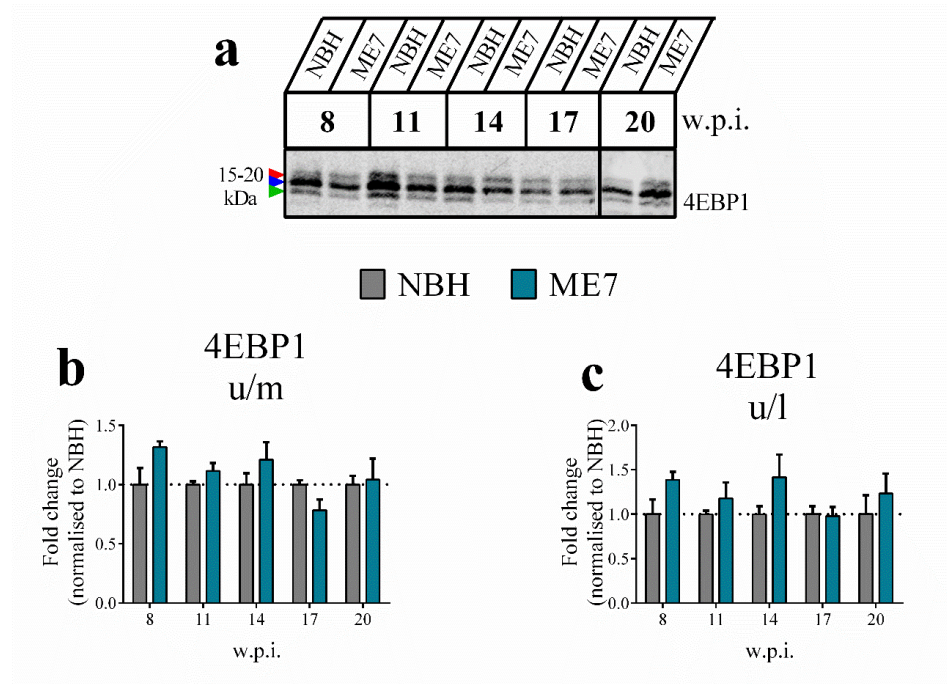


Figure 3.9 Quantification of the phosphorylation state of total 4EBP1 protein in ME7-animals.

Representative western blotting (a) and related quantification of total 4EBP1 (b-c) in SDS extracted hippocampi from NBH- and ME7-animals killed at different time-points (8-20 w.p.i.). Coloured arrowheads (a) mark upper (red) hyperphosphorylated (Thr37, Thr46, Ser65 and Thr7), middle (blue) phosphorylated (Thr37 and Thr46) and lower hypophosphorylated 4EBP1 (green). Data in bar graphs represents mean \pm SEM of the protein expression values from $n = 4$ animals per condition and time-point, except NBH- and ME7-animals at 20 w.p.i., where $n = 2$ and 3, respectively. Statistical test = repeated measures two-way ANOVA with Bonferroni post-analysis (8-17 w.p.i.) and unpaired Student's t -test, two-tails (20 w.p.i.). l, lower 4EBP1 band (hypophosphorylated); m, middle 4EBP1 band (phosphorylated); u, upper 4EBP1 band (hyperphosphorylated) and w.p.i., weeks post-inoculation.

Both qPCR and quantitative western blotting revealed little evidence for a UPR at the mRNA or protein level. A recent publication has shown that the ER localised molecule SIL1 (an adenine nucleotide exchange factor for BiP) protects against ER stress in motoneurons (Filezac de L'Etang et al., 2015). Levels of SIL1 mRNA were investigated in NBH- and ME7-animals between 14-20 w.p.i. to determine if SIL1 mRNA was increased in ME7-animals. Earlier time-points were not examined because significant changes in molecular responses were only seen between 14-20 w.p.i. (see below). qPCR analysis revealed that the levels of SIL1 mRNA were unchanged between NBH- and ME7-animals at both 14 and 20 w.p.i. (Figure 3.10). However, at 17 w.p.i. levels of SIL1 mRNA were significantly increased in ME7-animals (Figure 3.10). This result adds additional support to the observation that there is little evidence for a UPR in ME7-animals.

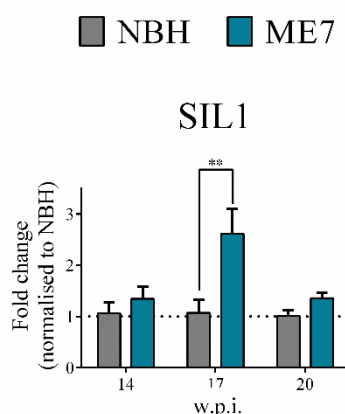


Figure 3.10 Quantification of SIL1 mRNA in ME7-animals.

qPCR analysis for SIL1 mRNA in hippocampal homogenates from NBH- and ME7-animals killed at different time-points (8-20 w.p.i.). Data in graphs represents mean \pm SEM of the mRNA expression values from $n = 4$ animals per condition and time-point. Statistical test = repeated measures two-way ANOVA with Bonferroni post-analysis. Statistical significance relative to NBH: ** $P \leq 0.01$. w.p.i., week's post-inoculation.

3.4.4 Expression of other stress-related response mRNAs in ME7-animals

The UPR is a response to ER stress, a specific type of intracellular stress. However, a large number of other molecules have been shown to be activated in response to other diverse cellular dysfunctions or stressors. Some of these molecules have been investigated in this thesis. These other stress-response related molecules have been grouped as immediate early genes, activity-induced immediate early genes and a cellular physiological and environmental damage stress sensor. These stress reporter molecules were selected based on their association with different models of neuronal dysfunction and neurodegeneration (section 1.7.4).

3.4.4.1 Expression of immediate early gene mRNAs in ME7-animals

Levels of ATF3 mRNA progressively increased in ME7-animals from 11 w.p.i. and this reached a statistical significance from ≥ 14 w.p.i. (Figure 3.11a). In contrast, c-Jun mRNA levels were unchanged between NBH- and ME7-animals between 8-17 w.p.i. (Figure 3.11b). However, at 20 w.p.i. levels of c-Jun mRNA were significantly increased in ME7-animals compared to NBH-animals (Figure 3.11b). Levels of c-Fos mRNA were not significantly different between NBH- and ME7-animals across the disease course, except for at 14 w.p.i. when levels of c-Fos mRNA were significantly increased in ME7-animals (Figure 3.11c).

3.4.4.2 Expression of activity-induced immediate early gene mRNAs in ME7-animals

Arc mRNA levels were not significantly different between NBH- and ME7-animals at any of the time-points investigated (Figure 3.12a). Similarly, Levels of Homer1a mRNA were unchanged between NBH- and ME7-animals across the ME7 disease time course, except for at 17 w.p.i., when levels of Homer1a were significantly increased in ME7-animals compared to NBH-animals (Figure 3.12b).

3.4.4.3 mRNA expression of the cellular physiological and environmental damage stress sensor, GADD45a, in ME7-animals

Like ATF3, levels of GADD45a mRNA progressively increased in ME7-animals and this occurred from 14 w.p.i. and this induction reached significance from ≥ 17 w.p.i. (Figure 3.13).

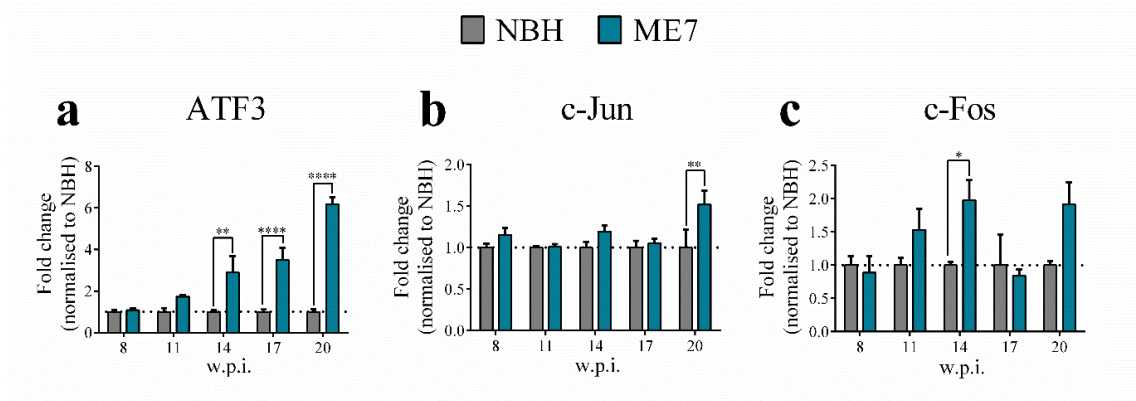


Figure 3.11 Quantification of immediate early gene mRNAs in ME7-animals.

qPCR analysis for ATF3 (a), c-Jun (b) and c-Fos (c) mRNAs in hippocampal homogenates from NBH- and ME7-animals killed at different time-points (8-20 w.p.i.). Data in graphs represents mean \pm SEM of the mRNA expression values from $n = 4$ animals per condition and time-point, except for c-Fos where NBH 8, 11 and 20 w.p.i. and ME7 8 w.p.i. represents $n = 3$ animals per condition and time-point. Statistical test = repeated measures two-way ANOVA with Bonferroni post-analysis. Statistical significance relative to NBH: * $P \leq 0.05$, ** $P \leq 0.01$ and **** $P \leq 0.0001$. w.p.i., weeks post-inoculation.

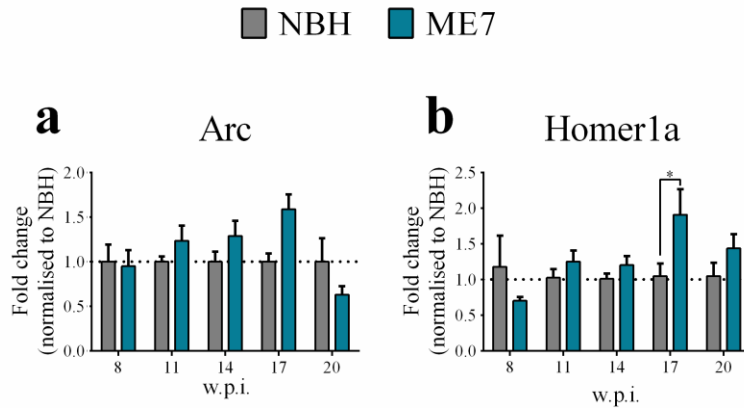


Figure 3.12 Quantification of activity-induced immediate early gene mRNAs in ME7-animals.

qPCR analysis for Arc (a) and Homer1a (b) mRNAs in hippocampal homogenates from NBH- and ME7-animals killed at different time points (8-20 w.p.i.). Data in graphs represents mean \pm SEM of the mRNA expression values from $n = 4$ animals per condition and time-point. Statistical test = repeated measures two-way ANOVA with Bonferroni post-analysis. Statistical significance relative to NBH: * $P \leq 0.05$. w.p.i., weeks post-inoculation.

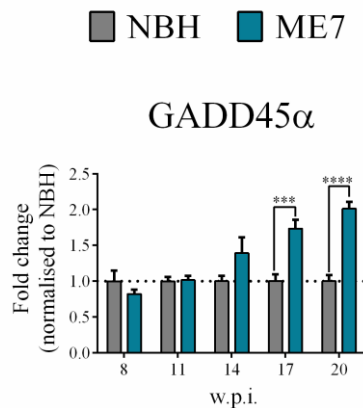


Figure 3.13 Quantification of the mRNA levels of the cellular physiological and environmental damage stress sensor, GADD45 α , in ME7-animals.

qPCR analysis for GADD45 α (a) mRNA in hippocampal homogenates from NBH- and ME7-animals killed at different time-points (8-20 w.p.i.). Data in graphs represents mean \pm SEM of the mRNA expression values from $n = 4$ animals per condition and time-point. Statistical test = repeated measures two-way ANOVA with Bonferroni post-analysis. Statistical significance relative to NBH: *** $P \leq 0.001$ and **** $P \leq 0.0001$. w.p.i., weeks post-inoculation.

3.4.5 Expression of other stress-related response proteins in ME7-animals

3.4.5.1 Western blotting

3.4.5.1.1 Expression of immediate early gene proteins in ME7-animals

ATF3, c-Jun and c-Fos protein levels were determined by quantitative western blotting of SDS extracted hippocampi. Levels of ATF3 protein were not significantly different between NBH- and ME7- animals at 8-17 w.p.i. (Figure 3.14a and b), despite increases in ATF3 mRNA in ME7-animals between 14-20 w.p.i. (Figure 3.11a). Immunoreactivity for ATF3 using quantitative western blotting in NBH- and ME7-animals could not be detected at 20 w.p.i. Similar to ATF3, c-Jun and c-Fos protein levels were not significantly different between NBH- and ME7-animals at any of the time-points investigated using quantitative western blotting (Figure 3.14a, c and d).

3.4.5.1.2 Protein expression of the cellular physiological and environmental damage stress sensor, GADD45 α , in ME7-animals

Levels of GADD45 α protein were not different between NBH- and ME7-animals, except for at 20 w.p.i., when levels of GADD45 α protein were significantly increased in ME7-animals (Figure 3.14a and e).

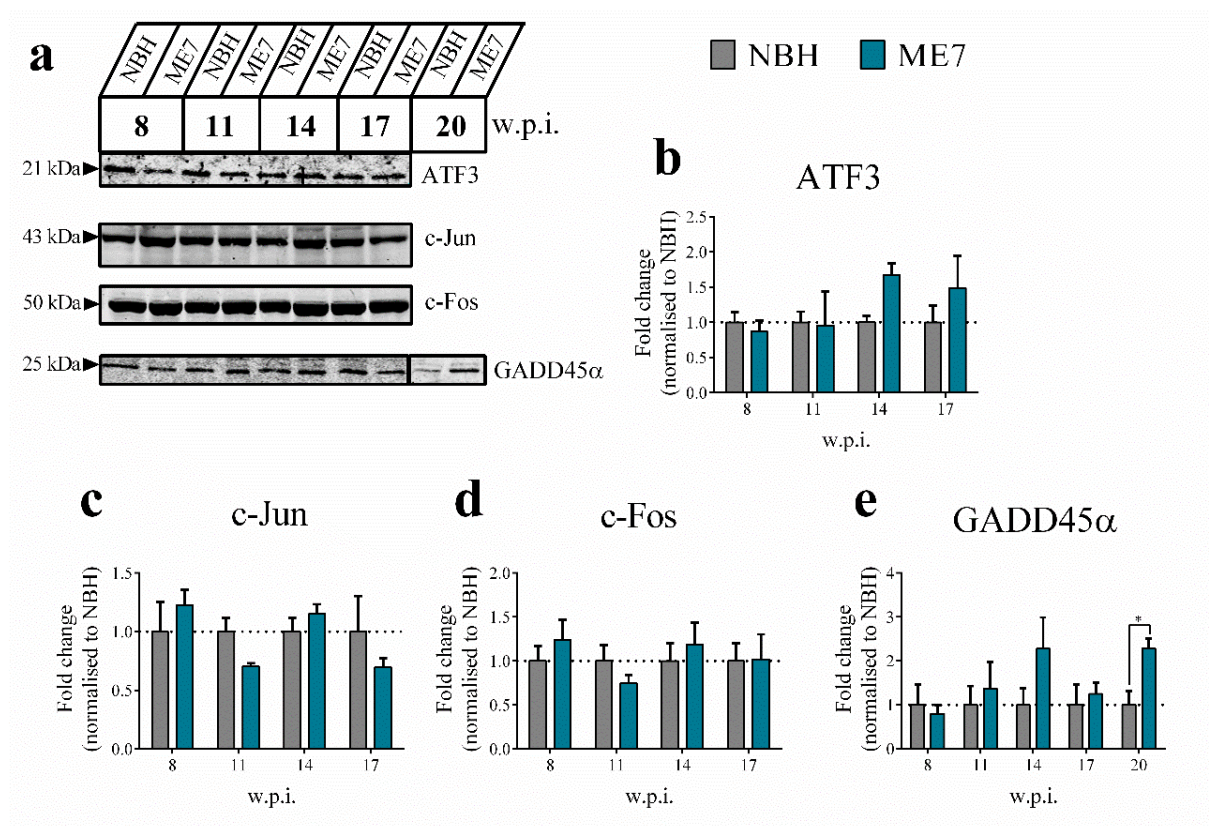


Figure 3.14 Quantification of immediate early gene proteins and the cellular physiological and environmental damage stress sensor protein, GADD45α, in ME7-animals.

Representative western blotting (a) and related quantification for ATF3 (b), c-Jun (c), c-Fos (d) and GADD45α (e) proteins in SDS extracted hippocampi from NBH- and ME7-animals killed at different time-points (8-20 w.p.i.). Data in graphs represents mean \pm SEM of the protein expression values from $n = 4$ animals per condition and time-point, except GADD45α at 20 w.p.i. and c-Jun and c-Fos (8-17 w.p.i.), where $n = 3$ animals per condition and time-point. Statistical tests = repeated measures two-way ANOVA with Bonferroni post-analysis was used for NBH- and ME7-animals between 8-17 w.p.i. and an Unpaired Student's t -test, two tails was used for NBH- and ME7-animals at 20 w.p.i.. Statistical significance relative to NBH: * $P \leq 0.05$. w.p.i., weeks post-inoculation.

3.4.5.2 Immunohistochemistry

Although GADD45 α protein was the only stress-related response protein increased in ME7-animals, as shown by quantitative western blotting (Figure 3.14), qPCR showed that the levels of ATF3, c-Jun, c-Fos and GADD45 α mRNAs were significantly increased in ME7-animals (Figure 3.11 and 3.13). Immunohistochemistry was performed to determine if increases in the levels of any of these proteins could be seen in specific neurons. This might explain why changes in the levels of these proteins was not detected in whole hippocampal tissue, where changes in discrete regions are likely to not be detected.

3.4.5.2.1 Cell loss and vacuolation in ME7-animals

Cell loss and vacuolation was confirmed in end-stage (21 w.p.i.) ME7-animals prior to assessing the levels of ATF3, c-Jun, c-Fos and GADD45 α protein expression. Figure 3.15 shows that ME7-animals at 21 w.p.i. had CA1 cell loss, as evidenced by the thin pyramidal layer of CA1 and vacuolation seen in the brain sections of the ME7-animals (Figure 3.15).

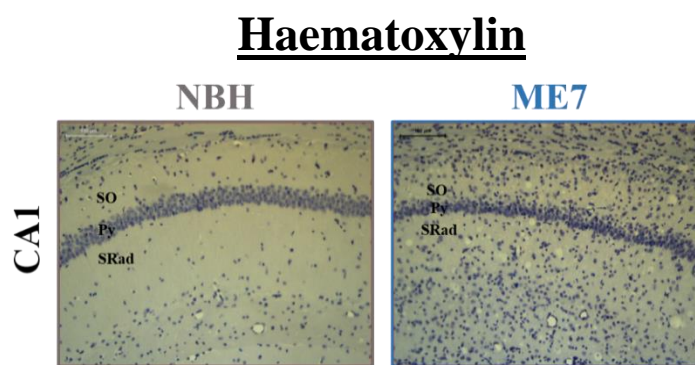


Figure 3.15 Haematoxylin staining of ME7-animals.

Representative haematoxylin staining of NBH- and ME7-animals hippocampi at 21 w.p.i. Scale bars for images are indicated under the ME7 image (100 μ m). $n = 3$ animals per condition. CA1, Cornu Ammonis region 1; Py; pyramidal layer; SO, stratum oriens; SRad, stratum radiatum and w.p.i., weeks post-inoculation. Staining performed by masters student, Matthew Cooper.

3.4.5.2.2 Expression of immediate early gene proteins in ME7-animals

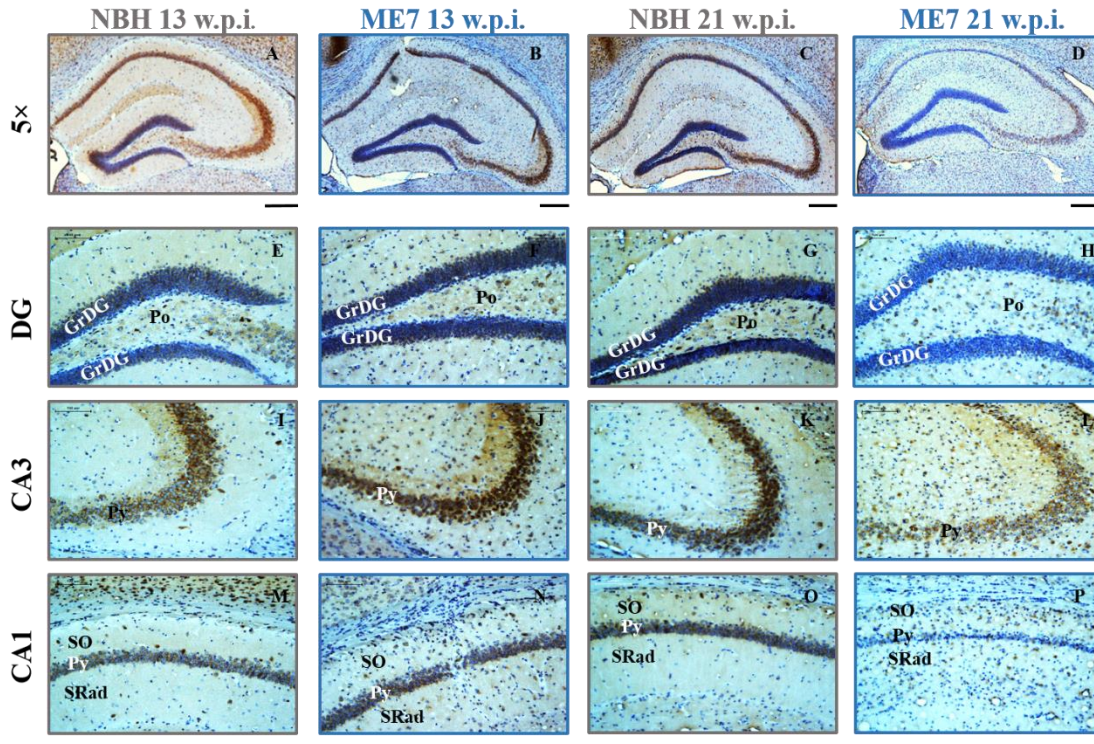
Restricted positive staining for ATF3 could be seen in the DG and CA1 regions of the hippocampus for both NBH- and ME7-animals (Figure 3.16a E-H and M-P). ATF3 staining could be seen in the CA3 region in both NBH- and ME7-animals at 13 w.p.i. (Figure 3.16a I-L) and quantitatively the expression of ATF3 staining was significantly increased in the pyramidal layer of the CA3 in ME7-animals compared to NBH-animals (Figure 3.16b).

c-Jun is constitutively expressed at a high level in nearly all neurons of the granule cell layer of the DG in NBH- and ME7-animals at 13 and 21 w.p.i. (Figure 3.17a E-H). It is also expressed in neurons of the pyramidal layer of CA3 and CA1. Qualitatively and quantitatively c-Jun staining is progressively increased in neurons of the pyramidal layer of CA3 and CA1 in ME7-animals from 13 w.p.i. (Figure 3.17a I-P and b and c). Statistically, however, c-Jun is only significantly increased in the pyramidal layer of CA1 in ME7-animals at 21 w.p.i. compared to NBH-animals (Figure 3.17c).

c-Fos was mainly expressed in neurons of the pyramidal layer of CA3 and CA1 in NBH-animals (Figure 3.18a I, K, M and O). c-Fos staining was increased in regions outside of the granule cell layer of the DG, but was more evidently increased in regions outside of the pyramidal layer of CA3 and CA1 in ME7-animals from 13 w.p.i. (Figure 3.18a E-P). However, statistically this was not significantly different between NBH- and ME7-animals at either 13 or 21 w.p.i. (Figure 3.18b and c).

ATF3

a



b

CA3 - 13 w.p.i.

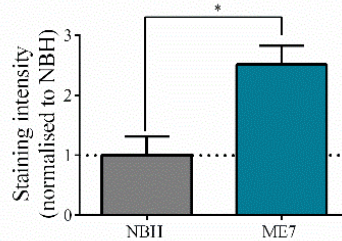


Figure 3.16 Immunohistochemical staining for ATF3 in ME7-animals.

Representative immunohistochemical staining (a) and related quantification of the staining intensity (b) for ATF3 in different regions of the hippocampus. Immunohistochemical staining was performed on NBH- and ME7-animals killed at 13 and 21 w.p.i. $n = 3$ animals per condition and time-point for immunohistochemical staining. Scale bars for 5x images are indicated under each of the images (300 μm) and the scale bar for DG, CA3 and CA1 images is indicated under image P (100 μm). Data in graphs represents mean \pm SEM of the staining intensity for ATF3 in the pyramidal layer of CA3. n is the same as in (a). Statistical test = Unpaired Student's t -test, two-tails. Statistical significance relative to NBH: $*P \leq 0.05$. CA1, Cornu Ammonis region 1; CA3, Cornu Ammonis region 3; DG, dentate gyrus; GrDG, granule cell layer of the DG; Po, polymorphic layer; Py, pyramidal layer; SO, stratum oriens; SRad,

stratum radiatum and w.p.i., weeks post-inoculation. Staining performed by masters student, Matthew Cooper.

c-Jun

a

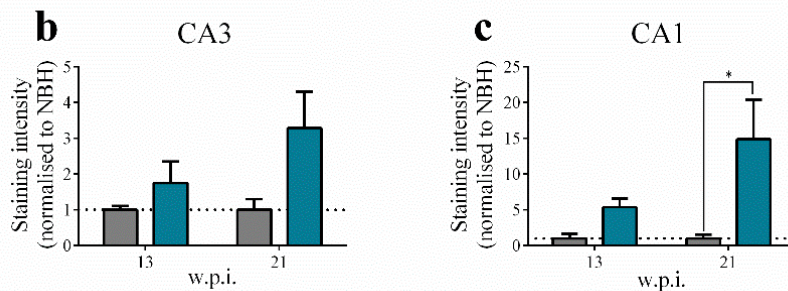
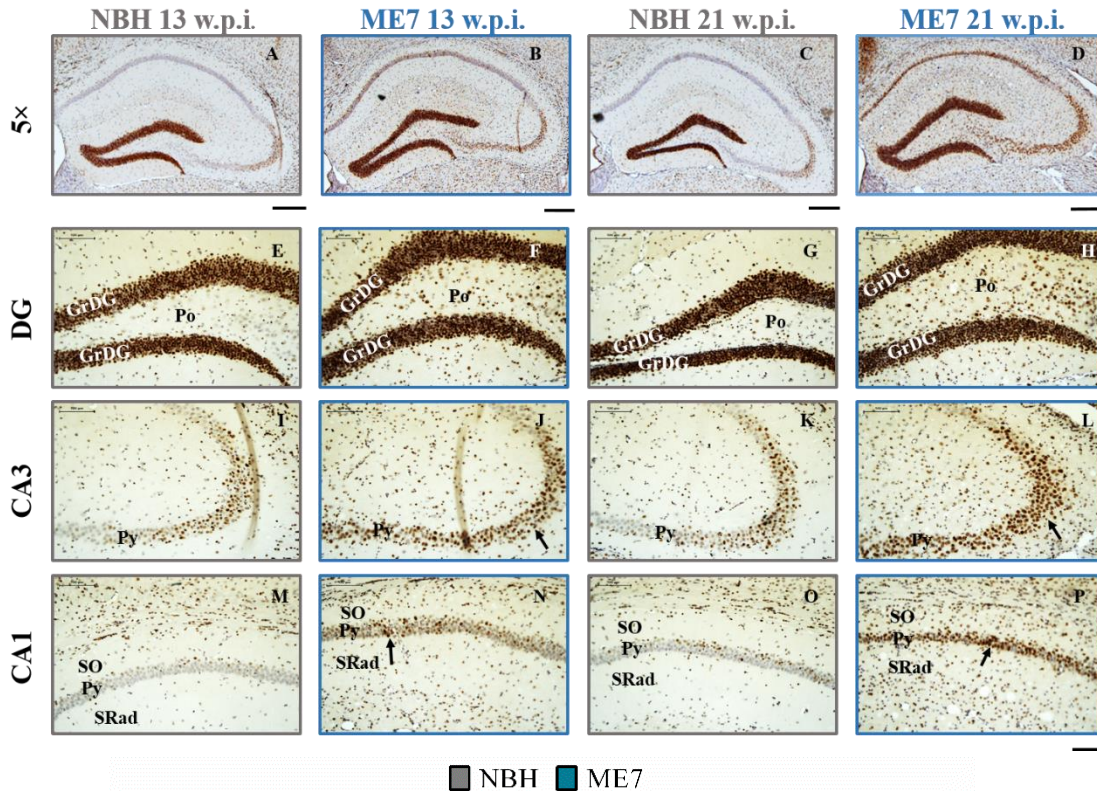


Figure 3.17 Immunohistochemical staining for c-Jun in ME7-animals.

Representative immunohistochemical staining (a) and related quantification of the staining intensity (b-c) for c-Jun in different regions of the hippocampus. Immunohistochemical staining was performed on NBH- and ME7-animals killed at 13 and 21 w.p.i. $n = 3$ animals per condition and time-point for immunohistochemical staining. Scale bars for 5x images are indicated under each of the images (300 μm) and the scale bar for DG, CA3 and CA1 images is indicated under image P (100 μm). Black arrows point to distinct increased staining in neurons of the pyramidal layer. Data in graphs represents mean \pm SEM of the staining intensity for c-Jun in the pyramidal layer of CA3 and CA1. n is the same as in (a). Statistical test = repeated measures two-way ANOVA with Bonferroni post-analysis. Statistical significance relative to NBH: $*P \leq 0.05$. CA1, Cornu Ammonis region 1; CA3, Cornu Ammonis region 3; DG, dentate

gyrus; GrDG, granule cell layer of the DG; Po, polymorphic layer; Py, pyramidal layer; SO, stratum oriens; SRad, stratum radiatum and w.p.i., weeks post-inoculation. Staining performed by masters student, Matthew Cooper.

c-Fos

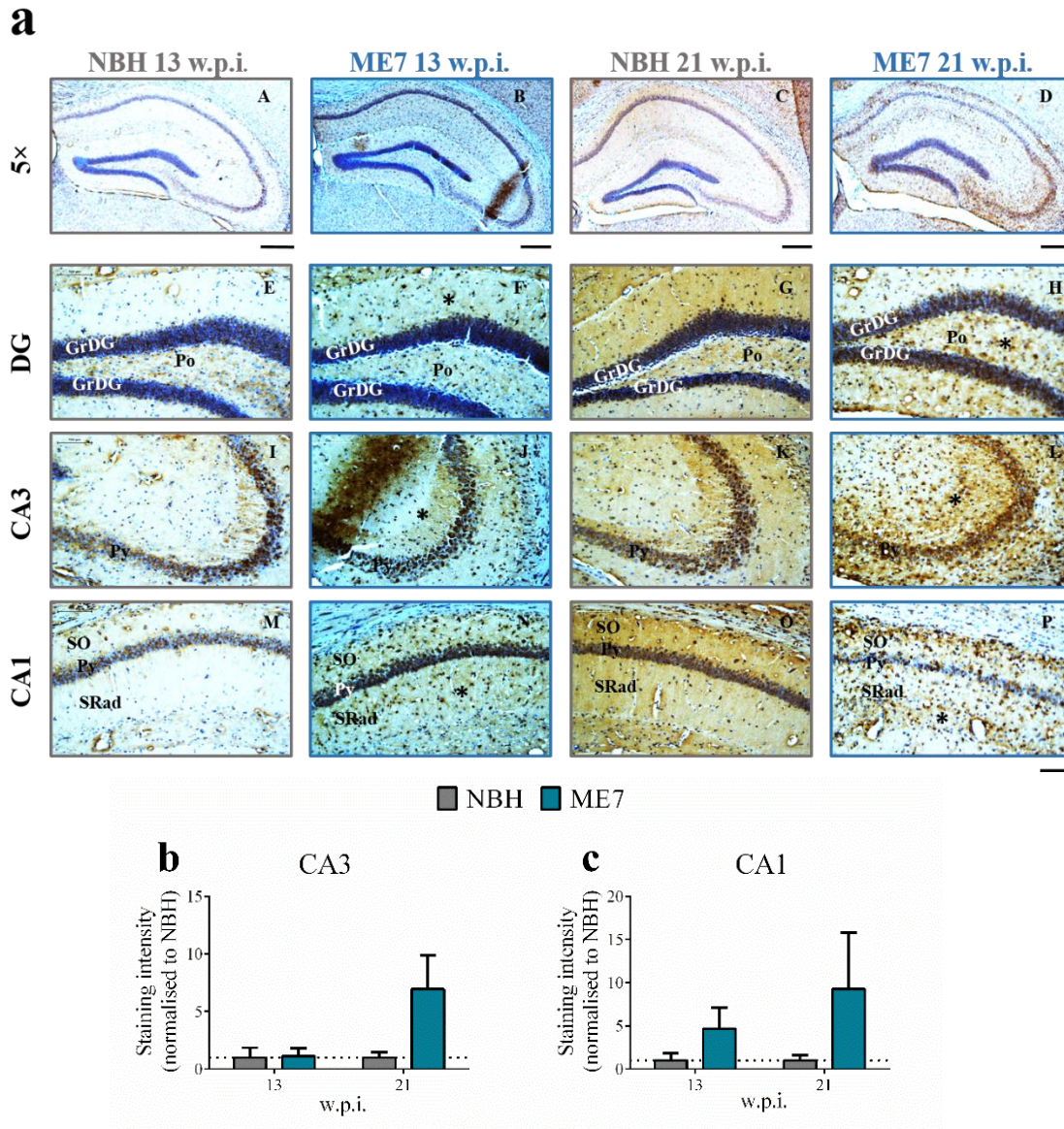


Figure 3.18 Immunohistochemical staining for c-Fos in ME7-animals.

Representative immunohistochemical staining (a) and related quantification of the staining intensity (b-c) for c-Fos in different regions of the hippocampus. Immunohistochemical staining was performed on NBH- and ME7-animals killed at 13 and 21 w.p.i. $n = 3$ animals per condition and time-point for immunohistochemical staining. Scale bars for 5 \times images are indicated under each of the images (300 μ m) and the scale bar for DG, CA3 and CA1 images is indicated under image P (100 μ m). Asterisks highlight regions of increased staining outside of the granule cell layer of the DG and pyramidal layer of CA3 and CA1. Data in graphs represents mean \pm SEM of the staining intensity for c-Fos in the CA3 and CA1 region. n is the same as in (a). Statistical test = repeated measures two-way ANOVA with Bonferroni post-analysis.

CA1, Cornu Ammonis region 1; CA3, Cornu Ammonis region 3; DG, dentate gyrus; GrDG, granule cell layer of the DG; Po, polymorphic layer; Py, pyramidal layer; SO, stratum oriens; SRad, stratum radiatum and w.p.i., weeks post-inoculation. Staining performed by masters student, Matthew Cooper.

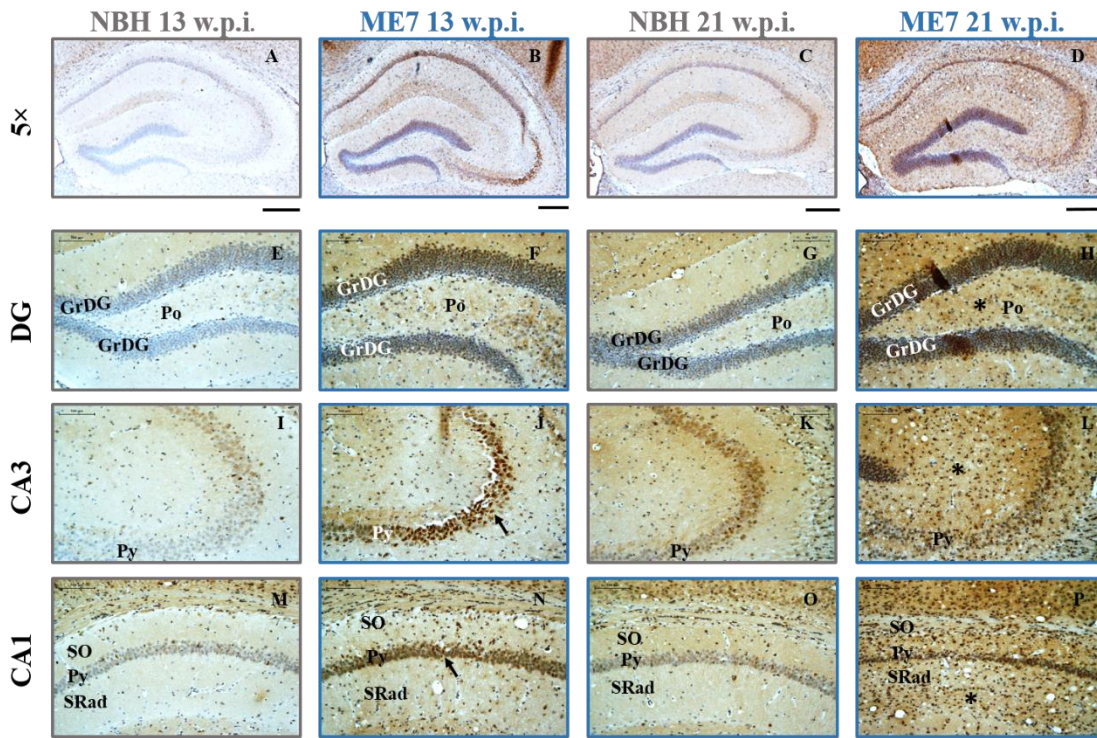
3.4.5.2.3 Expression of the cellular physiological and environmental damage stress sensor, GADD45 α , in ME7-animals

GADD45 α was expressed at low levels in the DG and CA1 regions of the hippocampus in NBH-animals at 13 and 21 w.p.i. (Figure 3.19a E, G, M and O). More abundant staining was seen in the CA3 pyramidal layer of NBH-animals (Figure 3.19a I and K). GADD45 α expression was increased in the granule cell layer of DG in ME7-animals at 13 w.p.i. but this was qualitatively more obvious in the pyramidal layers of CA3 and CA1 (Figure 3.19a J and N). However, quantification of the staining intensity for GADD45 α showed no statistical significance between NBH- and ME7-animals at 13 w.p.i (Figure 3.19b and d).

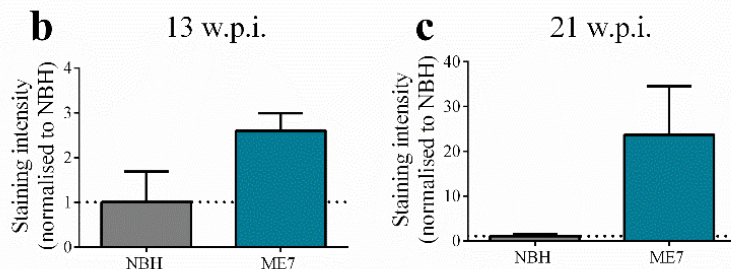
Qualitatively the staining intensity for GADD45 α was increased in ME7-animals at 21 w.p.i. in all regions but most apparent in the CA3 and CA1. However, unlike at 13 w.p.i. when this seemed confined to the pyramidal layer of those regions, staining of GADD45 α could also be seen in regions outside of the granule cell layer of the DG and pyramidal layer of CA3 and CA1 (Figure 3.19a H, L and P). However, quantification of the staining intensity for GADD45 α in CA3 and CA1 showed there was no significant increase in ME7-animals at 21 w.p.i. (Figure 3.19c and e).

GADD45 α

a



CA3



CA1

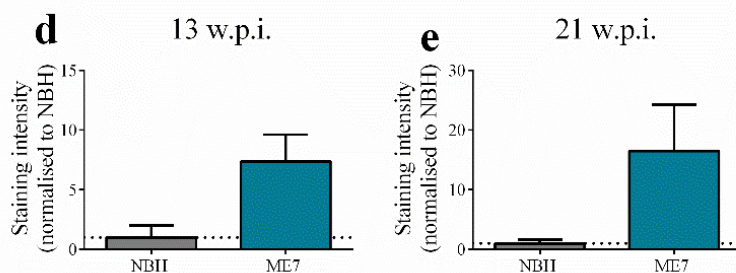


Figure 3.19 Immunohistochemical staining for GADD45 α in ME7-animals.

Representative immunohistochemical staining (a) and related quantification of the staining intensity (b-e) for GADD45 α in different regions of the hippocampus. Immunohistological staining was performed on NBH- and ME7-animals killed at 13 and

21 w.p.i. $n = 3$ animals per condition and time-point for immunohistochemical staining. Scale bars for 5x images are indicated under each of the images (300 μm) and the scale bar for DG, CA3 and CA1 images is indicated under image P (100 μm). Black arrows highlight distinct increased staining in neurons of the pyramidal layer and asterisks illustrate increased staining outside of the granule cell layer of the DG and pyramidal layer of CA3 and CA1. Data in graphs represents mean \pm SEM of the staining intensity for GADD45 α in the pyramidal layer of CA3 and CA1 (13 w.p.i.) and the entire CA3 and CA1 region (21 w.p.i.). n is the same as in (a). Statistical test = Unpaired Student's t -test, two-tails. CA1, Cornu Ammonis region 1; CA3, Cornu Ammonis region 3; DG, dentate gyrus; GrDG, granule cell layer of the DG; Po, polymorphic layer; Py, pyramidal layer; SO, stratum oriens; SRad, stratum radiatum and w.p.i., weeks post-inoculation. Staining performed by masters student, Matthew Cooper.

3.5 Discussion

The transmission of scrapie to mice in 1961 provided an *in vivo* laboratory model that could be used to study the neuropathology of prion disease (Chandler, 1961). ME7-infected brain homogenate is administered into the dorsal hippocampus, a region of the brain with well-defined neuroanatomy (Betmouni et al, 1996). The sequence of disease-associated events which are characteristic of ME7 prion disease include the deposition of PrP^{Sc}, the appearance of hypertrophied astrocytes, microglia proliferation and activation, which is then shortly followed by synapse loss in the stratum radiatum of the hippocampus (Cunningham et al., 2003, Gray et al., 2009). Neuronal loss is seen towards the end-stages of disease (Cunningham et al., 2003). The predictable manner in which pathology evolves enables a detailed investigation of molecular changes during disease progression.

In the ME7 model, a combination of western blotting, immunohistochemistry and electron microscopy, has been used to study synapse loss in ME7-animals (Cunningham et al., 2003, Gray et al., 2009, Sisková et al., 2009). Recently further resolution of the topology of synapse loss has been obtained using BDA tracing of CA3 pyramidal neurons (Al-Malki, 2012). Synapse bouton loss along the CA3 Schaffer collateral axons occurs progressively from 13 w.p.i. in ME7-animals. In addition, the appearance of axonal swellings and signs of axonal alterations are also apparent at 13 w.p.i. A reduced number of dendritic spines, reduced dendritic arborization and length was also seen on

the CA3 pyramidal neurons of ME7-animals as early as 13 w.p.i. (Al-Malki, 2012). Dendritic swellings could be seen at this time but changes in the size and morphology of the cell body was not seen until 16 w.p.i. in ME7-animals.

In this chapter, the ME7 prion model has been used to investigate if molecular changes, detected at either the mRNA and/or protein level might correlate with the morphological alternations observed during disease progression (Al-Malki, 2012). A combination of qPCR, quantitative western blotting and immunohistochemistry has been used to analyse the UPR and other stress-related response molecules in the hippocampus of ME7-animals. Both the UPR and other stress-related response molecules have been implicated in chronic neurodegenerative disease models and neuronal injury models (chapter 1).

3.5.1 PrP and GFAP protein expression is increased in ME7-animals at a time when synapse loss is occurring

Levels of GFAP protein are progressively increased in ME7-animals at the same time as when increases in total PrP protein expression were seen (Figure 3.2a, b and f and 3.3 A-F) in agreement with previous observations (Asuni et al., 2014). The presence of GFAP cleavage products are also apparent in ME7-animals (Figure 3.2a) as reported previously (Gray et al., 2006). Disorganisation of staining for the synaptic vesicle protein, synaptophysin, is seen at the same time as increases in the expression in total PrP and GFAP protein in ME7-animals (Figure 3.3 G-J). As disease progresses, staining for synaptophysin becomes increasingly disorganised in ME7-animals, in line with previous observations (Cunningham et al., 2003). The combination of increased PrP and GFAP expression and disorganised synaptic staining shows that the tissue used to investigate molecular stress responses has prion disease pathology.

3.5.2 Limited evidence for a UPR in ME7-animals

3.5.2.1 Expression of UPR mRNAs

qPCR analysis of UPR mRNAs failed to show a robust UPR in ME7-animals between 8-17 w.p.i. (Figure 3.4a, b, d and e). GADD34 was the only mRNA to be increased in ME7-animals during this time (14 w.p.i.) (Figure 3.4c), but the lack of induction of the other UPR mRNAs suggest that a classic UPR is not occurring. Induction of CHOP

mRNA (Figure 3.4d) in ME7-animals at 20 w.p.i. occurred independently of its upstream activators (ATF4 and eIF2 α -P) and, as a pro-apoptotic protein, is more likely to be involved in the apoptosis of CA1 neurons seen in late-stage ME7-animals (Cunningham et al., 2003, Gomez-Nicola et al., 2013, Williams et al., 1997). Similarly, a modest induction of BiP occurred at the mRNA level in ME7-animals only at 20 w.p.i. (Figure 3.4a).

SIL1 has been shown to be highly expressed in disease-resistant motoneurons but not in motoneurons which are vulnerable in ALS and undergo ER stress (Filezac de L'Etang et al., 2015). Induction of SIL1 mRNA was seen at 17 w.p.i. in ME7-animals (Figure 3.10), which further supports the UPR transcriptional data which suggests that the hippocampus of ME7-animals is not vulnerable to ER stress.

3.5.2.2 Expression of UPR proteins

There was no change in expression of BiP at the protein level between NBH- and ME7-animals at any of the time-points investigated, as detected either by quantitative western blotting or immunohistochemistry (Figure 3.5a and b and 3.6). However, the induction of BiP protein was clearly seen in tunicamycin treated HeLa cells, where the fold change in expression was 5.6 compared to untreated HeLa cells (appendix 6).

The levels of eIF2 α -P were not increased in ME7-animals at any of the time-points investigated at early-, middle- and late-stage disease (Figure 3.5a, c and d). In contrast, PEITC treated HeLa cells had a 2.2 fold induction in expression of eIF2 α -P compared to untreated HeLa cells (appendix 6). Immunoreactivity of PERK-P, ATF4 and CHOP was not detected in NBH- or ME7-animals at any of the time-points investigated (appendix 8). However, levels of ATF4 and CHOP protein are increased in tunicamycin treated HeLa cells (appendix 6), which shows that the reagents are capable of detecting these proteins. Analysis of the phosphorylation state of 4EBP1 also revealed no evidence that the cells in the hippocampus are translationally inactive in ME7-animals (Figure 3. 9).

3.5.3 Evidence supporting the activation of a UPR in prion disease

Evidence from both animal models and post-mortem human brain tissue has implicated ER stress and the UPR in a number of chronic neurodegenerative diseases, including AD, PD and ALS (section 1.7.3). In addition, an upregulation of BiP protein has been

shown in the cortex of post-mortem tissue from patients with vCJD and sCJD (Hetzel et al., 2003).

The eIF2 α -P arm of the UPR pathway has been implicated in a different infectious prion disease mouse model to the one used in this thesis (Moreno et al., 2013, Moreno et al., 2012). In this model, prion disease is initiated by the inoculation of Tg (Tg37^{+/-}) mice which overexpress PrP^C 3 fold higher than expressed in non-Tg mice, with the RML scrapie strain. In RML-animals, increasing levels of PrP^{Sc} led to the activation of the eIF2 α -P arm of the UPR which results in global translation repression and a concomitant reduction in the translation of key synaptic proteins – leading to synaptic transmission failure, synapse loss and neuronal death (Moreno et al., 2012). In the model used by Moreno et al., levels of PERK-P, eIF2 α -P, CHOP, ATF4 and BiP protein are increased in RML-animals compared to controls although levels of CHOP and ATF4 mRNA remain unchanged between control and RML-animals (Moreno et al., 2013, Moreno et al., 2012). Levels of BiP and eIF2 α -P protein were increased ~2.5 fold and ~3 fold, respectively, in RML-animals which suggests that in this model of prion disease a robust UPR is induced. In Tg37^{+/+} mice inoculated with RML, eIF2 α -P is increased at 6 w.p.i. and mice develop clinical symptoms earlier (Moreno et al., 2012).

The results in this chapter using ME7-animals disagree with those seen in RML-animals. This could be for a number of reasons. Firstly, the mice used in this chapter were wildtype non-Tg C57BL/6J mice, whereas the mice used by Moreno et al., were Tg37^{+/-} mice which express PrP^C 3 fold higher than in wildtype mice (Moreno et al., 2012). These animals have a faster disease progression (end-stage = 12 w.p.i. (RML) vs 20 w.p.i. (ME7)). Higher levels of PrP^C, which has to be modified and transported thorough the ER, may result in the misfolding of PrP^C – which could prime the ER to trigger the activation of a UPR. However, results have shown that wildtype mice infected with RML also leads to the activation of the eIF2 α -P arm of the UPR at 16 w.p.i. (Moreno et al., 2012). Secondly, in this chapter, ME7 was used as the strain of prion, whereas in Moreno et al., RML was used (Moreno et al., 2012). Analysis of the glycosylation patterns of total PrP, reveal that the ratio of un- and monoglycosylated PrP to diglycosylated PrP is higher in RML-animals compared to ME7-animals (Moreno et al., 2013, Moreno et al., 2012). The increase in forms of PrP which are not fully glycosylated, might suggest that the ER is perturbed in RML-animals, which may be a reason for a UPR in RML-animals, but not ME7-animals.

All the numerous cellular compartments including the ER have been suggested to be involved in the formation of misfolded PrP (Campana et al., 2005). Whilst PrP^C is predominantly found at the plasma membrane and not localised in the ER, mutant forms of PrP have been found associated with the ER in two neuroblastoma cell lines (Gu et al., 2003, Torres et al., 2010). However, the conversion of PrP^C to PrP^{Sc} in infectious prion disease occurs at the plasma membrane and within endosomal compartments not in the ER (Borchelt et al., 1992, Caughey and Raymond, 1991, Caughey et al., 1991, Goold et al., 2011, Marijanovic et al., 2009), therefore, it is unclear how PrP^{Sc} could cause ER stress and activate the UPR. It has been suggested that in the model used by Moreno et al., that the UPR is triggered by PrP^C in the ER as opposed to PrP^{Sc} (which is not formed in the ER) (Halliday and Mallucci, 2015). This is because in the RML model, PrP mRNA is increased with disease progression, as shown by qPCR data and this may therefore contribute to the misfolding of PrP^C within the ER and activation of the UPR (Moreno et al., 2012). However, observations in the ME7 model have shown that PrP mRNA is not increased in ME7-animals at any stage during disease progression (Asuni et al., 2014).

Whilst conversion of PrP^C to PrP^{Sc} does not occur in the ER in infectious prion disease, some mouse models of chronic neurodegenerative disease are associated with the appearance of disease associated misfolded protein in the ER, including ALS (Atkin et al., 2006) and PD (Bellucci et al., 2011, Colla et al., 2012a, Colla et al., 2012b). This would help explain the activation of the UPR in these models (section 1.7.3).

3.5.4 Evidence showing that the UPR is not activated in prion disease

In contrast to the proposed activation of a UPR in prion disease, others have reported little or no evidence for this. Analysis of sporadic, inherited and infectious human prion disease tissue reveals little/no expression of PERK-P, eIF2 α -P and the other eIF2 α kinase, PKR-P (Unterberger et al., 2006). In addition, PERK-P was rarely/ not expressed in the neurons of the brains of RML and sCJD and vCJD infected mice (Unterberger et al., 2006). The levels of PERK-P was higher in the RML models compared to human vCJD and sCJD mouse models (Unterberger et al., 2006). Variation in activation of PERK-P adds additional support to the fact that different strains of prion may be more or less effective in triggering the UPR. It also suggests that human forms of prion disease are less capable of mounting a UPR response.

The levels of PERK-P and eIF2 α -P are not increased in the hippocampus, thalamus or cerebellum of PrP Tg mice (Tg(PG14-A3^{+/-}), Tg(WT-E1^{+/+}), Tg(CJD-A21^{+/-}), Tg(CJD-66^{+/-}) and Tg(FFI-26^{+/-})) (Senatore et al., 2013) and splicing of XBP-1 did not occur in transgenic prion mouse models (Tg(PG14-A3^{+/-}), Tg(WT-E1^{+/+}), Tg(CJD-A21^{+/-})) (Quaglio et al., 2011). Similarly, BiP and CHOP immunoreactivity is not increased in these Tg mouse models (Tg(PG14-A3^{+/-}), (Tg(CJD-A21^{+/-})) (Quaglio et al., 2011). In another model of prion disease (139A scrapie strain, C57BL6/J mice), levels of BiP protein are not increased in the hippocampus, but are transiently increased in the cortex, thalamus and brainstem (Hetz et al., 2005). Levels of eIF2 α -P, CHOP and ATF4 protein are not increased in this model in late-stage prion disease animals (Hetz et al., 2008, Hetz et al., 2005).

3.5.4.1 **High-throughput analysis shows UPR transcripts are not induced in prion disease**

Microarray generated expression profiles of UPR mRNAs from the brains of RML and 301V scrapie inoculated C57BL/6J animals, reveals that ER stress and the UPR is not a prominent feature in these models (Gehlenborg et al., 2009) (Table 3.1). LCM of CA1 neurons from RML-inoculated mice revealed no induction of UPR mRNAs across disease progression, based on a false discovery rate of <0.1% and a 2.5 fold change (Majer et al., 2012). The exception was GADD34 mRNA, in which levels were induced by 2.4 fold in RML-animals early on in disease (~57 % disease progression) but the expression of GADD34 was reduced by 2.8 fold at end-stage disease (Majer et al., 2012). A microarray study on ME7-intracerebrally inoculated C57BLxVM/DK mice revealed no upregulation of BiP mRNA in the hippocampus and did not report an upregulation of any of the other UPR mRNAs analysed in this chapter (Brown et al., 2005). Therefore, the consensus from these different prions models is that there is little evidence for a conventional or profound UPR in the brains of mice with prion disease.

	Strain					
	RML		301V		ME7	
Transcript	Fold change (up)	Fold change (down)	Fold change (up)	Fold change (down)	Fold change (up)	Fold change (down)
BiP	1.1 (10 w.p.i.)	1.3 (8 w.p.i.)	1.3 (16 w.p.i.)	1.5 (8 w.p.i.)	1.5 (20 w.p.i.)	1.25 (8 w.p.i.)
GADD34	1.8 (12 w.p.i.)	1.1 (6 w.p.i.)	1.2 (28 w.p.i.)	2.4 (36 w.p.i.)	1.4 (14 w.p.i.)	N/A
ATF4	1.3 (12 w.p.i.)	1.2 (23 w.p.i.)	1.2 (41 w.p.i.)	1.3 (36 w.p.i.)	1.24 (17 w.p.i.)	N/A
CHOP	1.3 (23 w.p.i.)	1.0 (4 w.p.i.)	1.1 (41 w.p.i.)	1.2 (32 w.p.i.)	1.7 (20 w.p.i.)	1.1 (14 w.p.i.)

Table 3.1 Expression profiles of UPR mRNAs in RML- and 301V-inoculated animals compared to ME7-animals.

Highest fold change (up and down) for the UPR mRNAs shown across the full disease time course for each prion strain in C57BL/6J mice. Red refers to a fold change of >1.5. Time-point at which fold change occurred is in parentheses. RML end-stage is 23 w.p.i., 301V end-stage is 41 w.p.i. and ME7 end-stage is 21 w.p.i. Data for RML- and 301V-animals is taken from Gehlenborg et al., 2009.

3.5.5 Other stress-related response molecules are induced in ME7-animals

Other stress-related response molecules were investigated in ME7-animals to look for a biochemical correlate of the morphological changes seen during ME7 disease progression (Al-Malki, 2012). These other stress-related responses molecules included immediate early genes (ATF3, c-Jun and c-Fos), activity-induced immediate early genes (Arc and Homer1a) and a cellular physiological and environmental damage stress sensor (GADD45 α).

qPCR analysis revealed an induction of ATF3, GADD45 α , c-Jun, c-Fos and Homer1a mRNAs in ME7-animals compared to NBH-animals (Figure 3.11-3.13). ATF4 has been shown to lead to the induction of ATF3 and GADD45 α (Jiang et al., 2007, Jiang et al., 2004), however, this is unlikely to be the case here, as levels of ATF4 mRNA are not increased in ME7-animals. Levels of Arc mRNA were increased in ME7-animals but not to a statistically significant level (Figure 3.12a). Both Arc and Homer1a are upregulated in response to neuronal activity (Brakeman et al., 1997, Link et al., 1995,

Lyford et al., 1995). The induction of genes associated with NMDA receptor activation and excitability has been shown in another model of RML prion disease (Majer et al., 2012) and therefore upregulation of Arc and Homer1a in ME7-animals may be as a result of increased excitability in the hippocampus. PrP^C has been shown to be important for the regulation of NMDA-mediated excitability (Khosravani et al., 2008) and the conversion of PrP^C to PrP^{Sc} might lead to enhanced neuronal excitability. Arc mRNA is upregulated in brain regions in which there are activated microglia (Rosi et al., 2005). Activated microglia in ME7-animals may therefore modify neuronal networks and be responsible for the increased expression of Arc.

Despite significant induction of these stress-related mRNAs, quantitative western blotting revealed no difference in the levels of ATF3, GADD45 α , c-Jun and c-Fos proteins between NBH- and ME7-animals during disease progression (Figure 3.14). The only exception to this was GADD45 α which was increased in ME7-animals at 20 w.p.i. However, immunohistochemistry did reveal changes in protein expression between NBH- and ME7-animals. ATF3, GADD45 α and c-Jun staining was increased in neurons at 13 w.p.i., although this was only significant for ATF3 (CA3 pyramidal layer) (Figure 3.16, 3.17 and 3.19). c-Jun expression progressively increased in the pyramidal layer of CA3 and CA1 and at 21 w.p.i. was significantly increased in the pyramidal layer of CA1 in ME7-animals (Figure 3.17). Both GADD45 α and c-Fos had increased (but not statistically significant) expression in ME7-animals at 21 w.p.i. (Figure 3.18 and 3.19).

Induction of c-Jun protein (13 w.p.i.), and ATF3 mRNA (14 w.p.i.) and protein (13 w.p.i.) occurred in ME7-animals at a time when morphological changes are apparent in the synapse, axon, and dendrites of CA3 pyramidal neurons (Al-Malki, 2012). Expression of ATF3 and c-Jun in the CA3 and CA1 could be a response to the pathological alterations seen in ME7-animals at 13 w.p.i. and also to preceding events in CA1 pyramidal neurons prior to loss of these.

3.5.6 Evidence showing other stress-related response molecules are induced in prion disease

The other stress-related response molecules investigated here have also been shown to be upregulated in other mouse models and post-mortem brain tissue from a number of different chronic neurodegenerative diseases (section 1.7.4).

3.5.6.1 **High-throughput analysis shows other stress-related response mRNAs are induced in prion disease**

Microarray expression profiles of RML- and 301V-inoculated C57BL/6J mice revealed that other stress-related response mRNAs are implicated in disease pathogenesis (Gehlenborg et al., 2009) (Table 3.2). c-Jun protein has also been shown to be upregulated in the brains of VM/Dk mice inoculated with the 87V strain of scrapie from ~30% disease progression onwards (Jamieson et al., 2001).

The RML- and 301V-animal microarray analysis was done in whole brain tissue. Therefore, these transcriptional responses could be coming from neuronal, non-neuronal cells or a combination of both and from different brain regions other than the hippocampus. A study in RML-animals in which CA1 neurons were laser microdissected has shown that some of the stress-related response mRNAs are induced in CA1 neurons during RML prion disease (Majer et al., 2012). This is based on a false discovery rate of <0.1% and a 2.5 fold change. Although ATF3 mRNA was below the level of detection in this study, c-Jun, c-Fos, Homer1a and Arc mRNA were all increased in RML-animals at least at one time-point during disease progression (Majer et al., 2012). Arc, Homer1 and c-Fos mRNA are induced early on during disease and show a 3.8, 4.3 and 9.4 fold change, respectively, in RML-animals at ~44-57 % disease progression. These mRNAs are induced much earlier in this model than in ME7-animals and this might be down to strain differences or region specific expression differences (CA1 neurons (RML) vs whole hippocampus (ME7)). Homer1a expression is downregulated in RML-animals at ~83% disease progression (2.5 fold), which is not seen in ME7-animals. c-Jun mRNA is downregulated by 2.3 fold at ~44% disease progression in RML-animals. However, c-Jun mRNA is upregulated in end-stage RML-animals (10.3 fold change). The fold change seen here is much greater in microdissected CA1 neurons compared to the whole hippocampus in ME7-animals.

Despite a lack of evidence for a UPR in ME7-animals, an upregulation of other stress-related response molecules was seen. The induction of these stress-related response mRNAs in other mouse models of prion disease suggest that these might be common molecular signatures associated with prion disease and other chronic neurodegenerative diseases.

	Strain					
	RML		301V		ME7	
Transcript	Fold change (up)	Fold change (down)	Fold change (up)	Fold change (down)	Fold change (up)	Fold change (down)
ATF3	2.4 (23 w.p.i.)	1.1 (8 w.p.i.)	1.5 (36 w.p.i.)	1.1 (32 w.p.i.)	6.2 (20 w.p.i.)	N/A
GADD45 α	1.8 (20 w.p.i.)	1.3 (2 w.p.i.)	1.5 (24 w.p.i.)	1.3 (12 w.p.i.)	2 (20 w.p.i.)	1.25 (8 w.p.i.)
c-Jun	1.7 (23 w.p.i.)	1.1 (6 w.p.i.)	1.3 (16 w.p.i.)	1.3 (36 w.p.i.)	1.5 (20 w.p.i.)	N/A
c-Fos	2.2 (12 w.p.i.)	2.5 (2 w.p.i.)	4.2 (41 w.p.i.)	1.3 (8 w.p.i.)	2 (14 w.p.i.)	1.2 (17 w.p.i.)
Arc	2.7 (12 w.p.i.)	2.5 (2 w.p.i.)	2.7 (41 w.p.i.)	4.4 (36 w.p.i.)	1.6 (17 w.p.i.)	1.6 (20 w.p.i.)
Homer1	1.1 (6 w.p.i.)	1.9 (12 w.p.i.)	3.6 (36 w.p.i.)	1.3 (28 w.p.i.)	1.6 (17 w.p.i.)	1.4 (8 w.p.i.)

Table 3.2 Expression profiles of other stress-related response mRNAs in RML- and 301V-inoculated animals compared to ME7-animals.

Highest fold change (up and down) for stress-related response mRNAs shown across the full disease time courses for each prion strain in C57BL/6J mice. Red refers to a fold change of ≥ 1.5 . Time-point at which fold change occurred is in parentheses. RML end-stage is 23 w.p.i., 301V end-stage is 41 w.p.i. and ME7 end-stage is 21 w.p.i. Data for RML- and 301V-animals is taken from Gehlenborg et al., 2009.

3.6 Conclusion

The hippocampus of NBH- and ME7-animals was used to investigate UPR and other stress-related response molecules using a combination of biochemistry and immunohistochemistry. ME7-animals had increasing accumulation of PrP and GFAP protein and synapse loss. However, there was little evidence for a UPR in ME7-animals at any time during disease progression. In contrast, other stress-related response molecules were upregulated in ME7-animals. This included the immediate early genes: ATF3, c-Jun and c-Fos, the activity-induced immediate early genes: Arc and Homer1a and GADD45 α a cellular physiological and environmental damage stress sensor.

The induction of these other stress-related response molecules in ME7-animals, suggests these could be viable targets for pharmacological intervention. Identifying

molecular targets as early as possible still offers the best hope for delaying the progression of chronic neurodegenerative diseases.

Chapter 4: Investigation of the unfolded protein response and other stress-related responses in cysteine string protein α $-/-$ mice

4.1 Introduction

CSP α is a synaptic vesicle protein (Braun and Scheller, 1995, Chamberlain and Burgoyne, 2000). In conjunction with Hsc70 and SGT it chaperones SNAP-25 and dynamin-1 (Sharma et al., 2012a, Sharma et al., 2011, Zhang et al., 2012). This enables vesicle exocytosis-endocytosis coupling, which is essential for maintaining sustained synaptic transmission (Fernández-Chacón et al., 2004, García-Junco-Clemente et al., 2010, Schmitz et al., 2006).

The CSP α $-/-$ model is a model of neurodegeneration. CSP α $-/-$ mice are normal at birth compared to CSP α $+/+$ and CSP α $+/-$ littermates. However, after ~P15 CSP α $-/-$ animals develop a progressive muscle weakness, sensorimotor deficit and undergo synaptic loss and neurodegeneration after ~2 weeks of age (Fernández-Chacón et al., 2004, García-Junco-Clemente et al., 2010, Schmitz et al., 2006). CSP α $-/-$ animals start to perish at the end of the first postnatal month and no animals survive beyond three months of age (Fernández-Chacón et al., 2004). CSP α $+/-$ animals do not undergo neurodegeneration (Fernández-Chacón et al., 2004), which suggests a ~50% reduction in CSP α levels is insufficient to cause neurodegeneration. However, mutations in the human CSP α gene, DNAJC5, cause ANCL (Noskova et al., 2011, Zhang and Chandra, 2014).

CSP α is required for the maintenance of synaptic integrity and without it, SNAP-25 misfolds, SNARE-complex assembly is reduced and synapse dysfunction, loss and neurodegeneration ensues (Sharma et al., 2012a, Sharma et al., 2011). In the absence of complete chaperoning of SNAP-25 in CSP α $-/-$ animals, it has been hypothesised that SNAP-25 misfolds into a non-native form (Sharma et al., 2011). In CSP α $-/-$ animals a 40% increase in SNAP-25 ubiquitination has been shown (Sharma et al., 2011). Increased synaptic activity was shown to further promote SNAP-25 ubiquitination, whilst inhibition of synaptic activity reduced the ubiquitination of SNAP-25 (Sharma et al., 2011). Although SNAP-25 has not been shown to directly misfold in the ER in

CSP α $-/-$ mice, proteins which are associated with misfolding outside of the ER have been found to induce a UPR (Moreno et al., 2013, Moreno et al., 2012).

The CSP α $-/-$ model has been used in this chapter to build upon the observations made in the ME7 prion model (chapter 3), to determine whether UPR and other stress-related response molecules are induced in this model as a response to neuronal dysfunction. A similar induction of stress-related response pathways in the CSP α $-/-$ and ME7-animals may suggest common stress pathways initiated in neurodegenerative disease, regardless of the underlying initiating event.

4.2 Aims

Following on from chapter 3, the aim of this chapter was to investigate whether the UPR and other stress-related response molecules (immediate early genes, activity-induced immediate early genes and a cellular physiological and environmental damage stress sensor) were induced in CSP α $-/-$ animals. Tissue from CSP α $+/+$, $+/-$ and $-/-$ animals was taken across a time course, from shortly after birth up until when the animals had to be killed. Hippocampal tissue was taken for qPCR and quantitative western blotting and whole brain tissue sections (containing the hippocampus) was collected for immunohistochemistry. These techniques were used to:

- Quantify the expression of UPR and other stress-related response mRNAs
- Quantify the expression of UPR and other stress-related response proteins
- Investigate where in the hippocampus these molecules are expressed

The experimental outline for this study is shown in Figure 4.1.

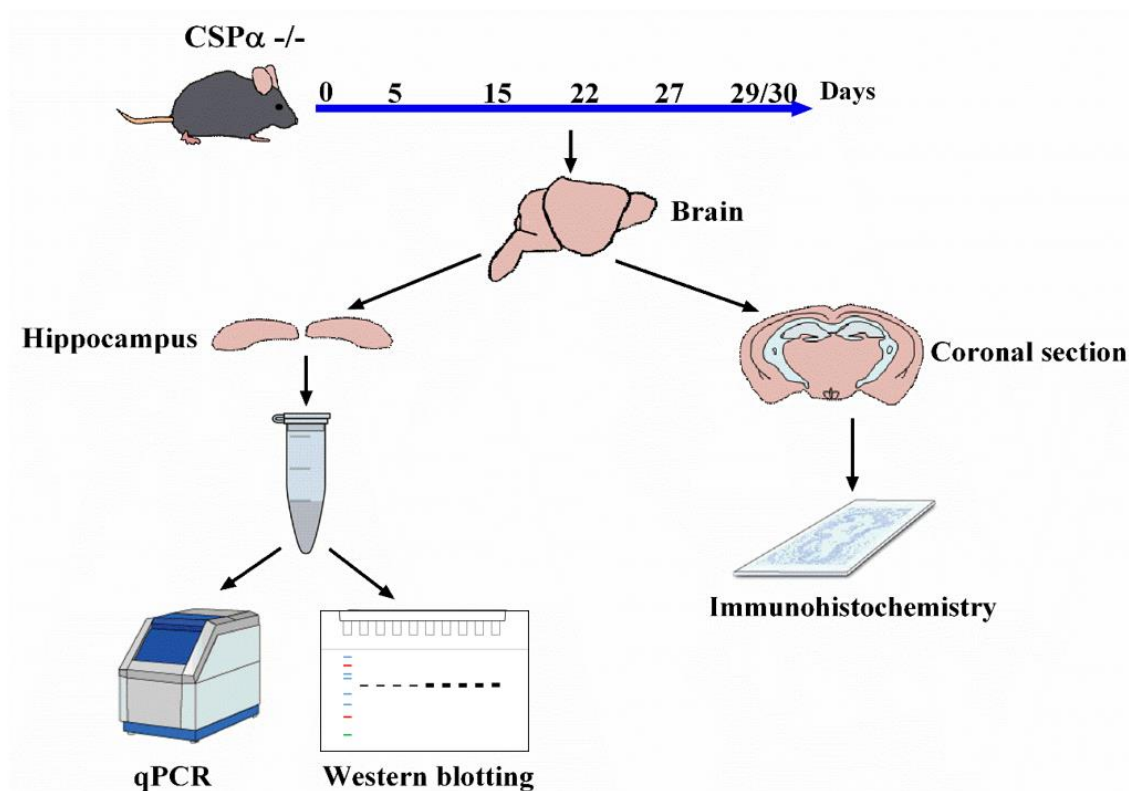


Figure 4.1 Experimental outline: investigating the UPR and other stress-related response molecules in $CSP\alpha^{-/-}$ animals.

$CSP\alpha^{+/+}$, $+/-$ and $-/-$ mice were killed by cervical dislocation without perfusion, at different time points (P5, P15, P22, P27 and P29/P30). The brain was removed and used for hippocampal dissection. The dissected hippocampus was homogenised and the homogenate split into two aliquots. One aliquot was used to isolate RNA and perform qPCR and the other to isolate protein and to perform quantitative western blotting. Coronal sections were cut from $CSP\alpha^{+/+}$, $+/-$ and $-/-$ animals at P29 and used for immunohistochemistry. $+/+$, wild-type; $+/-$, heterozygous; $-/-$, knockout and P, postnatal days.

4.3 Specific materials and methods

4.3.1 Breeding of CSP α mice

CSP α mice were kindly provided by Dr Rafael Fernández-Chacón (University of Seville, Spain) and subsequently bred in-house and maintained as CSP α +/- on a Charles River background. Breeding pairs were bred to obtain CSP α +/+, +/- and -/- mice. CSP α +/- mice were paired in a ratio of 2 females: 1 male. CSP α -/- mice can be distinguished from CSP α +/+ and CSP α +/- mice after ~P15 as they fail to gain weight, become increasingly lethargic and develop a progressive muscle weakness (Fernández-Chacón et al., 2004). Any mice thought to be CSP α -/- and not required for experimental studies were killed under Home Office Regulations, so as to avoid any unnecessary suffering. Litters were genotyped before any experiments were conducted (section 4.3.2).

4.3.2 Genotyping of CSP α mice

CSP α +/+, +/- and -/- mice were produced by crossing male and female CSP α +/- mice. Pups were genotyped 2-3 weeks after birth, using ear punches. Tail tips were used for confirmation of genotype.

4.3.2.1 Tissue collection

Mice 2-3 weeks of age were ear punched and this tissue was placed into a 1.5 ml Eppendorf. ≤ 2 mm of tail was removed using a scalpel blade and placed in a 1.5 ml Eppendorf for re-genotyping of these mice to be used as breeders. Lidocaine was applied to the tail 10 min before the tip was taken. The same protocol was used to extract DNA and genotype mice from both ear punches and tail tips as indicated below.

4.3.2.2 PK digestion

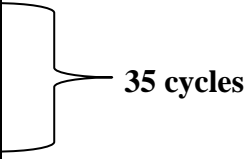
Lysis buffer contained 10 mM Tris pH 8, 10 mM EDTA, 100 mM NaCl, 0.5% SDS, 0.4 mg/ml PK and RNase-free water. Tissue was digested in 50 μ l lysis buffer and tails were digested in 100 μ l lysis buffer. Samples were incubated at 54 °C and were flicked every 5-15 min until the tissue had fully digested. For ear samples this was about 30 min and for tail tips this was about 45-60 min.

4.3.3 DNA extraction

After digestion, incubations were centrifuged for 10 min at 13,000 rpm. This pelleted hair and undigested material and the DNA remained in the supernatant. The supernatant was removed and placed into a 1.5 ml Eppendorf. 1 volume of isopropanol was added to the supernatant to precipitate the DNA. The isopropanol was mixed with the supernatant by flicking the Eppendorfs until the DNA became visible as white strands. The tubes were then centrifuged for 5 min at 10,000 rpm to pellet the DNA. The supernatant was discarded and the pellet washed in 70% ethanol followed by centrifugation for 5 min at 10,000 rpm. The ethanol was removed and the pellet subjected to a further wash in 70% ethanol. The final pellet was left to air-dry for 20 min before being resuspended with gentle mixing in either 25 µl (ear punch) or 50 µl (tail tip) RNase-free water. The DNA in solution was stored at 4 °C.

4.3.4 Genomic PCR for genotyping

1 µl of extracted DNA was used as the template in REDTaq PCR (section 2.6.2) with a distinct primer combination as described (Fernández-Chacón et al., 2004). Primers A (5'-TGGTAGACTAACCTAACATGGCCG-3') and C (5'-GAGCGCGCGCGGCGGA-GTTGTTGAC-3') are both sense primers whilst primer B (5'-TTGG-CCCACCAGCTGGAGAGTAC-3') is the antisense primer. Each DNA sample (section 4.3.3) was subjected to two PCR reactions, one containing primers A and B and the other primers C and B. The reaction mix was the same as in section 2.6.2. The reaction was incubated under the following cycling conditions:

Initial denaturation	94 °C	2 min	 35 cycles
Denaturation	94 °C	40 s	
Annealing	62 °C	30 s	
Extension	72 °C	2 min	
Final Extension	72 °C	10 min	
Hold	4 °C	∞	

PCR products were stored at 4 °C short-term and -20 °C long-term.

PCR products were separated on a 1% agarose gel (section 2.6.4) Primer A binds to exon 1 of the CSP α gene, whilst primer C binds to a neomycin insert which replaces

residues 1-36 in exon 1 of the CSP α knockout allele (Figure 4.2). The amplification product of primers A and B is 1.2 kb, whilst the amplification product from primers C and B is 900 bp. If the mice are CSP α $+/+$ a single band at 1.2 kb is amplified. If the mice are CSP α $+/-$ two products will be amplified, one at 1.2 kb and the other at 900 bp. If the mice are CSP α $-/-$ only a 900 bp would be amplified (Figure 4.3).

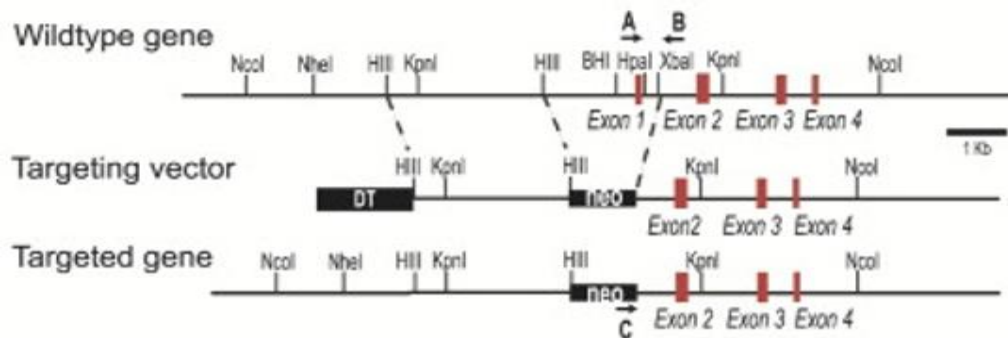


Figure 4.2 Wildtype CSP α gene, targeting vector and position of CSP α primers.

Targeting vector contains a neomycin insert (neo) which replaces exon 1 in the wildtype CSP α gene. The position of primers A, B and C in relation to wildtype and the targeted gene are shown. Image taken from Fernández-Chacón et al., 2004.

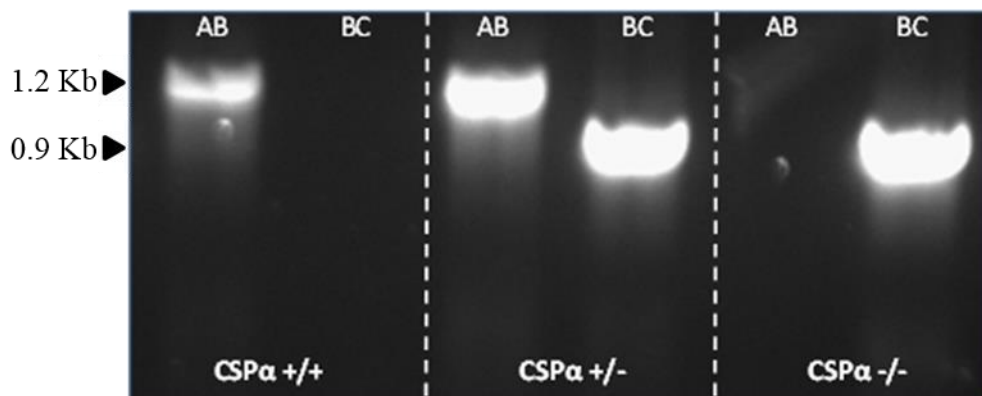


Figure 4.3 Example PCR gel image used to identify the genotype of CSP α mice.

One band at 1.2 Kb signifies that the mice are CSP α $+/+$. A band at 1.2 Kb and another at 0.9 Kb denotes that the mice are CSP α $+/-$. A single band at 0.9 Kb indicates that the mice are CSP α $-/-$. AB and BC refers to the primer combination. $+/+$, wildtype; $+/-$, heterozygous and $-/-$, knockout.

4.3.5 qPCR

mRNA expression was calculated as described (section 2.6.3.1) with the exception of Arc, Homer1a, ATF4 and SIL1 mRNA, which was calculated using the $2^{-\Delta\Delta C_t}$ method (section 2.6.3.2). Arc had a qPCR efficiency of 88.28%, Homer1a 79.86% and ATF4 87.69%, whilst GAPDH (used to normalise Arc, Homer1a and ATF4 expression) had a qPCR efficiency of 94.09%. SIL1 had a qPCR efficiency of 85.06% whilst GAPDH (used to normalise SIL1 expression) had a qPCR efficiency of 87.61%.

4.4 Results

CSP α $-/-$ animals and littermate $+/+$ and $+/-$ animals were used in this study up to a time point of P30. CSP α $-/-$ animals could not be collected past this point due to Home Office restrictions on weight loss and severity.

4.4.1 Expression of SNAP-25, SNARE-complex assembly and pre- and postsynaptic proteins in CSP α $-/-$ animals

The expression levels of CSP α were measured in CSP α $+/+$, $+/-$ and $-/-$ animals using quantitative western blotting. Levels of CSP α were reduced in CSP α $+/-$ animals to around ~50% expression compared to CSP α $+/+$ animals. Expression of CSP α was not seen in CSP α $-/-$ animals, consistent with their genotype (Figure 4.4a and b) and as previously shown (Fernández-Chacón et al., 2004).

Levels of SNAP-25 and SNARE-complex assembly have been previously shown to be significantly decreased in CSP α $-/-$ animals from P5 (Sharma et al., 2012a, Sharma et al., 2011). A comparison of the levels of SNAP-25 and SNARE-complexes in SDS extracted hippocampi from CSP $+/+$, $+/-$ and $-/-$ was made using quantitative western blotting. In early development (P5) levels of SNAP-25 and SNARE-complexes were lower than at later times consistent with ongoing synaptogenesis which occurs from birth up until P15. Levels of SNAP-25 protein progressively decreased from P15 in CSP α $-/-$ animals compared to CSP α $+/+$ and CSP α $+/-$ animals (Figure 4.4a and c). At P30 expression of SNAP-25 was significantly reduced by 58% in CSP α $-/-$ animals compared to CSP α $+/+$ animals. Consistent with a reduction in SNAP-25 levels, SNARE-complex assembly was progressively reduced in CSP α $-/-$ animals from P15

(Figure 4.4a and d). At P30 SNARE-complex assembly was significantly reduced by 43% in $CSP\alpha^{-/-}$ animals compared to $CSP\alpha^{+/+}$.

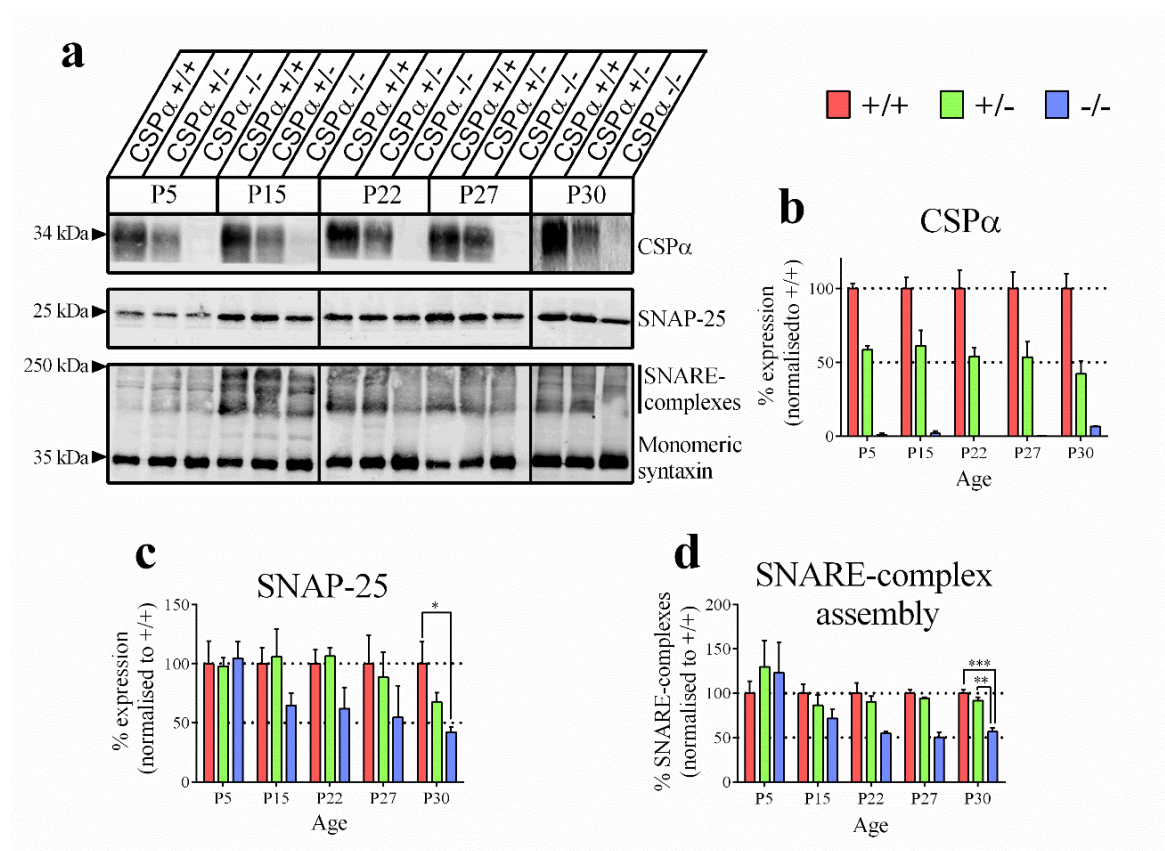


Figure 4.4 Quantification of $CSP\alpha$, SNAP-25 proteins and SNARE-complex assembly in $CSP\alpha^{-/-}$ animals.

Representative western blotting (a) and related quantification for $CSP\alpha$ (b), SNAP-25 (c) and SNARE-complex assembly (d) in SDS extracted hippocampi from $CSP\alpha^{+/+}$, $+/-$ and $-/-$ animals killed at different time points (P5-P30). SNARE-complexes were determined by western blotting for syntaxin from unboiled SDS extracted hippocampi. The immunoreactivity of monomeric syntaxin and SNARE-complexes was calculated. The fraction of total immunoreactivity (monomeric syntaxin + SNARE-complexes) which was contributed from the SNARE-complexes was determined (SNARE-complex immunoreactivity/SNARE-complex and syntaxin immunoreactivity) and this was expressed as a percentage of SNARE-complexes. $CSP\alpha^{+/+}$ animals were given a SNARE-complex value of 100% and SNARE-complexes for $CSP\alpha^{+/-}$ and $CSP\alpha^{-/-}$ animals were expressed relative to this. Data in graphs represents mean \pm SEM of the protein expression values from $n = 3$ animals per genotype and time-point, except $CSP\alpha^{-/-}$ animals at P30, where $n = 4$. Statistical tests = repeated measures two-way ANOVA with Bonferroni post-analysis (P5-P27) and one-way ANOVA with Bonferroni

post-analysis (P30). Statistical significance relative to CSP α +/+ and +/-: * $P \leq 0.05$, ** $P \leq 0.01$, and *** $P \leq 0.001$. +/+, wildtype; +/-, heterozygous; -/-, knockout and P, postnatal days. Data collected in collaboration with Dr Joanne Bailey.

Reduced levels of SNAP-25 protein and SNARE-complex assembly in CSP α -/- animals suggest that synapses within the hippocampus are dysfunctional. To determine if there was synaptic loss in CSP α -/- animals, levels of the presynaptic protein, synaptophysin and the postsynaptic protein, PSD-95, were determined by quantitative western blotting. Similar to SNAP-25 and SNARE-complexes, levels of synaptophysin and PSD-95 proteins were lower at P5 than at later time points (Figure 4.5a). Despite reduced levels of SNAP-25 protein and SNARE-complexes, no synaptic loss could be detected at any of the time-points investigated in the pre- or postsynaptic compartment in CSP α -/- animals (Figure 4.5a-c). These observations were followed by immunohistochemistry staining for synaptophysin to determine if reduced expression or disorganisation of staining in CSP α -/- animals could be seen. No clear qualitative differences in synaptophysin staining between the three CSP α genotypes could be seen at any of the time-points investigated (Figure 4.5d).

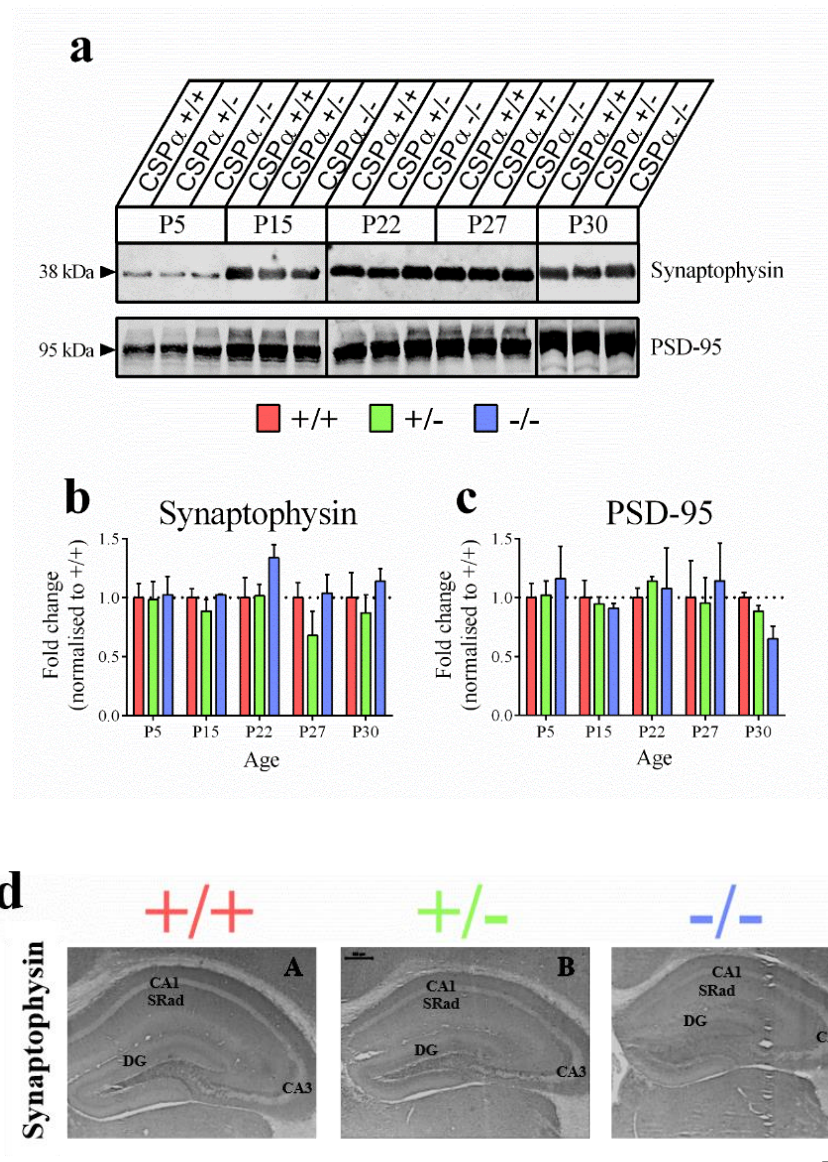


Figure 4.5 Quantification of synaptophysin and PSD-95 proteins in CSPα -/- animals.

Representative western blotting (a) and related quantification for synaptophysin (b) and PSD-95 (c) in SDS extracted hippocampi from CSPα +/+, +/- and -/- animals killed at different time points (P5-P30). Data in graphs represents mean ± SEM of the protein expression values from $n = 3$ animals per genotype and time-point, except CSPα -/- animals at P30, where $n = 4$. Statistical tests = repeated measures two-way ANOVA with Bonferroni post-analysis (P5-P27) and one-way ANOVA with Bonferroni post-analysis (P30). Representative immunohistochemical staining for synaptophysin (d) in the hippocampus of CSPα +/+, +/- and -/- animals. Immunohistochemical staining was performed on CSPα animals killed at P29. The scale bar is indicated under image C (300 μm). $n = 2$ animals per genotype, except for CSPα +/- animals, where $n = 3$. +/+,

wildtype; +/-, heterozygous; -/-, knockout; CA1, Cornu Ammonis region 1; CA3, Cornu Ammonis region 3; DG, dentate gyrus; P, postnatal days and SRad, stratum radiatum. Data collected in collaboration with Dr Joanne Bailey.

4.4.2 Expression of GFAP in CSP α -/- animals

Although synaptic loss was not detected biochemically in the hippocampus of CSP α -/- animals, the expression of GFAP, which is upregulated in response to disturbances in the hippocampal microenvironment, was investigated. Quantitative western blotting revealed that the levels of GFAP was significantly increased in CSP α -/- animals compared to CSP α +/+ and CSP α +/- animals at P27 (Figure 4.6b and c). However, at the mRNA level, GFAP mRNA was only significantly increased in CSP α -/- animals at P30 (Figure 4.6a).

Immunohistochemistry was performed to investigate the expression of GFAP protein in the DG, CA3 and CA1 regions of the hippocampus at P29, a time when SNAP-25 protein levels and SNARE-complex assembly is reduced (Figure 4.4c and d). Staining for GFAP revealed variation, in particular between the two CSP α -/- animals. One had a clear increase in the expression of GFAP but the other was more modest (Figure 4.7a). This is represented in the scatter plot in which the intensity of staining for GFAP in CSP α -/- animals is plotted relative to CSP α +/+ animals (Figure 4.7b). The increased staining intensity for GFAP in CSP α -/- animals was most evident in the CA3 (Figure 4.7a K and L). Taken together these results show that a modest gliosis occurs in CSP α -/- animals from P27-P30, despite no detectable synaptic loss or neurodegeneration. This is consistent with previous data using this model in which an astrogliosis is seen in CSP α -/- animals despite no detectable synaptic loss (Malfa, 2012).

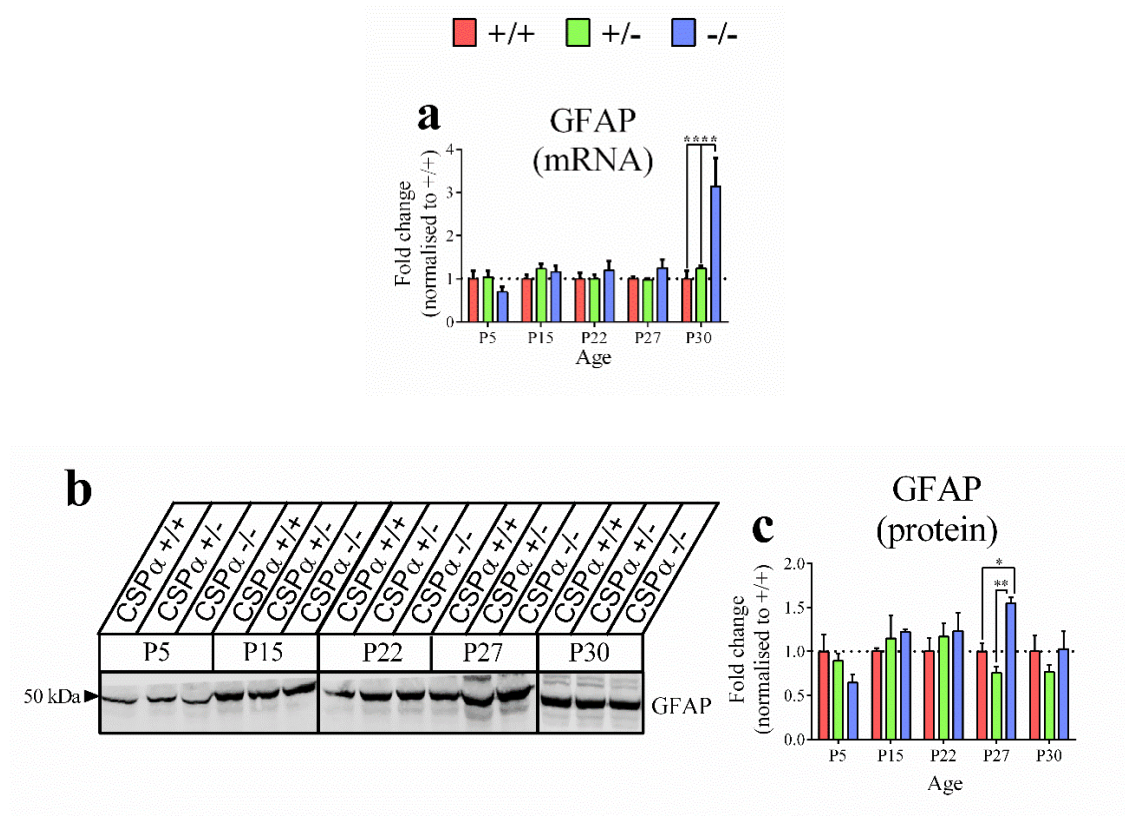


Figure 4.6 Quantification of GFAP to measure gliosis in CSPα -/- animals.

qPCR analysis for GFAP mRNA (a) in hippocampal homogenates from CSPα +/+, +/- and -/- animals killed at different time points (P5-P30). Data in graphs represents mean \pm SEM of the mRNA expression values from $n = 3$ animals per genotype and time-point. Statistical test = repeated measures two-way ANOVA with Bonferroni post-analysis. Statistical significance relative to CSPα +/+ and +/-: **** $P \leq 0.0001$. Representative western blotting (b) and related quantification (c) for GFAP in SDS extracted hippocampi from CSPα +/+, +/- and -/- animals killed at different time points (P5-P30). Data in graphs represents mean \pm SEM of the protein expression values from $n = 3$ animals per genotype and time-point, except -/- animals at P30, where $n = 4$. Statistical tests = repeated measures two-way ANOVA with Bonferroni post-analysis (P5-P27) and one-way ANOVA with Bonferroni post-analysis (P30). Statistical significance relative to CSPα +/+ and +/-: * $P \leq 0.05$ and ** $P \leq 0.01$.

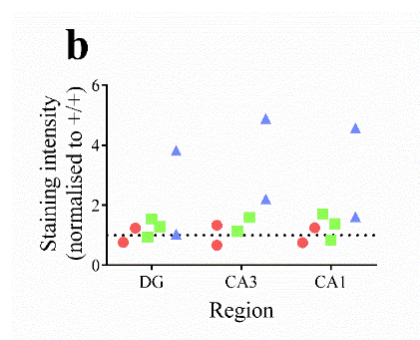
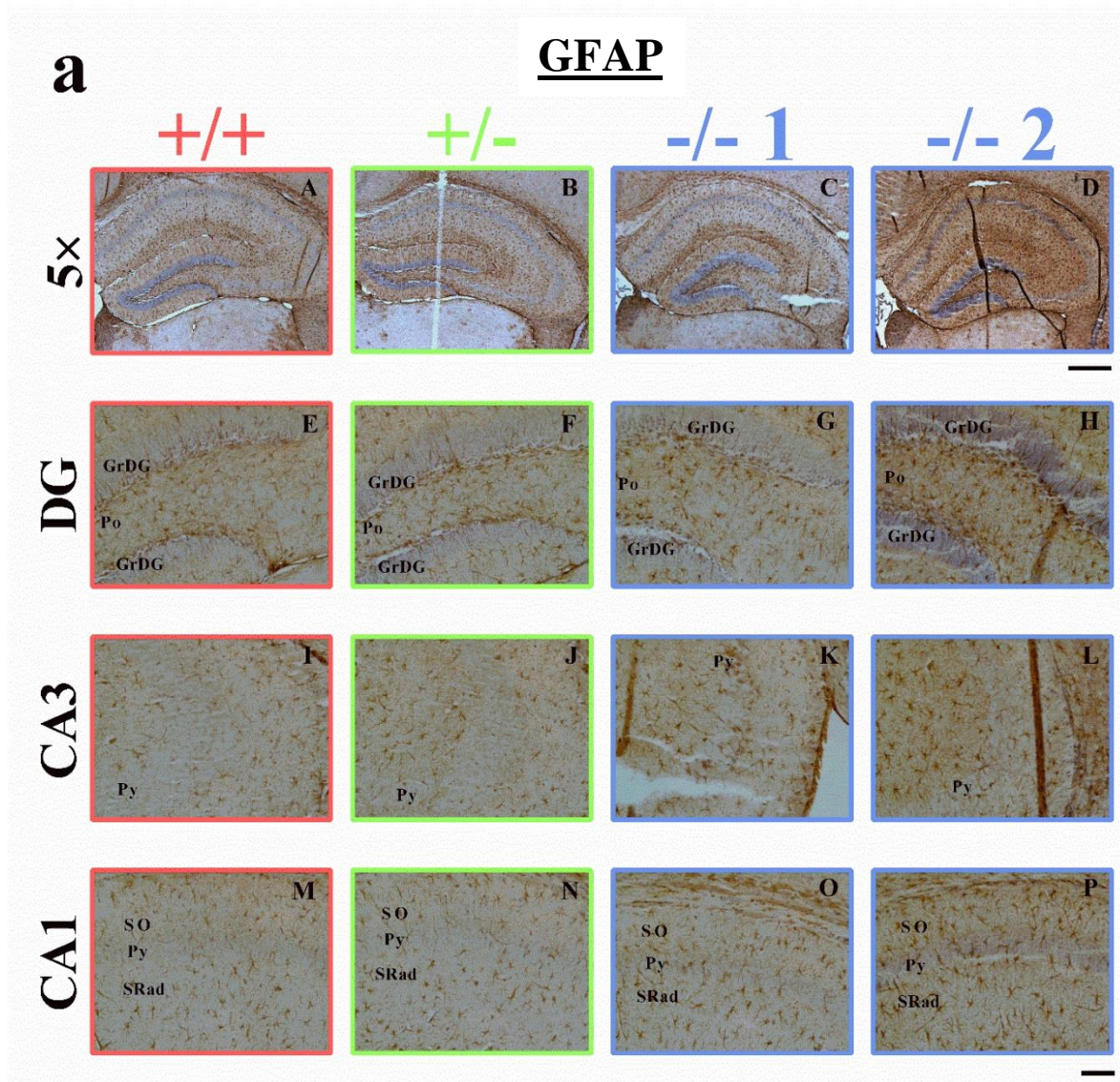


Figure 4. 7 Immunohistochemical staining for GFAP in CSP α $-/-$ animals.

Representative immunohistochemical staining for GFAP (a) and related quantification (b) in the hippocampus of CSP α $+/+$, $+/-$ and $-/-$ animals. Immunohistochemical staining was performed on CSP α animals killed at P29. Scale bars are indicated image D (300 μ m) and P (100 μ m). $-/-$ 1 and $-/-$ 2 refer to two different CSP α $-/-$ animals. Data in

scatter plot represents individual values of the staining intensity for GFAP in the DG, CA3 and CA1 regions. $n = 2$ animals per genotype, except for +/- animals, where $n = 3$. +/+, wildtype; +/-, heterozygous; -/-, knockout; CA1, Cornu Ammonis region 1; CA3, Cornu Ammonis region 3; DG, dentate gyrus; GrDG, granule cell layer of the DG; P, postnatal days; Po, polymorphic layer; Py, pyramidal layer; SO, stratum oriens and SRad, stratum radiatum. Data collected in collaboration with Dr Joanne Bailey.

4.4.3 Expression of UPR mRNAs in CSP α -/- animals

The investigation of the levels of SNAP-25, SNARE-complexes and expression of GFAP in CSP α -/- animals indicates neuronal dysfunction in the hippocampus. Although synaptic loss is not detected, the reduced levels of SNAP-25 and SNARE-complexes from P15 highlight synaptic perturbations. To investigate molecular responses associated with these perturbations reagents that were characterised and used in the preceding chapter (chapter 3) were taken advantage of to investigate the UPR in CSP α -/- animals.

mRNA and protein expression was determined for a number of UPR molecules using qPCR and quantitative western blotting. Investigation of the relative mRNA levels of BiP and spliced XBP-1 revealed that these were not significantly increased in CSP α -/- animals between P5-P30 (Figure 4.8a and b). Levels of GADD34 and CHOP mRNA were modestly increased (< 1.5 fold) in CSP α -/- animals at P22 and P27 (GADD34) and P22 (CHOP) only (Figure 4.8c and d). Levels of ATF4 mRNA were not significantly different between the three CSP α genotypes at P30 (Figure 4.8e).

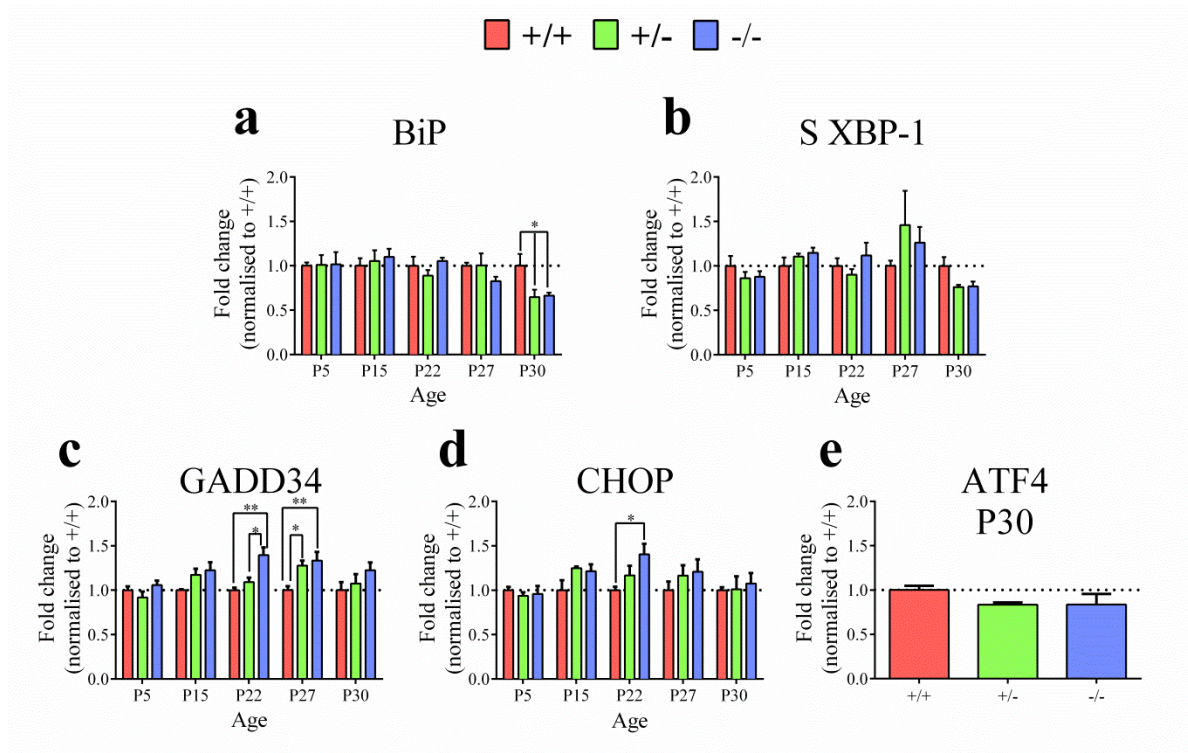


Figure 4.8 Quantification of UPR mRNAs in CSPα -/- animals.

qPCR analysis for BiP (a), spliced XBP-1 (b), GADD34 (c), CHOP (d) and ATF4 (P30 only) (e) mRNAs in hippocampal homogenates from CSPα +/+, +/- and -/- animals killed at different time points (P5-P30). Data in graphs represents mean ± SEM of the mRNA expression values from $n = 3$ animals per genotype and time-point. Statistical test = repeated measures two-way ANOVA with Bonferroni post-analysis (a-d) and one-way ANOVA with Bonferroni post-analysis (e). Statistical significance relative to CSPα +/+ and +/-: * $P \leq 0.05$ and ** $P \leq 0.01$. +/+, wildtype; +/-, heterozygous; -/-, knockout; P, postnatal days and S, spliced.

4.4.4 Expression of UPR proteins in CSP α -/- animals

Previous work on proteinopathy-induced synaptic dysfunction, has suggested that there can be discrete changes in correlates of UPR molecules not resolved by measuring the expression at the mRNA level (Moreno et al., 2012). Thus to extend the above analysis, the level of UPR proteins was also measured by probing for BiP and eIF2 α -P using quantitative western blotting. Immunoreactivity for PERK-P, ATF4 and CHOP which would serve as distinct measures of the UPR could not be detected in SDS extracted hippocampi from CSP α animals at any of the postnatal ages investigated (appendix 9).

Immunoreactivity for BiP protein between P5-P22 was unable to be detected, despite 40 μ g of protein being loaded and run on the SDS-PAGE gels. BiP immunoreactivity at P27 and P30 was detected, however, levels of BiP did not significantly differ between CSP α +/+, +/- and -/- animals at these time-points (Figure 4.9a and b). Similarly, the levels of eIF2 α -P did not significantly differ between the three CSP α genotypes (Figure 4.9a and c).

These observations were followed up by exploring whether there was a change in the phosphorylation state of 4EBP1, as an additional readout of translation. There were no significant changes in the ratios of hyperphosphorylated: phosphorylated/hypophosphorylated 4EBP1 in CSP α -/- animals between P5 and P30 (Figure 4. 9d and e). These results, in conjunction with the qPCR analysis of UPR mRNAs, reveal that the UPR is not activated in CSP α -/- animals between P5-P30.

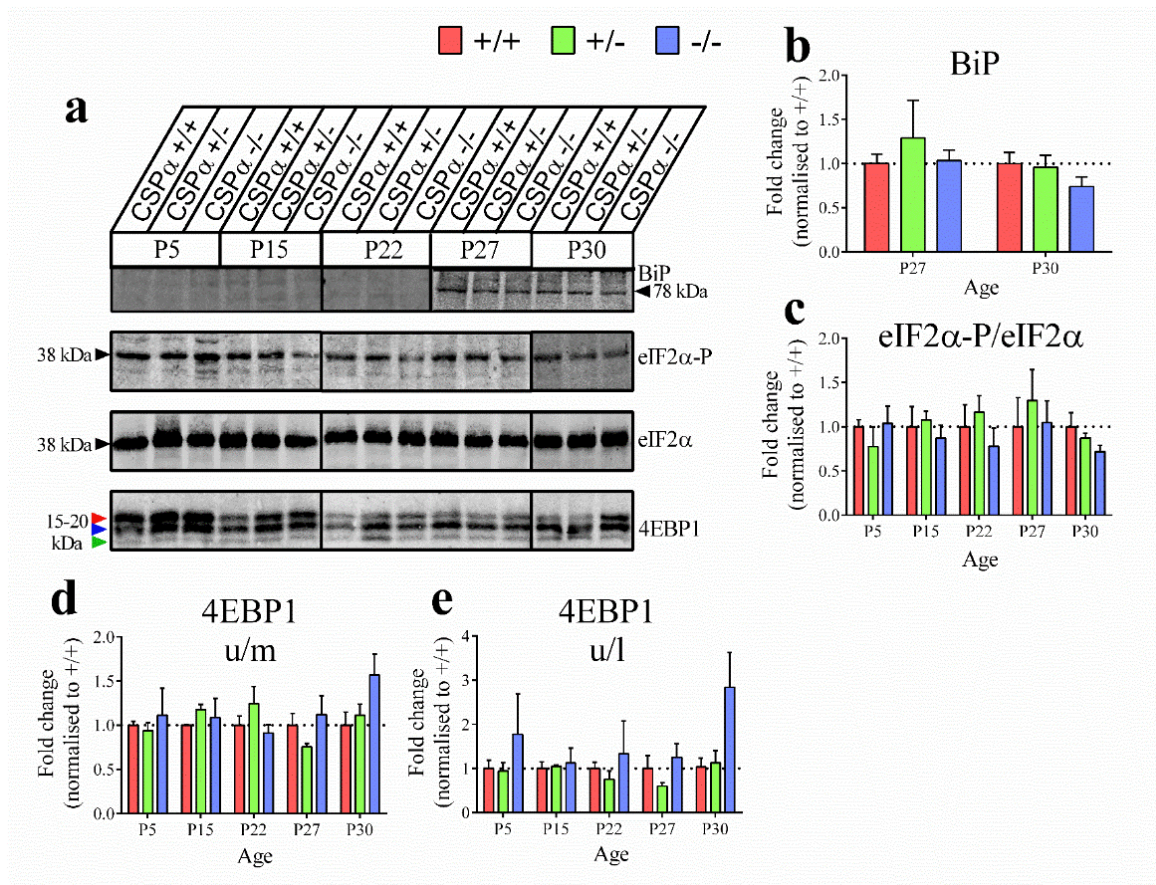


Figure 4.9 Quantification of UPR proteins and the phosphorylation state of 4EBP1 in CSPα -/- animals.

Representative western blotting (a) and related quantification for BiP (b), eIF2α-P (Ser51) (c) and 4EBP1 (d and e) in SDS extracted hippocampi from CSPα +/+, +/- and -/- animals killed at different time points (P5-P30). Coloured arrowheads (a) mark upper hyperphosphorylated (red) (Thr37, Thr46, Ser65 and Thr70), middle phosphorylated (blue) (Thr37 and Thr46) and lower hypophosphorylated (green) 4EBP1. Data in graphs represents mean ± SEM of the protein expression values from $n = 3$ animals per genotype and time-point, except CSPα -/- animals at P30, where $n = 4$. Statistical test = repeated measures two-way ANOVA with Bonferroni post-analysis (P5-P27, (c-e)) and one-way ANOVA with Bonferroni post-analysis (P27 (b) and P30 (b-e)). +/+, wildtype; +/-, heterozygous; -/-, knockout; l, lower 4EBP1 band (hypophosphorylated); m, middle 4EBP1 band (phosphorylated); P, postnatal days and u, upper 4EBP1 band (hyperphosphorylated). Data collected in collaboration with Dr Joanne Bailey.

The expression of SIL1 mRNA, previously investigated in chapter 3, was investigated in CSPα +/+, +/- and -/- animals. qPCR revealed a significant increase in the expression

of SIL1 mRNA in CSP α $-/-$ animals at P15 and P27 compared to CSP α $+/+$ animals (Figure 4.10).

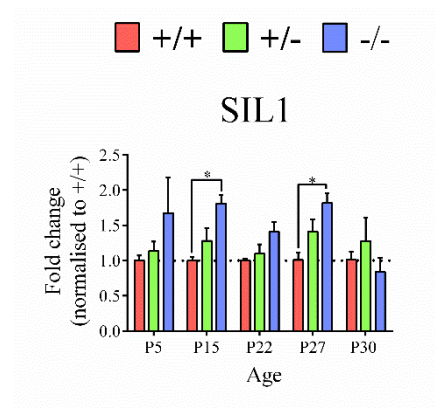


Figure 4.10 Quantification of SIL1 mRNA in CSP α $-/-$ animals.

qPCR analysis for SIL1 mRNA in hippocampal homogenates from CSP α $+/+$, $+/-$ and $-/-$ animals killed at different time points (P5-P30). Data in graphs represents mean \pm SEM of the mRNA expression values from $n = 3$ animals per genotype and time-point, except for CSP α $-/-$ animals at P30 where $n = 4$. Statistical test = repeated measures two-way ANOVA with Bonferroni post-analysis (P5-P27) and one-way ANOVA with Bonferroni post-analysis (P30). Statistical significance relative to CSP α $+/+$ and $+/-$: * $P \leq 0.05$. $+/+$, wildtype; $+/-$, heterozygous; $-/-$, knockout and P, postnatal days.

4.4.5 Expression of other stress-related response mRNAs levels in CSP α $-/-$ animals

Although the UPR was not induced in the CSP α $-/-$ animals at any of the time-points investigated, other stress-related response molecules investigated in chapter 3 were investigated here to see if some of these molecules were similarly induced.

4.4.5.1 Expression of immediate early gene mRNAs in CSP α $-/-$ animals

mRNA levels of ATF3 were unchanged and did not differ between the three CSP α genotypes between P5-P27, until P30 when levels of ATF3 mRNA were dramatically and significantly increased in CSP α $-/-$ (Figure 4.11a). Similarly, mRNA levels of c-Jun mRNA were unchanged between CSP α $+/+$, $+/-$ and $-/-$ animals until P30 when c-Jun mRNA expression was significantly increased in CSP α $-/-$ animals (Figure 4.11b). mRNA levels of c-Fos were below the limit for accurate quantification (section 2.6.3.1) between P5-P27. At P30 levels of c-Fos were quantifiable but there was no significant

difference between the levels of c-Fos mRNA in the three CSP α genotypes (Figure 4.11c).

4.4.5.2 Expression of activity-induced immediate early gene mRNAs in CSP α -/- animals

Arc mRNA levels were unchanged between the three CSP α genotypes between P5-P27 (Figure 4.12a) At P30, levels of Arc mRNA were increased in CSP α -/- animals, but this did not reach statistical significance (Figure 4.12a). mRNA levels of Homer1a were unchanged between all three CSP α genotypes until P30 when Homer1a mRNA was significantly increased in CSP α -/- animals (Figure 4.12b).

4.4.5.3 mRNA expression of the cellular physiological and environmental damage stress sensor, GADD45 α , in CSP α -/- animals

Levels of GADD45 α mRNA did not change significantly between CSP α +/+ and -/- animals except for at P22 when levels of GADD45 α mRNA were significantly increased in CSP α -/- animals (Figure 4.13).

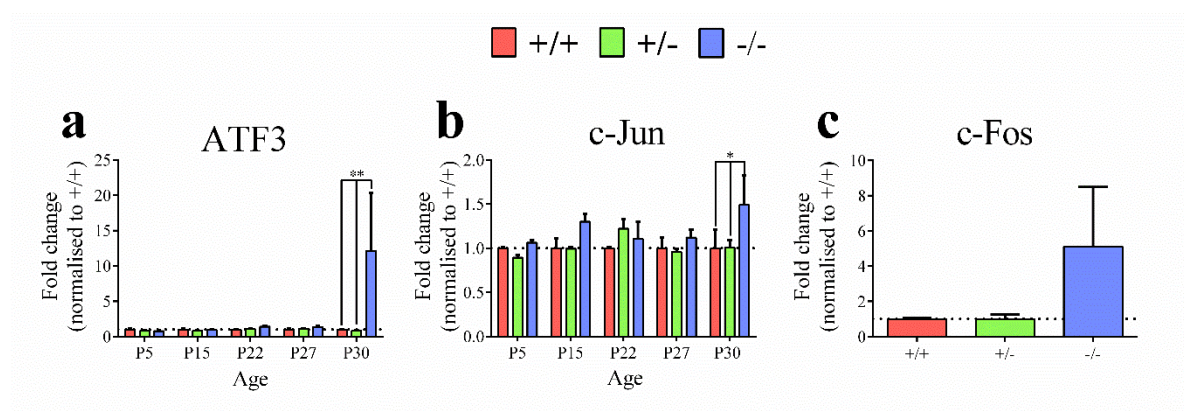


Figure 4.11 Quantification of immediate early gene mRNAs in CSP α -/- animals.

qPCR analysis for ATF3 (a), c-Jun (b) and c-Fos (c) mRNAs in the hippocampus of CSP α +/+, +/- and -/- animals killed at different time points (P5-P30). Data in graphs represents mean \pm SEM of the mRNA expression values from $n = 3$ animals per genotype and time-point. Statistical test = repeated measures two-way ANOVA with Bonferroni post-analysis (a and b) and one-way ANOVA with Bonferroni post-analysis (c). Statistical significance relative to CSP α +/+ and +/-: * $P \leq 0.05$ and ** $P \leq 0.01$. +/+, wildtype; +/-, heterozygous; -/-, knockout and P, postnatal days.

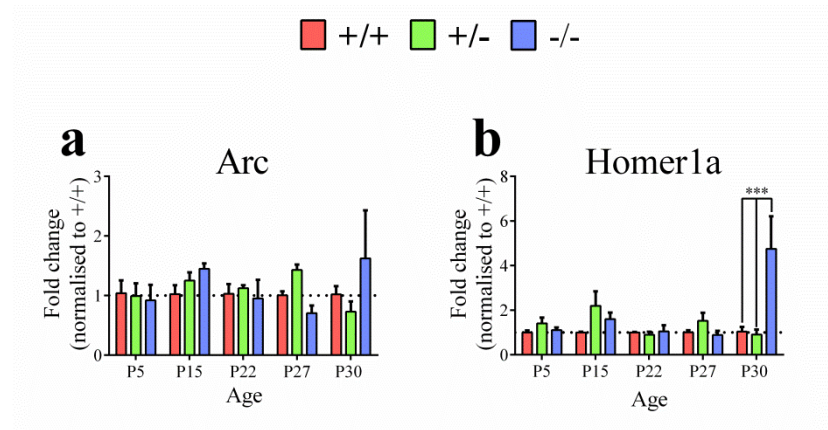


Figure 4.12 Quantification of activity-induced mRNAs in CSP α -/- animals.

qPCR analysis for Arc (a) and Homer1a (b) mRNAs in the hippocampus from CSP α +/+, +/- and -/- animals killed at different time points (P5-P30). Data in graphs represents mean \pm SEM mRNA expression values from $n = 3$ animals per genotype and time-point, except for Homer1a at P5 ($n = 2$ for CSP α +/+ and -/-) and at P22 ($n = 2$ for CSP α -/-). Statistical test = repeated measures two-way ANOVA with Bonferroni post-analysis (a and b) and one-way ANOVA with Bonferroni post-analysis (b, P5 and P22 only). Statistical significance relative to CSP α +/+ and +/-: *** $P \leq 0.001$. +/+, wildtype; +/-, heterozygous; -/-, knockout and P, postnatal days.

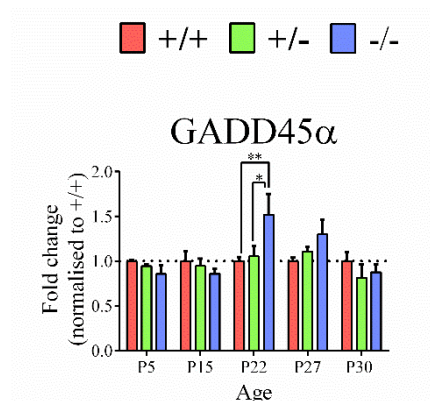


Figure 4.13 Quantification of the mRNA levels of the cellular physiological and environmental damage stress sensor GADD45 α in CSP α -/- animals.

qPCR analysis for GADD45 α mRNA in the hippocampus of CSP α +/+, +/- and -/- animals killed at different time points (P5-P30). Data in graphs represents mean \pm SEM of the mRNA expression values from $n = 3$ animals per genotype and time-point. Statistical test = repeated measures two-way ANOVA with Bonferroni post-analysis. Statistical significance relative to CSP α +/+ and +/-: * $P \leq 0.05$ and ** $P \leq 0.01$. +/+, wildtype; +/-, heterozygous; -/-, knockout and P, postnatal days.

4.4.6 Expression of other stress-related response proteins in CSP α -/- animals

4.4.6.1 Western blotting

Following the transcript profiling of stress-related response molecules, protein expression of some of these molecules was investigated by quantitative western blotting. Western blotting for ATF3, c-Jun, c-Fos and GADD45 α proteins was performed in CSP α animals at P27-P30, to encompass the time when transcriptional changes were seen. Immunoreactivity of GADD45 α could not be detected in the CSP α samples by western blotting, even with the loading of 40 μ g of protein. However, immunohistochemistry for GADD45 α was performed and immunoreactivity detected (section 4.4.6.2.4). Despite a significant transcript induction of ATF3 and c-Jun at P30 in CSP α -/- animals, no significant change was detected at the protein level (Figure 4.14a-c). Levels of c-Fos protein were not different between CSP α genotypes (Figure 4.14d).

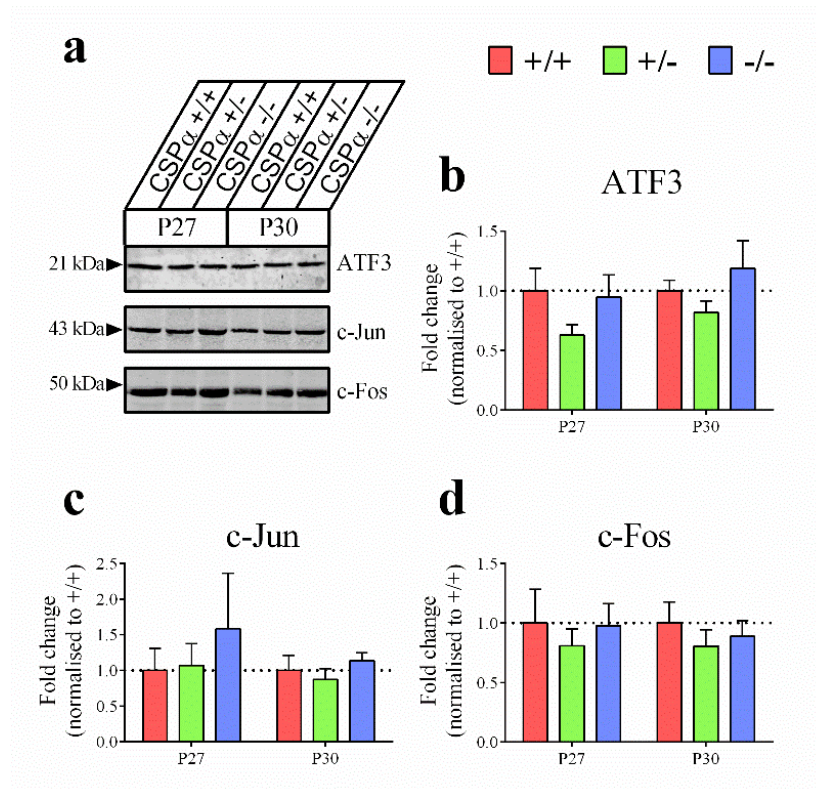


Figure 4.14 Quantification of immediate early gene proteins in CSP α -/- animals.

Representative western blotting (a) and related quantification for ATF3 (b), c-Jun (c) and c-Fos (d) in SDS extracted hippocampi from CSP α +/+, +/- and -/- animals killed at different time points (P5-P30). Data in graphs represents mean \pm SEM of the protein expression values from $n = 3$, except for CSP α -/- animals at P30, where $n = 4$. Statistical test = one-way ANOVA with Bonferroni post-analysis. +/+, wildtype; +/-, heterozygous; -/-, knockout; and P, postnatal days. Data collected in collaboration with Dr Joanne Bailey.

4.4.6.1 **Immunohistochemistry**

Although western blotting revealed no difference in the protein expression of stress-related response proteins in CSP α $-/-$ animals, immunohistochemistry was performed to determine if there was an induction of these proteins in specific regions of the hippocampus.

4.4.6.1.1 ATF3

Visual inspection of the whole hippocampus reveals low levels of expression for ATF3 (Figure 4.15a). Staining and subsequent quantification for ATF3 revealed that there was no clear difference in expression of ATF3 in the DG between CSP α $+/+$, $+/-$ and $-/-$ animals (Figure 4.15a E-H). The staining intensity for ATF3 was varied between the two CSP α $-/-$ animals in the CA3 (Figure 4.15a K and L). This is also reflected by the scatter plots for ATF3 staining intensity (Figure 4.15b). However, in CSP α $-/-$ animal 1 ATF3 staining was clearly induced in the CA3 pyramidal layer compared to CSP α $+/+$ and CSP α $+/-$ animals (Figure 4.15a K). There was little staining for ATF3 in the CA1 region in all 3 CSP α genotypes (Figure 4.15a M-P).

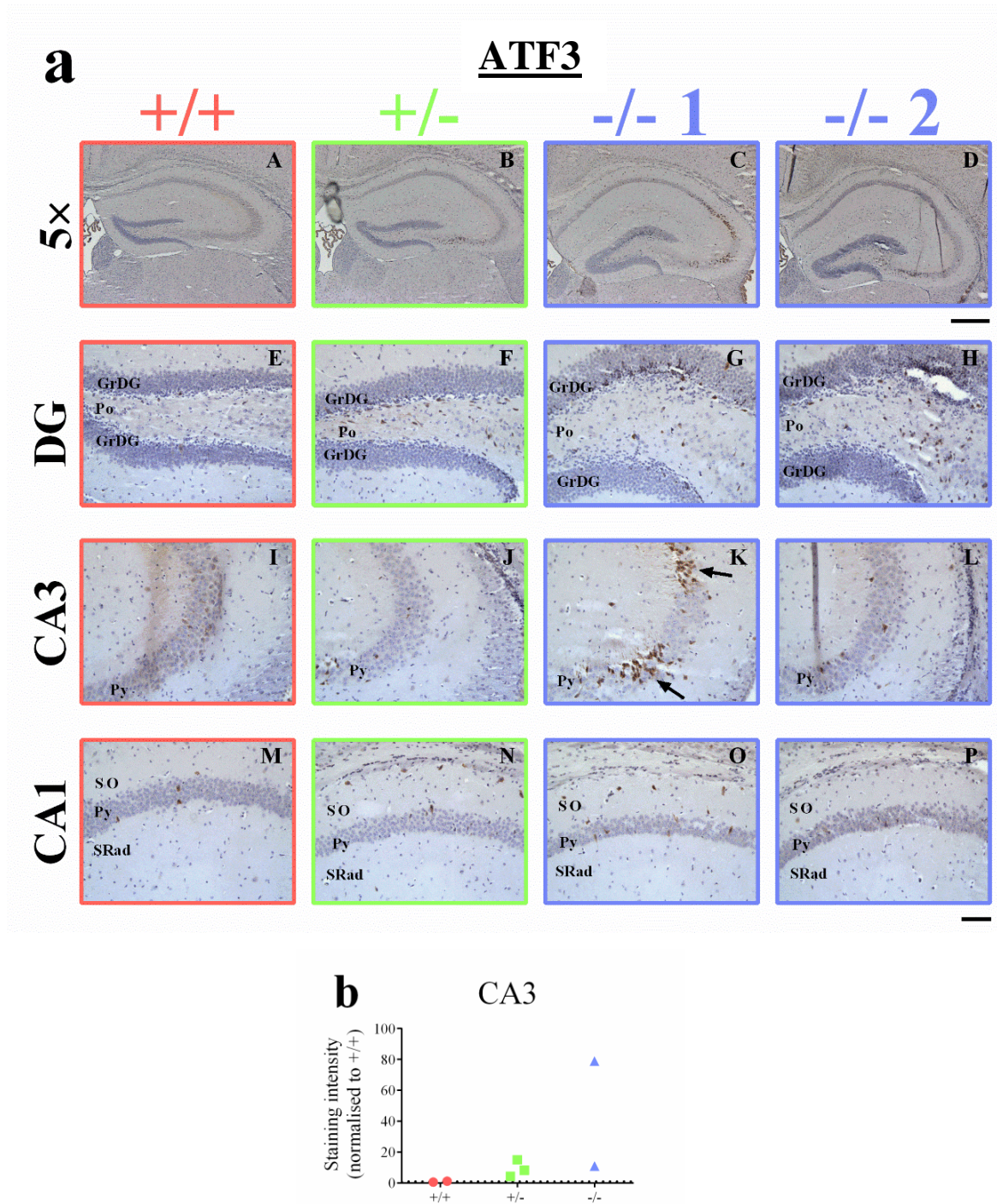


Figure 4.15 Immunohistochemical staining for ATF3 in CSP α -/- animals.

Immunohistochemical staining (a) and related quantification of the staining intensity (b) for ATF3 in different regions of the hippocampus. (a) Immunohistochemical staining was performed on CSP α animals killed at P29. $n = 2$ animals per genotype, except for CSP α +/- where $n = 3$. The scale bar for 5x images is indicated under image D (300 μ m) and the scale bar for all other images is indicated under image P (100 μ m). -/- 1 and -/- 2 refer to two different CSP α -/- animals. Black arrows represent distinct and

positive immunostaining. (b) Data in graphs represents individual values of the staining intensity for ATF3 in the pyramidal layer of CA3. *n* is the same as in (a). +/+, wildtype; +/-, heterozygous; -/-, knockout; CA1, Cornu Ammonis region 1; CA3, Cornu Ammonis region 3; DG, dentate gyrus; GrDG, granule cell layer of the DG; P, postnatal days, Po, polymorphic layer; Py, pyramidal layer; SO, stratum oriens and SRad, stratum radiatum. Data collected in collaboration with Dr Joanne Bailey.

4.4.6.1.2 c-Jun

c-Jun protein was expressed highly in the DG in all CSP α genotypes (Figure 4.16a E-H). However, the granule cell layer of the DG was less stained in CSP α -/- animal 1 (Figure 4.16a G). The expression of c-Jun protein in the CA3 was low for CSP α +/+, CSP α +/- and CSP α -/- animal 1 (Figure 4.16a I-K). However, c-Jun was expressed highly in the CA3 pyramidal layer of -/- animal 2 (Figure 4.16a L). In the CA1 pyramidal layer, c-Jun protein expression was increased in both CSP α -/- animals compared to CSP α +/+ and CSP α +/- animals (Figure 4.16a M-P and 4.16b).

4.4.6.1.3 c-Fos

c-Fos protein expression is low in the hippocampus and is not qualitatively different between the three CSP α genotypes (Figure 4.17).

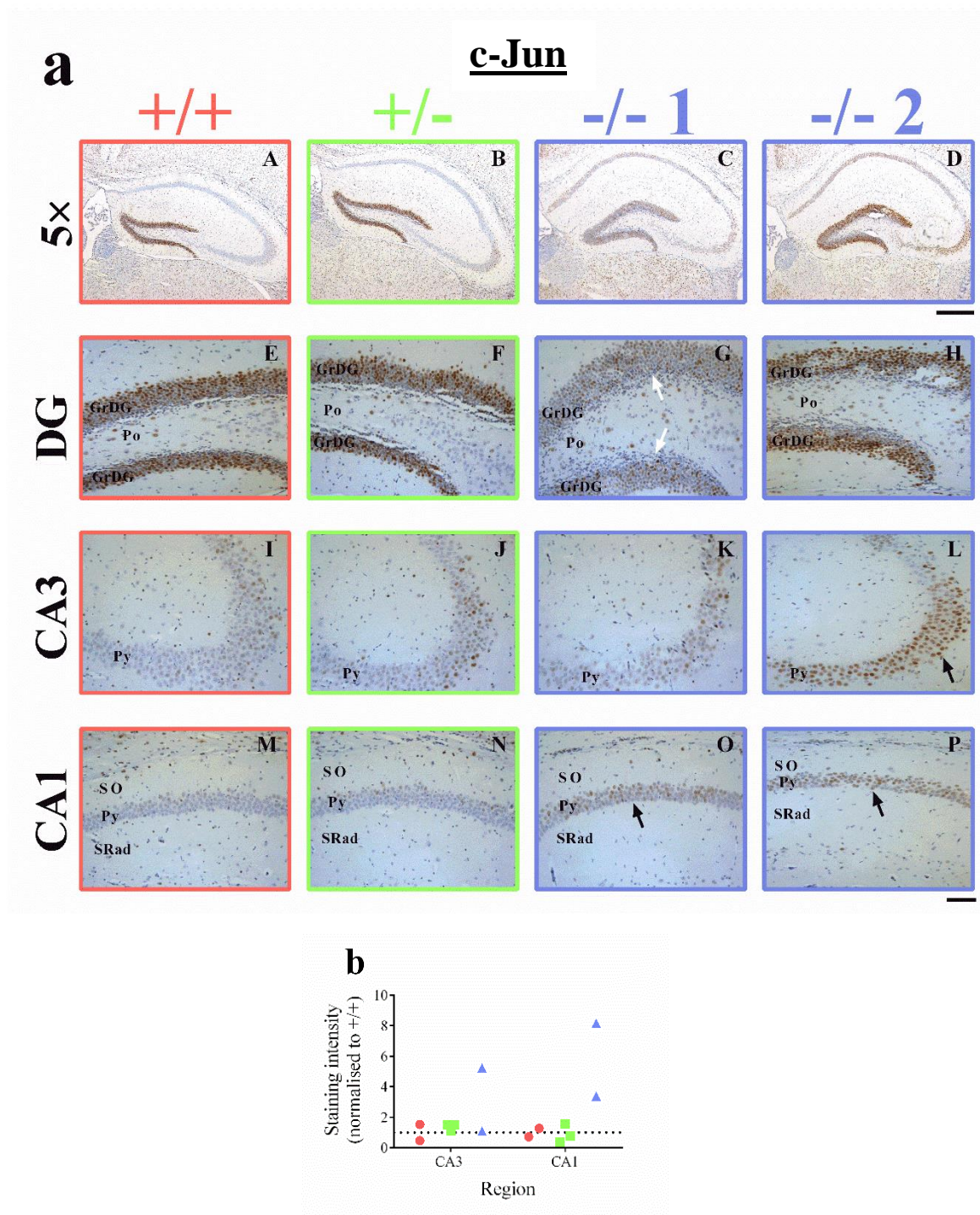


Figure 4.16 Immunohistochemical staining for c-Jun in CSP α $-/-$ animals.

Immunohistochemical staining (a) and related quantification of the staining intensity (b) for c-Jun in different regions of the hippocampus. (a) Immunohistochemical staining was performed on CSP α animals killed at P29. $n = 2$ animals per genotype, except for CSP α $+/-$ where $n = 3$. The scale bar for 5x images is indicated under image D (300 μm) and the scale bar for all other images is indicated under image P (100 μm). $-/-$ 1 and $-/-$ 2 refer to two different CSP α $-/-$ animals. Black arrows represent distinct and positive immunostaining. White arrows highlight reduced staining. (b) Data in graphs

represents individual values of the staining intensity for c-Jun in the pyramidal layer of CA3 and CA1. *n* = is the same as in (a) +/+, wildtype; +/-, heterozygous; -/-, knockout; CA1, Cornu Ammonis region 1; CA3, Cornu Ammonis region 3; DG, dentate gyrus; GrDG, granule cell layer of the DG; P, postnatal days, Po, polymorphic layer; Py, pyramidal layer; SO, stratum oriens and SRad, stratum radiatum. Data collected in collaboration with Dr Joanne Bailey.

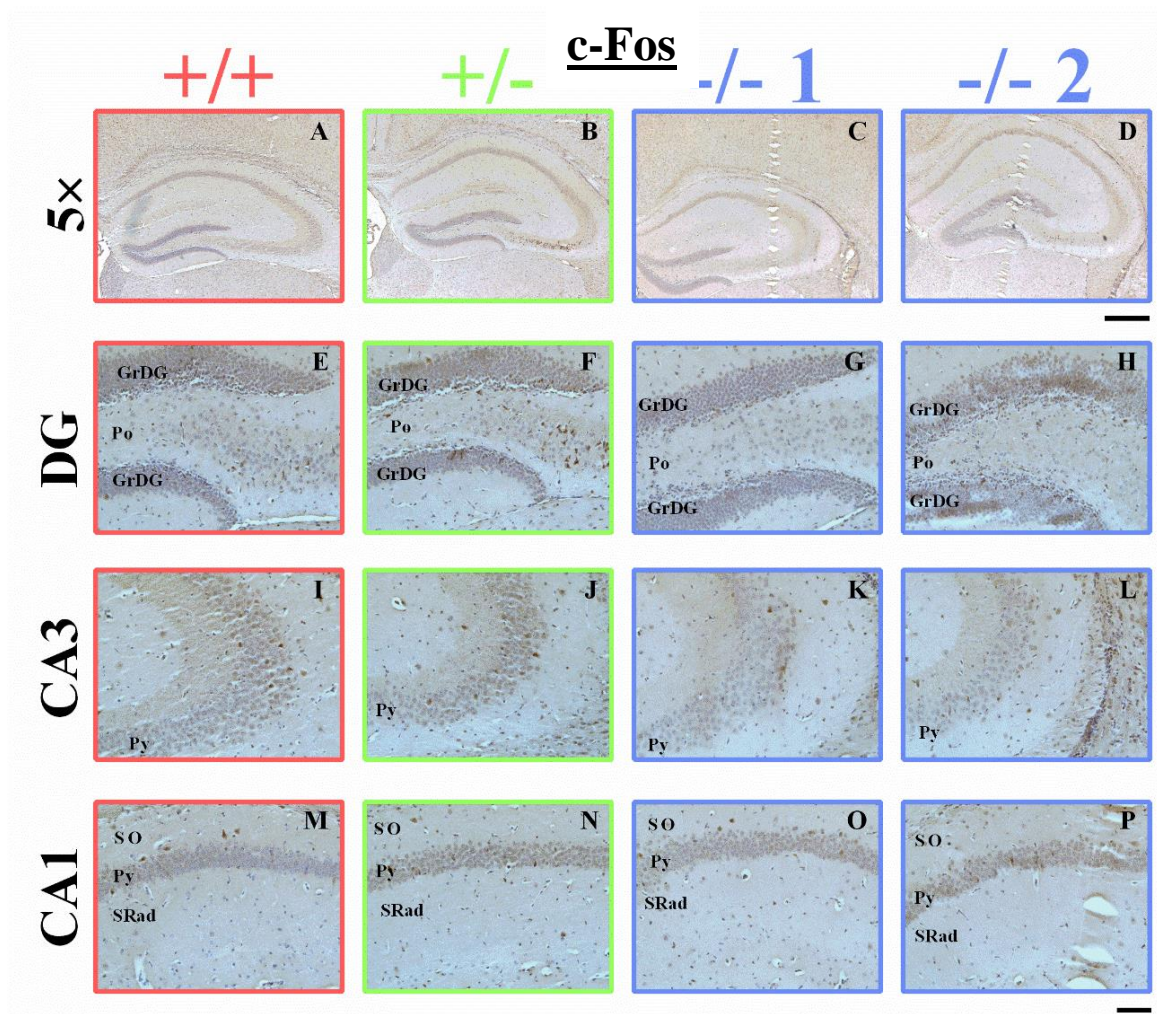


Figure 4.17 Immunohistochemical staining for c-Fos in CSPα -/- animals.

Immunohistochemical staining (a) and related quantification of the staining intensity (b) for c-Fos in different regions of the hippocampus. (a) Immunohistochemical staining was performed on CSPα animals killed at P29. $n = 2$ animals per genotype, except for CSPα +/- where $n = 3$. The scale bar for 5x images is indicated under image D (300 μm) and the scale bar for all other images is indicated under image P (100 μm). -/- 1 and -/- 2 refer to two different CSPα -/- animals. +/+, wildtype; +/-, heterozygous; -/-, knockout; CA1, Cornu Ammonis region 1; CA3, Cornu Ammonis region 3; DG, dentate gyrus; GrDG, granule cell layer of the DG; P, postnatal days, Po, polymorphic layer; Py, pyramidal layer; SO, stratum oriens and SRad, stratum radiatum. Data collected in collaboration with Dr Joanne Bailey.

4.4.6.1.4 Expression of the cellular physiological and environmental damage stress sensor, GADD45 α , in CSP α -/- animals

GADD45 α immunohistochemical staining revealed there was no qualitative difference in staining between CSP α +/+, CSP α +/- and CSP α -/- animals in the DG and CA1 (Figure 4.18a). Like ATF3, the staining intensity for GADD45 α was varied between the two CSP α -/- animals (Figure 4.18a K and L). However, in CSP α -/- animal 1 GADD45 α staining was clearly increased in the pyramidal layer compared to CSP α +/+ and CSP α +/- animals (Figure 4.18a K and 4.17b).

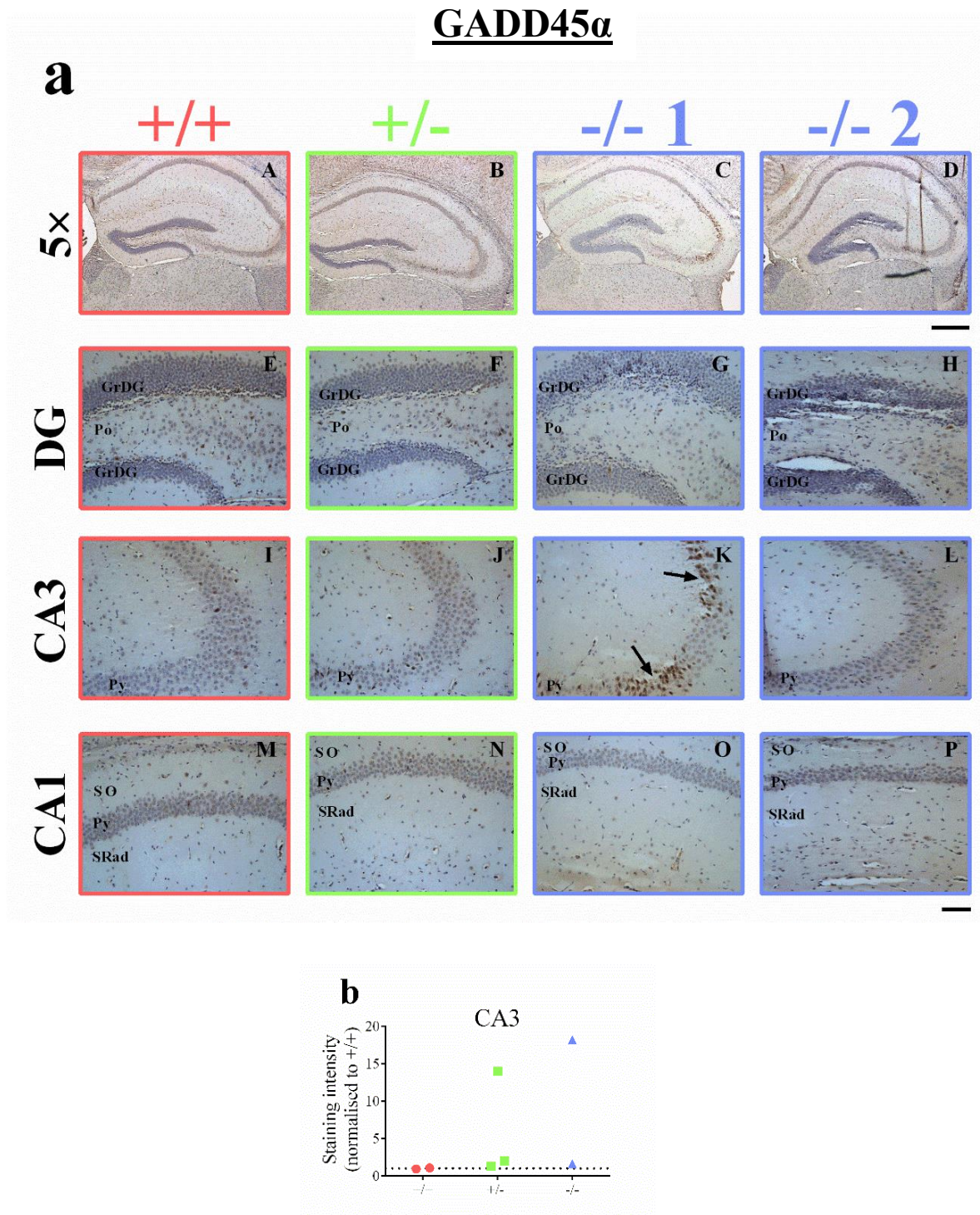


Figure 4.18 Immunohistochemical staining for GADD45 α in CSP α -/- animals.

Immunohistochemical staining (a) and related quantification of the staining intensity (b) for GADD45 α in different regions of the hippocampus. (a) Immunohistochemical staining was performed on CSP α animals killed at P29. $n = 2$ animals per genotype, except for CSP α +/- where $n = 3$. The scale bar for 5x images is indicated under image D (300 μ m) and the scale bar for all other images is indicated under image P (100 μ m). -/- 1 and -/- 2 refer to two different CSP α -/- animals. Black arrows represent distinct

and positive immunostaining. (b) Data in graphs represents individual values of the staining intensity for GADD45 α in the pyramidal layer of CA3. *n* is the same as in (a). +/+, wildtype; +/-, heterozygous; -/-, knockout; CA1, Cornu Ammonis region 1; CA3, Cornu Ammonis region 3; DG, dentate gyrus; GrDG, granule cell layer of the DG; P, postnatal days, Po, polymorphic layer; Py, pyramidal layer; SO, stratum oriens and SRad, stratum radiatum. Data collected in collaboration with Dr Joanne Bailey.

4.5 Discussion

Deletion of CSP α in mice is not embryonic lethal but CSP α -/- mice develop progressive neurodegeneration that occurs within 60 post-natal days (Fernández-Chacón et al., 2004). CSP α -/- mice begin to die rapidly after ~4 weeks and none survive beyond 3 months of age (Fernández-Chacón et al., 2004). In the analysis in this chapter, CSP α -/- animals fed soft food still lose $\geq 20\%$ of their body weight at ~P30 and therefore CSP α -/- animals could not be analysed past this time-point due to welfare considerations.

4.5.1 SNAP-25 protein levels and SNARE-complex assembly is reduced whilst synaptic loss is not detected in CSP α -/- animals

CSP α has been shown in combination with Hsc70 and SGT to chaperone SNAP-25 (Sharma et al., 2012a, Sharma et al., 2011). Previous studies have reported a ~40% - ~50% decrease in SNAP-25 and SNARE-complex assembly at P40 (Chandra et al., 2005, Sharma et al., 2011). In agreement with these results a decrease in the levels of SNAP-25 and SNARE-complex assembly was seen in CSP α -/- animals from P15 (Figure 4. 4a, c and d). In CSP α -/- animals at P30, levels of SNAP-25 and SNARE-complex assembly were reduced by 43% and 57%, respectively (Figure 4.4c and d). SNARE-complex assembly is also reduced in post-mortem brain tissue from AD and PD patients (Sharma et al., 2012b), which suggests, this might be an important primary pathological feature of human chronic neurodegenerative disease. Although, it also could be a consequence of gross synaptic loss and thus a secondary pathological feature.

Despite synaptic dysfunction (exemplified by reduced SNAP-25 levels and SNARE-complex assembly) in CSP α -/- animals, synaptic loss was not detected in CSP α -/- animals at the time-points investigated. Quantitative western blotting revealed

no significant difference in the levels of the presynaptic protein synaptophysin or the post-synaptic protein PSD-95 between the CSP α animals up to P30 (Figure 4.5a-c). Immunohistochemical staining for synaptophysin at P29 also failed to show any clear qualitative signs of presynaptic loss in CSP α $-/-$ animals (Figure 4.5d). It has been shown that in the hippocampus of CSP α $-/-$ mice, the inhibitory synaptotagmin 2, PV+ expressing basket cells are the most vulnerable to synaptic degeneration, with a loss of these synapses detected from P28 (García-Junco-Clemente et al., 2010). Therefore, significant synaptic loss might not occur until after P30 in the hippocampus of CSP α $-/-$ animals. This would explain why synaptic loss was not detected by quantitative western blotting and immunohistochemistry for synaptophysin and PSD-95, which are both abundant synaptic proteins.

4.5.2 GFAP upregulation follows SNAP-25 and SNARE-complex assembly reduction in CSP α $-/-$ animals

Whilst synaptic loss is not detected, an increase in the levels of GFAP mRNA and protein was detected in CSP α $-/-$ animals between P27-P30 (Figure 4.6). Immunohistochemical staining for GFAP suggests that the CA3 region might be more vulnerable to dysfunction in CSP α $-/-$ animals than the DG and CA1 region (Figure 4.7). This is in agreement with previous observations which also show an upregulation of GFAP in the CA3 of CSP α $-/-$ animals (Malfa, 2012). In addition, CSP immunoreactivity has been found to be high in the mossy fibres which synapse onto CA3 pyramidal neurons (Kohan et al., 1995). Therefore, a loss of CSP α here may render this region more vulnerable to dysfunction and may explain the increased astrogliosis selectively seen in the CA3.

The upregulation of GFAP (Figure 4.6-4.7) suggests hippocampal homeostasis has been perturbed. Increased GFAP expression has been shown to be widespread in the hippocampus of CSP α $-/-$ animals at P42 (Chandra et al., 2005). A similar induction of GFAP expression in all regions of the hippocampus might have been seen in the CSP α $-/-$ animals used in this study had they been able to be kept for an extended period of time. Astrocytes are extremely sensitive to changes in the nervous system and in the ME7 model astrogliosis precedes overt synaptic loss (Betmouni et al., 1996, Cunningham et al., 2003, Gray et al., 2009, Sisková et al., 2009). The increased

expression of GFAP in CSP α -/- animals in this study also reflects an early pathological change, which like the ME7 model, precedes synaptic loss.

As well as the associated astrogliosis seen in CSP α -/- animals, activation of microglia is seen in CSP α -/- animals from P26 (Malfa, 2012). This provides an additional readout of dysfunction seen in the CSP α -/- animals.

4.5.3 CSP α -/- mice do not undergo a UPR

The UPR was investigated in the CSP α -/- model to determine if either synaptic dysfunction (exemplified by reduced levels of SNAP-25 and SNARE-complex assembly) or the lost ability to chaperone CSP α client proteins would induce ER stress and engage the UPR pathway. Analysis of UPR mRNAs (BiP, spliced XBP-1, GADD34, CHOP and ATF4) failed to detect a robust UPR in CSP α -/- animals compared to CSP α +/+ animals (Figure 4.8). GADD34 mRNA was induced at P22 and P27 in CSP α -/- animals and CHOP mRNA was also increased in CSP α -/- animals at P27 (Figure 4.8c and d). However, this induction was modest (<1.5 fold) and not sustained and occurred at a time when no other UPR molecules were induced.

Similarly, analysis of BiP and eIF2 α -P at the protein level by quantitative western blotting failed to detect a UPR (Figure 4.9a-c). In support of these observations, Sharma et al., showed no difference in the protein expression of BiP between CSP α +/+ and CSP α -/- animals (Sharma et al., 2012b). Quantitative western blotting for 4EBP1 provided additional support to show that there is no detectable translational arrest occurring in the CSP α -/- animals at any of the time-points investigated (Figure 4.9a, d-e). In fact there is an increase in the ratio of hyperphosphorylated: phosphorylated/hypophosphorylated 4EBP1 in the CSP α -/- animals at P30. This in addition to the reduced levels of eIF2 α -P at P30, suggests that global translation is increased as opposed to repressed. It is possible that the loss of CSP α chaperoning of its client proteins (which leads to ubiquitination and degradation) (Sharma et al., 2011; Zhang et al., 2012) leads to increased protein translation as cells attempt to restore these protein levels.

The lack of a robust UPR in CSP α -/- animals is similar to that seen in ME7-animals (chapter 3) and suggests that the UPR is not implicated in these two distinct models, which both have different underlying etiologies.

Although ER stress is not occurring as reported by the levels of UPR mRNA or protein, treatment of CSP α $-/-$ mice with proteasome inhibitors alleviates CSP α mediated neurodegeneration (Sharma et al., 2012b), which suggests that proteostasis is impacted. Ubiquitination pathways independent of the ER might therefore be important. Interestingly, proteasome inhibition has been shown to lead to ER stress (Hetz et al., 2007) and unsurprisingly proteasome inhibition in CSP α $-/-$ animals causes an upregulation of BiP (Sharma et al., 2012b). However, in this context the upregulation of BiP coincides with an increase in SNAP-25 and SNARE-complex assembly and is not detrimental. Despite the lack of induction of BiP protein in the CSP α $-/-$ animals in this study or in the study by Sharma et al., levels of BiP protein are increased in AD and PD post-mortem brain tissue, where SNARE-complex assembly is reduced (Sharma et al., 2012b).

Similar to ME7-animals, SIL1 mRNA is significantly increased in CSP α $-/-$ animals compared to CSP α $+/+$ at P15 and P27 (Figure 4.10). The observation that SIL1 is induced in CSP α $-/-$ animals adds further support to the data which shows there is no classic UPR engaged in CSP α $-/-$ animals.

4.5.4 Other stress-related response molecules are induced in CSP α $-/-$ animals

Other stress-related response molecules which are induced in the ME7-animals (chapter 3) were investigated. This included the immediate early gene molecules: ATF3, c-Jun and c-Fos; the activity-induced immediate early gene molecules: Arc and Homer1a and the cellular physiological and environmental damage stress sensor GADD45 α .

In contrast to a lack of a UPR in CSP α $-/-$ animals, some of these other stress-related response mRNAs are increased in CSP α $-/-$ animals. mRNA levels of ATF3, c-Jun and Homer1a are significantly increased in CSP α $-/-$ animals compared to CSP α $+/+$ and CSP α $+/-$ at P30 (Figure 4.11a and b and 4.12b). mRNA levels of c-Fos and Arc are also increased at P30 but not to a statistically significant level (Figure 4.11c and 4.12a). In addition, GADD45 α mRNA levels were increased in CSP α $-/-$ animals at P22 (Figure 4.13).

Quantitative western blotting for ATF3, c-Jun and c-Fos proteins between P27-P30 failed to show an increase in the expression of any of these proteins (Figure 4.14a-d). Immunohistochemistry was therefore performed for all 3 proteins plus GADD45 α , to

determine whether changes at the protein level were restricted to certain regions in the hippocampus.

Immunohistochemical analysis revealed that ATF3 and GADD45 α was induced in the CA3 pyramidal layer of CSP α $-/-$ animals (Figure 4.15 and 4.18). However, this was variable between the two CSP α $-/-$ animals studied and this might represent the heterogeneity in illness severity seen in CSP α $-/-$ animals, with some animals appearing phenotypically worse than others. ATF3 and GADD45 α are likely to be expressed in the same cells, as shown by sequential DAB immunopositive staining.

c-Jun protein is endogenously expressed at high levels in the DG (Figure 4.16a E-H). Interestingly, c-Jun protein expression is reduced in the granule cell layer of the DG in CSP α $-/-$ animals, particularly in CSP α $-/-$ animal 1 (Figure 4.16a G). However, one CSP α $-/-$ animal had increased expression of c-Jun in the CA3 pyramidal layer and both CSP α $-/-$ animals had increased c-Jun expression in the CA1 pyramidal layer compared to CSP α $+/+$ and CSP α $+/-$ (Figure 4. 16a and b). Therefore, in contrast to the DG, where c-Jun expression is reduced in CSP α $-/-$ animals, c-Jun expression is increased in the CA3 and CA1 pyramidal layer. In contrast to c-Jun, levels of c-Fos protein were not increased in any of the hippocampal regions in CSP α $-/-$ animals (Figure 4. 17).

The expression of ATF3, c-Fos and GADD45 α proteins is increased in a sub-region of CA3, CA3b, in CSP α $-/-$ animals (appendix 10). Interestingly, these molecules are also highly expressed in the CA3b of CSP α $+/-$ animals compared to CSP α $+/+$. Therefore, immunohistochemical staining of stress-related response proteins in CSP α $+/-$ animals suggests that despite no obvious phenotypic differences compared to CSP α $+/+$ animals (Fernández-Chacón et al., 2004), differences can be seen at a biochemical level. This suggests that although a $\sim 50\%$ reduction in CSP α is not lethal, it is sufficient to drive neuronal stress responses.

Results from Sharma et al., have shown that CSP α $+/-$ animals are more vulnerable to neurodegeneration when an additional insult occurs (Sharma et al., 2012a). SNAP-25 knockdown in CSP α $+/-$ animals decreases SNARE-complex assembly, neuron and synapse density and increases apoptosis compared to CSP α $+/+$ animals. CSP α $+/-$ animals have been inoculated with ME7 prion to determine if this additional insult would render CSP α $+/-$ animals more vulnerable to neurodegeneration (Davies et al., 2015) (appendix 11).

There is variation observed between the two CSP α $-/-$ animals used for immunohistochemical analysis. An increased n number will be required to confidently assess the expression of these stress-related response molecules. In addition, in the future it would be useful to rate the severity of illness of each CSP α $-/-$ animal at late stage disease so this can be correlated post-mortem to differential biochemical changes seen in these animals.

Despite little evidence for a UPR, the induction of other stress-related response molecules at the mRNA level (ATF3, c-Jun and Homer1 α) and protein level (ATF3, GADD45 α and c-Jun) shown in this chapter is similar to that seen in ME7-animals (chapter 3). The upregulation of these molecules suggests common molecular pathways are activated in response to neuronal dysfunction seen in both of these models.

4.6 Conclusion

The hippocampus of CSP α $-/-$ mice was used to investigate the UPR and other stress-related response molecules using a combination of biochemistry and immunohistochemistry techniques. CSP α $-/-$ animals had reduced levels of SNAP-25 and SNARE-complex assembly, signifying synaptic dysfunction, however, synaptic loss was not detected. qPCR and quantitative western blotting revealed that the UPR was not robustly induced in CSP α $-/-$ animals. An increased expression of other stress-related response mRNAs (including immediate early gene molecules, activity-induced immediate early gene molecules and the cellular physiological and environmental damage stress sensor GADD45 α) was seen in CSP α $-/-$ animals. Quantitative western blotting revealed no difference in the expression of these other stress-related response proteins, but immunohistochemistry showed that these stress-related response proteins are induced in particular regions of the hippocampus in CSP α $-/-$ animals at P29. The selective expression of these molecules is likely to be the reason why they were not detected using whole hippocampal tissue.

Mechanistic insight into stress-related response molecules and pathways is needed to unravel the consequential expression of these molecules. Strategies which increase SNARE-complex assembly have been shown to be neuroprotective in mice deficient in CSP α . Manipulation of stress-related response molecules and pathways may provide an alternative approach for providing neuroprotection in CSP α $-/-$ animals.

Chapter 5: Is the unfolded protein response induced in a kainic acid model of excitotoxicity?

5.1 Introduction

The onset and progression of neurodegenerative disease pathology in the ME7 prion model evolves over a period of several months and a few weeks in the CSP α $-/-$ model (chapter 3 and 4). There was very little evidence for a UPR in either of these models. In order to assess whether the UPR can be evoked in other pathological conditions, a kainic acid (KA) model of excitotoxicity was used to investigate if the UPR is induced by an insult which leads to acute neurodegeneration (Kim et al., 2014, Sokka et al., 2007, Zhang et al., 2002).

KA is an excitatory amino acid extracted from seaweed (Ben-Ari and Cossart, 2000) and is an agonist of AMPA/kainate glutamate receptors (Wang et al., 2005). KA-driven neuronal excitation leads to depolarisation of the cell, increased intracellular levels of Ca²⁺ and activation of calcium-dependent pathways leading to apoptosis (Wang et al., 2005). The increased and excessive excitation driven by the administration of KA and subsequent neuronal damage is a form of excitotoxicity.

In rodents, systemic or intracerebral injection of KA induces, seizures, behavioural changes and neurodegeneration (Chen et al., 2002, Choi et al., 2011, McKhann et al., 2003, Zhang and Zhu, 2011). KA induced seizures have been used as a model of human temporal lobe epilepsy (Ben-Ari and Cossart, 2000). Excitotoxicity has also been implicated in stroke (Lai et al., 2014) and chronic neurodegenerative diseases including AD, PD, and ALS (Dong et al., 2009, Zheng et al., 2011). In addition, transcriptomic analysis of CA1 neurons from mice inoculated with the RML prion strain has revealed a molecular signature containing elements of pathways associated with neuronal excitation (Majer et al., 2012). The high density of kainate receptors in the hippocampus (Bahn et al., 1994, Werner et al., 1991) means that the hippocampus is particularly vulnerable to KA pathology (Ferrer et al., 2002, Zhang and Zhu, 2011). In particular the pyramidal neurons of CA3 are more susceptible to KA-induced pathology (Ben-Ari and Cossart, 2000, Lee et al., 2001, Nadler et al., 1978). The KA model has been used as a paradigm to unpick events leading to neurodegeneration caused by excitotoxicity *in vivo*

(Cardoso et al., 2010, Zhang and Zhu, 2011). Administration of KA leads to gliosis and neuronal death in the hippocampus (Chihara et al., 2009; Cardoso et al., 2010).

Acute neuronal dysfunction and degeneration, such as that brought on by injection of KA, triggers molecular cascades in response to such an insult (Francis et al., 2004). Stress-related response molecules including c-Jun and ATF3 induced in ME7-animals and CSP α $-/-$ animals are classic stress-response molecules upregulated in KA-injected animals (see discussion). In this chapter, KA-injected animals has been used to determine if the UPR is induced in an acute model of neuronal dysfunction. If the UPR is induced in KA-animals, it suggests that the UPR is implicated in acute neuronal dysfunction as opposed to more chronic and protracted neuronal dysfunction.

In addition, another model of acute neuronal injury – initiated by the acute coronal slicing of mouse brain tissue (Takano et al., 2014) has also been used in this chapter to investigate if the UPR proteins, BiP and eIF2 α -P are induced. This model provides an additional readout of the UPR in acute stress conditions, in which the primary injury is the mechanical lesioning of cell processes.

5.2 Aims

- 1) To investigate the UPR and other stress-related responses molecules (immediate early genes, activity-induced immediate early genes and a cellular physiological and environmental damage stress sensor), investigated in the previous two chapters in KA-injected animals. Hippocampal tissue was taken from control and KA-injected animals 6 hr, 24 hr and 3 d after treatment and used for quantitative western blotting and qPCR. Whole brain tissue sections (containing the hippocampus) was collected for immunohistochemistry. These techniques were used to:
 - Quantify the expression of UPR and other stress-related response mRNAs
 - Quantify the expression of UPR and other stress-related response proteins
 - Investigate where in the hippocampus these molecules are expressed

The experimental outline for this study is shown in Figure 5.1.

- 2) To investigate if the UPR proteins, BiP and eIF2 α -P are induced in brain tissue which has undergone acute coronal slicing.

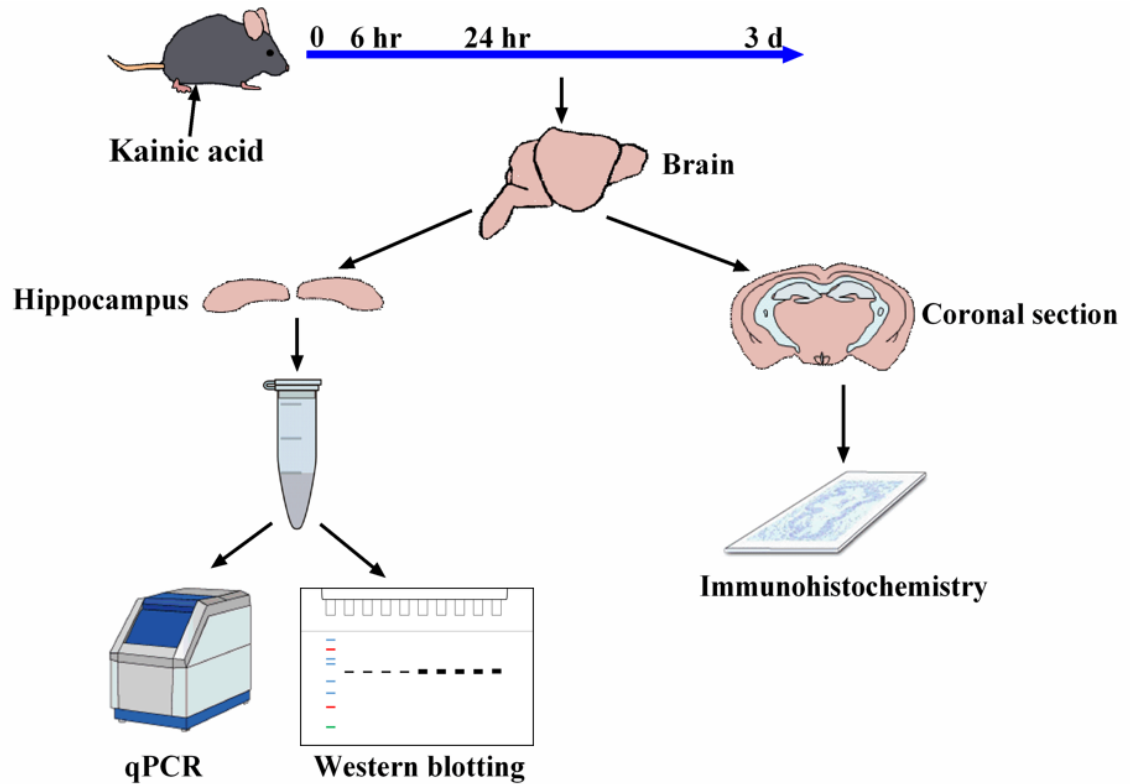


Figure 5.1 Experimental outline: investigating the UPR and other stress-related response molecules in KA-animals.

C57BL/6J female mice (8-13 weeks of age) were injected i.p. with saline (control) or KA. Control and KA-animals were killed 6 hr, 24 hr and 3 d after treatment. The brain was removed and used for hippocampal dissection. The dissected hippocampus was homogenised and the homogenate split into two aliquots. One aliquot was used to isolate RNA and perform qPCR and the other to isolate protein and to perform quantitative western blotting. Coronal sections were cut from control and KA-animals and used for immunohistochemistry. d, days; hr, hours; i.p., intraperitoneally and KA, kainic acid.

5.3 Specific materials and methods

5.3.1 KA administration

C57BL/6J mice female mice (8-13 weeks of age) were injected i.p. with KA at a dose of 20 mg/kg. Although seizure scores are lower at this dose than at higher doses, this dose was chosen as it was shown to induce stress response molecules and had a lower mortality rate than seen for higher doses of KA (Schauwecker and Steward, 1997, Zhang et al., 2002). Control mice were injected with an equivalent volume of 0.9% sterile saline. Mice which had been injected with KA showed signs of seizure activity (10 min after injection) including immobility, head bobbing and rearing. No seizure activity was observed for control mice.

5.3.2 qPCR

mRNA expression was calculated as described (section 2.6.3.1) with the exception of c-Fos, Arc, Homer1a and GFAP, which was calculated using the $2^{-\Delta\Delta C_t}$ method (section 2.6.3.2). c-Fos had a qPCR efficiency of 87.06%, Arc 83.53% and Homer1a 88.41%, whilst GAPDH (used to normalise c-Fos, Arc and Homer1a expression) had a qPCR efficiency of 98.90%. GFAP had a qPCR efficiency of 90.47%, whilst GAPDH (used to normalise GFAP expression) had a qPCR efficiency of 101.64%.

5.3.3 Immunohistochemistry - mouse brain slices

5.3.3.1 Preparation and slicing

Mouse brain slicing was performed by Chrysia-Maria Pegasiou. C57BL/6J female mice (8-13 weeks of age) were anaesthetised with terminal isoflurane and culled by decapitation in accordance with Home Office regulations. The brain was dissected in partially frozen artificial cerebrospinal fluid (ACSF), pH 7.2-7.4, with an osmolarity of approximately 300 mOsm and containing NaCl, 126 mM; KCl, 3 mM; NaH₂PO₄, 1.25 mM; MgSO₄, 2 mM; CaCl₂, 2 mM; NaHCO₃, 25 mM and glucose, 10mM. The brain was then transferred to a 50 ml falcon tube containing ice-cold ACSF and was transferred for slicing. The time taken between brain collection and slicing was <5 min.

Mouse brains were placed onto moist filter paper, on top of a frozen petri dish. The cerebellum was removed and the brain was positioned in front of a 4% agar block made with ACSF, using cyanoacrylate glue. The brain and block was then glued onto the cutting stage. A vibrating microtome (Intergaslice 7550 PSDS, Campden Instruments) was used to cut thick coronal sections at 4 °C. 400 µm and 150 µm coronal sections were cut for quantitative western blotting and immunohistochemistry, respectively. Coronal sections were placed in ice-cold ACSF and cut down the midline to obtain left and right hemispheres of the brain.

Sliced hemispheres were either collected immediately (0 hr) or bubbled with carbogen gas (95 % O₂/ 5 % CO₂) at room temperature for 4 or 8 hr. At 0, 4 and 8 hr, sliced hemispheres were either collected as whole for immunohistochemistry or were dissected to obtain the cortex, hippocampus and midbrain regions. Dissected tissue was placed into eppendorfs and snap-frozen and subsequently stored at -80 °C until required. Sliced hemispheres to be used for immunohistochemistry were fixed in 4% PFA for 1 hr at room temperature, then washed three times in 0.1 M phosphate buffer and stored at 4 °C in 0.1 M PB (2.4 g NaH₂PO₄, 11.36 g Na₂HPO₄ in 1 L ddH₂O, pH 7.4) until required. Tissue for western blotting was processed as described in section 2.9.

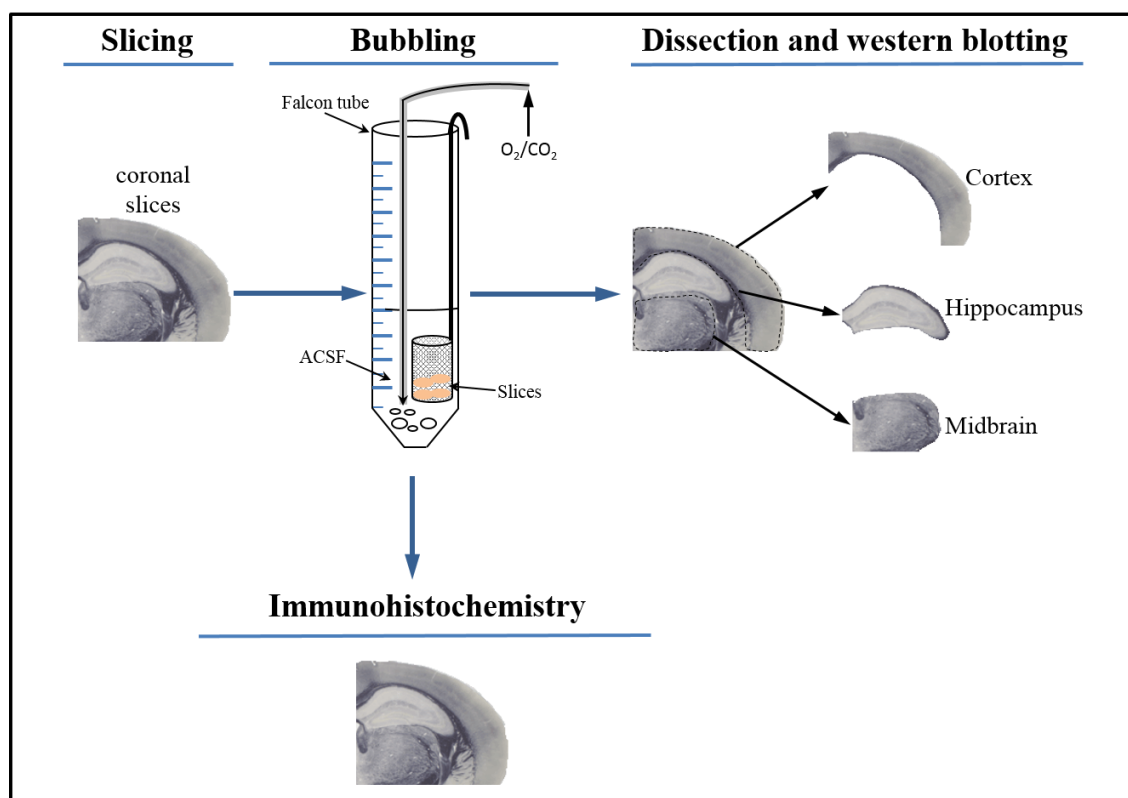


Figure 5.2 Experimental outline for coronal mouse brain slicing.

C57BL/6J female mice were killed, the brain was removed and coronal slices were cut on a vibrating microtome (400 μm for western blotting and 150 μm for immunohistochemistry). Coronal slices were cut down the midline to yield left and right hemispheres and were collected either immediately (0 hr) or bubbled in ACSF with O_2/CO_2 gas for 4 or 8 hr. Slices to be used for western blotting were dissected to obtain the cortex, hippocampus and midbrain. The whole hemisphere was used for immunohistochemistry. ACSF, artificial cerebrospinal fluid and hr, hour.

5.3.3.2 DAB staining

Free-floating immunohistochemistry was performed on mouse brain slices. Mouse brain slices in a 12 well-plate were washed three times (5 min/wash) in wash buffer (1 \times PBS, 0.1% Triton X-100). Sections were quenched and permeabilised in 0.3% hydrogen peroxide, 10% methanol in PBS containing 0.1% (v/v) Triton X-100. Following this sections were washed three times (5 min/wash) in wash buffer and then blocked in blocking buffer (5% (v/v) serum, 5% (w/v) BSA, 1 \times PBS, 0.2% (v/v) Triton X-100) for 1 hr at room temperature. Subsequent steps were the same as described in section 2.10.2, except wash steps were performed with wash buffer, primary and secondary antibody was incubated in blocking buffer and ABC solution was incubated in PBS

containing 0.1% (v/v) Triton X-100. Prior to DAB developing sections were mounted onto gelatinized slides. Counterstaining with haematoxylin was omitted from this protocol.

5.4 Results

5.4.1 Neuropathology in KA-animals

Haematoxylin staining of cell nuclei in the hippocampus of control and KA-animals was performed and qualitatively visualised. Staining revealed no clear neuronal cell loss in KA-animals between 6 hr and 3 d in the DG, CA3 and CA1 of KA-animals compared to controls (Figure 5.3).

qPCR analysis revealed that the mRNA levels of GFAP were significantly increased in KA-animals at 24 hr but declined by 3 d after KA administration (Figure 5.4a). This was associated with a significant induction of GFAP at the protein level in KA-animals 3 d after KA administration, as shown by quantitative western blotting (Figure 5.4b and c). Immunohistochemistry and related quantification for GFAP showed that GFAP expression was significantly increased in the DG of KA-animals 24 hr after KA-administration (Figure 5.5a and b). Increased staining for GFAP was also seen in the CA3 of KA-animals but this was not statistically significant from control animals (Figure 5.5a and c). Staining for GFAP was not increased in the CA1 of KA-animals (Figure 5.5a and d).

Haematoxylin

Control

Kainic acid

6 hr

24 hr

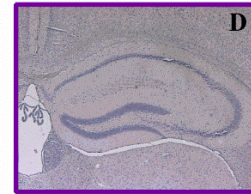
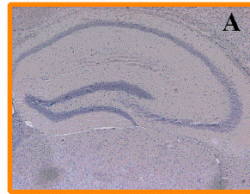
3 d

6 hr

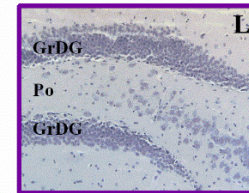
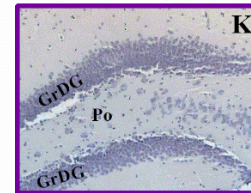
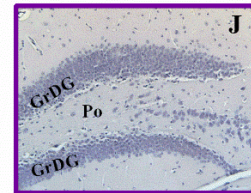
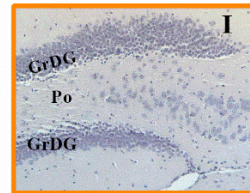
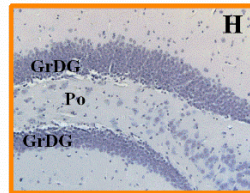
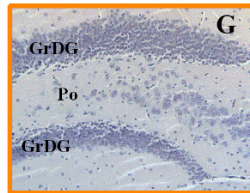
24 hr

3 d

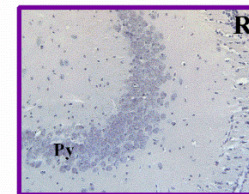
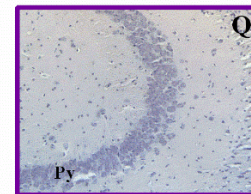
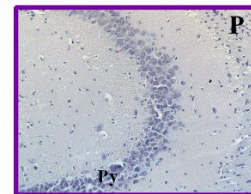
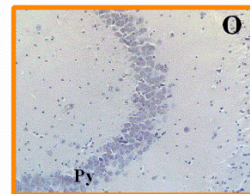
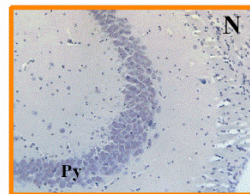
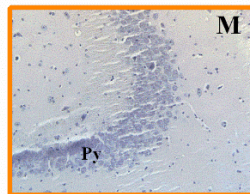
5×



DG



CA3



CA1

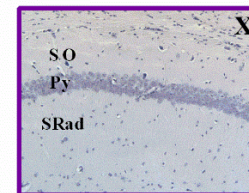
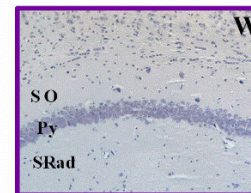
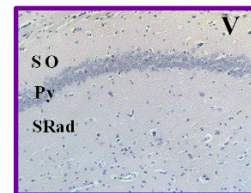
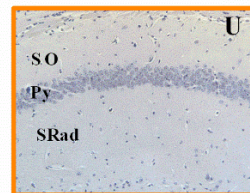
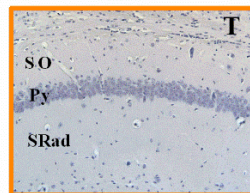
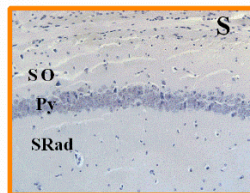


Figure 5.3 Haematoxylin staining of hippocampal sections from KA-animals.

Representative haematoxylin staining of hippocampal sections from control and KA-animals in different regions of the hippocampus. Staining was performed on brain sections from animals killed at 6 hr, 24 hr or 3 d after administration of saline (control) or KA. $n = 4$ animals per condition and time-point, except for KA-animals 24 hr after KA administration where $n = 3$. Scale bar for 5x images is indicated under image F (300 μm) and scale bar for the DG, CA3 and CA1 images is indicated under image X (100 μm). d, days; CA1, Cornu Ammonis region 1; CA3, Cornu Ammonis region 3; DG, dentate gyrus; GrDG, granule cell layer of the DG; hr, hours; KA, kainic acid; Po, polymorphic layer; Py, pyramidal layer; SO, stratum oriens and SRad, stratum radiatum.

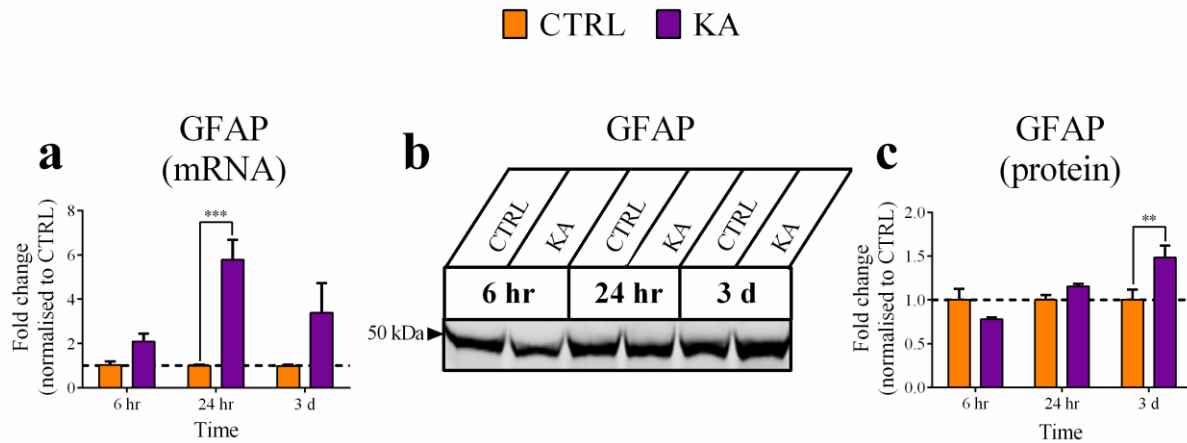
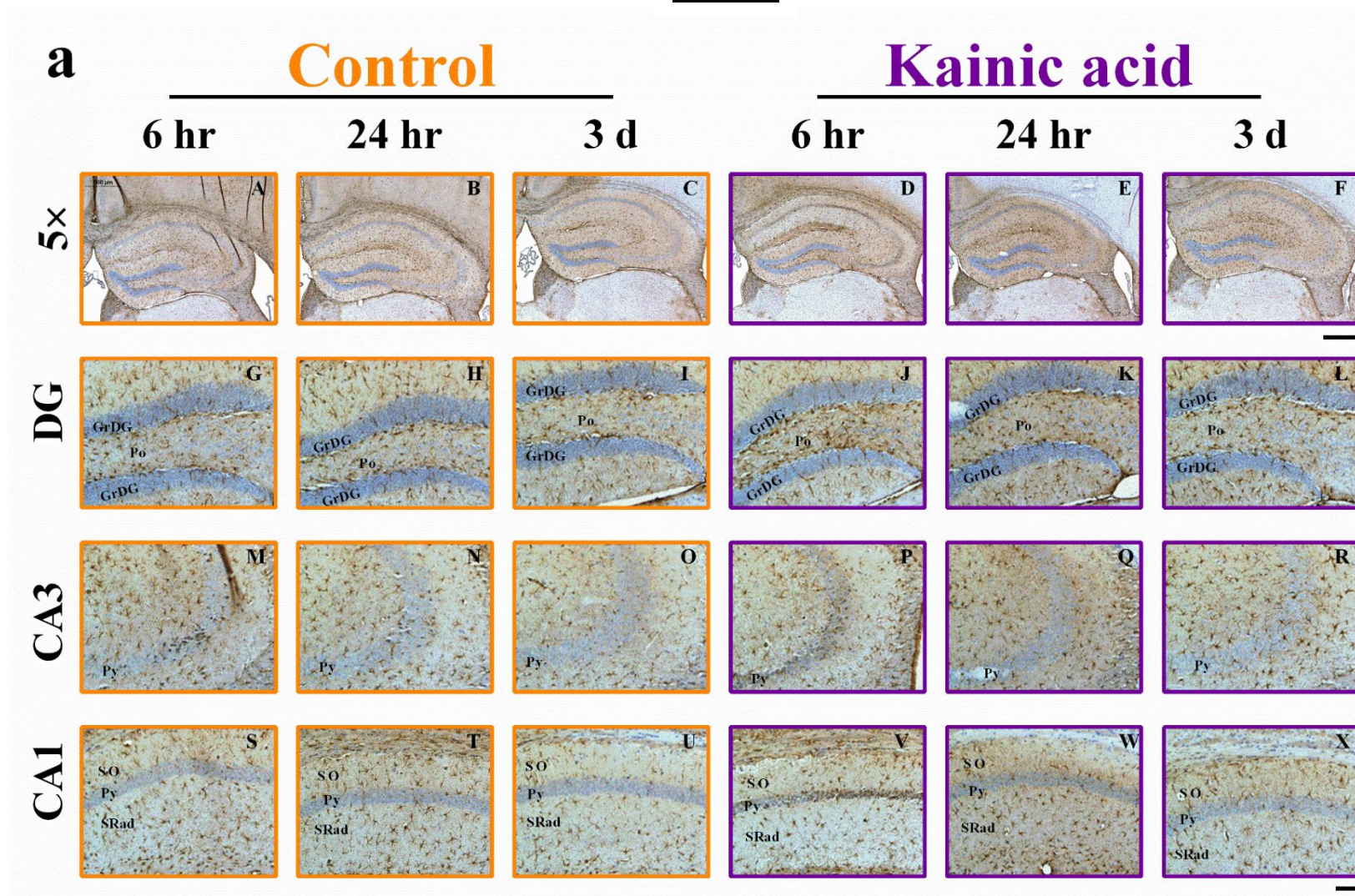


Figure 5.4 Quantification of GFAP mRNA and protein in KA-animals.

qPCR analysis (mRNA) (a), representative western blot (b) and related western blotting quantification (c) for GFAP in hippocampal homogenates (a) and from SDS-extracted hippocampi (b and c). qPCR and quantitative western blotting was performed on control and KA-animals killed 6 hr, 24 hr or 3 d after saline (control) or KA administration. Data in graphs represents mean \pm SEM of the mRNA and protein expression values from $n = 4$ animals per condition and time-point. Statistical test = repeated measures two-way ANOVA with Bonferroni post-analysis. Statistical significance relative to control: ** $P \leq 0.01$, and *** $P \leq 0.001$. d, days; CTRL, control; hr, hours and KA, kainic acid.

GFAP



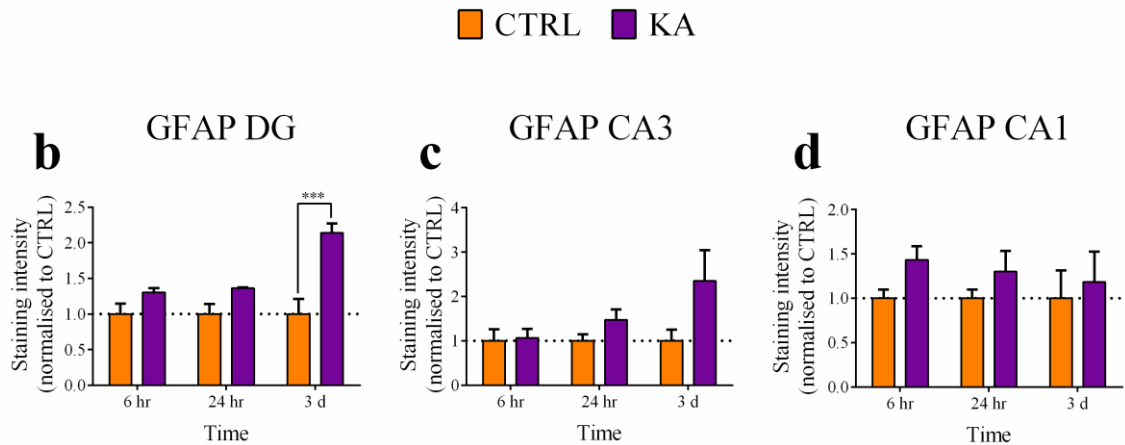


Figure 5.5 Immunohistochemical staining for GFAP in KA-animals.

Representative immunohistochemical staining (a) and related quantification (b-d) for GFAP in different regions of the hippocampus. (a) Immunohistochemical staining was performed on control and KA-animals killed 6 hr, 24 hr or 3 d after saline (control) or KA administration. $n = 4$ animals per condition and time-point, except for KA-animals 24 hours after KA administration where $n = 3$. Scale bar for 5× images is indicated under image F (300 μm) and scale bar for DG, CA3 and CA1 images is indicated under image X (100 μm). (b-d) Data in graphs represents mean \pm SEM of the staining intensity for GFAP in the DG, CA3 and CA1 region. n is the same as in (a). Statistical test = repeated measures two-way ANOVA with Bonferroni post-analysis (6 hr and 3 d) and an Unpaired Student's t -test, two tails (24 hr). Statistical significance relative to control: *** $P \leq 0.001$. d, days; CA1, Cornu Ammonis region 1; CA3, Cornu Ammonis region 3; DG, dentate gyrus; GrDG, granule cell layer of the DG; hr, hours; KA, kainic acid; Po, polymorphic layer; Py, pyramidal layer; SO, stratum oriens and SRad, stratum radiatum.

5.4.2 Expression of stress-related response molecules implicated in KA-induced excitotoxicity

c-Jun is a key molecular signature seen in KA-induced excitotoxicity (Schauwecker, 2000, Sng et al., 2005, Zhang et al., 2002). The levels of c-Jun were therefore investigated at the mRNA and protein level. Induction of this molecule, being seen as an indicator that the tissue in which the UPR will be investigated, has undergone a classic excitotoxicity stress response.

5.4.2.1 Expression of the immediate early gene c-Jun

The levels of c-Jun were determined using qPCR, quantitative western blotting and immunohistochemistry. qPCR analysis revealed that the levels of c-Jun mRNA were increased, albeit not significantly, in KA-animals at 6 hr after KA administration (Figure 5.6). The levels of c-Jun mRNA were not different between control and KA-animals at the two later time-points.

Although the increase in c-Jun mRNA was not statistically significant, quantitative western blotting for c-Jun showed that c-Jun protein levels were significantly increased in KA-animals 6 hr after KA-administration (Figure 5.7a and b). Immunohistochemical analysis for c-Jun also revealed qualitative changes in the DG, CA3 and CA1 region (Figure 5.8a). Quantitatively this was seen as a significant increase in the levels of c-Jun protein in the granule cell layer of the DG and pyramidal layer of CA3 6 hr after KA treatment (Figure 5.8a, b and c).

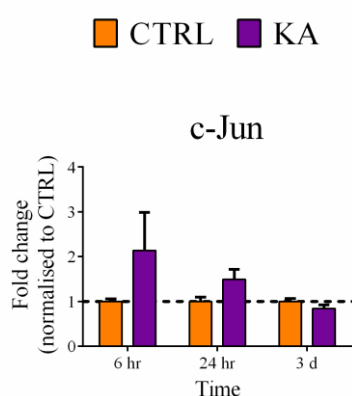


Figure 5.6 Quantification of c-Jun mRNA in KA-animals.

qPCR analysis for c-Jun mRNA in hippocampal homogenates from control and KA-animals animals killed at 6 hr, 24 hr or 3 d after saline (control) or KA treatment. Data in graphs represents mean \pm SEM of the mRNA expression values from $n = 4$ animals per condition and time-point. Statistical test = repeated measures two-way ANOVA with Bonferroni post-analysis. CTRL, control; d, days; hr, hours and KA, kainic acid.

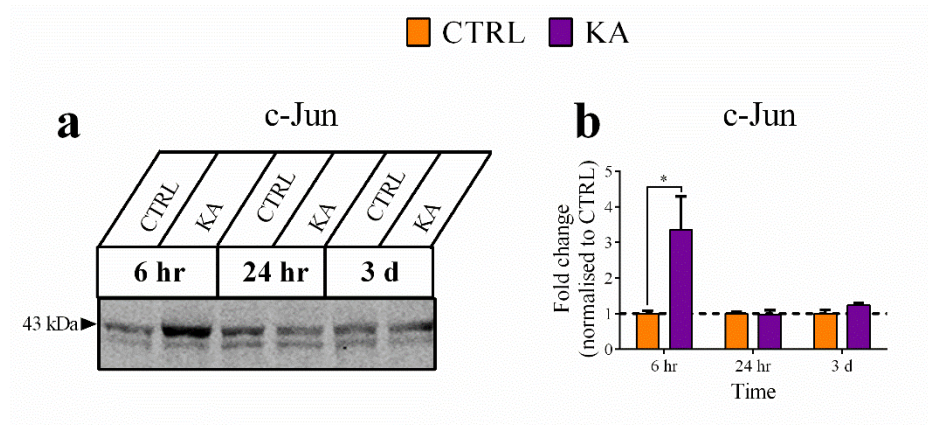
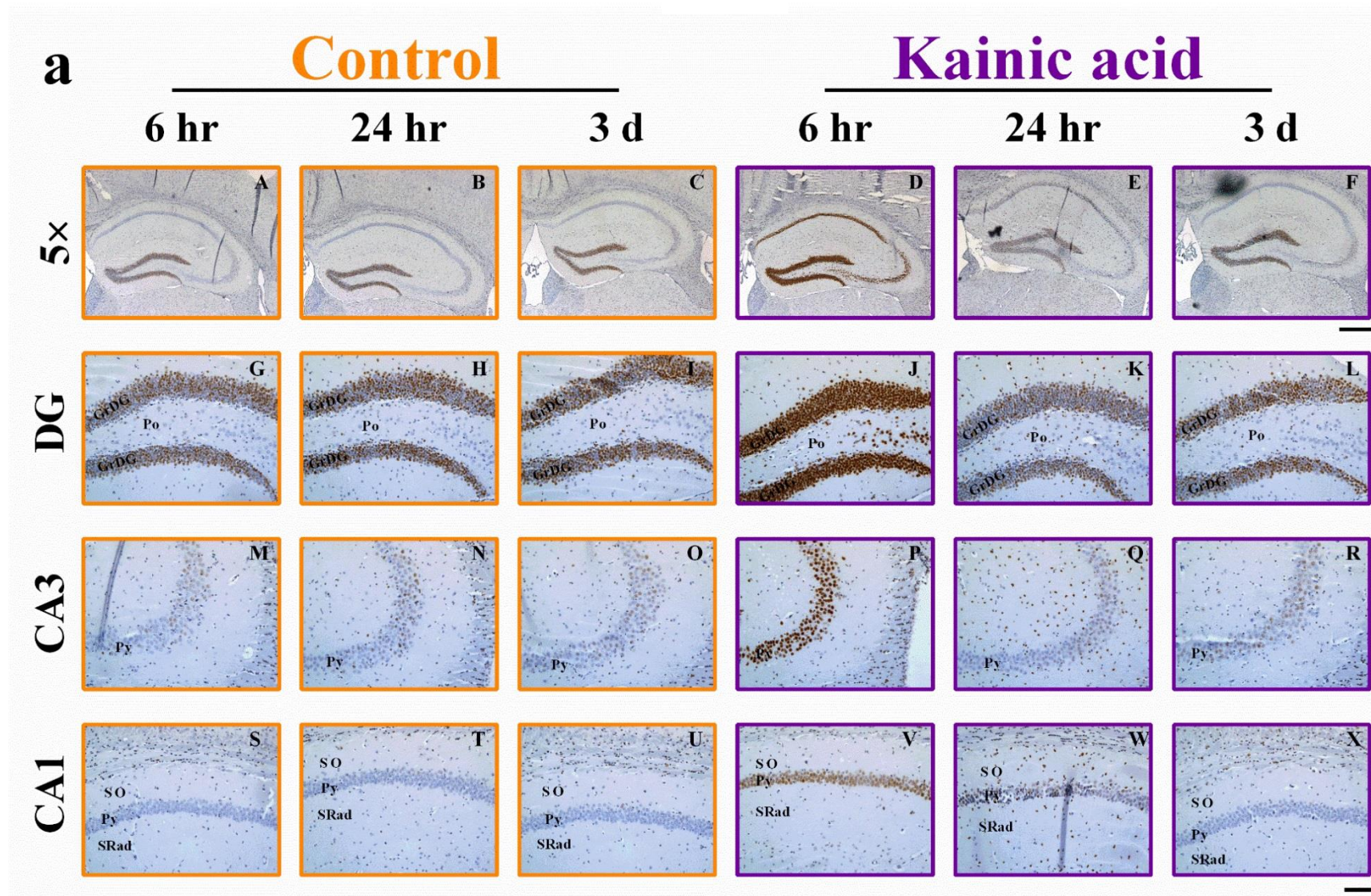


Figure 5.7 Quantification of c-Jun protein in KA-animals.

Representative western blot (a) and related quantification (b) for c-Jun in SDS-extracted hippocampi. Quantitative western blotting was performed on control and KA-animals killed 6 hr, 24 hr or 3 d after saline (control) or KA administration. Only the top band was quantified as c-Jun immunoreactivity. Data in bar charts represents mean \pm SEM of the protein expression values from $n = 4$ animals per condition and time-point, except for KA-animals at 6 hr, where $n = 3$. Statistical test = repeated measures two-way ANOVA with Bonferroni post-analysis (24 hr and 3 d) and Unpaired Student's *t*-test, two tails (6 hr). Statistical significance relative to control: * $P \leq 0.05$. d, days; CTRL, control; hr, hours and KA, kainic acid.

c-Jun



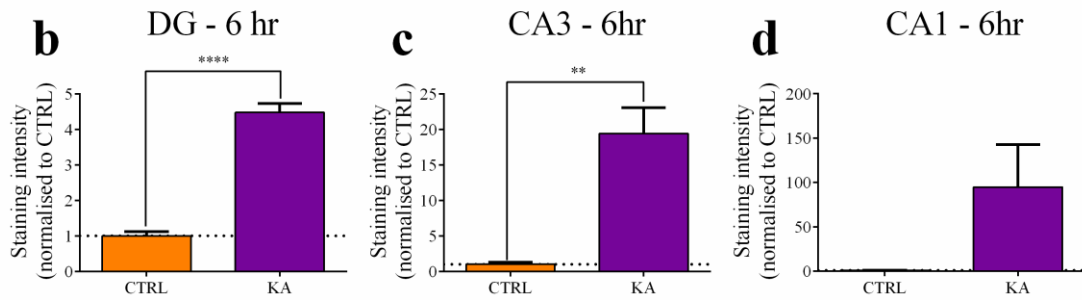


Figure 5.8 Immunohistochemical staining for c-Jun in KA-animals.

Representative immunohistochemical staining (a) and related quantification (b-d) for c-Jun in different regions of the hippocampus. (a) Immunohistological staining was performed on control and KA-animals killed 6 hr, 24 hr or 3 d after saline (control) or KA administration. $n = 4$ animals per condition and time-point, except for KA-animals 24 hours after KA administration where $n = 3$. Scale bar for 5 \times images is indicated under image F (300 μ m) and scale bar for DG, CA3 and CA1 images is indicated under image X (100 μ m). (b-d) Data in graphs represents mean \pm SEM of the staining intensity for c-Jun in the granule cell layer of the DG and the pyramidal layer of CA3 and CA1. n is the same as in (a). Statistical test = Unpaired Student's t -test, two tails. Statistical significance relative to control: ** $P \leq 0.01$ and **** $P \leq 0.0001$. d, days; CA1, Cornu Ammonis region 1; CA3, Corn Ammonis region 3; DG, dentate gyrus; GrDG, granule cell layer of the DG; hr, hours; KA, kainic acid; Po, polymorphic layer; Py, pyramidal layer; SO, stratum oriens and SRad, stratum radiatum.

5.4.2.2 Expression of other immediate early gene mRNAs

The levels of ATF3 and c-Fos mRNA were determined by qPCR. This analysis revealed a significant induction of ATF3 mRNA in KA-animals 6 hr after KA administration (Figure 5.9a). This increase was only seen at 6 hr after which levels of ATF3 mRNA were comparable to control treated animals. Levels of c-Fos mRNA were non-significantly increased in KA-animals at 6 hr after KA administration (Figure 5.9b). Levels of c-Fos were comparable between KA-animals and control-animals at the two later time-points.

5.4.2.3 Expression of activity-induced immediate early gene mRNAs

Levels of Arc and Homer1a mRNA previously investigated in ME7-animals and CSP α $-/-$ animals, were determined in KA-animals. The levels of Arc and Homer1a

mRNA were significantly increased in KA-animals 6 hr after KA-administration (Figure 5.10a and b). At 24 hr and 3 d post-KA treatment, levels of Arc and Homer1a were not different between control and KA-animals.

5.4.2.4 mRNA expression of the cellular physiological and environmental damage stress sensor GADD45 α

mRNA levels of GADD45 α were significantly increased in KA-animals at both 6 hr and 24 hr after KA-administration (Figure 5.11). There was no difference between control and KA-animals 3 d post-KA administration.

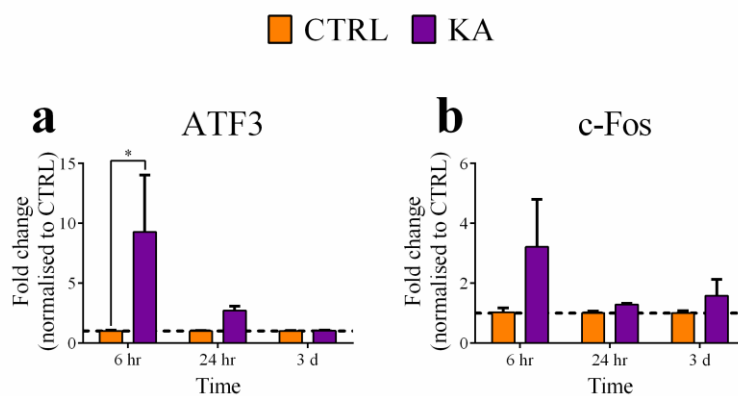


Figure 5.9 Quantification of ATF3 and c-Fos immediate early gene mRNAs in KA-animals.

qPCR analysis for ATF3 (a) and c-Fos (b) mRNAs in hippocampal homogenates from control and KA-animals animals killed 6 hr, 24 hr and 3d after control (saline) or KA treatment. Data in graphs represents mean \pm SEM mRNA expression values from $n = 4$ animals per condition and time-point. Statistical test = repeated measures two-way ANOVA with Bonferroni post-analysis. Statistical significance relative to control: * $P \leq 0.05$. CTRL, control; d, days; hr, hours and KA, kainic acid.

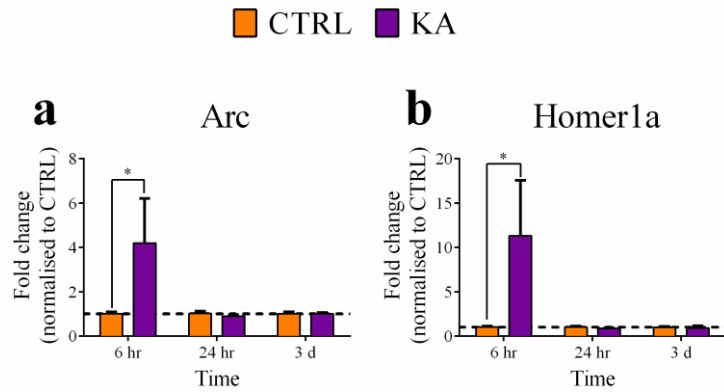


Figure 5.10 Quantification of activity-induced immediate early gene mRNAs in KA-animals.

qPCR analysis for Arc (a) and Homer1a (b) mRNAs in hippocampal homogenates from control and KA-animals animals killed 6 hr, 24 hr or 3 d after control (saline) or KA treatment. Data in graphs represents mean \pm SEM of the mRNA expression values from $n = 4$ animals per condition and time-point. Statistical test = repeated measures two-way ANOVA with Bonferroni post-analysis. Statistical significance relative to control: $*P \leq 0.05$. CTRL, control; d, days; hr, hours and KA, kainic acid.

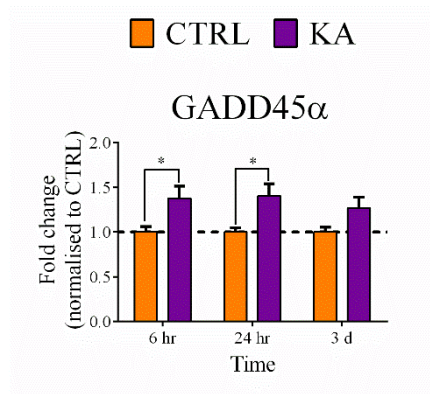


Figure 5.11 Quantification of the mRNA levels of the cellular physiological and environmental damage stress sensor GADD45 in KA-animals.

qPCR analysis for GADD45 α mRNA in hippocampal homogenates from control and KA-animals animals killed 6 hr, 24 hr or 3 d after control (saline) or KA treatment. Data in graphs represents mean \pm SEM of the mRNA expression values from $n = 4$ animals per condition and time-point. Statistical test = repeated measures two-way ANOVA with Bonferroni post-analysis. Statistical significance relative to control: $*P \leq 0.05$. CTRL, control; d, days; hr, hours and KA, kainic acid.

5.4.3 Expression of UPR mRNAs in KA-animals

The expression of UPR mRNAs investigated in ME7-animals and CSP α $-/-$ animals, was investigated here in KA-animals. qPCR analysis revealed that the levels of the UPR mRNAs BiP, spliced XBP-1, GADD34 and CHOP were not different between control and KA-animals at any of the time-points examined (Figure 5.12a-d). Only ATF4 mRNA was significantly increased in KA-animals and this was only seen 6 hr post-KA administration (Figure 5.12e).

5.4.4 Expression of UPR proteins in KA-animals

Quantitative western blotting was performed for BiP and eIF2 α -P in control and KA-animals. Quantitative western blotting revealed that the levels of BiP and eIF2 α -P were not different between control and KA-animals at any of the time-points examined (Figure 5. 13a-c).

Similar to quantitative western blotting, immunohistochemical staining for eIF2 α -P showed that the levels of eIF2 α -P were not increased in KA-animals at 6 hr, 24 hr or 3 d after KA treatment (Figure 5.15). However, despite no increase in BiP immunoreactivity from quantitative western blotting, immunohistochemical staining for BiP revealed modest qualitative changes in the expression of BiP in KA-animals (Figure 5. 14a). Quantitatively this was seen as a significant increase in BiP staining in the granule cell layer of the DG in KA-animals 6 hr post-KA treatment and in the pyramidal layer of CA1 in KA-animals 3 d after KA treatment (Figure 5.14b and c).

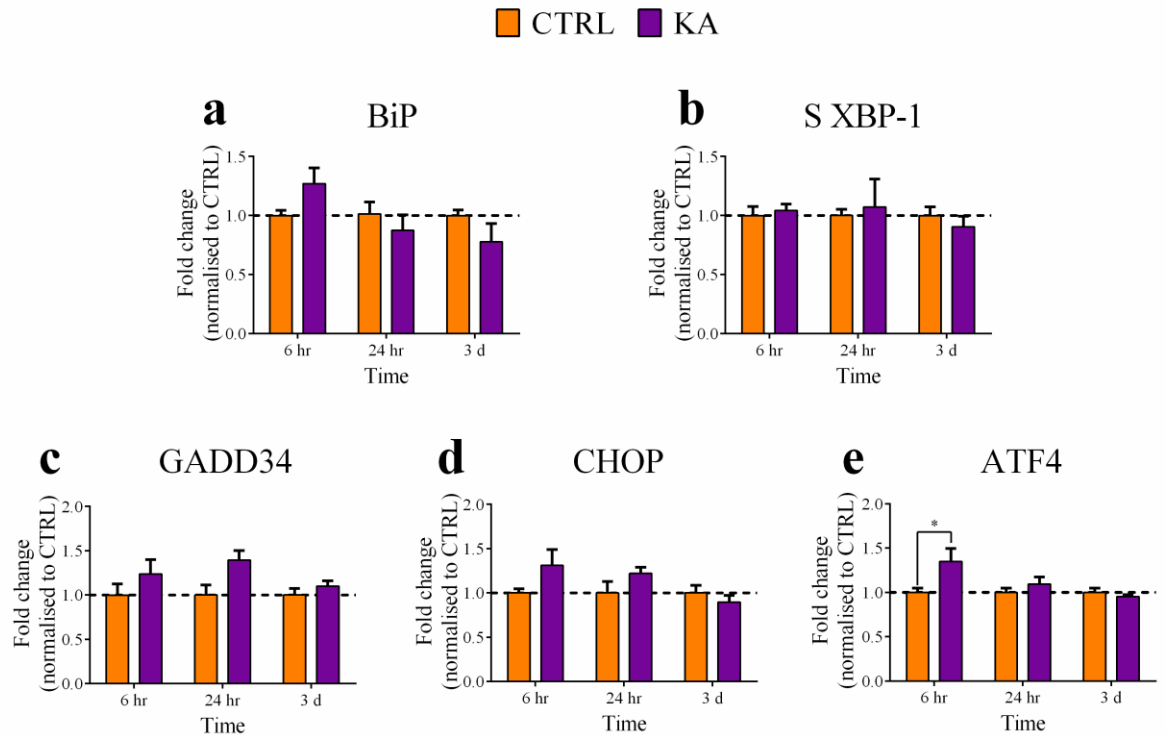


Figure 5.12 Quantification of UPR mRNAs in KA-animals.

qPCR analysis for BiP (a), S XBP-1 (b), GADD34 (c), CHOP (d) and ATF4 (e) mRNAs in hippocampal homogenates from control and KA-animals killed 6 hr, 24 hr or 3 d after saline (control) or KA treatment. Data in graphs represents mean \pm SEM of the mRNA expression values from $n = 4$ animals per condition and time-point. Statistical test = repeated measures two-way ANOVA with Bonferroni post-analysis. Statistical significance relative to control: $*P \leq 0.05$. CTRL, control; d, days; hr, hours and KA, kainic acid.

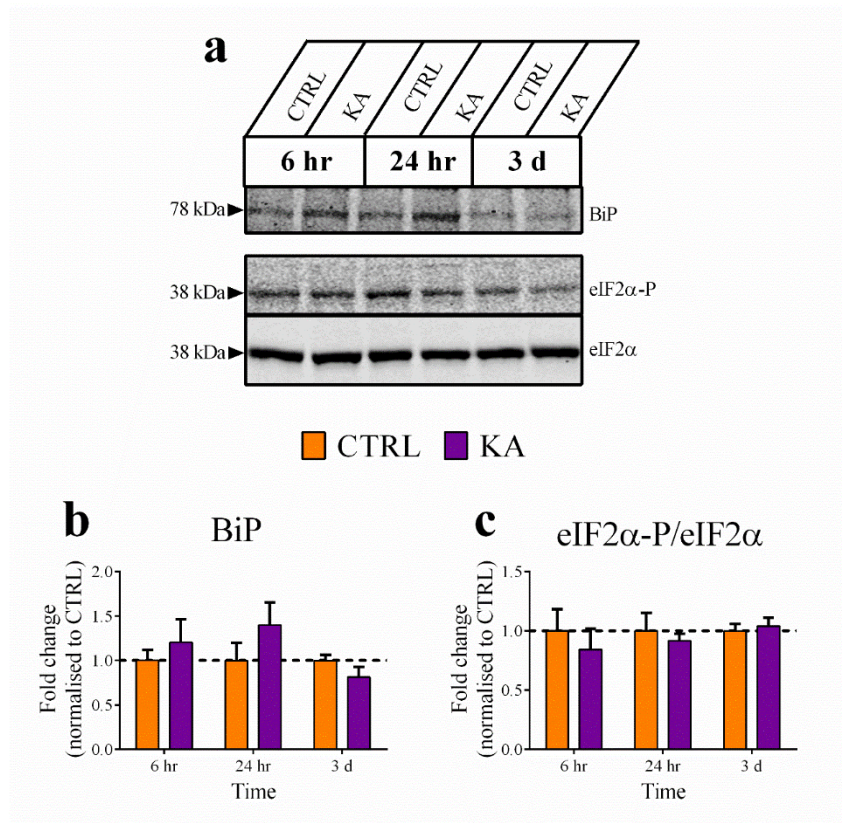
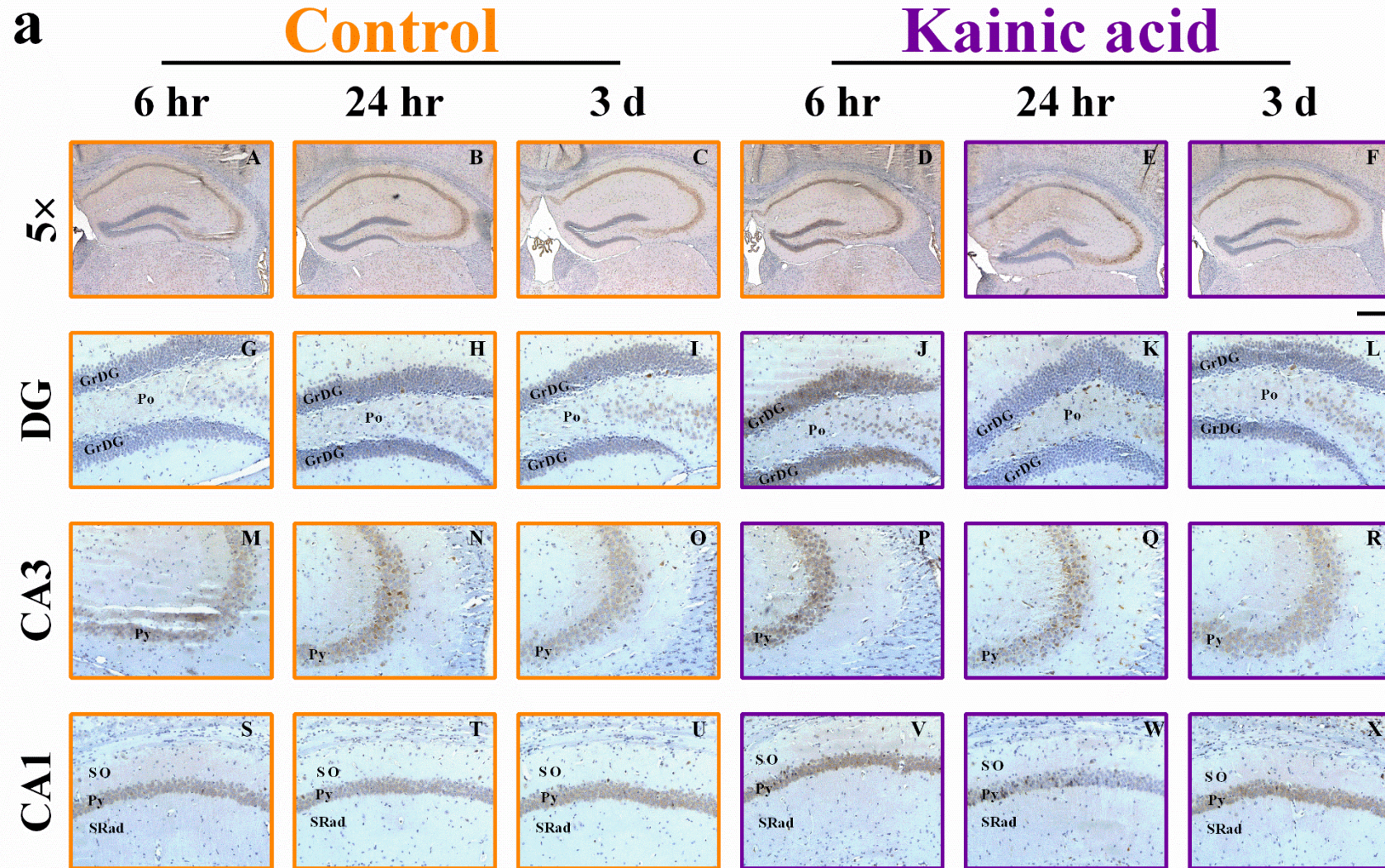


Figure 5.13 Quantification of UPR proteins in KA-animals.

Representative western blotting (a) and related quantification for BiP (b) and eIF2α-P (Ser51) (c) in SDS-extracted hippocampi. Quantitative western blotting was performed on control and KA-animals killed 6 hr, 24 hr and 3 d after saline (control) or KA administration. Data in bar charts represents mean \pm SEM of the protein expression values from $n = 4$ animals per condition and time-point, except for BiP where $n = 3$ animals per condition and time-point. Statistical test = repeated measures two-way ANOVA with Bonferroni post-analysis. d, days; CTRL, control; hr, hours and KA, kainic acid.

BiP



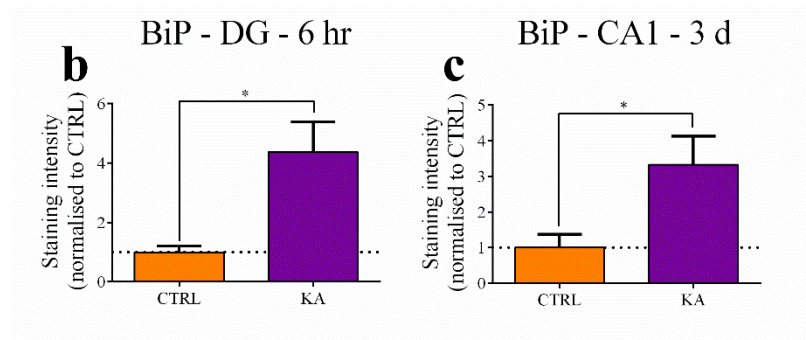


Figure 5.14 Immunohistochemical staining for BiP in KA-animals.

Representative immunohistochemical staining (a) and related quantification (b-c) for BiP in different regions of the hippocampus. Immunohistochemical staining was performed on control and KA-animals killed 6 hr, 24 hr and 3 d after saline (control) or KA administration. $n = 4$ animals per condition and time-point, except for KA-animals 24 hours after KA administration where $n = 3$. Scale bar for 5x images is indicated under image F (300 μm) and scale bar for DG, CA3 and CA1 images is indicated under image X (100 μm). (b-c) Data in graphs represents mean \pm SEM of the staining intensity for BiP protein in the granule cell layer of the DG and the pyramidal layer of CA1. n is the same as in (a). Statistical test = Unpaired Student's t -test, two tails. Statistical significance relative to controls: $*P \leq 0.05$. d, days; CA1, Cornu Ammonis region 1; CA3, Cornu Ammonis region 3; CTRL, control; DG, dentate gyrus; GrDG, granule cell layer of the DG; hr, hours; KA, kainic acid; Po, polymorphic layer; Py, pyramidal layer; SO, stratum oriens and SRad, stratum radiatum.

eIF2 α -P

Control

Kainic acid

6 hr

24 hr

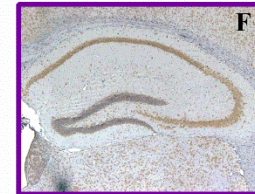
3 d

6 hr

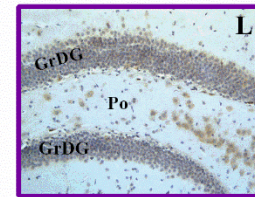
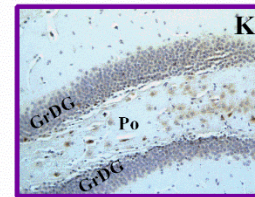
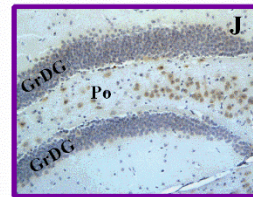
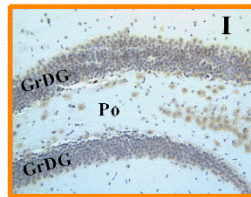
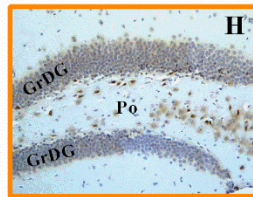
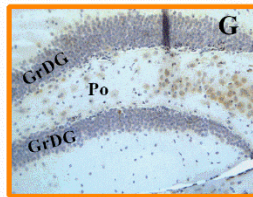
24 hr

3 d

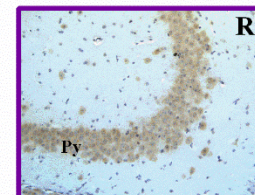
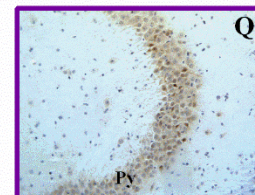
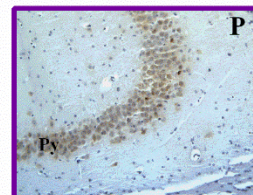
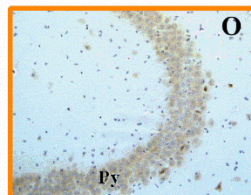
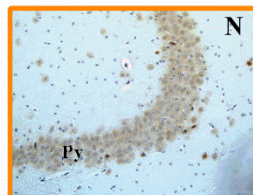
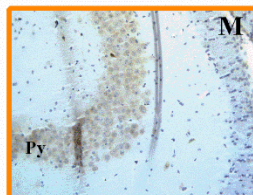
5 \times



DG



CA3



CA1

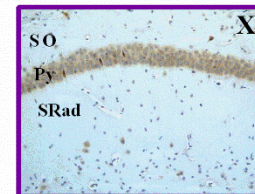
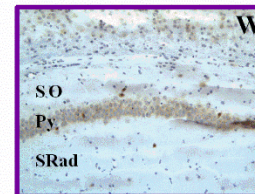
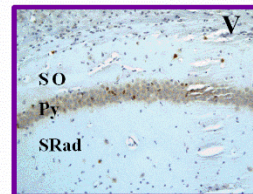
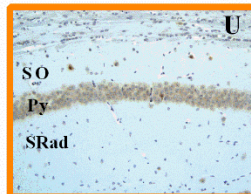
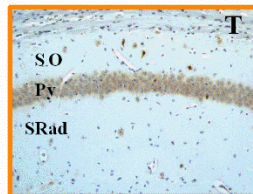
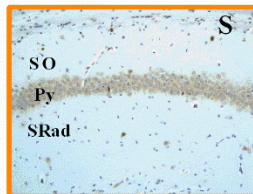


Figure 5.15 Immunohistochemical staining for eIF2 α -P in KA-animals.

Representative immunohistochemical staining for eIF2 α -P (Ser51) in different regions of the hippocampus. Immunohistochemical staining was performed on control and KA-animals killed 6 hr, 24 hr and 3 d after saline (control) or KA administration. $n = 4$ animals per condition and time-point, except for KA-animals 24 hours after KA administration where $n = 3$. Scale bar for 5 \times images is indicated under image F (300 μ m) and scale bar for DG, CA3 and CA1 images is indicated under image X (100 μ m). d, days; CA1, Cornu Ammonis region 1; CA3, Cornu Ammonis region 3; DG, dentate gyrus; GrDG, granule cell layer of the DG; hr, hours; KA, kainic acid; Po, polymorphic layer; Py, pyramidal layer; SO, stratum oriens and SRad, stratum radiatum.

5.4.5 Expression of BiP and eIF2 α -P proteins after acute coronal mouse brain slicing

A classic UPR has not been seen in ME7-animals and CSP α $-/-$ animals, nor has it been robustly induced in KA-animals. All of this data suggest that a classic and robust UPR is hard to initiate in mouse brain tissue, even though other cellular and/or molecular changes are apparent in all of the models used in this thesis.

As an attempt to try to drive the phosphorylation of eIF2 α , which has been documented as a key UPR molecule implicated in chronic neurodegenerative disease (Moreno et al., 2013, Moreno et al., 2012), coronal vibratome slicing of mouse brains was performed. This was done to determine if increased eIF2 α -P and also BiP could be detected in the brains of mice after this acute slicing-induced injury. Unsliced cortical tissue was compared to cortical tissue which had been sliced and harvested 0, 4 or 8 hr after slicing.

Quantitative western blotting showed that the levels of BiP protein were not different between sliced (0 hr, 4 hr or 8 hr) and unsliced cortical tissue (Figure 5.16a). However, levels of eIF2 α -P were significantly increased 4 hr after slicing (Figure 5.16a and b). Immunohistochemical staining for eIF2 α -P showed that eIF2 α -P was highly expressed in the cortex, hippocampus and midbrain after slicing (Figure 5.16c). In the hippocampus this was seen in the granule cell layer of the DG and the pyramidal layer of CA3 and CA1.

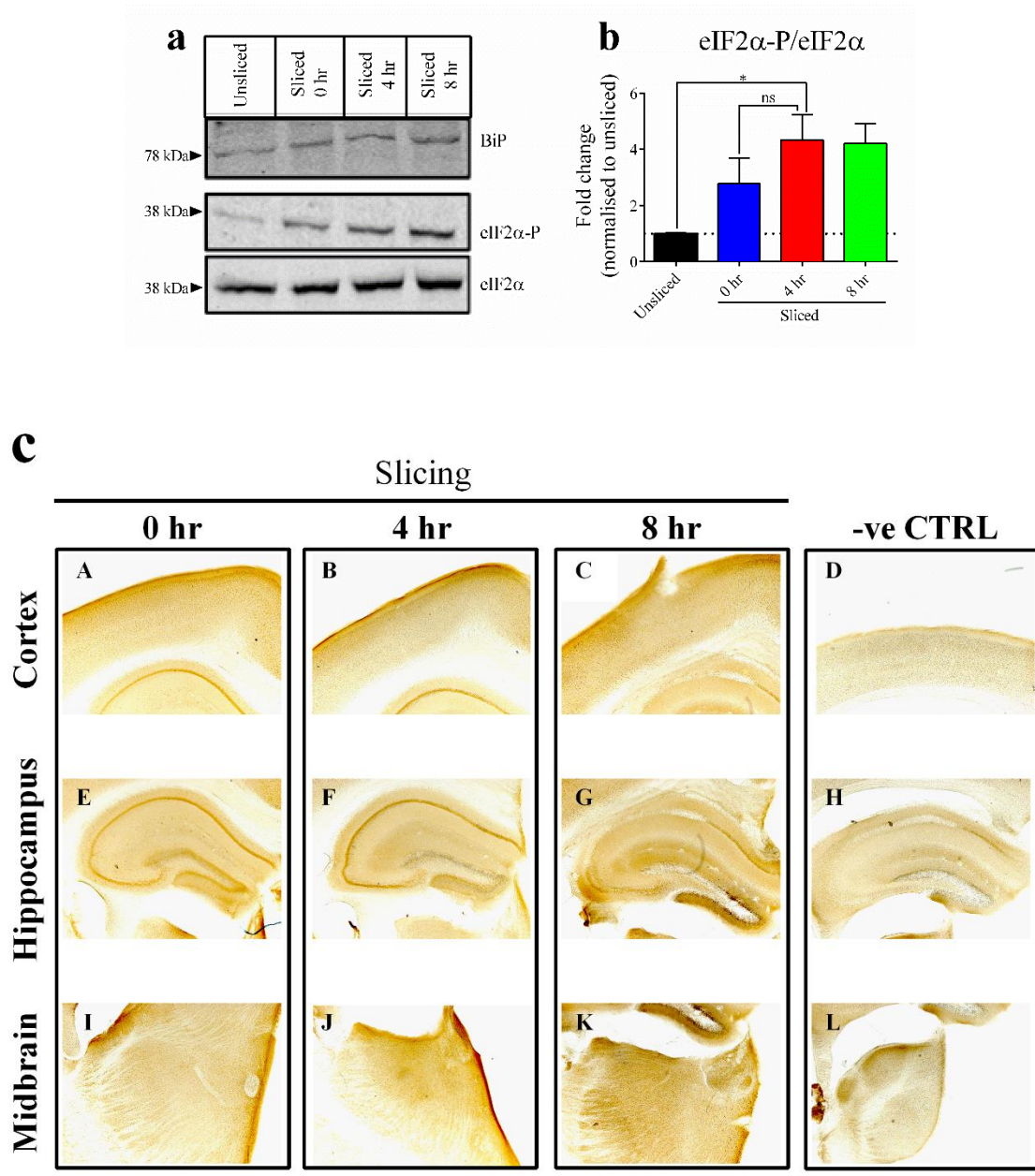


Figure 5.16 Quantification of BiP and eIF2α-P proteins after acute coronal mouse brain slicing.

Representative western blots for BiP and eIF2α-P (Ser51) (a) and related quantification for eIF2α-P (b) in SDS extracted unsliced and sliced cortex. 0 hr, 4 hr and 8 hr refers to the time after slicing. Data in graphs represents mean \pm SEM of the protein expression values from $n = 3$ animals per condition, except for 8 hr sliced where $n = 2$. (b) Statistical test = one-way ANOVA with Bonferroni post-analysis. Statistical significance relative to control (unsliced and 0 hr): $*P \leq 0.05$. (c) Representative immunohistochemical staining for eIF2α-P (Ser51) in different regions of the brain. Immunohistochemical staining for eIF2α-P was performed on unfixed sliced coronal

sections (150 μ m) collected at 0 hr, 4 hr or 8 hr after slicing. –ve CTRL refers to background staining in the absence of the primary antibody. Scale bar is indicated under image L (500 μ m). –ve, negative; CTRL, control, hr, hours and ns, non-significant. Western blotting and quantification performed by masters student, Joanna Penfold.

5.5 Discussion

There was no evidence for a UPR in the two distinct models of neurodegeneration – the ME7 model and CSP α -/- model (chapters 3 and 4). In this chapter, the UPR was investigated in KA-injected mice, as a model of excitotoxicity-induced acute neuronal injury and in another model of acute neuronal injury initiated by the coronal slicing of mouse brain tissue. A combination of qPCR, quantitative western blotting and immunohistochemistry was used to investigate whether the UPR was activated.

5.5.1 The dose of KA

In this chapter a dose of KA (20 mg/kg) was chosen (section 5.3.1). Although cell death did not occur (Figure 5.3), mortality rate was reduced (only 1 animal died in this study) and GFAP (Figure 5.4 and 5.5) and stress-related response molecules including c-Jun (see below) were induced (Figure 5.6-5.11) Cell death is often seen after KA treatment, however, C57BL/6J mice have been shown to be resistant to cell death compared to other mouse strains (McKhann et al., 2003, McLin and Steward, 2006, Schauwecker et al., 2000, Schauwecker and Steward, 1997). This is reflected in C57BL/6J mice requiring higher doses of KA to display even mild seizure activity (Benkovic et al., 2004). At higher doses of KA (≥ 35 mg/kg) cell death is apparent in C57BL/6J mice (Benkovic et al., 2004, Chen et al., 2002, Hu et al., 1998). At higher doses mortality rate is also increased (section 5.3.1).

5.5.2 Stress response molecules are upregulated in KA-animals

Stress-related response mRNAs upregulated in the ME7 and CSP α -/- model were investigated in KA-animals. In this chapter, an induction of c-Jun was used as a benchmark to show that the hippocampal tissue analysed has undergone a classic excitotoxicity-driven stress response. This is because c-Jun has been shown to be

rapidly (≥ 30 min) and transiently upregulated after KA treatment or exposure to glutamate (Cardoso et al., 2010, Sng et al., 2005).

In agreement with the studies above, in this chapter quantitative western blotting and immunohistochemistry showed that c-Jun protein was induced in KA-animals 6 hr after KA treatment (Figure 5.7 and 5.8).

In addition, levels of other stress-related response molecules including ATF3, Arc, Homer1a and GADD45 α mRNAs were also increased in KA-animals compared to controls (Figure 5.9a, 5.10 and 5.11). The induction of these stress-related response molecules agrees with observations made by others. KA administration has been shown to lead to an increase in ATF3 protein (Francis et al., 2004). This was a protective response as overexpression of ATF3 reduced CA3 neuronal cell death. c-Fos mRNA was increased in KA-animals (Figure 5.9b) but not significantly. However, c-Fos mRNA and protein has been shown to be rapidly upregulated (min-hr) after KA treatment in the granule cell layer and pyramidal layer of the hippocampus (Blendy et al., 1995, Schauwecker et al., 2000, Sng et al., 2005, Zhang et al., 2002). This upregulation has been shown to be protective, as seizures were more severe, astrogliosis was heightened and neuronal cell death was increased in mice with reduced c-Fos expression (Zhang et al., 2002).

Arc mRNA and protein have been shown to be upregulated early after KA treatment (2-3 hr) (Izumi et al., 2011, Li et al., 2005, Toyoda et al., 2010) and Homer1a protein is induced 3 hr after KA treatment (Jessberger and Kempermann, 2003). GADD45 α has also been shown to be upregulated at the mRNA and protein level after KA treatment (Choi et al., 2011).

These studies along with the results presented in this chapter show that stress-related response molecules are induced by acute KA exposure used in this study. Their induction, in addition to the increase in GFAP, suggest that the hippocampal tissue used in this chapter is consistent with an acute excitotoxic insult.

5.5.3 A robust and classic UPR is not activated in KA-animals

qPCR analysis revealed that the levels of the UPR mRNAs: BiP, spliced XBP-1, GADD34 and CHOP were not different between control and KA-animals at any of the

time-points investigated (Figure 5.12a-d). ATF4 mRNA was increased in KA-animals at 6 hr (Figure 5.12e), but the lack of induction of the other UPR mRNAs suggests this increase is not associated with a full UPR. Quantitative western blotting and immunohistochemistry showed that the levels of eIF2 α -P were not different between control and KA-animals at 6 hr, 24 hr or 3 d after KA treatment (Figure 5.13a and c and 5.15). Similarly, quantitative western blotting revealed that the levels of BiP were also not significantly different between control and KA-animals at any of the time-points investigated (Figure 5.13a and b). Despite this, there was qualitative and quantitative changes in the expression of BiP in KA-animals as shown by immunohistochemistry staining (Figure 5.14a, b and c). Therefore, the combination of results from biochemistry and immunohistochemistry shows that ATF4 (mRNA) and BiP (protein) are induced in KA-animals at least at one time-point after KA treatment. The induction of these two molecules occurs when other UPR molecules are not induced, which suggest that a classic and full-blown UPR is not activated.

The UPR has been shown to be induced in other models of KA-driven excitotoxicity. In one of these models (male ICR mice, KA 30 mg/kg i.p.), the levels of eIF2 α -P were increased ~1.5-2 fold 2 hr and 24 hr after KA treatment (Kim et al., 2014). Similarly, levels of ATF4 protein were also increased ~2 fold at 2 hr and 6 hr and CHOP protein was increased at 24 hr after the administration of KA. The results from this study show that the UPR is a prominent feature in KA-animals, however, this study was conducted on ICR mice which are more susceptible to neurodegeneration (McLin and Steward, 2006) compared to C57BL/6J mice. In addition, KA was administered at a significantly higher dose (30 mg/kg) than used in this chapter.

KA has been shown to induce ER membrane fragmentation and induce ER stress in another model of KA-induced excitotoxicity (male Wistar rats, KA 0.5 μ l (0.35 μ g/ μ l) into lateral ventricle) which was associated with increasing levels of calcium (Sokka et al., 2007). Both BiP and CHOP mRNA were upregulated ~1.5 fold 24 hr after KA treatment in hippocampal neuronal cultures treated with KA (100 μ M KA) and at the protein level *in vivo* (Sokka et al., 2007). Similarly, levels of ATF4 were increased ~3.5 fold up to 24 hr after KA treatment in hippocampal neuronal cultures. Splicing of XBP-1, however, did not occur in these neuronal cultures. PERK-P was increased at 3 hr and eIF2 α -P was increased between 3-48 hr *in vivo*. All of the experiments in this study (Sokka et al., 2007) were performed on rats. Some of the experiments by Sokka et

al., was done in hippocampal neuronal cultures and the experiments which were performed *in vivo* were done by injecting KA into the lateral ventricle, which lead to cell death in the CA3 region at 24 hr after KA administration. Therefore, this study differs from the one performed in this chapter: mice vs rats, culture vs *in vivo*, route of KA administration and subsequently the concentration of KA which reaches the brain.

In a KA model using C57BL/6J mice, BiP and ATF4 mRNA were upregulated ~2.5 and ~1.5 fold, respectively, 12 hr after treatment with KA (Chihara et al., 2009). The expression of BiP protein was shown to be expressed in both neurons and astrocytes, which suggests that astrocytes too can undergo ER stress and mount a UPR. These results were from mice injected with a significantly higher dose of KA (36 mg/kg) than used in this chapter. However, at a dose of 20 mg/kg they also showed an increase in BiP mRNA in KA-animals 12 hr after KA treatment (Chihara et al., 2009) and BiP protein has also been shown to be upregulated at 6 hr and 12 hr in rats after an i.p. injection of KA at a dose of 12 mg/kg (Jang et al., 2004). Other UPR molecules were not investigated in C57BL/6J mice injected i.p. with 20 mg/kg KA (Chihara et al., 2009).

The results from this chapter suggest that a classic and robust UPR is not activated in KA-animals. The results from others (see above) report an induction of UPR molecules. However, the induction of these molecules are modest and do not show the same level of induction as seen in HeLa cells treated with tunicamycin or PEITC (appendix 6).

5.5.4 Increased phosphorylation of eIF2 α in acute coronal mouse brain slices

Although acute excitotoxicity (based on gliosis and the induction of stress-related response molecules) mediated by KA treatment failed to induce a full UPR and an upregulation of eIF2 α -P, acute coronal slicing of mouse brains led to an increase in eIF2 α -P immediately after slicing (Figure 5.16a and b). This shows technically that an increase in eIF2 α -P can be detected in mouse brain tissue. The induction of eIF2 α -P mediated by acute coronal mouse brain slicing (4.3 fold) is greater than that seen in HeLa cells treated with tunicamycin (1.4 fold) or PEITC (2.2 fold) (appendix 6) or in hippocampal tissue from RML prion diseased animals (~2.9 fold) (Moreno et al., 2012).

A study has shown that protein synthesis is lower at both the upper and lower surfaces of rat hippocampal slices, which is thought to be because of limits on oxygen diffusion into

the tissue at these two interfaces (Hesse and Shashoua, 1990). Hypoxic conditions have been shown to lead to the increased phosphorylation of eIF2 α , through both PERK and GCN2 kinases (Koumenis et al., 2002, Liu et al., 2010). This response might contribute to the increase in phosphorylation of eIF2 α after 0 hr. Immunohistochemistry of eIF2 α -P, revealed that eIF2 α -P was expressed in the cortex, hippocampus and midbrain (Figure 5.16c). Closer examination of the hippocampus showed that eIF2 α -P was expressed in the granule cell layer of the DG and pyramidal layer of CA3 and CA1. eIF2 α -P has been shown to be increased in neuronal cell bodies in the cortex of the brain 4 hr following axotomy (Singleton et al., 2002).

Levels of BiP were not increased after immediate slicing or 4 hr or 8 hr after slicing (Figure 5.16a). The results in this thesis have shown that in chronic neurodegeneration (ME7 (months)), semi-chronic neurodegeneration (CSP α -/- (weeks)) and acute injury (KA (days)), levels of eIF2 α -P are not increased (chapters 3, 4 and 5). However, in acute neuronal injury, mediated by coronal mouse brain slicing, levels of eIF2 α -P are increased. This highlights the difference in response elicited during different temporally evolving injuries and suggests that in more protracted models of neuronal dysfunction, mechanisms might be at play to prevent the activation of a strong and detectable UPR.

5.6 Conclusion

KA was injected into mice as a model of excitotoxicity. The hippocampus of KA-animals was used to investigate the UPR using a combination of biochemistry and immunohistochemistry. KA-animals which were used for this investigation had increased levels of GFAP between 24 hr and 3 d after KA treatment, which signified a glial response, consistent with neuronal injury. The levels of c-Jun which have been well characterised in KA-animals revealed an induction, which was most evidently seen using immunohistochemistry. This in combination with the increased GFAP expression shows that the hippocampal tissue used from KA-animals was perturbed and displayed signs of dysfunction.

Analysis of other stress-related response mRNAs (also analysed in ME7-animals and CSP α -/- animals) revealed an induction in KA-animals 6 and 24 hr after KA treatment. qPCR and quantitative western blotting revealed no induction of the UPR in KA-animals at any of the time-points investigated. Despite this, small changes were

seen in BiP staining in the granule cell layer of the DG (6 hr) and the pyramidal layer of CA1 (3 d) in KA-animals.

The phosphorylation of eIF2 α has been shown to be an important determinant of disease progression in chronic neurodegenerative diseases. An increased phosphorylation of eIF2 α has not been seen in ME7-animals (chapter 3), CSP α -/- animals (chapter 4) and now KA-animals (chapter 5). Despite this, an increased phosphorylation of eIF2 α was driven by the acute coronal slicing of mouse brain tissue. This demonstrates that in *in vivo* mouse brain tissue the phosphorylation of eIF2 α can be activated and detected, although this does not readily occur in ME7-animals, CSP α -/- animals and KA-animals.

Chapter 6: Laser capture microdissection and transcript profiling of the CA3 hippocampal subfield in ME7 prion disease

6.1 Introduction

Synaptic loss in the stratum radiatum of the hippocampus has been shown to be a relatively early event in ME7-animals (Cunningham et al., 2003, Gray et al., 2009, Sisková et al., 2009). As previously discussed, BDA tracing has extended these findings and revealed progressive morphological alterations to CA3 pyramidal neurons from 13 w.p.i. in the hippocampus of ME7-animals during prion disease progression (Al-Malki, 2012). These include: synaptic bouton loss; the accumulation of abnormal axonal swellings; reduced dendritic spines; reduced density of dendritic branching and length of dendrites; dendritic swellings and altered cell body shape (Al-Malki, 2012). Molecular correlates of these morphological changes are ill-defined. However, an upregulation of UPR and other stress-related response mRNAs (ATF3 and GADD45), has been shown in laser microdissected cell bodies of motoneurons, in Tg ALS mice (SOD1, G93A) which develop motoneuron disease (Saxena et al, 2009). Changes in expression of these mRNAs are seen before synaptic and axonal loss. Although the UPR was not induced in whole hippocampal tissue from ME7-animals (chapter 3), it is still feasible that the UPR might be selectively induced in dysfunctional CA3 pyramidal neurons.

Within the hippocampus and the rest of the brain there is a complex mixture of cell types including non-neuronal cells such as the glial cells: microglia; astrocytes and oligodendrocytes. Under non-pathological conditions, the non-neuronal cells outnumber neurons by $\geq 10:1$ (Majer et al, 2012). In ME7 prion disease there is a significant gliosis response (Betmouni et al., 1996, Cunningham et al., 2003) and a proteomic study in the hippocampus of ME7-animals revealed that the pre-dominant proteomic signature was from astrocytes (Asuni et al., 2014). In addition, whole brain transcriptomics has revealed that the most significant changes seen in the expression of mRNAs in different prion disease mouse models, are from those associated with the microglia and astrocytes (Hwang et al., 2009). Therefore, identifying changes in the expression of mRNAs,

especially mRNAs expressed at low levels, in specific neurons is challenging, as changes in expression might be masked by alterations in other neurons and/or non-neuronal cells. The UPR might be induced in dysfunctional CA3 pyramidal neurons, but not detected in the analysis of the whole hippocampus because the signal was ‘diluted’ by other signals from other neurons and non-neuronal cells. LCM has been used in this chapter to isolate the CA3 pyramidal layer (containing the cell bodies of CA3 pyramidal neurons), to investigate the UPR and other stress-related response molecules.

LCM has proved useful for isolating specific cells in heterogeneous tissue composed of different cell types (Curran et al., 2000, Majer et al., 2012).

LCM has been used to isolate the CA1 neurons of RML-inoculated animals (Majer et al., 2012) and microarray analysis revealed an early upregulation of mRNAs associated with NMDA signalling and neuroprotective pathways. However, next-generation sequencing (NGS) technology is also widely used to investigate changes in the expression of large numbers of mRNAs. NGS is a high-throughput technique with advantages over microarray based approaches, including the ability to uncover new genes and exons (Mortazavi et al., 2008). One method known as RNA-sequencing (RNA-Seq) is used to sequence the transcriptome and then map these sequences to the genome of interest. Sequence reads are then counted and compared between samples to determine if a specific treatment or condition alters the expression of one or many thousand genes (Mortazavi et al., 2008).

6.2 Aims

1. To optimise the technique of LCM. mRNAs from laser microdissected CA3 of naïve mice was used to investigate:
 - If LCM can be used to enrich and de-enrich for mRNAs expressed in different hippocampal regions and in glial cells of the hippocampus
 - Measure the expression of some previously investigated UPR and other stress-related response (ATF3 and GADD45 α) mRNAs

2. Laser microdissected CA3 of NBH- and ME7-animals was taken at early- (8 w.p.i.), middle- (12 w.p.i.) and late-stages (20 w.p.i.) of disease. Total RNA was extracted and qPCR was performed to investigate the expression levels of:
 - UPR mRNAs
 - Other stress-related response mRNAs (ATF3, Homer1a and GADD45 α)
3. RNA from the laser microdissected CA3 of NBH- and ME7-animals was sequenced at the National Institute for Medical Research (NIMR). This was used to reveal:
 - Differentially expressed mRNAs between NBH- and ME7-animals during disease progression
 - Molecular pathways activated during prion disease progression

6.3 Specific materials and methods

6.3.1 Tissue sectioning for LCM

Mouse brains were covered in optimal cutting temperature compound (OCT) and then individually placed (olfactory bulb facing upwards) in tin-foil made moulds containing OCT. More OCT was added to completely submerge the brain and the moulds were placed in a beaker of isopentane on dry ice, to rapidly freeze the tissue. Tissue was stored at -80 °C until required. A cryostat (Leica Microsystems) was used to section brain tissue embedded in OCT. The inside of the cryostat was cleaned with 100% ethanol and the cryostat stage, blades, brushes, tweezers, and slide holders were treated with RNaseZap solution.

Inside the cryostat the tin-foil mould was removed and the OCT embedded brain tissue attached to a metal chuck by freezing with OCT. The brain tissue was left in the cryostat for 10 min to harden and to allow the tissue to equilibrate to the temperature of the cryostat (-18 °C). The tissue was placed and orientated onto the cryostat holder. The OCT-brain block was brought towards the knife's edge and trimmed (30 μ m) until brain tissue became visible. Once the hippocampus was reached the cutting thickness was set to 10 μ m. Coronal sections containing the hippocampus were cut and the sections were then adhered to room temperature PEN membrane glass slides (Applied Biosystems). 5-6 sections were collected per glass slide and approximately 50-60 coronal sections were collected per brain. Once all sections had been collected, slides were placed in a

slide box on dry ice whilst the rest of the tissue was cut and collected. All slides were placed in a tightly closed box with self-indicating silica gel and stored at -80 °C until required.

6.3.2 Tissue processing for LCM

Slide chambers and slide racks were treated with RNaseZap solution. Sections were processed by one of two methods. In the first method, sections were fixed in 75% ethanol for 30 s. Sections were then stained with 1% cresyl violet for 1 min. Tissue was dehydrated in increasing concentrations of ethanol: 75%; 95% and 100%, for 1 min each. Sections were then left to air-dry in a fume hood for 15 min, before proceeding to LCM (section 6.3.3).

The methodology of the second method was as described by the LCM staining kit (Ambion). In the second method, sections were fixed in 95% ethanol for 30 s and then hydrated in a decreasing series of ethanol concentrations (75% and 50%) for 30 s each. Sections were stained with 1% cresyl violet for 1 min and then washed with increasing ethanol concentrations: 50%; 75% and 95%, for 30 s each. Sections were dehydrated twice in 100% ethanol for 30 s each. Afterwards, they were transferred into xylene to rinse off any residual ethanol, before being placed in fresh xylene for 5 min. Sections were then left to air-dry in a fume hood for 15 min, before proceeding to LCM (section 6.3.3). All ethanol solutions used for both processing methods were made up with water treated with diethylpyrocarbonate (DEPC) to inactivate RNases.

6.3.3 LCM of CA3

The CA3 pyramidal layer of the hippocampus, containing the cell bodies of CA3 pyramidal neurons (referred to as laser microdissected CA3), was microdissected bilaterally using a machine capable of LCM (Leica Microsystems) with an ultra-violet (UV) laser (Figure 6.1). As many serial sections of the CA3 pyramidal layer as possible were laser microdissected in order to increase the overall RNA yield. This was typically around ~200 laser captured CA3 pyramidal layer regions per brain (of approximate size as shown in Figure 6.1). The laser microdissected CA3 tissue falls via gravity into the cap of a 0.5 ml thin-walled PCR tube containing 50 µl lysis buffer from the RNAqueous-micro kit. It took approximately 2 hr to laser microdissect the CA3 from

one brain. After every 30 min laser microdissected CA3 tissue in the lysis buffer was removed from the cap and transferred to a fresh 0.5 ml PCR tube. An additional 50 μ l lysis buffer was added to the cap to ensure all of the tissue and had been lysed and this was then transferred to the new PCR tube. The lysis buffer containing the CA3 tissue was placed on dry ice (to minimise RNA degradation) whilst the remaining tissue was microdissected. This process was repeated until LCM was complete. Laser microdissected CA3 tissue in lysis buffer was then stored at -80 °C until required.

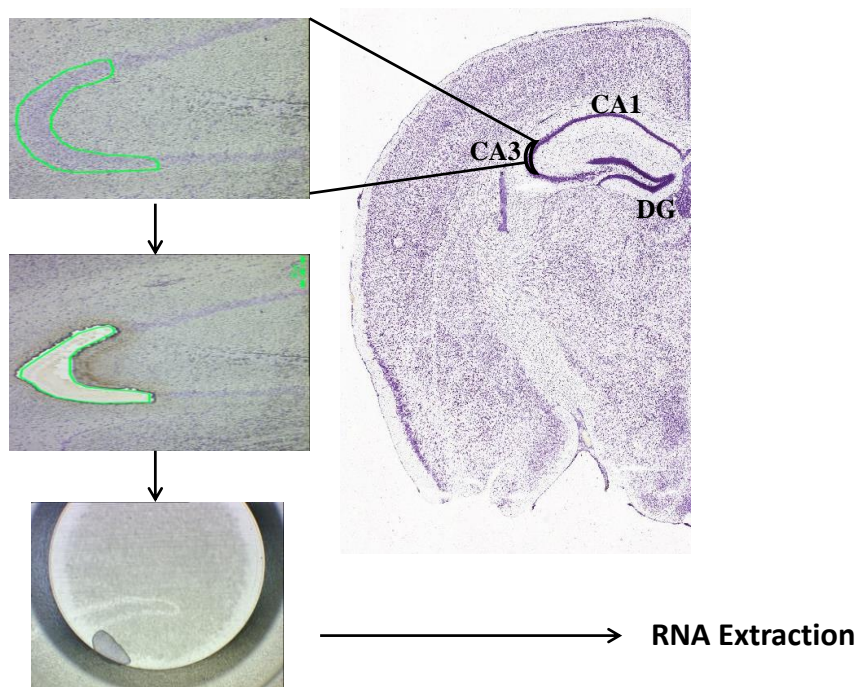


Figure 6.1 Laser microdissection of the CA3 pyramidal layer.

A line was drawn using a computer around the CA3 pyramidal layer (containing the cell bodies of CA3 pyramidal neurons) and a UV laser was used to microdissect this region. A mouse brain atlas was used throughout as a reference for identifying the CA3 boundary. The microdissected tissue falls via gravity into a PCR tube cap containing lysis buffer. Laser microdissected CA3 is then subjected to RNA extraction and downstream analysis. CA1, Cornu Ammonis region 1; CA3, Cornu Ammonis region 3; DG, dentate gyrus and UV, ultra-violet.

6.3.4 RNA extraction of laser microdissected CA3

RNA extraction of laser microdissected CA3 was carried out using the RNeasy-Micro kit according to the manufacturer's instructions. Laser

microdissected CA3 was pooled from 2 animals for each time-point to increase the RNA yield in order to perform downstream applications. RNA was eluted in 20 µl elution solution (RNAaqueous-Micro kit) and stored at -80 °C until required.

6.3.5 qPCR

mRNA expression was calculated as described (section 2.6.3.1) with the exception of GFAP, CD11b and Homer1a in NBH and ME7-animals, which was calculated using the $2^{-\Delta\Delta C_T}$ method (section 2.6.3.2). GFAP had a qPCR efficiency of 75.16%, CD11b 81.55% and Homer1a 88.41%, whilst GAPDH (used to normalise these genes) had an efficiency of 87.36%.

6.3.6 RNA-Seq

All of the following steps were performed by the genomics facility at the NIMR.

Total RNA was analysed using a Qubit fluorometer (Life Technologies) and Agilent 2100 Bioanalyser (Agilent Technologies) according to the manufacturer's instructions. The Qubit fluorometer was used to measure the concentration of RNA and the Agilent 2100 Bioanalyser was used to determine the integrity of the RNA. An example trace of one of the RNA samples analysed using the Agilent Bioanalyser 2100 is shown in Figure 6.2. The bioanalyser trace provides a visual assessment of the RNA quality. An RNA integrity number (RIN) score (1-10) is assigned to each RNA sample as an indicator of the degree of RNA degradation. A RIN score of 10 represents intact RNA and a RIN score of 1 represents degraded RNA. The RIN scores for the RNA samples given to the NIMR genomics facility are shown in Table 6.1. The RIN scores for all the samples were deemed to be acceptable to perform RNA-Seq.

Following this, 100 ng of total RNA was used to make cDNA and generate cDNA libraries for RNA-Seq using NuGEN Encore SP+ Complete DR Multiplex System 1-8 and 9-16 on a Mondrian SP+ Workstation (NuGEN). This protocol was used to enrich for non-ribosomal RNAs (rRNAs) and for sense-stranded RNA-Seq. Millions of cDNA clusters (each containing thousands of copies of template molecules) were formed using a cBot machine (Illumina). RNA-Seq was then carried on a Genome Analyser IIX machine (Illumina) using a paired-end 60 bp run. 80-100 million reads were produced

for each sample. FastQ files containing the nucleotide sequencing and a corresponding quality score were generated from the RNA-Seq.

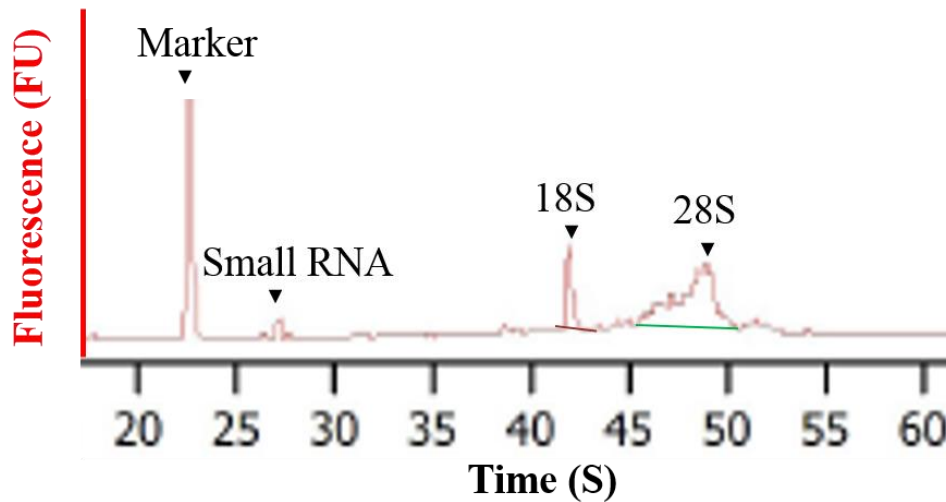


Figure 6.2 Representative Agilent 2100 Bioanalyser trace.

Trace of an NBH 8 w.p.i. RNA sample isolated by LCM. Electropherogram showing marker, small RNA, 18S and 28S ribosomal subunits. This trace represents relatively intact RNA. In degraded RNA the ratio of 18S to 28S ribosomal subunits decreases and there is an increase in the size of the small RNA peak. LCM, laser capture microdissection and w.p.i., weeks post-inoculation.

Sample	Concentration (ng/μl)	RIN score (1-10)
NBH 8 w.p.i. (1)	17.11	8.10
NBH 8 w.p.i. (2)	24.67	7.90
NBH 12 w.p.i. (1)	35.7	8.30
NBH 12 w.p.i. (2)	37.25	7.40
NBH 20 w.p.i. (1)	15.4	7.30
NBH 20 w.p.i. (2)	23.67	7.90
ME7 8 w.p.i. (1)	21.93	8.0
ME7 8 w.p.i. (2)	19.35	6.80
ME7 12 w.p.i. (1)	14.24	7.40
ME7 12 w.p.i. (2)	17.02	7.70
ME7 20 w.p.i. (1)	34.37	8.50
ME7 20 w.p.i. (2)	44.22	7.80

Table 6.1 Concentration and RIN score of RNA from laser microdissected CA3 of NBH- and ME7-animals.

Numbers in parentheses in sample column indicates independent samples for each condition and time-point. RIN, RNA integrity number.

6.3.7 RNA-Seq data analysis

FastQ files generated from RNA-Seq were given to a collaborating bioinformatics group (Dr Christopher Woelk, Michael Breen and Jeongmin Woo) in the Clinical and Experimental Science department at Southampton General Hospital. All analysis steps for the RNA-Seq data was performed by this team.

FastQ files were quality checked using FastQC to ensure high-quality nucleotide scores for each of the samples. Reads were then mapped to the mouse RefSeq genome (GenCode annotation (version M3 (GRCm38) – Ensembl 76)) using the programme TopHat. Reads were counted for each sample using the programme HT-Seq. Counted reads were then filtered (a minimum of 20 reads in at least 4 samples was required) and normalised via variance stabilising transformation (vst) normalisation (which normalises the variation seen between genes expressed at different levels) using the programme edgeR. Both non-normalised and normalised read counts were provided. The mean fold change was calculated by dividing the average normalised values for the ME7 samples by the average normalised values for the NBH samples.

6.4 Results

6.4.1 The optimisation of tissue processing for LCM

Coronal sections containing the hippocampus from a naïve mouse were sectioned at a range of different thickness between 10-30 μm . Coronal sections cut at both 20 μm and 30 μm could not be laser microdissected, as the laser was not powerful enough to cut tissue at these thicknesses. However, coronal sections cut at 10 μm could be microdissected by the laser. As a result all further experimentation using LCM was performed on coronal sections cut at 10 μm .

In order to try to optimise the processing of tissue prior to LCM, two different processing methods (section 6.3.2) were compared to maximise the concentration and quality of RNA which could be extracted from laser microdissected CA3 tissue. Coronal sections containing the hippocampus from a naïve mouse were cut and processed either by method 1 or method 2. 51 laser microdissected CA3 regions of approximately equal size were collected. RNA was extracted and the concentration and quality assessed using a NanoDrop spectrophotometer. Laser microdissected CA3 tissue which had been processed by method 1 had a higher concentration of RNA (16.2 ng/ μl), compared to that processed by method 2 (13.9 ng/ μl) (Figure 6.3). Reagent contaminants have absorbance values of 230 nm and 280 nm and proteins have an absorbance at 280 nm using the NanoDrop spectrophotometer. A higher ratio of absorbance at 260: 230 and 260: 280 is indicative of purer RNA. The 260: 280 ratio was similar for both tissue processing methods. Laser microdissected CA3 processed by method 1 had a 260:280 of 2.24 whilst the 260: 280 of laser microdissected CA3 processed by method 2 was 2.13. However, laser microdissected CA3 processed by method 1 had a higher 260:230 ratio (0.46), than laser microdissected CA3 processed by method 2 (0.08). Tissue processing method 1 was therefore selected for future experimentation on tissue to undergo LCM.

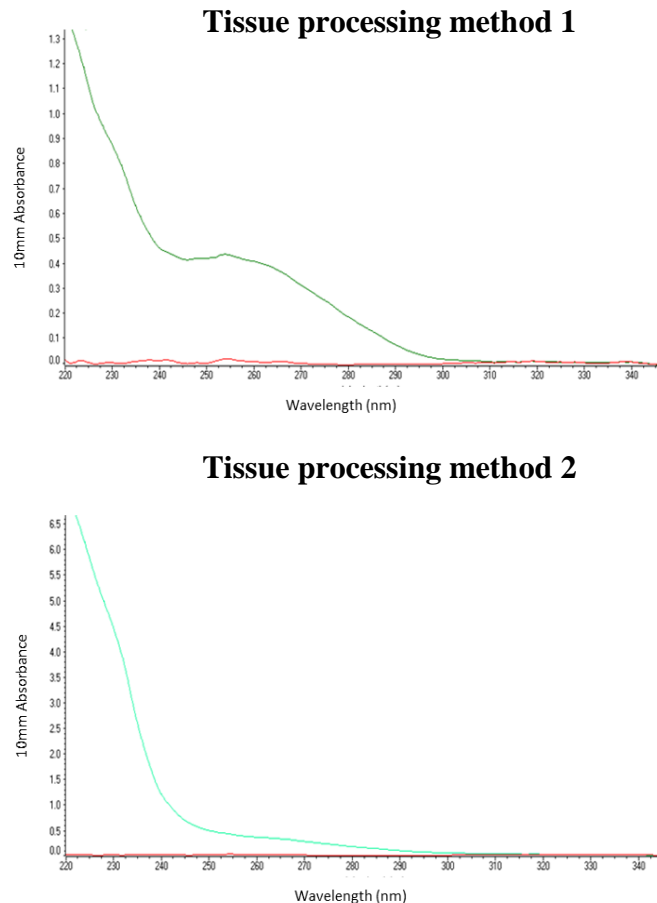


Figure 6.3 Quality of RNA from laser microdissected CA3 processed by method 1 or 2.

NanoDrop spectrophotometer traces of RNA extracted from laser microdissected CA3 (green line), which had been processed prior by method 1 or 2. The red line represents RNase-free water (negative control). Pure RNA has a maximum absorbance peak at 260 nm.

6.4.2 Using LCM to enrich and de-enrich for mRNAs expressed in different hippocampal regions and in glial cells

The expression of mRNAs which are enriched or restricted to anatomically defined regions of the hippocampus were searched for using literature searches and bioinformatics (Table 6.2). DNA microarray and *in situ* hybridisation data revealed a subset of mRNAs which were found to be enriched/restricted to the granule cell layer of the DG and the pyramidal layer of CA3 and CA1 (Lein et al., 2004). This was cross-referenced to *in situ* hybridization data from the Allen Brain Atlas (<http://www.brain-map.org/>) and from another secondary source of data (Table 6.2).

Two mRNAs enriched in the CA3 pyramidal layer were chosen along with one mRNA from the CA1 pyramidal layer and one mRNA from the DG granule cell layer. These were chosen to assess the differential abundance of these mRNAs between laser microdissected CA3 tissue and whole hippocampal tissue.

Region	Gene	Primary source of information	Secondary source of information
CA3 pyramidal layer	BCL-2-related ovarian killer protein (Bok)	<i>In situ</i> hybridisation and DNA microarrays (Lein et al., 2004)	<i>In situ</i> hybridisation (Lein et al., 2005) PCR (Hatazaki et al., 2007) Allen Brain Atlas
	Testican (Spock1)	<i>In situ</i> hybridisation and DNA microarrays (Lein et al., 2004)	<i>In situ</i> hybridisation (Bonnet et al., 1996) Allen Brain Atlas
CA1 pyramidal layer	Nephroblastoma overexpressed gene (Nov)	<i>In situ</i> hybridisation and DNA microarrays (Lein et al., 2004)	<i>In situ</i> hybridisation (Zhao et al., 2001) Allen Brain Atlas
DG granule cell layer	Desmoplakin (Dsp)	<i>In situ</i> hybridisation and DNA microarrays (Lein et al., 2004)	Microarray (Hagihara et al., 2009) Allen Brain Atlas

Table 6.2 mRNAs enriched in different regions of the hippocampus.

Primary and secondary data sources which support the region specific expression patterns of these mRNAs is shown. CA1, Cornu Ammonis region 1; CA3, Cornu Ammonis region 3 and DG, dentate gyrus.

Total RNA was extracted from laser microdissected CA3 of a naïve mouse and from the whole hippocampus of a naïve mouse as shown in Figure 6.4. 43 ng of RNA from both the laser microdissected CA3 and whole hippocampus was then reverse transcribed into cDNA and qPCR was used to measure the relative expression levels of the selected mRNAs (Table 6.2).

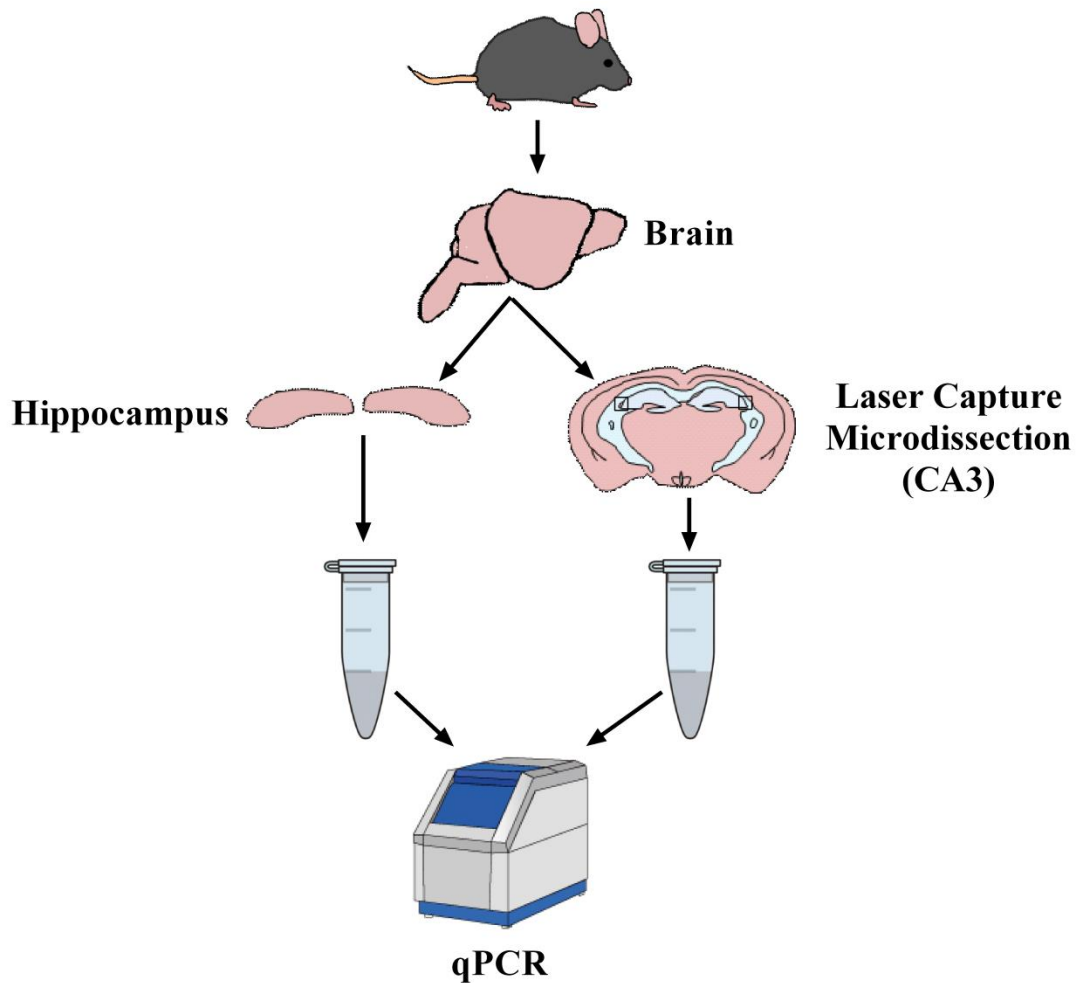


Figure 6.4 Experimental outline: the expression of mRNAs in the whole hippocampus compared to laser microdissected CA3.

Naïve C57BL/6J mice were killed. The brain was removed and used for either hippocampal dissection or for cutting coronal sections containing the hippocampus. LCM was performed on coronal brain sections to microdissect the CA3 pyramidal layer. The dissected hippocampus and laser microdissected CA3 was used to isolate RNA and perform qPCR. CA3, Cornu Ammonis region 3 and LCM, laser capture microdissection.

In situ hybridisation shows that both Bcl-2-related ovarian killer protein (Bok) and Testican (Spock1) mRNAs are enriched within the CA3 pyramidal layer of the hippocampus (Lein et al., 2004) (Figure 6.5a and b). qPCR analysis shows that the relative expression of both of these mRNAs is increased in laser microdissected CA3 compared to the whole hippocampus (Figure 6.5a and b).

In situ hybridisation shows that the expression of Desmoplakin (Dsp) mRNA is restricted to the DG granule cell layer (Lein et al., 2004) (Figure 6.6a) and the

expression of Nephroblastoma overexpressed gene (Nov) mRNA is restricted to CA1 pyramidal layer (Lein et al., 2004) (Figure 6.6b). qPCR analysis shows that both Dsp and Nov mRNAs are detected in whole hippocampal tissue (Figure 6.6a and b). However, qPCR shows that Dsp and Nov mRNAs are not detected within the laser microdissected CA3 tissue, as expected (Figure 6.6a and b).

In addition, the expression levels of synaptic and glial cell mRNAs in laser microdissected CA3 was compared to the whole hippocampus. The expression of the synaptic mRNA synaptophysin, was slightly higher in laser microdissected CA3 compared to the whole hippocampus (Figure 6.7b). The astrocyte specific mRNA, GFAP, is expressed at a much higher level in the whole hippocampus as opposed to laser microdissected CA3 (Figure 6.7a). The CT values of the microglia associated mRNA, CD11b, in both the whole hippocampus and in laser microdissected CA3, was below the range for accurate quantification (section 2.6.3.1). However, when the amplified samples were run on an agarose gel it can be clearly seen that CD11b mRNA is expressed at a much higher level in the whole hippocampus compared to laser microdissected CA3 (Figure 6.7c).

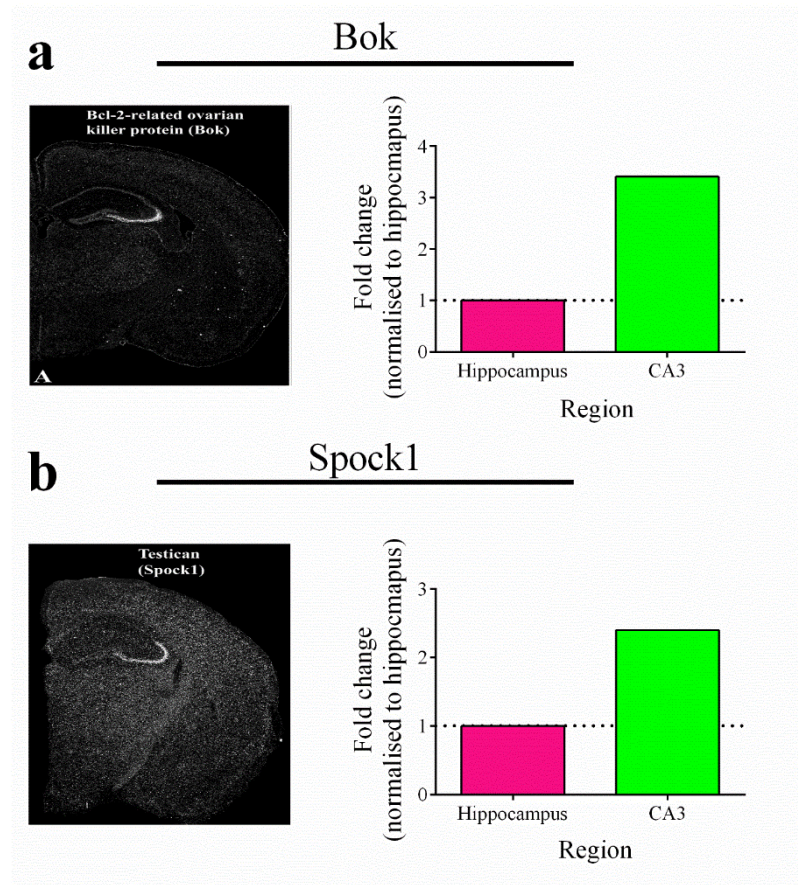


Figure 6.5 Quantification of Bok and Spock1 mRNAs in laser microdissected CA3.

In situ hybridisation and qPCR analysis for Bok (a) and Spock1 (b) mRNAs. *In situ* hybridisation data is from Lein et al., 2004. Data in graphs represents qPCR derived mRNA expression values from whole hippocampal tissue and laser microdissected CA3 tissue. $n = 1$ naïve animal. CA3, Cornu Ammonis region 3.

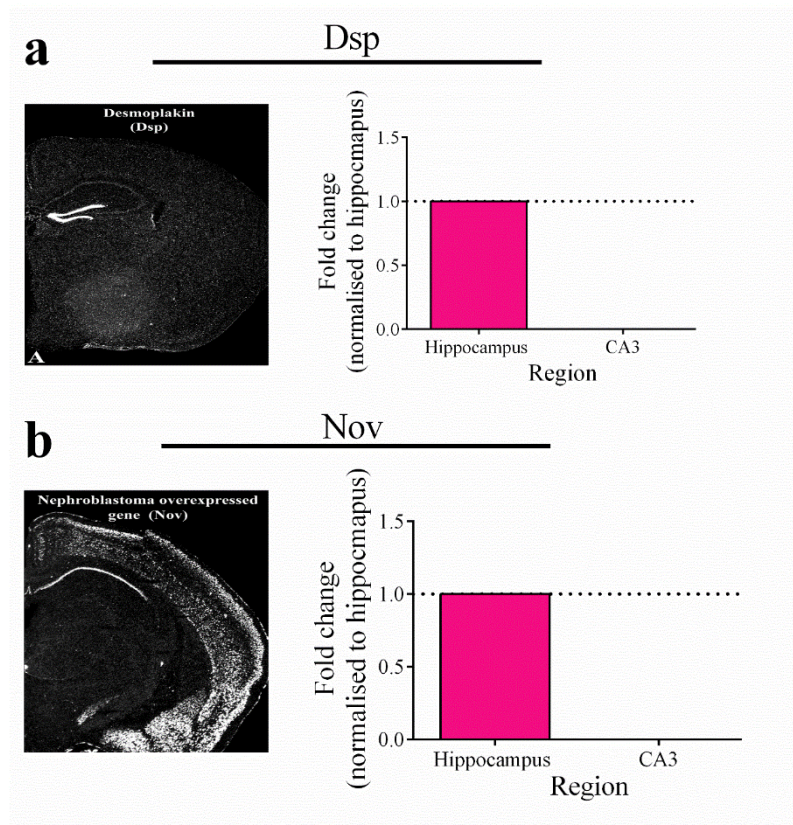


Figure 6.6 Quantification of Dsp and Nov mRNAs in laser microdissected CA3.

In situ hybridisation and qPCR analysis for Dsp (a) and Nov (b) mRNAs. *In situ* hybridisation data is from Lein et al., 2004. Data in graphs represents qPCR derived mRNA expression values from whole hippocampal tissue and laser microdissected CA3. $n = 1$ naïve animal. CA3, Cornu Ammonis region 3.

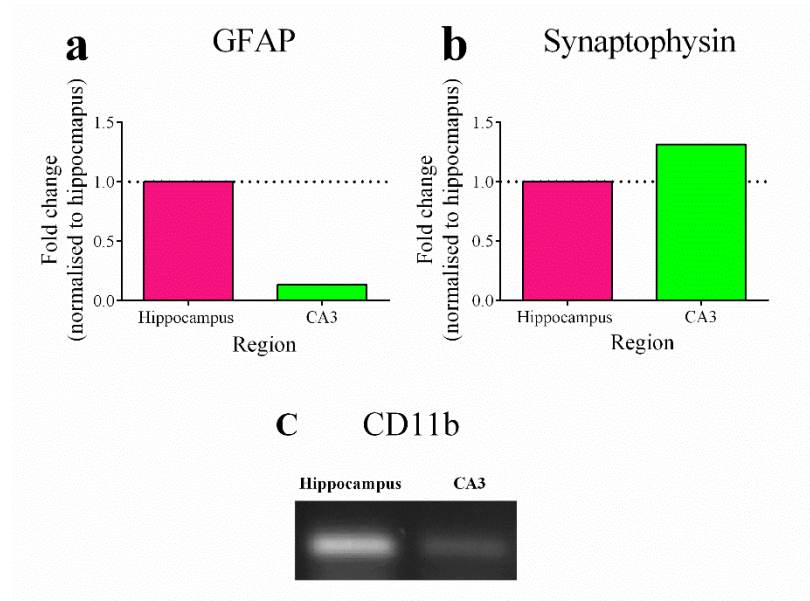


Figure 6.7 Quantification of GFAP and synaptophysin mRNAs and levels of CD11b mRNA in laser microdissected CA3.

qPCR analysis for GFAP (a), synaptophysin (b) and CD11b (c) mRNAs. Data in graphs represents the mRNA expression values from whole hippocampal tissue and laser microdissected CA3. $n = 1$ naïve animal. CA3, Cornu Ammonis region 3.

6.4.3 The expression of UPR and other stress-related response mRNAs in laser microdissected CA3

The constitutive expression of three UPR mRNAs (BiP, CHOP and ATF4) and two other stress-related response mRNAs (ATF3 and GADD45 α) was investigated using qPCR, to determine if these mRNAs were enriched in laser microdissected CA3 compared to the whole hippocampus of naïve animals. Both BiP and CHOP mRNA was reduced ~2 fold in laser microdissected CA3 compared to the whole hippocampus (Figure 6.8a and b). However, the expression of ATF4 mRNA was 1.5 fold higher in laser microdissected CA3 compared to the whole hippocampus (Figure 6.8c). The expression of ATF3 mRNA was very low in the whole hippocampus ($C_T = \sim 29$), but was below the range for accurate quantification (section 2.6.3.1) in laser microdissected CA3 ($C_T = > 32$) (Figure 6.8d). Levels of GADD45 α mRNA were slightly higher in the whole hippocampus compared to laser microdissected CA3 (Figure 6.8e).

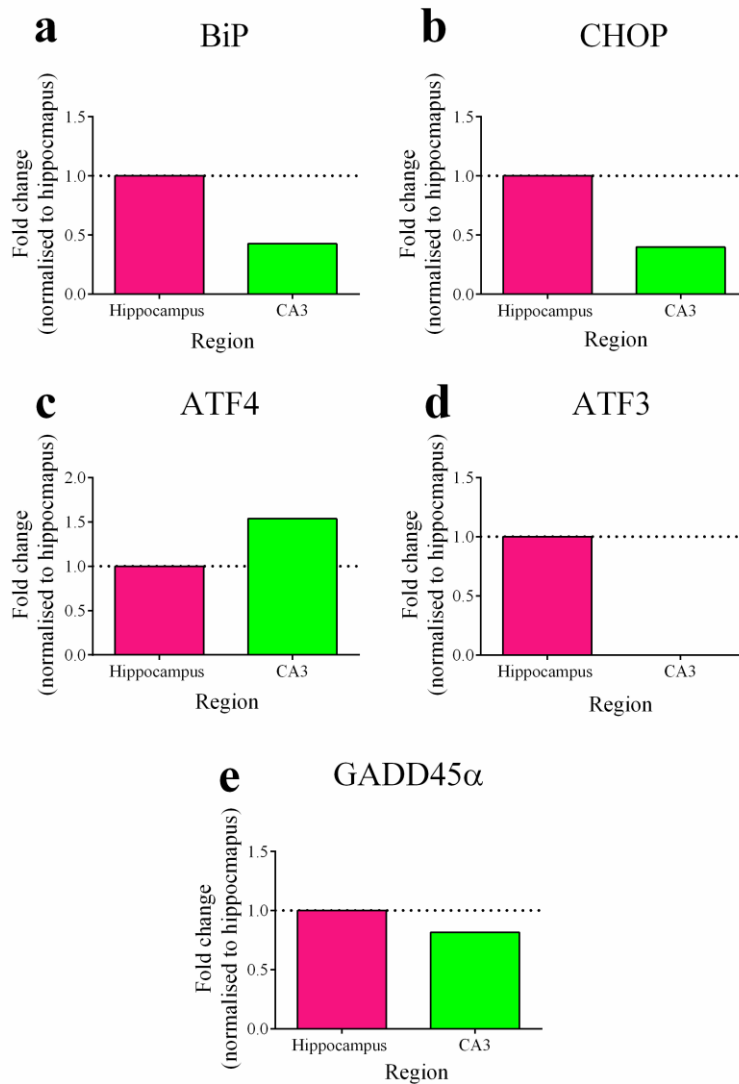


Figure 6.8 Quantification of UPR and stress-related response mRNAs in laser microdissected CA3.

qPCR analysis for BiP (a), CHOP (b), ATF4 (c) ATF3 (d) and GADD45α (e) mRNAs. Data in graphs represents the mRNA expression values from whole hippocampal and laser microdissected CA3. $n = 1$ naïve animal. CA3, Cornu Ammonis region 3.

6.4.4 The expression of astrocyte and microglia-associated molecules in the laser microdissected CA3 of ME7-animals

RNA extracted from laser microdissected CA3 of NBH- and ME7-animals, across a full disease time course, was collected and used for qPCR (section 6.4.4 and 6.4.5) and RNA-Seq (section 6.4.6) (Figure 6.9).

qPCR was performed to determine the relative expression of astrocyte and microglia-associated mRNAs in the laser microdissected CA3. qPCR revealed that the levels of GFAP mRNA progressively increased in ME7-animals from 2.7 fold at 8 w.p.i. to 102 fold at 20 w.p.i. (Figure 6.10a). The levels of CD11b mRNA were 1.7 fold higher in ME7-animals at 8 and 12 w.p.i. and at 20 w.p.i. CD11b mRNA levels were 6.2 fold higher in ME7-animals compared to NBH-animals (Figure 6.10b). Expression of complement (C1q) is associated with the presence of reactive astrocytes and microglia (Alexander et al., 2008). Similar to GFAP mRNA, the expression of C1qB mRNA progressively increased in ME7-animals and at 20 w.p.i. the levels of C1qB mRNA were 15.7 fold higher in ME7-animals compared to NBH-animals (Figure 6.10c).

To confirm the presence of both astrocytes and microglia in the CA3 pyramidal layer of ME7-animals, immunohistochemistry was performed. Immunohistochemical staining for GFAP and the microglia marker IBA1, showed an increased presence of astrocytes and microglia (including the cell body and processes) in the pyramidal layer of CA3 in ME7-animals from 12 w.p.i. (Figure 6.11a and b).

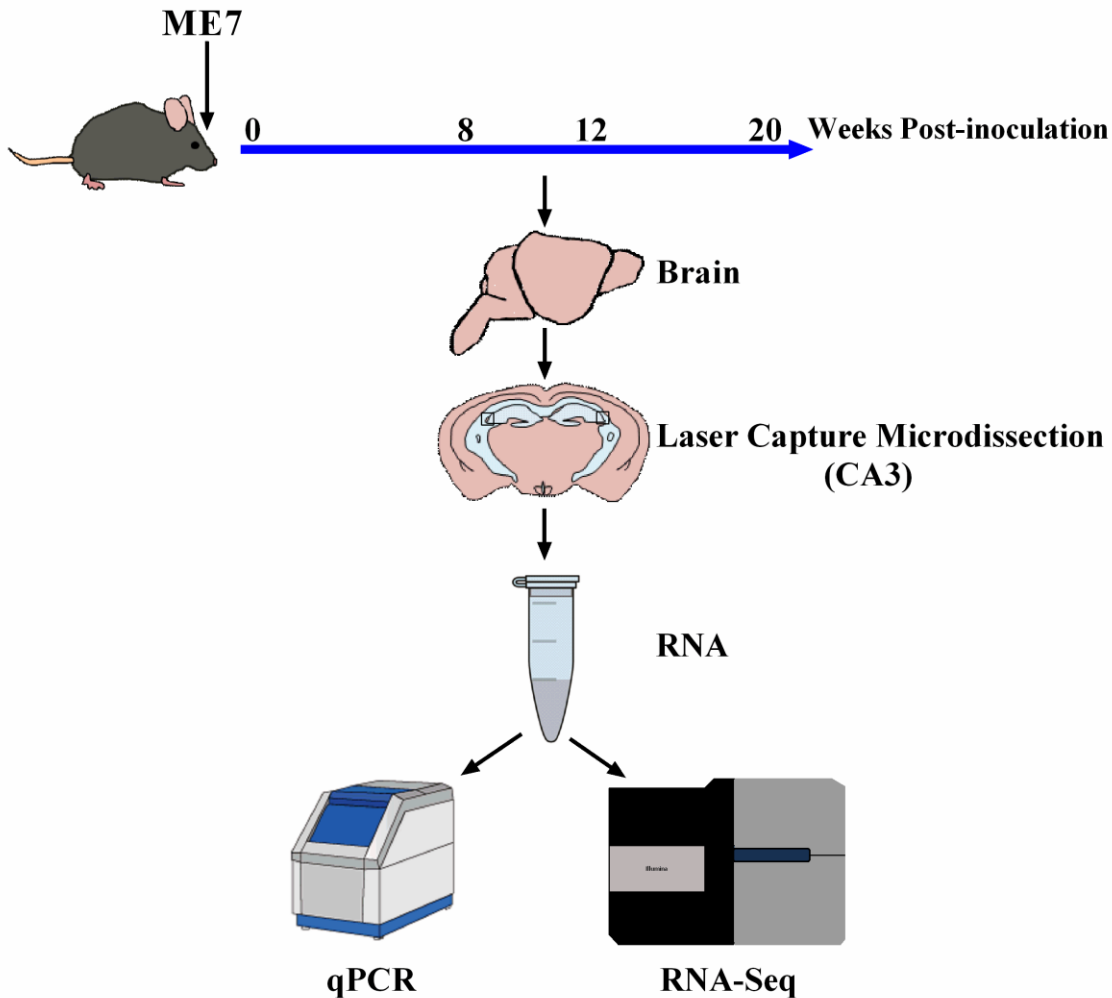


Figure 6.9 Experimental outline: investigating transcriptional responses in laser microdissected CA3 of ME7-animals.

C57BL/6J female mice were injected with 1 μ l of NBH or ME7 brain homogenate bilaterally into the dorsal hippocampus. Mice were killed at different time points spanning early- (8 w.p.i.) middle- (12 w.p.i.) and late-stages (20 w.p.i.) of disease. The brain was removed and coronal sections containing the hippocampus were cut. LCM was performed on coronal brain sections to microdissect the CA3 pyramidal layer. Laser microdissected CA3 was used to isolate RNA. Some of the RNA was used to perform qPCR and the remainder was used for RNA-Seq. LCM, laser capture microdissection; RNA-Seq, RNA sequencing and w.p.i., weeks post-inoculation.

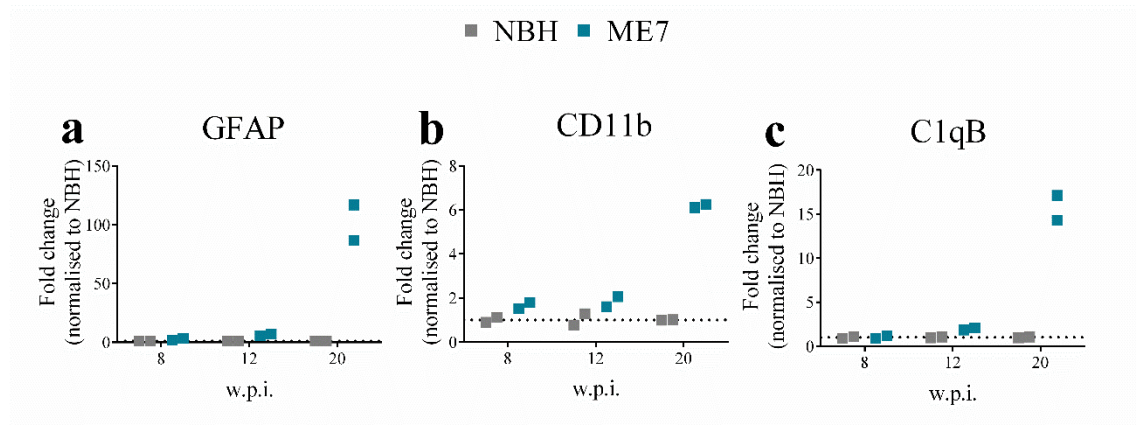


Figure 6.10 Quantification of GFAP, CD11b and C1qB mRNAs in laser microdissected CA3 of ME7-animals.

qPCR analysis for GFAP (a), CD11b (b) and C1qB (c) mRNAs in laser microdissected CA3 of NBH- and ME7-animals killed at 8, 12 and 20 w.p.i. Scatter plots show independent mRNA expression values from $n = 2$ animals per condition and time-point. CA3, Cornu Ammonis region 3 and w.p.i., weeks post-inoculation.

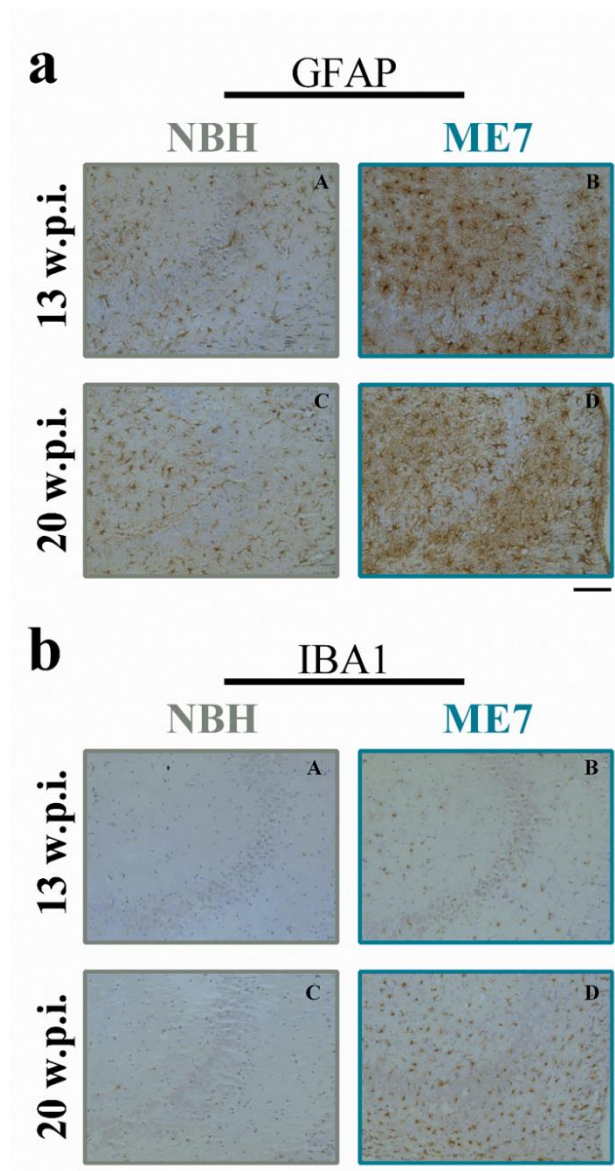


Figure 6.11 Immunohistochemical staining for GFAP and IBA1 in ME7-animals.

Representative immunohistochemical staining for GFAP (a) and IBA1 (b) in the CA3 of the hippocampus of NBH- and ME7-animals killed at 12 and 20 w.p.i. Scale bars are indicated under the panel of images (100 μ m). $n = 4$ animals per condition and time-point. CA3, Cornu Ammonis region 3 and w.p.i., weeks post-inoculation. Staining was performed by Dr Diego Gomez-Nicola.

6.4.5 Expression of UPR and other stress-related response mRNAs in laser microdissected CA3 of ME7-animals

The expression of the UPR mRNAs, BiP and spliced XBP-1 were not distinctly different between NBH- and ME7-animals (Figure 6.12a and b). The expression of GADD34 and CHOP mRNAs were not different between NBH- and ME7-animals at 8 and 12 w.p.i., however, at 20 w.p.i. levels of GADD34 and CHOP mRNAs were increased ~1.5 fold in ME7-animals (Figure 6.12c and d). Expression of ATF4 mRNA was increased in ME7-animals at 8 w.p.i. when levels were 1.7 fold higher in ME7-animals compared to NBH-animals (Figure 6.12e). The mRNA levels of eIF2 α were examined. Although phosphorylation of eIF2 α is associated with a UPR, eIF2 α mRNA has been shown to be upregulated in the cell bodies of motoneurons early on in mice which succumb to motoneuron disease (Saxena et al., 2009). Expression of eIF2 α mRNAs was higher in ME7-animals at 8 w.p.i. (1.4 fold) and 12 w.p.i. (1.6 fold), although at 20 w.p.i. levels of eIF2 α mRNA were lower in ME7-animals compared to NBH-animals (Figure 6.12f).

The expression of the stress-related response transcripts: ATF3; GADD45 α and Homer1a were also investigated in laser microdissected CA3 of ME7-animals. ATF3 is expressed at low levels and most C_T values for the samples were below the limit for accurate quantification. However, ATF3 mRNA could be accurately detected at 20 w.p.i. Both of the NBH samples had very different expression levels of ATF3 (Figure 6.13a). However, the expression of ATF3 mRNAs was not increased in ME7-animals compared to NBH-animals (Figure 6.13a). Expression of GADD45 α mRNAs progressively increased in ME7-animals from 1.3 fold at 8 w.p.i. to 1.6 fold at 20 w.p.i. (Figure 6.13b). No clear differences were seen in the expression of Homer1a mRNA between NBH- and ME7-animals (Figure 6.13c).

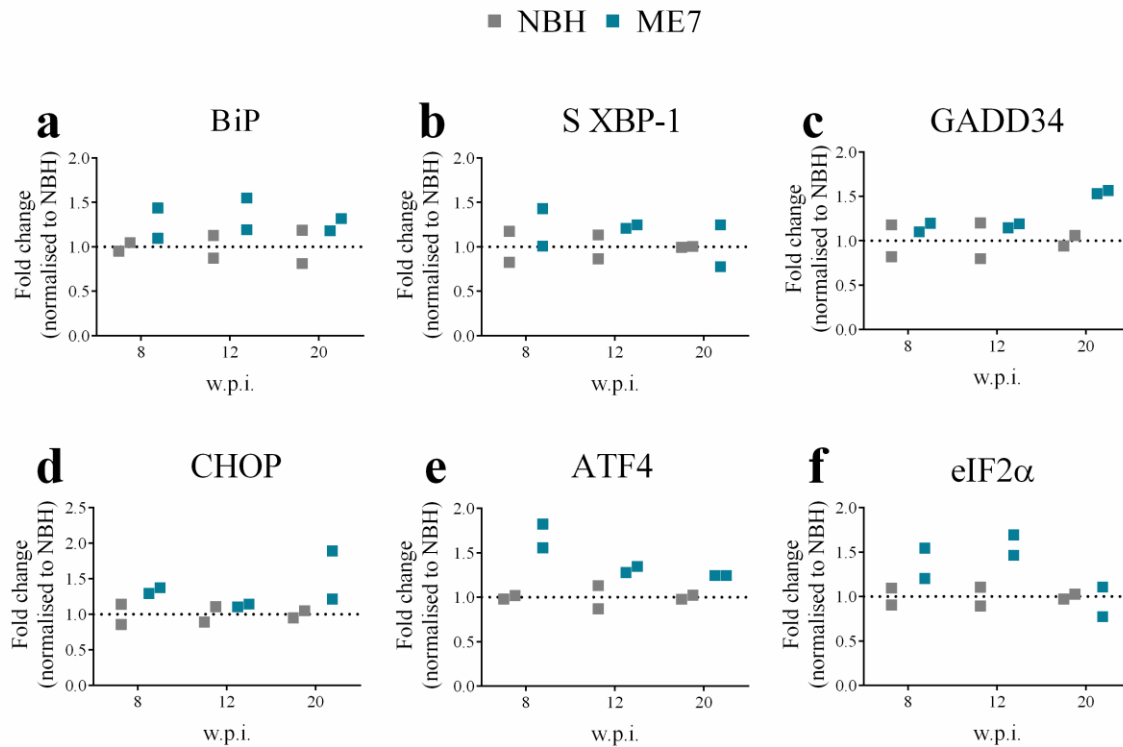


Figure 6.12 Quantification of UPR mRNAs in laser microdissected CA3 of ME7-animals.

qPCR analysis for BiP (a), spliced XBP-1 (b), GADD34 (c), CHOP (d), ATF4 (e) and eIF2α (f) mRNAs in laser microdissected CA3 from NBH- and ME7-animals killed at 8, 12 and 20 w.p.i. Scatter plots show independent mRNA expression values from $n = 2$ animals per condition and time-point. CA3, Cornu Ammonis region 3; S XBP-1, spliced XBP-1; and w.p.i., weeks post-inoculation.

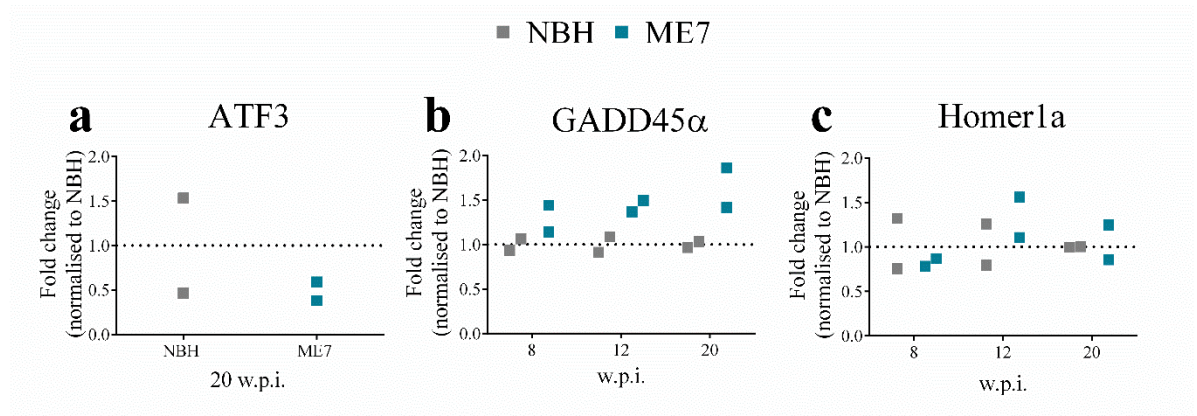


Figure 6.13 Quantification of other stress-related response mRNAs in laser microdissected CA3 of ME7-animals.

qPCR analysis for ATF3 (a), GADD45 α (b) and Homer1a (c) mRNAs in laser microdissected CA3 of NBH- and ME7-animals killed at 8, 12 and 20 w.p.i.. Scatter plots show independent mRNA expression values from $n = 2$ animals per condition and time-point. CA3, Cornu Ammonis region 3 and w.p.i., weeks post-inoculation.

6.4.6 RNA-Seq analysis

RNA-Seq was performed on total RNA from laser microdissected CA3 of NBH- and ME7-animals 8, 12 and 20 w.p.i. (section 6.3.6 and 6.3.7).

mRNA reads were detected for 24,060 mRNAs. As expected and owing to its abundance the read count for GAPDH was much higher than for other mRNAs such as GFAP, CD11b and C1qB. However, there was heterogeneity in the read count for GAPDH between samples of the same condition (Table 6.3). This became less heterogeneous after normalisation (Table 6.3). The read count and normalised read count for GFAP, CD11b and C1qB mRNAs from NBH and ME7 samples is displayed in the tables below. These mRNAs were analysed based on their striking differences in expression between NBH and ME7 samples, as shown by qPCR analysis (Figure 6.10a, b and c).

The fold change (based on normalised reads) in the expression of mRNAs between NBH and ME7 samples was compared between the RNA-Seq and qPCR data. The comparison shows that the fold change in expression of GFAP (Table 6.4), CD11b (Table 6.5) and C1qB (Table 6.6) mRNAs is very different between the RNA-Seq and qPCR datasets. The progressive increase in expression in these three mRNAs in the ME7 samples, seen using qPCR, is not seen in the RNA-Seq data. Unlike the qPCR

analysis, the RNA-Seq data shows that the expression of these three mRNAs is not different between NBH and ME7 samples at any of the time-points examined.

Because of the inability of RNA-Seq to replicate the clear expression changes seen in these mRNAs using qPCR, no further analysis was performed by the bioinformatics group on this RNA-Seq database.

Sample	Read count	Normalised read count
NBH 8 w.p.i. (1)	233	7.94
NBH 8 w.p.i. (2)	431	8.48
ME7 8 w.p.i. (1)	549	8.76
ME7 8 w.p.i. (2)	267	7.55
NBH 12 w.p.i. (1)	299	7.65
NBH 12 w.p.i. (2)	943	9.55
ME7 12 w.p.i. (1)	323	8.29
ME7 12 w.p.i. (2)	288	7.62
NBH 20 w.p.i. (1)	448	8.65
NBH 20 w.p.i. (2)	259	7.70
ME7 20 w.p.i. (1)	287	7.68
ME7 20 w.p.i. (2)	330	7.61

Table 6.3 Read count and normalised read count for GAPDH mRNA in laser microdissected CA3 of NBH- and ME7-animals.

Numbers in parentheses in sample column indicates independent samples for each condition and time-point. w.p.i., weeks post-inoculation.

Sample	Read count	Normalised read count	Mean fold change normalised to NBH (RNA-Seq)	Mean fold change normalised to NBH (qPCR)
NBH 8 w.p.i. (1)	38	5.3	1.02	2.65
NBH 8 w.p.i. (2)	30	4.7		
ME7 8 w.p.i. (1)	46	5.2		
ME7 8 w.p.i. (2)	46	5.0		
NBH 12 w.p.i. (1)	49	5.0	1.0	6.42
NBH 12 w.p.i. (2)	57	5.5		
ME7 12 w.p.i. (1)	56	5.8		
ME7 12 w.p.i. (2)	40	4.8		
NBH 20 w.p.i. (1)	35	5.0	1.12	101.72
NBH 20 w.p.i. (2)	53	5.4		
ME7 20 w.p.i. (1)	38	4.8		
ME7 20 w.p.i. (2)	198	6.9		

Table 6.4 RNA-Seq vs qPCR: mean fold change of GFAP mRNA between laser microdissected CA3 of NBH- and ME7-animals.

Numbers in parentheses in sample column indicates independent samples for each condition and time-point. w.p.i., weeks post-inoculation.

Sample	Read count	Normalised read count	Mean fold change normalised to NBH (RNA-Seq)	Mean fold change normalised to NBH (qPCR)
NBH 8 w.p.i. (1)	31	5.05	1.02	1.66
NBH 8 w.p.i. (2)	47	5.30		
ME7 8 w.p.i. (1)	40	5.0		
ME7 8 w.p.i. (2)	67	5.56		
NBH 12 w.p.i. (1)	74	5.64	1.03	1.84
NBH 12 w.p.i. (2)	40	5.0		
ME7 12 w.p.i. (1)	40	5.29		
ME7 12 w.p.i. (2)	77	5.72		
NBH 20 w.p.i. (1)	17	3.97	1.20	6.18
NBH 20 w.p.i. (2)	48	5.28		
ME7 20 w.p.i. (1)	66	5.57		
ME7 20 w.p.i. (2)	66	5.30		

Table 6.5 RNA-Seq vs qPCR: mean fold change of CD11b mRNA in laser microdissected CA3 of NBH- and ME7-animals.

Numbers in parentheses in sample column indicates independent samples for each condition and time-point. w.p.i., weeks post-inoculation.

Sample	Read count	Normalised read count	Mean fold change normalised to NBH (RNA-Seq)	Mean fold change normalised to NBH (qPCR)
NBH 8 w.p.i. (1)	5	2.53	1.18	1.03
NBH 8 w.p.i. (2)	8	2.82		
ME7 8 w.p.i. (1)	12	3.30		
ME7 8 w.p.i. (2)	11	3.01		
NBH 12 w.p.i. (1)	13	3.17	1.26	1.97
NBH 12 w.p.i. (2)	10	3.06		
ME7 12 w.p.i. (1)	16	3.99		
ME7 12 w.p.i. (2)	21	3.87		
NBH 20 w.p.i. (1)	8	2.93	1.20	15.71
NBH 20 w.p.i. (2)	11	3.20		
ME7 20 w.p.i. (1)	10	2.91		
ME7 20 w.p.i. (2)	36	4.44		

Table 6.6 RNA-Seq vs qPCR: mean fold change of C1qB mRNA between laser microdissected CA3 of NBH- and ME7-animals.

Numbers in parentheses in sample column indicates independent samples for each condition and time-point. w.p.i., weeks post-inoculation.

6.5 Discussion

6.5.1 Optimisation of LCM

Two different tissue processing methods were used prior to performing LCM and were compared to determine which method would produce RNA of the highest concentration and quality. The first tissue processing method produced RNA which was of a higher concentration and a higher 260: 230 absorbance (Figure 6.3). The first tissue processing method had a reduced number of steps for fixing, staining and dehydrating the tissue (5 steps for method 1 vs 11 steps for method 2). The reduced number of steps required for processing tissue to undergo LCM may have helped preserve RNA integrity.

6.5.2 Enriching for genes expressed in the CA3 pyramidal layer and de-enriching for genes expressed outside of the CA3 pyramidal layer

Genes expressed in different regions of the hippocampus were searched for (Table 6.2). LCM was used to try to enrich and de-enrich for these selected mRNAs. As expected mRNAs which were predominantly expressed in the CA3 pyramidal layer (Bok and Spock1) had a higher level of expression in laser microdissected CA3 tissue compared to whole hippocampal tissue (Figure 6.5a and b). mRNAs which are expressed in other neuronal layers (CA1 and DG) were not detected within the laser microdissected CA3 (Figure 6.6a and b). Similarly, the expression of mRNAs associated with glial cells (astrocytes and microglia) are much lower in laser microdissected CA3 as opposed to the whole hippocampus (Figure 6.7a and c). On the other hand, synaptophysin mRNA was enriched in laser microdissected CA3 tissue (Figure 6.7b). In agreement with a previous study, SNAP-25 mRNA has been found to be enriched in laser microdissected CA1 neurons (Majer et al., 2012). This data shows that LCM can also be used to selectively de-enrich for mRNAs which are expressed in other neurons and/or non-neuronal cells.

Studies looking at mRNA expression levels in whole anatomical regions of the brain, which contain different neuronal types and non-neuronal cells are not representative of molecular changes in specific cells. In this chapter, LCM was used to selectively isolate the CA3 pyramidal layer (containing the cell bodies of CA3 pyramidal neurons) to study molecular responses during chronic neurodegeneration.

6.5.3 The majority of UPR and other stress-related response mRNAs are de-enriched in laser microdissected CA3

Some of the UPR (BiP, CHOP and ATF4) and other stress-related response mRNAs (ATF3 and GADD45 α) were investigated to determine their expression in laser microdissected CA3 of naïve animals. The results showed that in naïve animals, BiP, CHOP, ATF3 and GADD45 α mRNAs are expressed at a higher extent in the whole hippocampus as opposed to laser microdissected CA3 (Figure 6. 8a, b, d and e). ATF4 mRNA was the only mRNA to be expressed at higher level in the laser microdissected CA3 compared to the whole hippocampus (Figure 6. 8c). Therefore, in naïve mice,

other neurons and/or non-neuronal cells have higher levels of expression of these mRNAs.

6.5.4 Using LCM to investigate the molecular changes occurring in the CA3 pyramidal neurons of ME7-animals

ME7 prion disease is associated with morphological alterations of the CA3 pyramidal neurons (Al-Malki, 2012). These morphological changes may lead to transcriptional responses. Transcript changes in the CA3 pyramidal neurons could also potentially be initiated by:

- 1) The accumulation of PrP^{Sc}
- 2) Signals released by activated microglia and astrocytes in response to either the accumulation of PrP^{Sc} or morphological changes to the CA3 pyramidal neurons (see below).
- 3) Loss of CA1 pyramidal neurons. Degeneration of these neurons could lead to changes in network homeostasis and consequently lead to a transcriptional response in the CA3 pyramidal neurons.

The appearance of PrP^{Sc} and activation of microglia and astrocytes are early events in ME7-animals (≥ 8 w.p.i.). Morphological changes seen in CA3 pyramidal neurons occur from ≥ 13 w.p.i. and neuronal cell death of CA1 pyramidal neurons is not seen until late-stage disease ≥ 18 w.p.i. This implies that different molecular responses are likely to occur as prion disease evolves. To understand the evolution of transcriptional responses during the course of ME7 prion disease, laser microdissected CA3 from NBH- and ME7-animals has been captured across the course of prion disease progression.

6.5.5 Astrocytes and microglia infiltrate the CA3 pyramidal layer of ME7-animals

Prior to assessing transcriptional responses in the laser microdissected CA3, the levels of astrocyte and microglia associated mRNAs was determined. qPCR showed that GFAP, CD11b and C1qB mRNAs progressively increased in laser microdissected CA3 from 8-20 w.p.i. in ME7-animals (Figure 6.10a, b and c). This suggests that during prion disease progression there is an increase in astrocytes and microglia in the pyramidal layer of CA3. Immunohistochemistry confirmed this and showed that as

disease progressed there was an increase in the number of astrocytes and microglia in the CA3 pyramidal layer (Figure 6.11a and b). Similarly, laser microdissected CA1 neurons of RML-animals at end-stage disease showed an increase in the presence of both astrocytes and microglia (Majer et al., 2012). C1qB mRNA was increased 7.4 fold in the laser microdissected CA1 neurons of RML-animals (Majer et al., 2012).

These results suggest that LCM still has its limitations, especially in diseases such as prion disease which is associated with a strong glial pathology. In addition, it highlights the need for caution when analysing gene expression changes especially from late-stage ME7 tissue, when the astrocytes and/or microglia may be contributing to changes in expression levels of mRNAs.

6.5.6 Limited evidence for a robust UPR in laser microdissected CA3 of ME7-animals

The expression of BiP, spliced XBP-1, GADD34 and CHOP mRNAs were all ≤ 1.6 fold in ME7-animals compared to NBH-animals (Figure 6.12). ATF4 mRNA was increased 1.7 fold in ME7-animals at 8 w.p.i., but this was at a time when none of the other UPR mRNAs were increased (Figure 6.12e). The phosphorylation of eIF2 α is associated with a UPR response not the transcriptional induction of eIF2 α . However, eIF2 α mRNA has been shown to be induced in the cell bodies of motoneurons in Tg ALS mice (SOD1, G93A) which succumb to motoneuron disease (Saxena et al., 2009). Investigation of eIF2 α mRNA in laser microdissected CA3 from NBH- and ME7-animals revealed that eIF2 α mRNA was modestly increased in ME7-animals, with a fold change of 1.6 at 12 w.p.i (Figure 6.12f). Although, at 20 w.p.i. there was no difference in expression between NBH- and ME7-animals. In line with these findings, laser microdissected CA1 neurons from RML-animals showed no robust induction of these UPR mRNAs, except for GADD34 mRNA which was upregulated early on during the course of RML prion disease (Majer et al., 2012).

6.5.7 GADD45 α but not ATF3 or Homer1a mRNA, is increased in laser microdissected CA3 of ME7-animals

ATF3 mRNA levels were below the limit for accurate quantification for most NBH and ME7 samples. In laser microdissected CA1 neurons from RML-animals, ATF3 was also

below the limit of detection for this microarray analysis (Majer et al., 2012). At 20 w.p.i. in the ME7 model, ATF3 was detected in both NBH and ME7 samples, although this was again at the lower end of the detection limit for this qPCR. Although ATF3 was detected here there was no induction of ATF3 mRNA in laser microdissected CA3 of ME7-animals (Figure 6.13a). This was in contrast to what is seen in whole hippocampal tissue from ME7-animals (Figure 3.11a). This suggests that the induction of ATF3 mRNA from other neurons and/or non-neuronal (glial) cells.

The levels of GADD45 α mRNA progressively increased in the laser microdissected CA3 of ME7-animals (Figure 6.13b). However, the fold change in GADD45 α is less in laser microdissected CA3 than seen in whole hippocampal tissue (Figure 3.13) which suggests that other neurons and/or non-neuronal (glial) cells are more responsible for the increased expression of GADD45 α in whole hippocampal tissue of ME7-animals. The induction of GADD45 α in laser microdissected CA3 of ME7-animals at 20 w.p.i., should be interpreted with caution, since astrocytes and microglia signals are found in laser microdissected CA3 at this time and might therefore be at least in part responsible for this transcriptional change. Although levels of GADD45 α mRNA was increased in laser microdissected CA3 of ME7-animals, there was no significant induction of GADD45 α mRNA in laser microdissected CA1 neurons of RML-animals (Majer et al., 2012). This might be because of the more stringent criteria for detecting a statistical significance in the RML model (2.5 fold change and <0.1% FDR), but also because of differences between the two models.

At 60-70% of the disease time-course (analogous to 12-14 w.p.i. in the ME7 model) in RML-animals, the level of Homer1a mRNA is significantly increased in laser microdissected CA1 neurons of RML-animals (Majer et al., 2012). Although, by end-stage disease Homer1a mRNA is downregulated (Majer et al., 2012). In the analysis in this chapter, there was no difference in Homer1a expression between NBH- and ME7-animals (Figure 6. 13c).

6.5.8 RNA-Seq did not resolve changes seen using qPCR

Gene expression changes determined by microarray analysis in whole brain tissue and in the hippocampus of mice with prion disease have been performed (Brown et al., 2005, Gehlenborg et al., 2009, Hwang et al., 2009, Sorensen et al., 2008). However,

although informative these studies do not reveal which neurons are responsible for the transcriptional changes reported. In fact, many of these changes might be non-neuronal.

In this chapter the CA3 pyramidal layer of the hippocampus was laser microdissected and this is the first known report of this, although the CA1 pyramidal layer has been laser microdissected in RML-animals (Majer et al., 2012). Although over 20,000 genes were detected results produced using qPCR were not recapitulated in the RNA-Seq dataset. The increased expression of GFAP, CD11b and C1qB mRNAs in the laser microdissected CA3 of ME7-animals as seen by qPCR, was not seen in the data produced from RNA-Seq (Table 6.4, 6.5 and 6.6). This was despite their presence in the library.

Therefore, mRNAs which are most likely to define the transcriptional changes in laser microdissected CA3, are probably not detected as changing in the data set captured. The quality and concentration of RNA from laser microdissected CA3 was lower than that produced from whole hippocampal tissue (data not shown). Pooling two samples per time-point may have contributed to variability between samples. Despite this, qPCR performed on these pooled samples did resolve clear differences between NBH- and ME7-animals especially for GFAP and C1qB mRNAs.

6.6 Conclusion

LCM was used to isolate the pyramidal layer of CA3 containing the cell bodies of CA3 pyramidal neurons. These neurons were chosen because of their early morphological alterations during prion disease. LCM was optimised to produce RNA which could be successfully used to perform qPCR. LCM was then used to determine if it could be used to enrich for genes expressed in the CA3 pyramidal layer and de-enrich for genes expressed outside of this region. In addition, expression of some previously investigated UPR and other stress-related response mRNAs was measured in laser microdissected CA3 and whole hippocampi of naïve and ME7-animals.

Laser microdissected CA3 of NBH- and ME7-animals was used for qPCR and RNA-Seq. RNA for qPCR was used to investigate the expression of UPR, ATF3, GADD45 α and Homer1a mRNAs. There was little evidence for a robust UPR and neither ATF3 nor Homer1a mRNAs were increased in ME7-animals. GADD45 α mRNA levels were increased but this was at a time when the levels of GFAP, CD11b

and C1qB mRNAs were increased and when both astrocytes and microglia could be found within the pyramidal layer of CA3 in ME7-animals.

RNA-Seq did not resolve the most pertinent changes in mRNA expression seen using qPCR. Although RNA-Seq did not resolve these changes, it is likely to be an important technique for high-throughput analysis of changes in gene expression in prion disease and other chronic neurodegenerative diseases. Isolation of specific neurons is needed to understand molecular responses occurring within these cells. Although challenging because of the large glial response, it offers a powerful approach for deciphering molecular responses in vulnerable neurons and identifying pathways which could be targeted pharmacologically.

Chapter 7: Overview and future work

7.1 Overview

Work in a Tg mouse model of ALS (SOD1, G93A) showed that the UPR was activated in the cell bodies of motoneurons early on during the course of disease, prior to synaptic and axonal loss (Saxena et al., 2009). At the same time other stress-related response molecules including ATF3 and GADD45 were also induced in the cell bodies of these vulnerable motoneurons (Saxena et al., 2009).

A study in an RML prion mouse model showed that the UPR was activated. Specifically, activation of PERK and the subsequent phosphorylation of eIF2 α (Moreno et al., 2012). eIF2 α -P leads to global translation repression and an associated decline in synaptic proteins. This resulted in synaptic dysfunction and subsequently neurodegeneration.

Targeting protein synthesis/translation is a promising therapeutic target because protein synthesis has been shown to be important for memory formation and memory loss is a major feature of dementia-associated chronic neurodegenerative diseases such as AD (Halliday and Mallucci, 2015). In RML prion mice a proof-of-principle experiment was performed in which genetic targeting of the eIF2 α -P pathway was performed (Moreno et al., 2012). Genetic inhibition of eIF2 α phosphorylation by injecting lentivirus expressing GADD34 or RNAi knockdown of PrP led to a reduction in eIF2 α -P levels and increased global translation rates. The reduction in eIF2 α -P was neuroprotective in RML-animals, preventing behavioural deficits, synaptic dysfunction and loss. In addition, spongiosis was reduced, neuronal loss was prevented and the survival of RML-animals was increased (Moreno et al., 2012).

These findings were extended by pharmacological targeting of the eIF2 α -P pathway in RML prion animals. The molecule, GSK2606414, is an orally-available, PERK inhibitor. It was developed by GlaxoSmithKline as a cancer therapeutic (Axten et al., 2012). This drug was given to RML-animals which led to global translation rates being restored to 100% (Moreno et al., 2013). Like the genetic manipulations described above, this was shown to be neuroprotective in RML-animals, preventing behavioural and memory deficits and protecting against spongiosis and neuronal loss. However, because

of the effects of the PERK inhibitor on pancreatic function the animals suffered from severe weight loss and mild hyperglycaemia (Moreno et al., 2013).

The use of another small molecule inhibitor, ISRIB, has been shown to partially restore global translation rates (Halliday et al., 2015). This molecule works downstream of eIF2 α -P and its effects do not cause pancreatic toxicity. Administration of ISRIB was neuroprotective in RML-animals preventing spongiosis and neurodegeneration and increasing survival (Halliday et al., 2015). However, the high insolubility of ISRIB means that it cannot be used clinically. The effects of both GSK2606414 and ISRIB are independent of prion replication and accumulation. This shows that the neuroprotective effects conferred by these molecules is independent of the disease-specific misfolded protein and is a more generic targeted approach. Such an approach could therefore be used to treat other chronic neurodegenerative diseases such as AD.

The GSK2606414 compound has also been shown to be neuroprotective in rTg4510 mice expressing high levels of mutant tau (Radford et al., 2015). Treating these mice with this inhibitor, at a time when the UPR was activated and neuronal loss had started to occur, reduced the levels of phosphorylated tau (via a reduction in the levels of active GSK-3 β), PERK-P, eIF2 α -P and ATF4 compared to untreated mice (Radford et al., 2015). This effect was also associated with increased levels of general protein translation, increased neuronal cell number, reduced brain atrophy and the prevention of clinical signs of disease (Radford et al., 2015).

Therefore the inhibition of eIF2 α phosphorylation is neuroprotective in RML prion infected mice and in rTg4510 mice, a mouse model of frontotemporal dementia. However, in RML-infected mice increasing the levels of eIF2 α -P has been shown to exacerbate prion disease. Treatment with the compound, salubrinal, which inhibits the dephosphorylation of eIF2 α -P, further reduced global translation levels and survival of RML-animals (Moreno et al., 2013). However, inhibiting the dephosphorylation of eIF2 α -P using salubrinal has been shown to be neuroprotective in PD and ALS Tg mouse models (Colla et al., 2012a, Saxena et al., 2009). The drug guanabenz, which also inhibits the dephosphorylation of eIF2 α -P has been also been shown to be neuroprotective in Tg338 mice injected with the 127S scrapie strain and in a Tg ALS mouse model (SOD1, G93A) (Jiang et al., 2014, Tribouillard-Tanvier et al., 2008).

More recently, Sephin 1, a drug which also inhibits the dephosphorylation of eIF2 α -P has been shown to be protective in Tg ALS (SOD1, G93A) mice (Das et al., 2015).

In KA-animals, pre-treatment with salubrinal has been shown to be neuroprotective, preventing cell death and increasing survival (Kim et al., 2014, Sokka et al., 2007). If the UPR is an important pathway in neurodegenerative diseases, the above observations suggests that therapeutic approaches will need to be tailored differently for different diseases.

The above studies suggest that the UPR is an important molecular pathway which has an impact on the outcome of disease. In addition, the study in Tg ALS mice (SOD1, G93A) suggests other stress-related response molecules might also be important in chronic neurodegenerative diseases and may also be potential targets for drug agents. In this thesis, classic UPR-associated molecules were investigated. Other stress-related response molecules including immediate early genes (ATF3, c-Jun and c-Fos), activity-induced immediate early genes (Arc and Homer1a) and a cellular physiological and environmental damage stress sensor (GADD45 α) were also investigated to determine if they too might be important determinants of disease pathogenesis. The UPR and other stress-related response molecules were investigated in the hippocampi of mice using a combination of qPCR, quantitative western blotting and immunohistochemistry. These molecules were investigated in three distinct models of neurodegeneration: the ME7 prion disease model; the CSP α -/- model and in a KA model of excitotoxicity. These three models each have different time-courses from the initiation of the insult to when neurodegeneration occurs.

In ME7-animals, CSP α -/- animals and KA-animals there was limited evidence for a robust UPR at the mRNA and protein levels at any of the time-points investigated. Despite this, analysis of other stress-related response molecules in ME7-animals, CSP α -/- animals and KA-animals revealed an induction at the mRNA and protein level. The induction of the stress-related response proteins, ATF3 and c-Jun (shown by immunohistochemistry) in ME7-animals occurred at the same time as morphological changes in CA3 pyramidal neurons becomes apparent (Al-Malki, 2012). The induction of the ATF3, c-Jun and GADD45 α proteins in CSP α -/- animals occurred at a time when neuronal dysfunction was seen but before detectable synaptic loss. This shows that the induction of these stress-related response molecules are relatively early events in these

models. Treating neurodegenerative diseases as early as possible offers the best hope for slowing the progression of these diseases.

A common molecular change seen in the ME7-animals and CSP α -/- animals was the induction of SIL1 mRNA at 17 w.p.i. and P15 and P27, respectively, and this is the first known report of this in these two models. SIL1 is an adenine nucleotide exchange factor for BiP, which exchanges ADP for ATP enabling BiP to become unbound from its substrate. BiP can then bind further substrate and assist in the correct folding of proteins (section 1.7.3.3). In the absence of correct protein folding a UPR is initiated (section 1.7.1). SIL1 is mutated in Marinesco-Sjögren syndrome, an autosomal recessive disorder characterised by cerebral ataxia, mental retardation and skeletal myopathy (Filezac de L'Etang et al., 2015). The mouse model of Marinesco-Sjögren syndrome, the woozy mouse, is associated with increased levels of ER stress (Saxena et al., 2009). In addition, in a Tg mouse model of ALS (SOD1, G93A) the UPR is the earliest identified molecular response induced in disease vulnerable motoneurons (Saxena et al., 2009). In the same ALS mouse model SIL1 has been shown to be highly expressed in motoneurons resistant to ALS pathology and ER stress but decreased in motoneurons which are vulnerable to ER stress and ALS pathology (Filezac de L'Etang et al., 2015). Reducing the levels of SIL1 in this model leads to exacerbated ER stress and ALS pathology, whilst overexpression helps to restore ER homeostasis and is neuroprotective (Filezac de L'Etang et al., 2015). SIL1 expression seems to be mediated by neuronal excitability, as increasing levels of neuronal excitability increases the expression of SIL1 (Filezac de L'Etang et al., 2015). Conversely, decreasing neuronal excitability leads to the decreased expression of SIL1 (Filezac de L'Etang et al., 2015).

In the woozy mouse model and the ALS mouse model (see above) SIL1 seems to act as a failsafe mechanism, regulating ER homeostasis, thereby preventing a UPR and disease pathology. In addition, the induction of SIL1 in ME7-animals and CSP α -/- animals might be protecting against a UPR and this induction help help explain why the UPR is not seen in these two distinct models. Because of the implications of ER stress and the UPR in other chronic neurodegenerative diseases, SIL1 might prove to be a pivotal molecule regulating whether neurons are susceptible to ER stress or not. Future work studying the effects of the enhancement of SIL1 expression in other mouse models of chronic neurodegenerative diseases would be useful and might help to shed light on to a

molecule which could be universally targetted in different chronic neurodegenerative diseases.

Finally, analysis of the UPR and other stress-related response molecules was extended to study these molecules discretely in the CA3 pyramidal layer (containing the cell bodies of CA3 pyramidal neurons) of ME7-animals. In laser microdissected CA3, like whole hippocampal tissue, there was limited evidence for a robust UPR. ATF3 and Homer1a mRNAs were not induced in the laser microdissected CA3 of ME7-animals, although there was an upregulation of GADD45 α mRNA late in disease. ATF3 and Homer1a mRNAs are induced in whole hippocampal tissue from ME7-animals. This suggests that the induction of these mRNAs occurs in other cells.

The remaining RNA from laser microdissected CA3 was used for RNA-Seq. RNA-Seq produced reads for over 20,000 mRNAs. Comparison of the relative expression of GFAP, CD11b and C1qB mRNAs as shown by qPCR and RNA-Seq revealed a lack of correlation. Whereas qPCR analysis showed that these mRNAs were robustly induced in the laser microdissected CA3 of ME7-animals, RNA-Seq did not reveal any differences in the expression of these mRNAs between NBH- and ME7-animals. Because these distinct changes in expression as shown by qPCR, were not resolved using RNA-Seq, no further analysis has been performed on this dataset.

Although there is limited evidence for a robust UPR in the three models investigated in this thesis, the induction of other stress-related response molecules was detected. However, many questions still remain. What pathways are leading to the induction of these stress-related response molecules? Is their induction neuroprotective or detrimental in these models and other models of neurodegeneration? In a Tg mouse model of ALS (SOD1, G93A), Tg overexpression of ATF3 was shown to be neuroprotective (Seijffers et al., 2014). In this model there was an increase in motoneuron survival, a delay in atrophy of the muscle, increase grip strength, delayed disease onset and modestly increased lifespan (Seijffers et al., 2014). Could manipulation of these stress-related response molecules be used for therapeutic intervention in neurodegenerative disease? Could they also/alternatively be used as biomarkers of disease? ATF3 has been previously used as a biomarker of early cell dysfunction and stress in a Tg rat model of ALS (SOD1, G93A) (Malaspina et al., 2010).

7.2 Future work

- 1) A key issue in this work was the failure to replicate previous studies demonstrating a UPR in murine prion disease. Future work is required to investigate:
 - Whether the activation of the UPR is prion strain or prion model dependent (e.g. Tg vs non-Tg animals). To address this, different prion strains could be injected into the dorsal hippocampus of wildtype non-Tg C57BL/6J mice and Tg mice. The UPR could then be investigated across the time-course for each prion strain and mouse background.
 - Whether the UPR is relevant to human neurodegenerative diseases? A detailed analysis of human post-mortem tissue, using an array of UPR molecules, is required to investigate whether the UPR is involved in human chronic neurodegenerative diseases.
- 2) Although there is no evidence for a robust UPR in ME7-animals or CSP α $-/-$ animals, there is clearly an upregulation of other stress-related response molecules in these two models. Future work will be aimed at:
 - Investigating the molecular pathways which lead to the induction of these stress-related response molecules. Neuronal activity and NMDA-Ca²⁺-CREB signalling leads to the induction of the immediate early genes, Arc and Homer1a (section 1.7.4.2). Similarly, other immediate early genes such as ATF3, c-Jun and c-Fos can also be activated by similar signalling cascades (Guzowski, 2002, Hunt et al., 2012). ATF3 can also be induced by other molecular pathways (section 1.7.4.1.1), including via ATF4 which can also induce the expression of GADD45 α . Upregulation of ATF3 and c-Jun protein occurs at the same time in ME7-animals and CSP α $-/-$ animals and these two molecules can heterodimerise with one another. However, the expression of ATF3 protein is restricted to the CA3 pyramidal layer in both models, whilst c-Jun is also upregulated in the CA1 pyramidal layer in both models. This suggests that distinct pathways are activating c-Jun in the CA1. An analysis of upstream molecules will help to decipher which pathways are activated in ME7-animals and CSP α $-/-$ animals.
 - Investigating if the induction of these stress-related response molecules is a pro-survival or pro-death response. To determine this, knockout mice harbouring a deletion of one of the stress-related response molecules could be inoculated

with ME7 brain homogenate. In addition, mice with a double deletion of both CSP α and a stress-related response molecule such as ATF3 could be used. Alternatively, lentivirus overexpressing one or more of the stress-related response molecules could be injected into ME7-animals or CSP α $-/-$ animals. Pathology, behavioural changes and lifespan could be assessed in these animals. Understanding whether a response is pro-survival or pro-death is important if drugs were to be made to target such molecules and pathways.

- Investigating stress-related response molecules in Tg α -synuclein \times CSP α $-/-$ mice. Tg overexpression of α -synuclein prevents neurodegeneration in CSP α $-/-$ mice (Chandra et al., 2005). This neuroprotective effect might be associated with the induction of protective stress response molecular pathways. Identifying and boosting such pathways is needed to try to help slow the progression of neurodegenerative diseases.
- 3) The role of stress response pathways in selected cell types has not been addressed in detail in models of chronic neurodegenerative diseases. The methods used in this thesis (LCM + qPCR/RNA-Seq) are a way forward to understand how different cells respond during evolving chronic neurodegeneration. To address this similar methods need to be adopted in different models of chronic neurodegeneration. Different cell types then need to be analysed for stress response pathways activated during the progression of disease. A knowledge of how cell types respond differently will enable better targeted therapies aimed at ‘vulnerable’ cell populations in chronic neurodegenerative diseases.

List of References

- Abid, K. & Soto, C. 2006. The intriguing prion disorders. *Cell Mol Life Sci*, 63, 2342-51.
- Abisambra, J. F., Jinwal, U. K., Blair, L. J., O'Leary, J. C., 3rd, Li, Q., Brady, S., Wang, L., Guidi, C. E., Zhang, B., Nordhues, B. A., Cockman, M., Suntharalingham, A., Li, P., Jin, Y., Atkins, C. A. & Dickey, C. A. 2013. Tau accumulation activates the unfolded protein response by impairing endoplasmic reticulum-associated degradation. *J Neurosci*, 33, 9498-507.
- Adalbert, R., Nogradi, A., Babetto, E., Janeckova, L., Walker, S. A., Kerschensteiner, M., Misgeld, T. & Coleman, M. P. 2009. Severely dystrophic axons at amyloid plaques remain continuous and connected to viable cell bodies. *Brain*, 132, 402-16.
- Aguzzi, A. & Heikenwalder, M. 2006. Pathogenesis of prion diseases: current status and future outlook. *Nat Rev Microbiol*, 4, 765-775.
- Aguzzi, A. & Polymenidou, M. 2004. Mammalian prion biology: one century of evolving concepts. *Cell*, 116, 313-327.
- Ahlgren, H., Bas-Orth, C., Freitag, H. E., Hellwig, A., Ottersen, O. P. & Bading, H. 2014. The nuclear calcium signaling target, activating transcription factor 3 (ATF3), protects against dendrotoxicity and facilitates the recovery of synaptic transmission after an excitotoxic insult. *J Biol Chem*, 289, 9970-82.
- Al-Malki, H. 2012. Synaptic degeneration: a morphological study in a mouse model of prion disease. *University of Southampton, Biological Sciences, Doctoral Thesis*.
- Alexander, J. J., Anderson, A. J., Barnum, S. R., Stevens, B. & Tenner, A. J. 2008. The complement cascade: Yin-Yang in neuroinflammation--neuro-protection and -degeneration. *J Neurochem*, 107, 1169-87.
- Alper, T., Cramp, W., Haig, D. & Clarke, M. 1967. Does the agent of scrapie replicate without nucleic acid? *Nature*, 214, 764-766.
- Andersen, P., Morris, R., Amaral, D., Bliss, T. & O'Keefe, J. 2006. *The Hippocampus Book*, Oxford University Press, USA.
- Anderson, A. J., Su, J. H. & Cotman, C. W. 1996. DNA damage and apoptosis in Alzheimer's disease: colocalization with c-Jun immunoreactivity, relationship to brain area, and effect of postmortem delay. *J Neurosci*, 16, 1710-9.
- Asuni, A. A., Gray, B., Bailey, J., Skipp, P., Perry, V. H. & O'Connor, V. 2014. Analysis of the hippocampal proteome in ME7 prion disease reveals a predominant astrocytic signature and highlights the brain-restricted production of clusterin in chronic neurodegeneration. *J Biol Chem*, 289, 4532-45.
- Atkin, J. D., Farg, M. A., Turner, B. J., Tomas, D., Lysaght, J. A., Nunan, J., Rembach, A., Nagley, P., Beart, P. M., Cheema, S. S. & Horne, M. K. 2006. Induction of the unfolded protein response in familial amyotrophic lateral sclerosis and association of protein-disulfide isomerase with superoxide dismutase 1. *J Biol Chem*, 281, 30152-65.
- Atkin, J. D., Farg, M. A., Walker, A. K., McLean, C., Tomas, D. & Horne, M. K. 2008. Endoplasmic reticulum stress and induction of the unfolded protein response in human sporadic amyotrophic lateral sclerosis. *Neurobiol Dis*, 30, 400-7.
- Axten, J. M., Medina, J. R., Feng, Y., Shu, A., Romeril, S. P., Grant, S. W., Li, W. H., Heerding, D. A., Minthorn, E., Mencken, T., Atkins, C., Liu, Q., Rabindran, S., Kumar, R., Hong, X., Goetz, A., Stanley, T., Taylor, J. D., Sigethy, S. D., Tomberlin, G. H., Hassell, A. M., Kahler, K. M., Shewchuk, L. M. & Gampe, R. T. 2012. Discovery of 7-methyl-5-(1-([3-(trifluoromethyl)phenyl]acetyl))-2,3-

- dihydro-1H-indol-5-yl)-7H-pyrrolo[2,3-d]pyrimidin-4-amine (GSK2606414), a potent and selective first-in-class inhibitor of protein kinase R (PKR)-like endoplasmic reticulum kinase (PERK). *J Med Chem*, 55, 7193-207.
- Bahn, S., Volk, B. & Wisden, W. 1994. Kainate receptor gene expression in the developing rat brain. *J Neurosci*, 14, 5525-47.
- Baleriola, J., Walker, C. A., Jean, Y. Y., Crary, J. F., Troy, C. M., Nagy, P. L. & Hengst, U. 2014. Axonally synthesized ATF4 transmits a neurodegenerative signal across brain regions. *Cell*, 158, 1159-72.
- Basler, K., Oesch, B., Scott, M., Westaway, D., Walchli, M., Groth, D., McKinley, M., Prusiner, S. & Weissmann, C. 1986. Scrapie and cellular PrP isoforms are encoded by the same chromosomal gene. *Cell*, 46, 417-428.
- Befort, K., Karchewski, L., Lanoue, C. & Woolf, C. J. 2003. Selective up-regulation of the growth arrest DNA damage-inducible gene Gadd45 alpha in sensory and motor neurons after peripheral nerve injury. *Eur J Neurosci*, 18, 911-22.
- Belichenko, P. V., Brown, D., Jeffrey, M. & Fraser, J. R. 2000. Dendritic and synaptic alterations of hippocampal pyramidal neurones in scrapie-infected mice. *Neuropathol Appl Neurobiol*, 26, 143-9.
- Bellucci, A., Navarria, L., Zaltieri, M., Falarti, E., Bodei, S., Sigala, S., Battistin, L., Spillantini, M., Missale, C. & Spano, P. 2011. Induction of the unfolded protein response by alpha-synuclein in experimental models of Parkinson's disease. *J Neurochem*, 116, 588-605.
- Ben-Ari, Y. & Cossart, R. 2000. Kainate, a double agent that generates seizures: two decades of progress. *Trends Neurosci*, 23, 580-7.
- Benkovic, S. A., O'Callaghan, J. P. & Miller, D. B. 2004. Sensitive indicators of injury reveal hippocampal damage in C57BL/6J mice treated with kainic acid in the absence of tonic-clonic seizures. *Brain Res*, 1024, 59-76.
- Betmouni, S., Perry, V. & Gordon, J. 1996. Evidence for an early inflammatory response in the central nervous system of mice with scrapie. *Neuroscience*, 74, 1-5.
- Bezard, E., Yue, Z., Kirik, D. & Spillantini, M. G. 2013. Animal models of Parkinson's disease: limits and relevance to neuroprotection studies. *Mov Disord*, 28, 61-70.
- Blendy, J. A., Schmid, W., Kiessling, M., Schutz, G. & Gass, P. 1995. Effects of kainic acid induced seizures on immediate early gene expression in mice with a targeted mutation of the CREB gene. *Brain Res*, 681, 8-14.
- Bolton, D. C., McKinley, M. P. & Prusiner, S. B. 1982. Identification of a protein that purifies with the scrapie prion. *Science*, 218, 1309-1311.
- Bonnet, F., Périn, J. P., Charbonnier, F., Camuzat, A., Roussel, G., Nussbaum, J. L. & Alliel, P. M. 1996. Structure and cellular distribution of mouse brain testican. *J Biol Chem*, 271, 4373.
- Borchelt, D. R., Taraboulos, A. & Prusiner, S. B. 1992. Evidence for synthesis of scrapie prion proteins in the endocytic pathway. *J Biol Chem*, 267, 16188-99.
- Bouybayoune, I., Mantovani, S., Del Gallo, F., Bertani, I., Restelli, E., Comerio, L., Tapella, L., Baracchi, F., Fernandez-Borges, N., Mangieri, M., Bisighini, C., Beznoussenko, G. V., Paladini, A., Balducci, C., Micotti, E., Forloni, G., Castilla, J., Fiordaliso, F., Tagliavini, F., Imeri, L. & Chiesa, R. 2015. Transgenic fatal familial insomnia mice indicate prion infectivity-independent mechanisms of pathogenesis and phenotypic expression of disease. *PLoS Pathog*, 11, e1004796.
- Bove, J., Martinez-Vicente, M. & Vila, M. 2011. Fighting neurodegeneration with rapamycin: mechanistic insights. *Nat Rev Neurosci*, 12, 437-52.

- Brakeman, P., Lanahan, A., O'Brien, R., Roche, K., Barnes, C., Huganir, R. & Worley, P. 1997. Homer: a protein that selectively binds metabotropic glutamate receptors. *Nature*, 386, 284-8.
- Braun, J. E. & Scheller, R. H. 1995. Cysteine string protein, a DnaJ family member, is present on diverse secretory vesicles. *Neuropharmacology*, 34, 1361-9.
- Braun, J. E. A., Wilbanks, S. M. & Scheller, R. H. 1996. The cysteine string secretory vesicle protein activates Hsc70 ATPase. *J Biol Chem*, 271, 25989-25993.
- Brautigam, H., Steele, J. W., Westaway, D., Fraser, P. E., St George-Hyslop, P. H., Gandy, S., Hof, P. R. & Dickstein, D. L. 2012. The isotropic fractionator provides evidence for differential loss of hippocampal neurons in two mouse models of Alzheimer's disease. *Mol Neurodegener*, 7, 58.
- Broadie, K. S. 1995. Genetic dissection of the molecular mechanisms of transmitter vesicle release during synaptic transmission. *J Physiol Paris*, 89, 59-70.
- Brown, A. R., Rebus, S., McKimmie, C. S., Robertson, K., Williams, A. & Fazakerley, J. K. 2005. Gene expression profiling of the preclinical scrapie-infected hippocampus. *Biochem Biophys Res Commun*, 334, 86-95.
- Brown, D. R. 2001a. Copper and prion disease. *Brain Res Bull*, 55, 165-73.
- Brown, D. R. 2001b. Prion and prejudice: normal protein and the synapse. *Trends Neurosci*, 24, 85-90.
- Brown, P., Preece, M., Brandel, J. P., Sato, T., McShane, L., Zerr, I., Fletcher, A., Will, R. G., Pocchiari, M., Cashman, N. R., d'Aignaux, J. H., Cervenáková, L., Fradkin, J., Schonberger, L. B. & Collins, S. J. 2000. Iatrogenic Creutzfeldt-Jakob disease at the millennium. *Neurology*, 55, 1075-81.
- Bruce, M. E., McConnell, I., Fraser, H. & Dickinson, A. G. 1991. The disease characteristics of different strains of scrapie in Sinc congenic mouse lines: implications for the nature of the agent and host control of pathogenesis. *J Gen Virol*, 72 (Pt 3), 595-603.
- Büeler, H., Aguzzi, A., Sailer, A., Greiner, R. A., Autenried, P., Aguet, M. & Weissmann, C. 1993. Mice devoid of PrP are resistant to scrapie. *Cell*, 73, 1339-1347.
- Büeler, H., Fischer, M., Lang, Y., Bluethmann, H., Lipp, H. P., DeArmond, S. J., Prusiner, S. B., Aguet, M. & Weissmann, C. 1992. Normal development and behaviour of mice lacking the neuronal cell-surface PrP protein. *Nature*, 356, 577-582.
- Campana, V., Sarnataro, D. & Zurzolo, C. 2005. The highways and byways of prion protein trafficking. *Trends Cell Biol*, 15, 102-11.
- Cardoso, A. L., Costa, P., de Almeida, L. P., Simoes, S., Plesnila, N., Culmsee, C., Wagner, E. & de Lima, M. C. 2010. Tf-lipoplex-mediated c-Jun silencing improves neuronal survival following excitotoxic damage in vivo. *J Contr Rel*, 142, 392-403.
- Caughey, B., Race, R. E., Ernst, D., Buchmeier, M. J. & Chesebro, B. 1989. Prion protein biosynthesis in scrapie-infected and uninfected neuroblastoma cells. *J Virol*, 63, 175-181.
- Caughey, B. & Raymond, G. J. 1991. The scrapie-associated form of PrP is made from a cell surface precursor that is both protease- and phospholipase-sensitive. *J Biol Chem*, 266, 18217-23.
- Caughey, B., Raymond, G. J., Ernst, D. & Race, R. E. 1991. N-terminal truncation of the scrapie-associated form of PrP by lysosomal protease(s): implications regarding the site of conversion of PrP to the protease-resistant state. *J Virol*, 65, 6597-603.

- Cavell, B. E. 2012. *In vitro analysis of potential anticancer effects associated with watercress*. Doctoral, University of Southampton.
- Chamberlain, L. H. & Burgoyne, R. D. 1997a. Activation of the ATPase activity of heat-shock proteins Hsc70/Hsp70 by cysteine-string protein. *Biochem J*, 322, 853-8.
- Chamberlain, L. H. & Burgoyne, R. D. 1997b. The molecular chaperone function of the secretory vesicle cysteine string proteins. *J Biol Chem*, 272, 31420-6.
- Chamberlain, L. H. & Burgoyne, R. D. 1998. The cysteine-string domain of the secretory vesicle cysteine-string protein is required for membrane targeting. *Biochem J*, 335 205-9.
- Chamberlain, L. H. & Burgoyne, R. D. 2000. Cysteine-string protein: the chaperone at the synapse. *J Neurochem*, 74, 1781-9.
- Chandler, R. L. 1961. Encephalopathy in mice produced by inoculation with scrapie brain material. *Lancet*, 1, 1378-1379.
- Chandra, S., Gallardo, G., Fernández-Chacón, R., Schlüter, O. M. & Südhof, T. C. 2005. α -Synuclein cooperates with CSP α in preventing neurodegeneration. *Cell*, 123, 383-396.
- Chang, R. C., Wong, A. K., Ng, H. K. & Hugon, J. 2002. Phosphorylation of eukaryotic initiation factor-2 α (eIF2 α) is associated with neuronal degeneration in Alzheimer's disease. *Neuroreport*, 13, 2429-32.
- Chen, Z., Ljunggren, H. G., Bogdanovic, N., Nennesmo, I., Winblad, B. & Zhu, J. 2002. Excitotoxic neurodegeneration induced by intranasal administration of kainic acid in C57BL/6 mice. *Brain Res*, 931, 135-45.
- Chesebro, B., Race, R., Wehrly, K., Nishio, J., Bloom, M., Lechner, D., Bergstrom, S., Robbins, K., Mayer, L. & Keith, J. M. 1985. Identification of scrapie prion protein-specific mRNA in scrapie-infected and uninfected brain. *Nature*, 315, 331-333.
- Chesebro, B., Trifilo, M., Race, R., Meade-White, K., Teng, C., LaCasse, R., Raymond, L., Favara, C., Baron, G., Priola, S., Caughey, B., Masliah, E. & Oldstone, M. 2005. Anchorless prion protein results in infectious amyloid disease without clinical scrapie. *Science*, 308, 1435-9.
- Chiesa, R., Piccardo, P., Dossena, S., Nowoslawski, L., Roth, K. A., Ghetti, B. & Harris, D. A. 2005. Bax deletion prevents neuronal loss but not neurological symptoms in a transgenic model of inherited prion disease. *Proc Natl Acad Sci U S A*, 102, 238-243.
- Chiesa, R., Piccardo, P., Ghetti, B. & Harris, D. A. 1998. Neurological illness in transgenic mice expressing a prion protein with an insertional mutation. *Neuron*, 21, 1339-51.
- Chihara, K., Saito, A., Murakami, T., Hino, S., Aoki, Y., Sekiya, H., Aikawa, Y., Wanaka, A. & Imaizumi, K. 2009. Increased vulnerability of hippocampal pyramidal neurons to the toxicity of kainic acid in OASIS-deficient mice. *J Neurochem*, 110, 956-65.
- Chinenov, Y. & Kerppola, T. K. 2001. Close encounters of many kinds: Fos-Jun interactions that mediate transcription regulatory specificity. *Oncogene*, 20, 2438-52.
- Chiti, Z., Knutsen, O. M., Betmouni, S. & Greene, J. R. 2006. An integrated, temporal study of the behavioural, electrophysiological and neuropathological consequences of murine prion disease. *Neurobiol Dis*, 22, 363-73.

- Choi, H. J., Kang, K. S., Fukui, M. & Zhu, B. T. 2011. Critical role of the JNK-p53-GADD45 α apoptotic cascade in mediating oxidative cytotoxicity in hippocampal neurons. *Br J Pharmacol*, 162, 175-92.
- Chowdhury, S., Shepherd, J. D., Okuno, H., Lyford, G., Petralia, R. S., Plath, N., Kuhl, D., Huganir, R. L. & Worley, P. F. 2006. Arc/Arg3.1 interacts with the endocytic machinery to regulate AMPA receptor trafficking. *Neuron*, 52, 445-59.
- Chung, K. T., Shen, Y. & Hendershot, L. M. 2002. BAP, a mammalian BiP-associated protein, is a nucleotide exchange factor that regulates the ATPase activity of BiP. *J Biol Chem*, 277, 47557-63.
- Cohen, F. E., Pan, K. M., Huang, Z., Baldwin, M., Fletterick, R. J. & Prusiner, S. B. 1994. Structural clues to prion replication. *Science*, 264, 530-531.
- Cole, A. J., Abu-Shakra, S., Saffen, D. W., Baraban, J. M. & Worley, P. F. 1990. Rapid rise in transcription factor mRNAs in rat brain after electroshock-induced seizures. *J Neurochem*, 55, 1920-7.
- Colla, E., Coune, P., Liu, Y., Pletnikova, O., Troncoso, J. C., Iwatsubo, T., Schneider, B. L. & Lee, M. K. 2012a. Endoplasmic reticulum stress is important for the manifestations of alpha-synucleinopathy in vivo. *J Neurosci*, 32, 3306-20.
- Colla, E., Jensen, P. H., Pletnikova, O., Troncoso, J. C., Glabe, C. & Lee, M. K. 2012b. Accumulation of toxic alpha-synuclein oligomer within endoplasmic reticulum occurs in alpha-synucleinopathy in vivo. *J Neurosci*, 32, 3301-5.
- Colling, S. B., Collinge, J. & Jefferys, J. G. 1996. Hippocampal slices from prion protein null mice: disrupted Ca(2+)-activated K⁺ currents. *Neurosci Lett*, 209, 49-52.
- Collinge, J., Whittington, M. A., Sidle, K. C., Smith, C. J., Palmer, M. S., Clarke, A. R. & Jefferys, J. G. 1994. Prion protein is necessary for normal synaptic function. *Nature*, 370, 295-7.
- Combrinck, M., Perry, V. & Cunningham, C. 2002. Peripheral infection evokes exaggerated sickness behaviour in pre-clinical murine prion disease. *Neuroscience*, 112, 7-11.
- Csicsvari, J., Hirase, H., Czurko, A., Mamiya, A. & Buzsaki, G. 1999. Oscillatory coupling of hippocampal pyramidal cells and interneurons in the behaving rat. *J Neurosci*, 19, 274-87.
- Cunningham, C., Champion, S., Lunnon, K., Murray, C. L., Woods, J. F., Deacon, R. M., Rawlins, J. N. & Perry, V. H. 2009. Systemic inflammation induces acute behavioral and cognitive changes and accelerates neurodegenerative disease. *Biol Psychiatry*, 65, 304-12.
- Cunningham, C., Deacon, R., Wells, H., Boche, D., Waters, S., Diniz, C. P., Scott, H., Rawlins, J. & Perry, V. 2003. Synaptic changes characterize early behavioural signs in the ME7 model of murine prion disease. *Eur J Neurosci*, 17, 2147-2155.
- Curran, S., McKay, J. A., McLeod, H. L. & Murray, G. I. 2000. Laser capture microscopy. *Mol Pathol*, 53, 64-8.
- Das, I., Krzyzosiak, A., Schneider, K., Wrabetz, L., D'Antonio, M., Barry, N., Sigurdardottir, A. & Bertolotti, A. 2015. Preventing proteostasis diseases by selective inhibition of a phosphatase regulatory subunit. *Science*, 348, 239-42.
- Davies, M. J., Cooper, M., Perry, V. H. & O'Connor, V. 2015. Reduced expression of the presynaptic co-chaperone cysteine string protein alpha (CSP α) does not exacerbate experimentally-induced ME7 prion disease. *Neurosci Lett*, 589, 138-43.

- Dawson, T. M., Ko, H. S. & Dawson, V. L. 2010. Genetic animal models of Parkinson's disease. *Neuron*, 66, 646-61.
- Deacon, R. M., Croucher, A. & Rawlins, J. N. 2002. Hippocampal cytotoxic lesion effects on species-typical behaviours in mice. *Behav Brain Res*, 132, 203-13.
- Deacon, R. M., Reisel, D., Perry, V. H., Nicholas, J. & Rawlins, P. 2005. Hippocampal scrapie infection impairs operant DRL performance in mice. *Behav Brain Res*, 157, 99-105.
- Devi, L. & Ohno, M. 2014. PERK mediates eIF2alpha phosphorylation responsible for BACE1 elevation, CREB dysfunction and neurodegeneration in a mouse model of Alzheimer's disease. *Neurobiol Aging*, 35, 2272-81.
- Dickey, C. A., Loring, J. F., Montgomery, J., Gordon, M. N., Eastman, P. S. & Morgan, D. 2003. Selectively reduced expression of synaptic plasticity-related genes in amyloid precursor protein + presenilin-1 transgenic mice. *J Neurosci*, 23, 5219-26.
- Dong, X. X., Wang, Y. & Qin, Z. H. 2009. Molecular mechanisms of excitotoxicity and their relevance to pathogenesis of neurodegenerative diseases. *Acta Pharmacol Sin*, 30, 379-87.
- Dossena, S., Imeri, L., Mangieri, M., Garofoli, A., Ferrari, L., Senatore, A., Restelli, E., Balducci, C., Fiordaliso, F., Salio, M., Bianchi, S., Fioriti, L., Morbin, M., Pincherle, A., Marcon, G., Villani, F., Carli, M., Tagliavini, F., Forloni, G. & Chiesa, R. 2008. Mutant prion protein expression causes motor and memory deficits and abnormal sleep patterns in a transgenic mouse model. *Neuron*, 60, 598-609.
- Doyle, K. M., Kennedy, D., Gorman, A. M., Gupta, S., Healy, S. J. & Samali, A. 2011. Unfolded proteins and endoplasmic reticulum stress in neurodegenerative disorders. *J Cell Mol Med*, 15, 2025-39.
- Dudal, S., Krzywkowski, P., Paquette, J., Morissette, C., Lacombe, D., Tremblay, P. & Gervais, F. 2004. Inflammation occurs early during the Abeta deposition process in TgCRND8 mice. *Neurobiol Aging*, 25, 861-71.
- Evans, G. J., Morgan, A. & Burgoyne, R. D. 2003. Tying everything together: the multiple roles of cysteine string protein (CSP) in regulated exocytosis. *Traffic*, 4, 653-9.
- Fernández-Chacón, R., Wölfel, M., Nishimune, H., Tabares, L., Schmitz, F., Castellano-Muñoz, M., Rosenmund, C., Montesinos, M. L., Sanes, J. R., Schneggenburger, R. & Südhof, T. C. 2004. The synaptic vesicle protein CSP alpha prevents presynaptic degeneration. *Neuron*, 42, 237-251.
- Ferrer, I., Blanco, R., Carmona, M., Puig, B., Dominguez, I. & Vinals, F. 2002. Active, phosphorylation-dependent MAP kinases, MAPK/ERK, SAPK/JNK and p38, and specific transcription factor substrates are differentially expressed following systemic administration of kainic acid to the adult rat. *Acta Neuropathol*, 103, 391-407.
- Filezac de L'Etang, A., Maharjan, N., Cordeiro Brana, M., Ruegsegger, C., Rehmann, R., Goswami, A., Roos, A., Troost, D., Schneider, B. L., Weis, J. & Saxena, S. 2015. Marinesco-Sjögren syndrome protein SIL1 regulates motor neuron subtype-selective ER stress in ALS. *Nat Neurosci*, 18, 227-38.
- Fischer, L. R., Culver, D. G., Tennant, P., Davis, A. A., Wang, M., Castellano-Sanchez, A., Khan, J., Polak, M. A. & Glass, J. D. 2004. Amyotrophic lateral sclerosis is a distal axonopathy: evidence in mice and man. *Exp Neurol*, 185, 232-40.
- Fornace, A. J., Jr., Alamo, I., Jr. & Hollander, M. C. 1988. DNA damage-inducible transcripts in mammalian cells. *Proc Natl Acad Sci U S A*, 85, 8800-4.

- Fornace, A. J., Jr., Jackman, J., Hollander, M. C., Hoffman-Liebermann, B. & Liebermann, D. A. 1992. Genotoxic-stress-response genes and growth-arrest genes. gadd, MyD, and other genes induced by treatments eliciting growth arrest. *Ann N Y Acad Sci*, 663, 139-53.
- Francis, J. S., Dragunow, M. & During, M. J. 2004. Over expression of ATF-3 protects rat hippocampal neurons from in vivo injection of kainic acid. *Mol Brain Res*, 124, 199-203.
- Fraser, H. 1993. Diversity in the neuropathology of scrapie-like diseases in animals. *Brit Med Bull*, 49, 792-809.
- Frerking, M., Schulte, J., Wiebe, S. P. & Stäubli, U. 2005. Spike timing in CA3 pyramidal cells during behavior: implications for synaptic transmission. *J Neurophysiol*, 94, 1528-40.
- Frey, D., Schneider, C., Xu, L., Borg, J., Spooren, W. & Caroni, P. 2000. Early and selective loss of neuromuscular synapse subtypes with low sprouting competence in motoneuron diseases. *J Neurosci*, 20, 2534-2542.
- Gajdusek, D. C., Gibbs, C. J. & Alpers, M. 1966. Experimental transmission of a kuru-like syndrome to chimpanzees. *Nature*, 209, 794-796.
- Gajdusek, D. C., Gibbs, C. J. & Alpers, M. 1967. Transmission and passage of experimental 'kuru' to chimpanzees. *Science*, 155, 212-214.
- García-Junco-Clemente, P., Cantero, G., Gómez-Sánchez, L., Linares-Clemente, P., Martínez-López, J. A., Luján, R. & Fernández-Chacón, R. 2010. Cysteine string protein- α prevents activity-dependent degeneration in GABAergic synapses. *J Neurosci*, 30, 7377-7391.
- Gehlenborg, N., Hwang, D., Lee, I. Y., Yoo, H., Baxter, D., Petritis, B., Pitstick, R., Marzolf, B., Dearmond, S. J., Carlson, G. A. & Hood, L. 2009. The Prion Disease Database: a comprehensive transcriptome resource for systems biology research in prion diseases. *Database (Oxford)*, 2009, bap011.
- Gibbs, C. J., Gajdusek, D. C., Asher, D. M., Alpers, M., Beck, E., Daniel, P. M. & Matthews, W. 1968. Creutzfeldt-Jakob disease (spongiform encephalopathy): transmission to the chimpanzee. *Science*, 161, 388-389.
- Gillardon, F., Skutella, T., Uhlmann, E., Holsboer, F., Zimmermann, M. & Behl, C. 1996. Activation of c-Fos contributes to amyloid beta-peptide-induced neurotoxicity. *Brain Res*, 706, 169-72.
- Goedert, M. 2004. Tau protein and neurodegeneration. *Semin Cell Dev Biol*, 15, 45-9.
- Gomez-Nicola, D., Fransen, N. L., Suzzi, S. & Perry, V. H. 2013. Regulation of microglial proliferation during chronic neurodegeneration. *J Neurosci*, 33, 2481-93.
- Goold, R., Rabbanian, S., Sutton, L., Andre, R., Arora, P., Moonga, J., Clarke, A. R., Schiavo, G., Jat, P., Collinge, J. & Tabrizi, S. J. 2011. Rapid cell-surface prion protein conversion revealed using a novel cell system. *Nat Commun*, 2, 281.
- Gordon, M. N., Holcomb, L. A., Jantzen, P. T., DiCarlo, G., Wilcock, D., Boyett, K. W., Connor, K., Melachrinou, J., O'Callaghan, J. P. & Morgan, D. 2002. Time course of the development of Alzheimer-like pathology in the doubly transgenic PS1+APP mouse. *Exp Neurol*, 173, 183-95.
- Götz, J. & Ittner, L. M. 2008. Animal models of Alzheimer's disease and frontotemporal dementia. *Nat Rev Neurosci*, 9, 532-44.
- Götz, J., Probst, A., Spillantini, M. G., Schäfer, T., Jakes, R., Bürki, K. & Goedert, M. 1995. Somatodendritic localization and hyperphosphorylation of tau protein in transgenic mice expressing the longest human brain tau isoform. *EMBO J*, 14, 1304-13.

- Gray, B. C., Sisková, Z., Perry, V. H. & O'Connor, V. 2009. Selective presynaptic degeneration in the synaptopathy associated with ME7-induced hippocampal pathology. *Neurobiol Dis*, 35, 63-74.
- Gray, B. C., Skipp, P., O'Connor, V. M. & Perry, V. H. 2006. Increased expression of glial fibrillary acidic protein fragments and mu-calpain activation within the hippocampus of prion-infected mice. *Biochem Soc Trans*, 34, 51-4.
- Grinevich, V., Kolleker, A., Eliava, M., Takada, N., Takuma, H., Fukazawa, Y., Shigemoto, R., Kuhl, D., Waters, J. & Seeburg, P. H. 2009. Fluorescent Arc/Arg3.1 indicator mice: a versatile tool to study brain activity changes in vitro and in vivo. *Journal Neurosci Meth*, 184, 25-36.
- Gu, Y., Verghese, S., Mishra, R. S., Xu, X., Shi, Y. & Singh, N. 2003. Mutant prion protein-mediated aggregation of normal prion protein in the endoplasmic reticulum: implications for prion propagation and neurotoxicity. *J Neurochem*, 84, 10-22.
- Guenther, K., Deacon, R. M., Perry, V. H. & Rawlins, J. N. 2001. Early behavioural changes in scrapie-affected mice and the influence of dapsone. *Eur J Neurosci*, 14, 401-9.
- Guerriero, C. J. & Brodsky, J. L. 2012. The delicate balance between secreted protein folding and endoplasmic reticulum-associated degradation in human physiology. *Physiol Rev*, 92, 537-76.
- Gundersen, C. B., Kohan, S. A., Souda, P., Whitelegge, J. P. & Umbach, J. A. 2010. Cysteine string protein beta is prominently associated with nerve terminals and secretory organelles in mouse brain. *Brain Res*, 1332, 1-11.
- Gupta, M., Gupta, S. K., Balliet, A. G., Hollander, M. C., Fornace, A. J., Hoffman, B. & Liebermann, D. A. 2005. Hematopoietic cells from Gadd45a- and Gadd45b-deficient mice are sensitized to genotoxic-stress-induced apoptosis. *Oncogene*, 24, 7170-9.
- Guzowski, J. F. 2002. Insights into immediate-early gene function in hippocampal memory consolidation using antisense oligonucleotide and fluorescent imaging approaches. *Hippocampus*, 12, 86-104.
- Guzowski, J. F., Lyford, G. L., Stevenson, G. D., Houston, F. P., McGaugh, J. L., Worley, P. F. & Barnes, C. A. 2000. Inhibition of activity-dependent arc protein expression in the rat hippocampus impairs the maintenance of long-term potentiation and the consolidation of long-term memory. *J Neurosci*, 20, 3993-4001.
- Hagihara, H., Toyama, K., Yamasaki, N. & Miyakawa, T. 2009. Dissection of Hippocampal Dentate Gyrus from Adult Mouse. *J Vis Exp*, 17.
- Hai, T. & Curran, T. 1991. Cross-family dimerization of transcription factors Fos/Jun and ATF/CREB alters DNA binding specificity. *Proc Natl Acad Sci U S A*, 88, 3720-4.
- Hai, T. & Hartman, M. G. 2001. The molecular biology and nomenclature of the activating transcription factor/cAMP responsive element binding family of transcription factors: activating transcription factor proteins and homeostasis. *Gene*, 273, 1-11.
- Hai, T., Wolfgang, C. D., Marsee, D. K., Allen, A. E. & Sivaprasad, U. 1999. ATF3 and stress responses. *Gene Expr*, 7, 321-35.
- Halliday, M. & Mallucci, G. R. 2015. Review: Modulating the unfolded protein response to prevent neurodegeneration and enhance memory. *Neuropathol Appl Neurobiol*, 41, 414-27.

- Halliday, M., Radford, H., Sekine, Y., Moreno, J., Verity, N., le Quesne, J., Otori, C. A., Barrett, D. A., Fromont, C., Fischer, P. M., Harding, H. P., Ron, D. & Mallucci, G. R. 2015. Partial restoration of protein synthesis rates by the small molecule ISRIB prevents neurodegeneration without pancreatic toxicity. *Cell Death Dis*, 6, e1672.
- Harris, D. A. 2003. Trafficking, turnover and membrane topology of PrP. *Br Med Bull*, 66, 71-85.
- Hatazaki, S., Bellver-Estelles, C., Jimenez-Mateos, E., Meller, R., Bonner, C., Murphy, N., Matsushima, S., Taki, W., Prehn, J. & Simon, R. 2007. Microarray profile of seizure damage-refractory hippocampal CA3 in a mouse model of epileptic preconditioning. *Neuroscience*, 150, 467-477.
- Hayashi, T., Saito, A., Okuno, S., Ferrand-Drake, M., Dodd, R. L. & Chan, P. H. 2005. Damage to the endoplasmic reticulum and activation of apoptotic machinery by oxidative stress in ischemic neurons. *J Cereb Blood Flow Metab*, 25, 41-53.
- Heiseke, A., Aguib, Y. & Schatzl, H. M. 2010. Autophagy, prion infection and their mutual interactions. *Curr Iss Mol Biol*, 12, 87-97.
- Heneka, M. T., Sastre, M., Dumitrescu-Ozimek, L., Dewachter, I., Walter, J., Klockgether, T. & Van Leuven, F. 2005. Focal glial activation coincides with increased BACE1 activation and precedes amyloid plaque deposition in APP[V717I] transgenic mice. *J Neuroinflamm*, 2, 22.
- Herdegen, T. & Leah, J. D. 1998. Inducible and constitutive transcription factors in the mammalian nervous system: control of gene expression by Jun, Fos and Krox, and CREB/ATF proteins. *Brain Res Rev*, 28, 370-490.
- Herdegen, T., Skene, P. & Bähr, M. 1997. The c-Jun transcription factor--bipotential mediator of neuronal death, survival and regeneration. *Trends Neurosci*, 20, 227-31.
- Herrera, D. G. & Robertson, H. A. 1996. Activation of c-fos in the brain. *Prog Neurobiol*, 50, 83-107.
- Hesse, G. W. & Shashoua, V. E. 1990. Protein synthesis as a function of depth in slices of rat hippocampus. *Neurosci Lett*, 109, 186-90.
- Hetz, C., Castilla, J. & Soto, C. 2007. Perturbation of endoplasmic reticulum homeostasis facilitates prion replication. *J Biol Chem*, 282, 12725-12733.
- Hetz, C., Lee, A. H., Gonzalez-Romero, D., Thielen, P., Castilla, J., Soto, C. & Glimcher, L. H. 2008. Unfolded protein response transcription factor XBP-1 does not influence prion replication or pathogenesis. *Proc Natl Acad Sci U S A*, 105, 757-62.
- Hetz, C., Russelakis-Carneiro, M., Maundrell, K., Castilla, J. & Soto, C. 2003. Caspase-12 and endoplasmic reticulum stress mediate neurotoxicity of pathological prion protein. *EMBO J*, 22, 5435-45.
- Hetz, C., Russelakis-Carneiro, M., Walchli, S., Carboni, S., Vial-Knecht, E., Maundrell, K., Castilla, J. & Soto, C. 2005. The disulfide isomerase Grp58 is a protective factor against prion neurotoxicity. *J Neurosci*, 25, 2793-802.
- Hetz, C., Thielen, P., Matus, S., Nassif, M., Court, F., Kiffin, R., Martinez, G., Cuervo, A. M., Brown, R. H. & Glimcher, L. H. 2009. XBP-1 deficiency in the nervous system protects against amyotrophic lateral sclerosis by increasing autophagy. *Genes Dev*, 23, 2294-306.
- Hill, A. F., Desbruslais, M., Joiner, S., Sidle, K. C. L., Gowland, I., Collinge, J., Doey, L. J. & Lantos, P. 1997. The same prion strain causes vCJD and BSE. *Nature*, 389, 448-450.

- Hilton, K. J., Cunningham, C., Reynolds, R. A. & Perry, V. H. 2013. Early hippocampal synaptic loss precedes neuronal loss and associates with early behavioural deficits in three distinct strains of prion disease. *PLoS One*, 8, e68062.
- Hinnebusch, A. G. & Lorsch, J. R. 2012. The mechanism of eukaryotic translation initiation: new insights and challenges. *Cold Spring Harb Perspect Biol*, 4.
- Hitomi, J., Katayama, T., Eguchi, Y., Kudo, T., Taniguchi, M., Koyama, Y., Manabe, T., Yamagishi, S., Bando, Y. & Imaizumi, K. 2004. Involvement of caspase-4 in endoplasmic reticulum stress-induced apoptosis and A β -induced cell death. *J Cell Biol*, 165, 347-356.
- Hollien, J. & Weissman, J. S. 2006. Decay of endoplasmic reticulum-localized mRNAs during the unfolded protein response. *Science's STKE*, 313, 104-107.
- Hoozemans, J., Van Haastert, E., Eikelenboom, P., De Vos, R., Rozemuller, J. & Scheper, W. 2007. Activation of the unfolded protein response in Parkinson's disease. *Biochem Biophys Res Commun*, 354, 707-711.
- Hoozemans, J. J., van Haastert, E. S., Nijholt, D. A., Rozemuller, A. J., Eikelenboom, P. & Scheper, W. 2009. The unfolded protein response is activated in pretangle neurons in Alzheimer's disease hippocampus. *Am J Pathol*, 174, 1241-51.
- Hoozemans, J. J., Veerhuis, R., Van Haastert, E. S., Rozemuller, J. M., Baas, F., Eikelenboom, P. & Scheper, W. 2005. The unfolded protein response is activated in Alzheimer's disease. *Acta Neuropathol*, 110, 165-72.
- Hsiao, K., Baker, H. F., Crow, T. J., Poulter, M., Owen, F., Terwilliger, J. D., Westaway, D., Ott, J. & Prusiner, S. B. 1989. Linkage of a prion protein missense variant to Gerstmann-Sträussler syndrome. *Nature*, 338, 342-345.
- Hu, B., Martone, M., Jones, Y. & Liu, C. 2000. Protein aggregation after transient cerebral ischemia. *J Neurosci*, 20, 3191-3199.
- Hu, J. H., Park, J. M., Park, S., Xiao, B., Dehoff, M. H., Kim, S., Hayashi, T., Schwarz, M. K., Haganir, R. L., Seeburg, P. H., Linden, D. J. & Worley, P. F. 2010. Homeostatic scaling requires group I mGluR activation mediated by Homer1a. *Neuron*, 68, 1128-42.
- Hu, R. Q., Koh, S., Torgerson, T. & Cole, A. J. 1998. Neuronal stress and injury in C57/BL mice after systemic kainic acid administration. *Brain Res*, 810, 229-40.
- Hu, Y., Park, K. K., Yang, L., Wei, X., Yang, Q., Cho, K. S., Thielen, P., Lee, A. H., Cartoni, R., Glimcher, L. H., Chen, D. F. & He, Z. 2012. Differential effects of unfolded protein response pathways on axon injury-induced death of retinal ganglion cells. *Neuron*, 73, 445-52.
- Hughes, P. E., Alexi, T., Walton, M., Williams, C. E., Dragunow, M., Clark, R. G. & Gluckman, P. D. 1999. Activity and injury-dependent expression of inducible transcription factors, growth factors and apoptosis-related genes within the central nervous system. *Prog Neurobiol*, 57, 421-50.
- Hunt, D., Raivich, G. & Anderson, P. N. 2012. Activating transcription factor 3 and the nervous system. *Front Mol Neurosci*, 5, 7.
- Hutton, M., Lendon, C. L., Rizzu, P., Baker, M., Froelich, S., Houlden, H., Pickering-Brown, S., Chakraverty, S., Isaacs, A., Grover, A., Hackett, J., Adamson, J., Lincoln, S., Dickson, D., Davies, P., Petersen, R. C., Stevens, M., de Graaff, E., Wauters, E., van Baren, J., Hillebrand, M., Joosse, M., Kwon, J. M., Nowotny, P., Che, L. K., Norton, J., Morris, J. C., Reed, L. A., Trojanowski, J., Basun, H., Lannfelt, L., Neystat, M., Fahn, S., Dark, F., Tannenberg, T., Dodd, P. R., Hayward, N., Kwok, J. B., Schofield, P. R., Andreadis, A., Snowden, J., Craufurd, D., Neary, D., Owen, F., Oostra, B. A., Hardy, J., Goate, A., van Swieten, J., Mann, D., Lynch, T. & Heutink, P. 1998. Association of missense

- and 5'-splice-site mutations in tau with the inherited dementia FTDP-17. *Nature*, 393, 702-5.
- Hwang, D., Lee, I. Y., Yoo, H., Gehlenborg, N., Cho, J. H., Petritis, B., Baxter, D., Pitstick, R., Young, R., Spicer, D., Price, N. D., Hohmann, J. G., Dearmond, S. J., Carlson, G. A. & Hood, L. E. 2009. A systems approach to prion disease. *Mol Syst Biol*, 5, 252.
- Imai, Y., Soda, M. & Takahashi, R. 2000. Parkin suppresses unfolded protein stress-induced cell death through its E3 ubiquitin-protein ligase activity. *Journal Biol Chem*, 275, 35661-35664.
- Ironside, J. W. 2012. Variant Creutzfeldt-Jakob disease: an update. *Folia Neuropathol*, 50, 50-6.
- Ishizuka, N., Weber, J. & Amaral, D. G. 1990. Organization of intrahippocampal projections originating from CA3 pyramidal cells in the rat. *J Comp Neurol*, 295, 580-623.
- Izumi, H., Ishimoto, T., Yamamoto, H., Nishijo, H. & Mori, H. 2011. Bioluminescence imaging of Arc expression enables detection of activity-dependent and plastic changes in the visual cortex of adult mice. *Brain Struct Funct*, 216, 91-104.
- Jaarsma, D., Holstege, J. C., Troost, D., Davis, M., Kennis, J., Haasdijk, E. D. & de Jong, V. J. 1996. Induction of c-Jun immunoreactivity in spinal cord and brainstem neurons in a transgenic mouse model for amyotrophic lateral sclerosis. *Neurosci Lett*, 219, 179-82.
- Jamieson, E., Jeffrey, M., Ironside, J. W. & Fraser, J. R. 2001. Apoptosis and dendritic dysfunction precede prion protein accumulation in 87V scrapie. *Neuroreport*, 12, 2147-53.
- Jang, Y. S., Lee, M. Y., Choi, S. H., Kim, M. Y., Chin, H., Jeong, S. W., Kim, I. K. & Kwon, O. J. 2004. Expression of B/K protein in the hippocampus of kainate-induced rat seizure model. *Brain Res*, 999, 203-11.
- Jeffrey, M., Goodsir, C. M., Race, R. E. & Chesebro, B. 2004. Scrapie-specific neuronal lesions are independent of neuronal PrP expression. *Ann Neurol*, 55, 781-92.
- Jeffrey, M., Halliday, W., Bell, J., Johnston, A., MacLeod, N., Ingham, C., Sayers, A., Brown, D. & Fraser, J. 2000. Synapse loss associated with abnormal PrP precedes neuronal degeneration in the scrapie-infected murine hippocampus. *Neuropathol App Neurobiol*, 26, 41-54.
- Jessberger, S. & Kempermann, G. 2003. Adult-born hippocampal neurons mature into activity-dependent responsiveness. *Eur J Neurosci*, 18, 2707-12.
- Jiang, H. Q., Ren, M., Jiang, H. Z., Wang, J., Zhang, J., Yin, X., Wang, S. Y., Qi, Y., Wang, X. D. & Feng, H. L. 2014. Guanabenz delays the onset of disease symptoms, extends lifespan, improves motor performance and attenuates motor neuron loss in the SOD1 G93A mouse model of amyotrophic lateral sclerosis. *Neuroscience*, 277, 132-8.
- Jiang, H. Y., Jiang, L. & Wek, R. C. 2007. The eukaryotic initiation factor-2 kinase pathway facilitates differential GADD45a expression in response to environmental stress. *J Biol Chem*, 282, 3755-65.
- Jiang, H. Y., Wek, S. A., McGrath, B. C., Lu, D., Hai, T., Harding, H. P., Wang, X., Ron, D., Cavener, D. R. & Wek, R. C. 2004. Activating transcription factor 3 is integral to the eukaryotic initiation factor 2 kinase stress response. *Mol Cell Biol*, 24, 1365-77.
- Jochum, W., Passegue, E. & Wagner, E. F. 2001. AP-1 in mouse development and tumorigenesis. *Oncogene*, 20, 2401-12.

- Johnston, A. R., Fraser, J. R., Jeffrey, M. & MacLeod, N. 1998. Synaptic plasticity in the CA1 area of the hippocampus of scrapie-infected mice. *Neurobiol Dis*, 5, 188-195.
- Joyce, P. I., Fratta, P., Fisher, E. M. & Acevedo-Arozena, A. 2011. SOD1 and TDP-43 animal models of amyotrophic lateral sclerosis: recent advances in understanding disease toward the development of clinical treatments. *Mamm Genome*, 22, 420-48.
- Kanekura, K., Suzuki, H., Aiso, S. & Matsuoka, M. 2009. ER stress and unfolded protein response in amyotrophic lateral sclerosis. *Mol Neurobiol*, 39, 81-89.
- Kang, S. W., Rane, N. S., Kim, S. J., Garrison, J. L., Taunton, J. & Hegde, R. S. 2006. Substrate-specific translocational attenuation during ER stress defines a pre-emptive quality control pathway. *Cell*, 127, 999-1013.
- Kastan, M. B., Zhan, Q., el-Deiry, W. S., Carrier, F., Jacks, T., Walsh, W. V., Plunkett, B. S., Vogelstein, B. & Fornace, A. J., Jr. 1992. A mammalian cell cycle checkpoint pathway utilizing p53 and GADD45 is defective in ataxia-telangiectasia. *Cell*, 71, 587-97.
- Katayama, T., Imaizumi, K., Sato, N., Miyoshi, K., Kudo, T., Hitomi, J., Morihara, T., Yoneda, T., Gomi, F. & Mori, Y. 1999. Presenilin-1 mutations downregulate the signalling pathway of the unfolded-protein response. *Nat Cell Biol*, 1, 479-485.
- Kaufman, R. J. 1999. Stress signaling from the lumen of the endoplasmic reticulum: coordination of gene transcriptional and translational controls. *Genes Dev*, 13, 1211-1233.
- Kerrigan, T. L. & Randall, A. D. 2013. A new player in the "synaptopathy" of Alzheimer's disease - arc/arg 3.1. *Front Neurol*, 4, 9.
- Khosravani, H., Zhang, Y., Tsutsui, S., Hameed, S., Altier, C., Hamid, J., Chen, L., Villemaine, M., Ali, Z., Jirik, F. R. & Zamponi, G. W. 2008. Prion protein attenuates excitotoxicity by inhibiting NMDA receptors. *J Cell Biol*, 181, 551-65.
- Kim, J. S., Heo, R. W., Kim, H., Yi, C. O., Shin, H. J., Han, J. W. & Roh, G. S. 2014. Salubrinal, ER stress inhibitor, attenuates kainic acid-induced hippocampal cell death. *J Neural Transm*, 121, 1233-43.
- Kohan, S. A., Pescatori, M., Brecha, N. C., Mastrogiacomo, A., Umbach, J. A. & Gundersen, C. B. 1995. Cysteine string protein immunoreactivity in the nervous system and adrenal gland of rat. *J Neurosci*, 15, 6230-8.
- Koumenis, C., Naczki, C., Koritzinsky, M., Rastani, S., Diehl, A., Sonenberg, N., Koromilas, A. & Wouters, B. G. 2002. Regulation of protein synthesis by hypoxia via activation of the endoplasmic reticulum kinase PERK and phosphorylation of the translation initiation factor eIF2alpha. *Mol Cell Biol*, 22, 7405-16.
- Kumar, R., Azam, S., Sullivan, J. M., Owen, C., Cavener, D. R., Zhang, P., Ron, D., Harding, H. P., Chen, J. J. & Han, A. 2001. Brain ischemia and reperfusion activates the eukaryotic initiation factor 2 α kinase, PERK. *J Neurochem*, 77, 1418-1421.
- Kyle, B. D., Ahrendt, E., Braun, A. P. & Braun, J. E. 2013. The large conductance, calcium-activated K⁺ (BK) channel is regulated by cysteine string protein. *Sci Rep*, 3, 2447.
- Lacor, P. N., Buniel, M. C., Chang, L., Fernandez, S. J., Gong, Y., Viola, K. L., Lambert, M. P., Velasco, P. T., Bigio, E. H., Finch, C. E., Krafft, G. A. & Klein, W. L. 2004. Synaptic targeting by Alzheimer's-related amyloid beta oligomers. *J Neurosci*, 24, 10191-200.

- Lai, T. W., Zhang, S. & Wang, Y. T. 2014. Excitotoxicity and stroke: identifying novel targets for neuroprotection. *Prog Neurobiol*, 115, 157-88.
- Langevin, C., Andreoletti, O., Le Dur, A., Laude, H. & Beringue, V. 2011. Marked influence of the route of infection on prion strain apparent phenotype in a scrapie transgenic mouse model. *Neurobiol Dis*, 41, 219-25.
- Larner, S. F., Hayes, R. L., McKinsey, D. M., Pike, B. R. & Wang, K. K. W. 2004. Increased expression and processing of caspase-12 after traumatic brain injury in rats. *J Neurochem*, 88, 78-90.
- Lee, M. C., Rho, J. L., Kim, M. K., Woo, Y. J., Kim, J. H., Nam, S. C., Suh, J. J., Chung, W. K., Moon, J. D. & Kim, H. I. 2001. c-JUN expression and apoptotic cell death in kainate-induced temporal lobe epilepsy. *J Kor Med Sci*, 16, 649-56.
- Lee, M. K., Stirling, W., Xu, Y., Xu, X., Qui, D., Mandir, A. S., Dawson, T. M., Copeland, N. G., Jenkins, N. A. & Price, D. L. 2002. Human alpha-synuclein-harboring familial Parkinson's disease-linked Ala-53 --> Thr mutation causes neurodegenerative disease with alpha-synuclein aggregation in transgenic mice. *Proc Natl Acad Sci U S A*, 99, 8968-73.
- Lein, E. S., Callaway, E. M., Albright, T. D. & Gage, F. H. 2005. Redefining the boundaries of the hippocampal CA2 subfield in the mouse using gene expression and 3-dimensional reconstruction. *J Comp Neurol*, 485, 1-10.
- Lein, E. S., Zhao, X. & Gage, F. H. 2004. Defining a molecular atlas of the hippocampus using DNA microarrays and high-throughput in situ hybridization. *J Neurosci*, 24, 3879.
- Li, L., Carter, J., Gao, X., Whitehead, J. & Tourtellotte, W. G. 2005. The neuroplasticity-associated arc gene is a direct transcriptional target of early growth response (Egr) transcription factors. *Mol Cell Biol*, 25, 10286-300.
- Li, X. G., Somogyi, P., Ylinen, A. & Buzsaki, G. 1994. The hippocampal CA3 network: an in vivo intracellular labeling study. *J Comp Neurol*, 339, 181-208.
- Liebermann, D. A. & Hoffman, B. 2008. Gadd45 in stress signaling. *J Mol Signal*, 3, 15.
- Lin, C. R., Yang, C. H., Huang, C. E., Wu, C. H., Chen, Y. S., Sheen-Chen, S. M., Huang, H. W. & Chen, K. H. 2011. GADD45A protects against cell death in dorsal root ganglion neurons following peripheral nerve injury. *J Neurosci Res*, 89, 689-99.
- Lin, M. K. & Farrer, M. J. 2014. Genetics and genomics of Parkinson's disease. *Genome Med*, 6, 48.
- Linden, R., Martins, V. R., Prado, M. A., Cammarota, M., Izquierdo, I. & Brentani, R. 2008. Physiology of the prion protein. *Physiol Rev*, 88, 673-728.
- Lindholm, D., Wootz, H. & Korhonen, L. 2006. ER stress and neurodegenerative diseases. *Cell Death Differ*, 13, 385-392.
- Lindwall, C. & Kanje, M. 2005. Retrograde axonal transport of JNK signaling molecules influence injury induced nuclear changes in p-c-Jun and ATF3 in adult rat sensory neurons. *Mol Cell Neurosci*, 29, 269-82.
- Link, W., Konietzko, U., Kauselmann, G., Krug, M., Schwanke, B., Frey, U. & Kuhl, D. 1995. Somatodendritic expression of an immediate early gene is regulated by synaptic activity. *Proc Natl Acad Sci U S A*, 92, 5734-8.
- Liscic, R. M. & Breljak, D. 2011. Molecular basis of amyotrophic lateral sclerosis. *Prog Neuropsychopharmacol Biol Psychiat*, 35, 370-2.
- Liu, Y., Laszlo, C., Liu, Y., Liu, W., Chen, X., Evans, S. C. & Wu, S. 2010. Regulation of G(1) arrest and apoptosis in hypoxia by PERK and GCN2-mediated eIF2alpha phosphorylation. *Neoplasia*, 12, 61-8.

- Lu, P. D., Harding, H. P. & Ron, D. 2004. Translation reinitiation at alternative open reading frames regulates gene expression in an integrated stress response. *J Cell Biol*, 167, 27-33.
- Luk, K. C., Kehm, V., Carroll, J., Zhang, B., O'Brien, P., Trojanowski, J. Q. & Lee, V. M. 2012a. Pathological alpha-synuclein transmission initiates Parkinson-like neurodegeneration in nontransgenic mice. *Science*, 338, 949-53.
- Luk, K. C., Kehm, V. M., Zhang, B., O'Brien, P., Trojanowski, J. Q. & Lee, V. M. 2012b. Intracerebral inoculation of pathological alpha-synuclein initiates a rapidly progressive neurodegenerative alpha-synucleinopathy in mice. *J Exp Med*, 209, 975-86.
- Lyford, G. L., Yamagata, K., Kaufmann, W. E., Barnes, C. A., Sanders, L. K., Copeland, N. G., Gilbert, D. J., Jenkins, N. A., Lanahan, A. A. & Worley, P. F. 1995. Arc, a growth factor and activity-regulated gene, encodes a novel cytoskeleton-associated protein that is enriched in neuronal dendrites. *Neuron*, 14, 433-445.
- Ma, T., Trinh, M. A., Wexler, A. J., Bourbon, C., Gatti, E., Pierre, P., Cavener, D. R. & Klann, E. 2013. Suppression of eIF2alpha kinases alleviates Alzheimer's disease-related plasticity and memory deficits. *Nat Neurosci*, 16, 1299-305.
- Majer, A., Medina, S. J., Niu, Y., Abrenica, B., Manguiat, K. J., Frost, K. L., Philipson, C. S., Sorensen, D. L. & Booth, S. A. 2012. Early mechanisms of pathobiology are revealed by transcriptional temporal dynamics in hippocampal CA1 neurons of prion infected mice. *PLoS Pathog*, 8, e1003002.
- Malaspina, A., Ngoh, S., Ward, R., Hall, J., Tai, F., Yip, P., Jones, C., Jokic, N., Averill, S. & Michael-Titus, A. 2010. Activation transcription factor-3 activation and the development of spinal cord degeneration in a rat model of amyotrophic lateral sclerosis. *Neuroscience*, 169, 812-827.
- Malfa, K. 2012. The role of complement in synaptic degeneration. *Univeristy of Southampton, Biological Sciences, Masters Thesis*.
- Mallucci, G., Dickinson, A., Linehan, J., Klöhn, P. C., Brandner, S. & Collinge, J. 2003. Depleting neuronal PrP in prion infection prevents disease and reverses spongiosis. *Science*, 302, 871-874.
- Mallucci, G. R. 2009. Prion neurodegeneration: starts and stops at the synapse. *Prion*, 3, 195-201.
- Mallucci, G. R., Ratte, S., Asante, E. A., Linehan, J., Gowland, I., Jefferys, J. G. & Collinge, J. 2002. Post-natal knockout of prion protein alters hippocampal CA1 properties, but does not result in neurodegeneration. *EMBO J*, 21, 202-10.
- Manson, J. C., Clarke, A. R., Hooper, M. L., Aitchison, L., McConnell, I. & Hope, J. 1994. 129/Ola mice carrying a null mutation in PrP that abolishes mRNA production are developmentally normal. *Mol Neurobiol*, 8, 121-7.
- Manson, J. C., Hope, J., Clarke, A. R., Johnston, A., Black, C. & MacLeod, N. 1995. PrP gene dosage and long term potentiation. *Neurodegeneration*, 4, 113-4.
- Marciniak, S. J., Yun, C. Y., Oyadomari, S., Novoa, I., Zhang, Y., Jungreis, R., Nagata, K., Harding, H. P. & Ron, D. 2004. CHOP induces death by promoting protein synthesis and oxidation in the stressed endoplasmic reticulum. *Genes Dev*, 18, 3066-3077.
- Marcus, D. L., Strafaci, J. A., Miller, D. C., Masia, S., Thomas, C. G., Rosman, J., Hussain, S. & Freedman, M. L. 1998. Quantitative neuronal c-fos and c-jun expression in Alzheimer's disease. *Neurobiol Aging*, 19, 393-400.
- Marijanovic, Z., Caputo, A., Campana, V. & Zurzolo, C. 2009. Identification of an intracellular site of prion conversion. *PLoS Pathog*, 5, e1000426.

- Martin, L. J., Pan, Y., Price, A. C., Sterling, W., Copeland, N. G., Jenkins, N. A., Price, D. L. & Lee, M. K. 2006. Parkinson's disease alpha-synuclein transgenic mice develop neuronal mitochondrial degeneration and cell death. *J Neurosci*, 26, 41-50.
- Mastrogriacomo, A. & Gundersen, C. B. 1995. The nucleotide and deduced amino acid sequence of a rat cysteine string protein. *Mol Brain Res*, 28, 12-8.
- Mastrogriacomo, A., Parsons, S. M., Zampighi, G. A., Jenden, D. J., Umbach, J. A. & Gundersen, C. B. 1994. Cysteine string proteins: a potential link between synaptic vesicles and presynaptic Ca²⁺ channels. *Science*, 263, 981-2.
- Matus, S., Glimcher, L. H. & Hetz, C. 2011. Protein folding stress in neurodegenerative diseases: a glimpse into the ER. *Curr Opin Cell Biol*, 23, 239-252.
- Matus, S., Lisbona, F., Torres, M., Leon, C., Thielen, P. & Hetz, C. 2008. The stress rheostat: an interplay between the unfolded protein response (UPR) and autophagy in neurodegeneration. *Curr Mol Med*, 8, 157-172.
- McKhann, G. M., 2nd, Wenzel, H. J., Robbins, C. A., Sosunov, A. A. & Schwartzkroin, P. A. 2003. Mouse strain differences in kainic acid sensitivity, seizure behavior, mortality, and hippocampal pathology. *Neuroscience*, 122, 551-61.
- McKinley, M. P., Bolton, D. C. & Prusiner, S. B. 1983. A protease-resistant protein is a structural component of the scrapie prion. *Cell*, 35, 57-62.
- McLin, J. P. & Steward, O. 2006. Comparison of seizure phenotype and neurodegeneration induced by systemic kainic acid in inbred, outbred, and hybrid mouse strains. *Eur J Neurosci*, 24, 2191-202.
- Meng, Q. & Xia, Y. 2011. c-Jun, at the crossroad of the signaling network. *Protein Cell*, 2, 889-98.
- Meusser, B., Hirsch, C., Jarosch, E. & Sommer, T. 2005. ERAD: the long road to destruction. *Nat Cell Biol*, 7, 766-72.
- Meyer, R. K., McKinley, M. P., Bowman, K. A., Braunfeld, M. B., Barry, R. A. & Prusiner, S. B. 1986. Separation and properties of cellular and scrapie prion proteins. *Proc Natl Acad Sci U S A*, 83, 2310-2314.
- Miller, M. 2009. The importance of being flexible: the case of basic region leucine zipper transcriptional regulators. *Curr Protein Pept Sci*, 10, 244-69.
- Mirabile, I., Jat, P. S., Brandner, S. & Collinge, J. 2015. Identification of clinical target areas in the brainstem of prion-infected mice. *Neuropathol Appl Neurobiol*, 41, 613-30.
- Moore, D. L. & Goldberg, J. L. 2011. Multiple transcription factor families regulate axon growth and regeneration. *Dev Neurobiol*, 71, 1186-211.
- Moreno, J. A., Halliday, M., Molloy, C., Radford, H., Verity, N., Axten, J. M., Ortori, C. A., Willis, A. E., Fischer, P. M., Barrett, D. A. & Mallucci, G. R. 2013. Oral treatment targeting the unfolded protein response prevents neurodegeneration and clinical disease in prion-infected mice. *Sci Transl Med*, 5, 206ra138.
- Moreno, J. A., Radford, H., Peretti, D., Steinert, J. R., Verity, N., Martin, M. G., Halliday, M., Morgan, J., Dinsdale, D., Ortori, C. A., Barrett, D. A., Tsaytler, P., Bertolotti, A., Willis, A. E., Bushell, M. & Mallucci, G. R. 2012. Sustained translational repression by eIF2alpha-P mediates prion neurodegeneration. *Nature*, 485, 507-11.
- Mortazavi, A., Williams, B. A., McCue, K., Schaeffer, L. & Wold, B. 2008. Mapping and quantifying mammalian transcriptomes by RNA-Seq. *Nat Meth*, 5, 621-8.
- Moser, M., Colello, R. J., Pott, U. & Oesch, B. 1995. Developmental expression of the prion protein gene in glial cells. *Neuron*, 14, 509-517.

- Moskalev, A. A., Smit-McBride, Z., Shaposhnikov, M. V., Plyusnina, E. N., Zhavoronkov, A., Budovsky, A., Tacutu, R. & Fraifeld, V. E. 2012. Gadd45 proteins: relevance to aging, longevity and age-related pathologies. *Ageing Res Rev*, 11, 51-66.
- Nadler, J. V., Perry, B. W. & Cotman, C. W. 1978. Intraventricular kainic acid preferentially destroys hippocampal pyramidal cells. *Nature*, 271, 676-7.
- Nakagawa, T., Zhu, H., Morishima, N., Li, E., Xu, J., Yankner, B. A. & Yuan, J. 2000. Caspase-12 mediates endoplasmic-reticulum-specific apoptosis and cytotoxicity by amyloid- β . *Nature*, 403, 98-103.
- Nijholt, D. A., van Haastert, E. S., Rozemuller, A. J., Scheper, W. & Hoozemans, J. J. 2012. The unfolded protein response is associated with early tau pathology in the hippocampus of tauopathies. *J Pathol*, 226, 693-702.
- Noskova, L., Stranecky, V., Hartmannova, H., Pristoupilova, A., Baresova, V., Ivanek, R., Hulkova, H., Jahnova, H., van der Zee, J., Staropoli, J. F., Sims, K. B., Tyynela, J., Van Broeckhoven, C., Nijssen, P. C., Mole, S. E., Elleder, M. & Kmoch, S. 2011. Mutations in DNAJC5, encoding cysteine-string protein alpha, cause autosomal-dominant adult-onset neuronal ceroid lipofuscinosis. *Am J Hum Genet*, 89, 241-52.
- Novoa, I., Zeng, H., Harding, H. P. & Ron, D. 2001. Feedback inhibition of the unfolded protein response by GADD34-mediated dephosphorylation of eIF2alpha. *J Cell Biol*, 153, 1011-22.
- Nunziante, M., Ackermann, K., Dietrich, K., Wolf, H., Gädtke, L., Gilch, S., Vorberg, I., Groschup, M. & Schätzl, H. M. 2011. Proteasomal Dysfunction and Endoplasmic Reticulum Stress Enhance Trafficking of Prion Protein Aggregates through the Secretory Pathway and Increase Accumulation of Pathologic Prion Protein. *J Biol Chem*, 286, 33942-33953.
- O'Connor, T., Sadleir, K. R., Maus, E., Velliquette, R. A., Zhao, J., Cole, S. L., Eimer, W. A., Hitt, B., Bembinster, L. A., Lammich, S., Lichtenthaler, S. F., Hebert, S. S., De Strooper, B., Haass, C., Bennett, D. A. & Vassar, R. 2008. Phosphorylation of the translation initiation factor eIF2alpha increases BACE1 levels and promotes amyloidogenesis. *Neuron*, 60, 988-1009.
- Oakley, H., Cole, S. L., Logan, S., Maus, E., Shao, P., Craft, J., Guillozet-Bongaarts, A., Ohno, M., Disterhoft, J., Van Eldik, L., Berry, R. & Vassar, R. 2006. Intraneuronal beta-amyloid aggregates, neurodegeneration, and neuron loss in transgenic mice with five familial Alzheimer's disease mutations: potential factors in amyloid plaque formation. *J Neurosci*, 26, 10129-40.
- Oesch, B., Westaway, D., Walchli, M., McKinley, M. P., Kent, S. B. H., Aebersold, R., Barry, R. A., Tempst, P. & Teplow, D. B. 1985. A cellular gene encodes scrapie PrP 27-30 protein. *Cell*, 40, 735-746.
- Oyadomari, S. & Mori, M. 2003. Roles of CHOP/GADD153 in endoplasmic reticulum stress. *Cell Death Differ*, 11, 381-389.
- Pan, K. M., Baldwin, M., Nguyen, J., Gasset, M., Serban, A., Groth, D., Mehlhorn, I., Huang, Z., Fletterick, R. J. & Cohen, F. E. 1993. Conversion of alpha-helices into beta-sheets features in the formation of the scrapie prion proteins. *Proc Natl Acad Sci U S A*, 90, 10962-10966.
- Park, B. G., Lee, J. S., Lee, J. Y., Song, D. Y., Jeong, S. W. & Cho, B. P. 2011. Co-localization of activating transcription factor 3 and phosphorylated c-Jun in axotomized facial motoneurons. *Anat Cell Biol*, 44, 226-37.

- Paschen, W., Aufenberg, C., Hotop, S. & Mengesdorf, T. 2003. Transient cerebral ischemia activates processing of xbp1 messenger RNA indicative of endoplasmic reticulum stress. *J Cereb Blood Flow Metab*, 23, 449-461.
- Paschen, W. & Frandsen, A. 2001. Endoplasmic reticulum dysfunction—a common denominator for cell injury in acute and degenerative diseases of the brain? *J Neurochem*, 79, 719-725.
- Paschen, W. & Mengesdorf, T. 2005. Endoplasmic reticulum stress response and neurodegeneration. *Cell Calcium*, 38, 409-415.
- Pearson, A. G., Byrne, U. T., MacGibbon, G. A., Faull, R. L. & Dragunow, M. 2006. Activated c-Jun is present in neurofibrillary tangles in Alzheimer's disease brains. *Neurosci Lett*, 398, 246-50.
- Perez-Cruz, C., Nolte, M. W., van Gaalen, M. M., Rustay, N. R., Termont, A., Tanghe, A., Kirchhoff, F. & Ebert, U. 2011. Reduced spine density in specific regions of CA1 pyramidal neurons in two transgenic mouse models of Alzheimer's disease. *J Neurosci*, 31, 3926-34.
- Perez, S. E., Dar, S., Ikonomic, M. D., DeKosky, S. T. & Mufson, E. J. 2007. Cholinergic forebrain degeneration in the APPswe/PS1DeltaE9 transgenic mouse. *Neurobiol Dis*, 28, 3-15.
- Perez, S. E., Lumayag, S., Kovacs, B., Mufson, E. J. & Xu, S. 2009. Beta-amyloid deposition and functional impairment in the retina of the APPswe/PS1DeltaE9 transgenic mouse model of Alzheimer's disease. *Invest Ophthalmol Vis Sci*, 50, 793-800.
- Perry, V. H. & O'Connor, V. 2010. The role of microglia in synaptic stripping and synaptic degeneration: a revised perspective. *ASN neuro*, 2, 281-291.
- Pievani, M., Filippini, N., van den Heuvel, M. P., Cappa, S. F. & Frisoni, G. B. 2014. Brain connectivity in neurodegenerative diseases—from phenotype to proteinopathy. *Nat Rev Neurol*, 10, 620-33.
- Plath, N., Ohana, O., Dammermann, B., Errington, M. L., Schmitz, D., Gross, C., Mao, X., Engelsberg, A., Mahlke, C., Welzl, H., Kobalz, U., Stawrakakis, A., Fernandez, E., Waltereit, R., Bick-Sander, A., Therstappen, E., Cooke, S. F., Blanquet, V., Wurst, W., Salmen, B., Bosl, M. R., Lipp, H. P., Grant, S. G., Bliss, T. V., Wolfer, D. P. & Kuhl, D. 2006. Arc/Arg3.1 is essential for the consolidation of synaptic plasticity and memories. *Neuron*, 52, 437-44.
- Polymenidou, M. & Cleveland, D. W. 2012. Prion-like spread of protein aggregates in neurodegeneration. *J Exp Med*, 209, 889-93.
- Poorkaj, P., Bird, T. D., Wijsman, E., Nemens, E., Garruto, R. M., Anderson, L., Andreadis, A., Wiederholt, W. C., Raskind, M. & Schellenberg, G. D. 1998. Tau is a candidate gene for chromosome 17 frontotemporal dementia. *Ann Neurol*, 43, 815-25.
- Prusiner, S. B. 1982. Novel proteinaceous infectious particles cause scrapie. *Science*, 216, 136-144.
- Prusiner, S. B. 1991. Molecular biology of prion diseases. *Science*, 252, 1515-1522.
- Prusiner, S. B. 1996. Molecular biology and pathogenesis of prion diseases. *Trends Biochem Sci*, 21, 482-487.
- Prusiner, S. B. 1998. Prions. *Proc Natl Acad Sci U S A*, 95, 13363-13383.
- Quaglio, E., Restelli, E., Garofoli, A., Dossena, S., De Luigi, A., Tagliavacca, L., Imperiale, D., Migheli, A., Salmona, M., Sitia, R., Forloni, G. & Chiesa, R. 2011. Expression of mutant or cytosolic PrP in transgenic mice and cells is not associated with endoplasmic reticulum stress or proteasome dysfunction. *PLoS One*, 6, e19339.

- Radford, H., Moreno, J. A., Verity, N., Halliday, M. & Mallucci, G. R. 2015. PERK inhibition prevents tau-mediated neurodegeneration in a mouse model of frontotemporal dementia. *Acta Neuropathol*, 130, 633-42.
- Radford, H. E. & Mallucci, G. R. 2010. The role of GPI-anchored PrP C in mediating the neurotoxic effect of scrapie prions in neurons. *Curr Iss Mol Biol*, 12, 119-27.
- Raivich, G. & Behrens, A. 2006. Role of the AP-1 transcription factor c-Jun in developing, adult and injured brain. *Prog Neurobiol*, 78, 347-63.
- Ramsden, M., Kotilinek, L., Forster, C., Paulson, J., McGowan, E., SantaCruz, K., Guimaraes, A., Yue, M., Lewis, J., Carlson, G., Hutton, M. & Ashe, K. H. 2005. Age-dependent neurofibrillary tangle formation, neuron loss, and memory impairment in a mouse model of human tauopathy (P301L). *J Neurosci*, 25, 10637-47.
- Ridley, R. M. & Baker, H. F. 1998. *Fatal protein: The story of CJD, BSE, and other prion diseases*, Oxford University Press Oxford.
- Rocher, A. B., Crimins, J. L., Amatrudo, J. M., Kinson, M. S., Todd-Brown, M. A., Lewis, J. & Luebke, J. I. 2010. Structural and functional changes in tau mutant mice neurons are not linked to the presence of NFTs. *Exp Neurol*, 223, 385-93.
- Ron, D. & Walter, P. 2007. Signal integration in the endoplasmic reticulum unfolded protein response. *Nat Rev Mol Cell Biol*, 8, 519-29.
- Rosemary Sifakas, A. & Richardson, D. R. 2009. Growth arrest and DNA damage-45 alpha (GADD45alpha). *Int J Biochem Cell Biol*, 41, 986-9.
- Rosi, S., Ramirez-Amaya, V., Vazdarjanova, A., Worley, P. F., Barnes, C. A. & Wenk, G. L. 2005. Neuroinflammation alters the hippocampal pattern of behaviorally induced Arc expression. *J Neurosci*, 25, 723-731.
- Rozas, J. L., Gomez-Sanchez, L., Mircheski, J., Linares-Clemente, P., Nieto-Gonzalez, J. L., Vazquez, M. E., Lujan, R. & Fernández-Chacón, R. 2012. Motoneurons require cysteine string protein-alpha to maintain the readily releasable vesicular pool and synaptic vesicle recycling. *Neuron*, 74, 151-65.
- Rutkowski, D. T. & Kaufman, R. J. 2007. That which does not kill me makes me stronger: adapting to chronic ER stress. *Trends Biochem Sci*, 32, 469-476.
- Sadowski, M., Pankiewicz, J., Scholtzova, H., Ji, Y., Quartermain, D., Jensen, C. H., Duff, K., Nixon, R. A., Gruen, R. J. & Wisniewski, T. 2004. Amyloid-beta deposition is associated with decreased hippocampal glucose metabolism and spatial memory impairment in APP/PS1 mice. *J Neuropathol Exp Neurol*, 63, 418-28.
- Safar, J., Wille, H., Itri, V., Groth, D., Serban, H., Torchia, M., Cohen, F. E. & Prusiner, S. B. 1998. Eight prion strains have PrP(Sc) molecules with different conformations. *Nat Med*, 4, 1157-65.
- Santiard-Baron, D., Gosset, P., Nicole, A., Sinet, P. M., Christen, Y. & Ceballos-Picot, I. 1999. Identification of beta-amyloid-responsive genes by RNA differential display: early induction of a DNA damage-inducible gene, gadd45. *Exp Neurol*, 158, 206-13.
- Sato, N., Urano, F., Yoon Leem, J., Kim, S. H., Li, M., Donoviel, D., Bernstein, A., Lee, A. S., Ron, D., Veselits, M. L., Sisodia, S. S. & Thinakaran, G. 2000. Upregulation of BiP and CHOP by the unfolded-protein response is independent of presenilin expression. *Nat Cell Biol*, 2, 863-70.
- Saxena, S., Cabuy, E. & Caroni, P. 2009. A role for motoneuron subtype-selective ER stress in disease manifestations of FALS mice. *Nat Neurosci*, 12, 627-636.
- Saxena, S. & Caroni, P. 2011. Selective neuronal vulnerability in neurodegenerative diseases: from stressor thresholds to degeneration. *Neuron*, 71, 35-48.

- Schauwecker, P. E. 2000. Seizure-induced neuronal death is associated with induction of c-Jun N-terminal kinase and is dependent on genetic background. *Brain Res*, 884, 116-28.
- Schauwecker, P. E., Ramirez, J. J. & Steward, O. 2000. Genetic dissection of the signals that induce synaptic reorganization. *Exp Neurol*, 161, 139-52.
- Schauwecker, P. E. & Steward, O. 1997. Genetic determinants of susceptibility to excitotoxic cell death: implications for gene targeting approaches. *Proc Natl Acad Sci U S A*, 94, 4103-8.
- Schmitz, F., Tabares, L., Khimich, D., Strenzke, N., de La Villa-Polo, P., Castellano-Muñoz, M., Bulankina, A., Moser, T., Fernández-Chacón, R. & Südhof, T. C. 2006. CSP α -deficiency causes massive and rapid photoreceptor degeneration. *Proc Natl Acad Sci U S A*, 103, 2926-2931.
- Schröder, M. & Kaufman, R. J. 2005. ER stress and the unfolded protein response. *Mutat Res*, 569, 29-63.
- Sclip, A., Antoniou, X., Colombo, A., Camici, G. G., Pozzi, L., Cardinetti, D., Feligioni, M., Veglianesi, P., Bahlmann, F. H., Cervo, L., Balducci, C., Costa, C., Tozzi, A., Calabresi, P., Forloni, G. & Borsello, T. 2011. c-Jun N-terminal kinase regulates soluble A β oligomers and cognitive impairment in AD mouse model. *J Biol Chem*, 286, 43871-80.
- Seijffers, R., Zhang, J., Matthews, J. C., Chen, A., Tamrazian, E., Babaniyi, O., Selig, M., Hynynen, M., Woolf, C. J. & Brown, R. H., Jr. 2014. ATF3 expression improves motor function in the ALS mouse model by promoting motor neuron survival and retaining muscle innervation. *Proc Natl Acad Sci U S A*, 111, 1622-7.
- Senatore, A., Restelli, E. & Chiesa, R. 2013. Synaptic dysfunction in prion diseases: a trafficking problem? *Int J Cell Biol*, 2013, 543803.
- Sharma, M., Burre, J., Bronk, P., Zhang, Y., Xu, W. & Südhof, T. C. 2012a. CSP α knockout causes neurodegeneration by impairing SNAP-25 function. *EMBO J*, 31, 829-41.
- Sharma, M., Burre, J. & Südhof, T. C. 2011. CSP α promotes SNARE-complex assembly by chaperoning SNAP-25 during synaptic activity. *Nat Cell Biol*, 13, 30-9.
- Sharma, M., Burre, J. & Südhof, T. C. 2012b. Proteasome inhibition alleviates SNARE-dependent neurodegeneration. *Sci Transl Med*, 4, 147ra113.
- Sheikh, M. S., Hollander, M. C. & Fornace, A. J., Jr. 2000. Role of Gadd45 in apoptosis. *Biochem Pharmacol*, 59, 43-5.
- Shepherd, J. D., Rumbaugh, G., Wu, J., Chowdhury, S., Plath, N., Kuhl, D., Huganir, R. L. & Worley, P. F. 2006. Arc/Arg3.1 mediates homeostatic synaptic scaling of AMPA receptors. *Neuron*, 52, 475-84.
- Sidrauski, C., Acosta-Alvear, D., Khoutorsky, A., Vedantham, P., Hearn, B. R., Li, H., Gamache, K., Gallagher, C. M., Ang, K. K., Wilson, C., Okreglak, V., Ashkenazi, A., Hann, B., Nader, K., Arkin, M. R., Renslo, A. R., Sonenberg, N. & Walter, P. 2013. Pharmacological brake-release of mRNA translation enhances cognitive memory. *Elife*, 2, e00498.
- Silveira, J. R., Raymond, G. J., Hughson, A. G., Race, R. E., Sim, V. L., Hayes, S. F. & Caughey, B. 2005. The most infectious prion protein particles. *Nature*, 437, 257-261.
- Singleton, R. H., Zhu, J., Stone, J. R. & Povlishock, J. T. 2002. Traumatically induced axotomy adjacent to the soma does not result in acute neuronal death. *J Neurosci*, 22, 791-802.

- Sisková, Z., Page, A., O'Connor, V. & Perry, V. H. 2009. Degenerating synaptic boutons in prion disease: microglia activation without synaptic stripping. *Am J Pathol*, 175, 1610-21.
- Sisková, Z., Reynolds, R. A., O'Connor, V. & Perry, V. H. 2013. Brain region specific pre-synaptic and post-synaptic degeneration are early components of neuropathology in prion disease. *PLoS One*, 8, e55004.
- Sisková, Z., Sanyal, N. K., Orban, A., O'Connor, V. & Perry, V. H. 2010. Reactive hypertrophy of synaptic varicosities within the hippocampus of prion-infected mice. *Biochem Soc Trans*, 38, 471-475.
- Siso, S., Puig, B., Varea, R., Vidal, E., Acin, C., Prinz, M., Montrasio, F., Badiola, J., Aguzzi, A., Pumarola, M. & Ferrer, I. 2002. Abnormal synaptic protein expression and cell death in murine scrapie. *Acta Neuropathol*, 103, 615-26.
- Skovronsky, D. M., Lee, V. M. & Trojanowski, J. Q. 2006. Neurodegenerative diseases: new concepts of pathogenesis and their therapeutic implications. *Annu Rev Pathol*, 1, 151-70.
- Smith, M. L., Chen, I. T., Zhan, Q., Bae, I., Chen, C. Y., Gilmer, T. M., Kastan, M. B., O'Connor, P. M. & Fornace, A. J., Jr. 1994. Interaction of the p53-regulated protein Gadd45 with proliferating cell nuclear antigen. *Science*, 266, 1376-80.
- Smith, M. L., Ford, J. M., Hollander, M. C., Bortnick, R. A., Amundson, S. A., Seo, Y. R., Deng, C. X., Hanawalt, P. C. & Fornace, A. J., Jr. 2000. p53-mediated DNA repair responses to UV radiation: studies of mouse cells lacking p53, p21, and/or gadd45 genes. *Mol Cell Biol*, 20, 3705-14.
- Sng, J. C., Taniura, H. & Yoneda, Y. 2005. Inhibition of histone deacetylation by trichostatin A intensifies the transcriptions of neuronal c-fos and c-jun genes after kainate stimulation. *Neurosci Lett*, 386, 150-5.
- Sokka, A. L., Putkonen, N., Mudo, G., Pryazhnikov, E., Reijonen, S., Khiroug, L., Belluardo, N., Lindholm, D. & Korhonen, L. 2007. Endoplasmic reticulum stress inhibition protects against excitotoxic neuronal injury in the rat brain. *J Neurosci*, 27, 901-8.
- Sonenberg, N. & Hinnebusch, A. G. 2009. Regulation of translation initiation in eukaryotes: mechanisms and biological targets. *Cell*, 136, 731-45.
- Song, D. Y., Yang, Y. C., Shin, D. H., Sugama, S., Kim, Y. S., Lee, B. H., Joh, T. H. & Cho, B. P. 2008. Axotomy-induced dopaminergic neurodegeneration is accompanied with c-Jun phosphorylation and activation transcription factor 3 expression. *Exp Neurol*, 209, 268-78.
- Sorensen, G., Medina, S., Parchaliuk, D., Phillipson, C., Robertson, C. & Booth, S. A. 2008. Comprehensive transcriptional profiling of prion infection in mouse models reveals networks of responsive genes. *BMC Genom*, 9, 114.
- Spillantini, M. G., Murrell, J. R., Goedert, M., Farlow, M. R., Klug, A. & Ghetti, B. 1998. Mutation in the tau gene in familial multiple system tauopathy with presenile dementia. *Proc Natl Acad Sci U S A*, 95, 7737-41.
- Spillantini, M. G., Schmidt, M. L., Lee, V. M., Trojanowski, J. Q., Jakes, R. & Goedert, M. 1997. Alpha-synuclein in Lewy bodies. *Nature*, 388, 839-40.
- Spires, T. L., Orne, J. D., SantaCruz, K., Pitstick, R., Carlson, G. A., Ashe, K. H. & Hyman, B. T. 2006. Region-specific dissociation of neuronal loss and neurofibrillary pathology in a mouse model of tauopathy. *Am J Pathol*, 168, 1598-607.
- Stefani, M. & Dobson, C. M. 2003. Protein aggregation and aggregate toxicity: new insights into protein folding, misfolding diseases and biological evolution. *J Mol Med*, 81, 678-699.

- Steward, O., Wallace, C. S., Lyford, G. L. & Worley, P. F. 1998. Synaptic activation causes the mRNA for the IEG Arc to localize selectively near activated postsynaptic sites on dendrites. *Neuron*, 21, 741-51.
- Swayne, L. A., Beck, K. E. & Braun, J. E. 2006. The cysteine string protein multimeric complex. *Biochem Biophys Res Commun*, 348, 83-91.
- Tabas, I. & Ron, D. 2011. Integrating the mechanisms of apoptosis induced by endoplasmic reticulum stress. *Nat Cell Biol*, 13, 184-90.
- Tajiri, S., Oyadomari, S., Yano, S., Morioka, M., Gotoh, T., Hamada, J., Ushio, Y. & Mori, M. 2004. Ischemia-induced neuronal cell death is mediated by the endoplasmic reticulum stress pathway involving CHOP. *Cell Death Differ*, 11, 403-415.
- Takano, T., He, W., Han, X., Wang, F., Xu, Q., Wang, X., Oberheim Bush, N. A., Cruz, N., Dienel, G. A. & Nedergaard, M. 2014. Rapid manifestation of reactive astrogliosis in acute hippocampal brain slices. *Glia*, 62, 78-95.
- Taylor, J. P., Hardy, J. & Fischbeck, K. H. 2002. Toxic proteins in neurodegenerative disease. *Science*, 296, 1991-1995.
- Telling, G. C., Scott, M., Mastrianni, J., Gabizon, R., Torchia, M., Cohen, F. E., DeArmond, S. J. & Prusiner, S. B. 1995. Prion propagation in mice expressing human and chimeric PrP transgenes implicates the interaction of cellular PrP with another protein. *Cell*, 83, 79-90.
- Terry, R. D., Masliah, E., Salmon, D. P., Butters, N., DeTeresa, R., Hill, R., Hansen, L. A. & Katzman, R. 1991. Physical basis of cognitive alterations in Alzheimer's disease: synapse loss is the major correlate of cognitive impairment. *Ann Neurol*, 30, 572-580.
- Thakur, A., Wang, X., Siedlak, S. L., Perry, G., Smith, M. A. & Zhu, X. 2007. c-Jun phosphorylation in Alzheimer disease. *J Neurosci Res*, 85, 1668-73.
- Tiwari, S. S., d'Orange, M., Troakes, C., Shurovi, B. N., Engmann, O., Noble, W., Hortobagyi, T. & Giese, K. P. 2015. Evidence that the presynaptic vesicle protein CSPalpha is a key player in synaptic degeneration and protection in Alzheimer's disease. *Mol Brain*, 8, 6.
- Tobaben, S., Thakur, P., Fernández-Chacón, R., Südhof, T. C., Rettig, J. & Stahl, B. 2001. A trimeric protein complex functions as a synaptic chaperone machine. *Neuron*, 31, 987-999.
- Tofaris, G. K., Garcia Reitböck, P., Humby, T., Lambourne, S. L., O'Connell, M., Ghetti, B., Gossage, H., Emson, P. C., Wilkinson, L. S., Goedert, M. & Spillantini, M. G. 2006. Pathological changes in dopaminergic nerve cells of the substantia nigra and olfactory bulb in mice transgenic for truncated human alpha-synuclein(1-120): implications for Lewy body disorders. *J Neurosci*, 26, 3942-50.
- Torp, R., Su, J. H., Deng, G. & Cotman, C. W. 1998. GADD45 is induced in Alzheimer's disease, and protects against apoptosis in vitro. *Neurobiol Dis*, 5, 245-52.
- Torres, M., Castillo, K., Armisen, R., Stutzin, A., Soto, C. & Hetz, C. 2010. Prion protein misfolding affects calcium homeostasis and sensitizes cells to endoplasmic reticulum stress. *PLoS One*, 5, e15658.
- Torres, M., Matamala, J. M., Duran-Aniotz, C., Cornejo, V. H., Foley, A. & Hetz, C. 2014. ER stress signaling and neurodegeneration: At the intersection between Alzheimer's disease and Prion-related disorders. *Virus Res*, 207, 69-75.

- Toyoda, T., Nomura, H., Hashikawa, K., Nonaka, A. & Matsuki, N. 2010. Persistent neural activity regulates Arc/Arg3.1 transcription in the dentate gyrus. *J Neurosci Res*, 88, 3060-6.
- Tribouillard-Tanvier, D., Beringue, V., Desban, N., Gug, F., Bach, S., Voisset, C., Galons, H., Laude, H., Vilette, D. & Blondel, M. 2008. Antihypertensive drug guanabenz is active in vivo against both yeast and mammalian prions. *PLoS One*, 3, e1981.
- Tsujino, H., Kondo, E., Fukuoka, T., Dai, Y., Tokunaga, A., Miki, K., Yonenobu, K., Ochi, T. & Noguchi, K. 2000. Activating transcription factor 3 (ATF3) induction by axotomy in sensory and motoneurons: A novel neuronal marker of nerve injury. *Mol Cell Neurosci*, 15, 170-82.
- Tu, J. C., Xiao, B., Yuan, J. P., Lanahan, A. A., Leoffert, K., Li, M., Linden, D. J. & Worley, P. F. 1998. Homer binds a novel proline-rich motif and links group 1 metabotropic glutamate receptors with IP3 receptors. *Neuron*, 21, 717-26.
- Tzingounis, A. V. & Nicoll, R. A. 2006. Arc/Arg3.1: linking gene expression to synaptic plasticity and memory. *Neuron*, 52, 403-7.
- Umbach, J. A., Zinsmaier, K. E., Eberle, K. K., Buchner, E., Benzer, S. & Gundersen, C. B. 1994. Presynaptic dysfunction in *Drosophila* csp mutants. *Neuron*, 13, 899-907.
- Unterberger, U., Hoftberger, R., Gelpi, E., Flicker, H., Budka, H. & Voigtlander, T. 2006. Endoplasmic reticulum stress features are prominent in Alzheimer disease but not in prion diseases in vivo. *J Neuropathol Exp Neurol*, 65, 348-57.
- Urano, F., Wang, X. Z., Bertolotti, A., Zhang, Y., Chung, P., Harding, H. P. & Ron, D. 2000. Coupling of stress in the ER to activation of JNK protein kinases by transmembrane protein kinase IRE1. *Science's STKE*, 287, 664-666.
- Vairapandi, M., Balliet, A. G., Fornace, A. J., Jr., Hoffman, B. & Liebermann, D. A. 1996. The differentiation primary response gene MyD118, related to GADD45, encodes for a nuclear protein which interacts with PCNA and p21WAF1/CIP1. *Oncogene*, 12, 2579-94.
- Vairapandi, M., Balliet, A. G., Hoffman, B. & Liebermann, D. A. 2002. GADD45b and GADD45g are cdc2/cyclinB1 kinase inhibitors with a role in S and G2/M cell cycle checkpoints induced by genotoxic stress. *J Cell Physiol*, 192, 327-38.
- Vazdarjanova, A., Ramirez-Amaya, V., Insel, N., Plummer, T. K., Rosi, S., Chowdhury, S., Mikhael, D., Worley, P. F., Guzowski, J. F. & Barnes, C. A. 2006. Spatial exploration induces ARC, a plasticity-related immediate-early gene, only in calcium/calmodulin-dependent protein kinase II-positive principal excitatory and inhibitory neurons of the rat forebrain. *J Comp Neurol*, 498, 317-29.
- Vendrell, M., Curran, T. & Morgan, J. I. 1993. Glutamate, immediate-early genes, and cell death in the nervous system. *Ann N Y Acad Sci*, 679, 132-41.
- Verity, N. C. & Mallucci, G. R. 2011. Rescuing neurons in prion disease. *Biochem J*, 433, 19-29.
- Vesely, P. W., Staber, P. B., Hoefler, G. & Kenner, L. 2009. Translational regulation mechanisms of AP-1 proteins. *Mutat Res*, 682, 7-12.
- Virgo, L. & de Belleruche, J. 1995. Induction of the immediate early gene c-jun in human spinal cord in amyotrophic lateral sclerosis with concomitant loss of NMDA receptor NR-1 and glycine transporter mRNA. *Brain Res*, 676, 196-204.
- Vlug, A. S., Teuling, E., Haasdijk, E. D., French, P., Hoogenraad, C. C. & Jaarsma, D. 2005. ATF3 expression precedes death of spinal motoneurons in amyotrophic lateral sclerosis-SOD1 transgenic mice and correlates with c-Jun

- phosphorylation, CHOP expression, somato-dendritic ubiquitination and Golgi fragmentation. *Eur J Neurosci*, 22, 1881-94.
- Wang, L., Deng, H. X., Grisotti, G., Zhai, H., Siddique, T. & Roos, R. P. 2009. Wild-type SOD1 overexpression accelerates disease onset of a G85R SOD1 mouse. *Hum Mol Genet*, 18, 1642-51.
- Wang, L., Popko, B. & Roos, R. P. 2011. The unfolded protein response in familial amyotrophic lateral sclerosis. *Hum Mol Genet*, 20, 1008-15.
- Wang, Q., Yu, S., Simonyi, A., Sun, G. Y. & Sun, A. Y. 2005. Kainic acid-mediated excitotoxicity as a model for neurodegeneration. *Mol Neurobiol*, 31, 3-16.
- Wang, X. W., Zhan, Q., Coursen, J. D., Khan, M. A., Kontny, H. U., Yu, L., Hollander, M. C., O'Connor, P. M., Fornace, A. J., Jr. & Harris, C. C. 1999. GADD45 induction of a G2/M cell cycle checkpoint. *Proc Natl Acad Sci U S A*, 96, 3706-11.
- Washbourne, P., Thompson, P. M., Carta, M., Costa, E. T., Mathews, J. R., Lopez-Bendito, G., Molnar, Z., Becher, M. W., Valenzuela, C. F., Partridge, L. D. & Wilson, M. C. 2002. Genetic ablation of the t-SNARE SNAP-25 distinguishes mechanisms of neuroexocytosis. *Nat Neurosci*, 5, 19-26.
- Watt, N. T. & Hooper, N. M. 2003. The prion protein and neuronal zinc homeostasis. *Trends Biochem Sci*, 28, 406-10.
- Watts, J. C. & Prusiner, S. B. 2014. Mouse models for studying the formation and propagation of prions. *J Biol Chem*, 289, 19841-9.
- Wegorzewska, I., Bell, S., Cairns, N. J., Miller, T. M. & Baloh, R. H. 2009. TDP-43 mutant transgenic mice develop features of ALS and frontotemporal lobar degeneration. *Proc Natl Acad Sci U S A*, 106, 18809-14.
- Wek, R. C., Jiang, H. Y. & Anthony, T. G. 2006. Coping with stress: eIF2 kinases and translational control. *Biochem Soc Trans*, 34, 7-11.
- Werner, P., Voigt, M., Keinänen, K., Wisden, W. & Seeburg, P. H. 1991. Cloning of a putative high-affinity kainate receptor expressed predominantly in hippocampal CA3 cells. *Nature*, 351, 742-4.
- White, M. D., Farmer, M., Mirabile, I., Brandner, S., Collinge, J. & Mallucci, G. R. 2008. Single treatment with RNAi against prion protein rescues early neuronal dysfunction and prolongs survival in mice with prion disease. *Proc Natl Acad Sci U S A*, 105, 10238-10243.
- Will, R., Ironside, J., Zeidler, M., Estibeiro, K., Cousens, S., Smith, P., Alperovitch, A., Poser, S., Pocchiari, M. & Hofman, A. 1996. A new variant of Creutzfeldt-Jakob disease in the UK. *Lancet*, 347, 921-925.
- Williams, A., Lucassen, P. J., Ritchie, D. & Bruce, M. 1997. PrP deposition, microglial activation, and neuronal apoptosis in murine scrapie. *Exp Neurol*, 144, 433-8.
- Wittner, L., Henze, D. A., Zaborszky, L. & Buzsaki, G. 2007. Three-dimensional reconstruction of the axon arbor of a CA3 pyramidal cell recorded and filled in vivo. *Brain Struct Funct*, 212, 75-83.
- Wolfgang, C. D., Liang, G., Okamoto, Y., Allen, A. E. & Hai, T. 2000. Transcriptional autorepression of the stress-inducible gene ATF3. *J Biol Chem*, 275, 16865-70.
- Wu, J., Petralia, R. S., Kurushima, H., Patel, H., Jung, M. Y., Volk, L., Chowdhury, S., Shepherd, J. D., Dehoff, M., Li, Y., Kuhl, D., Haganir, R. L., Price, D. L., Scannevin, R., Troncoso, J. C., Wong, P. C. & Worley, P. F. 2011. Arc/Arg3.1 regulates an endosomal pathway essential for activity-dependent beta-amyloid generation. *Cell*, 147, 615-28.
- Xu, Y. F., Gendron, T. F., Zhang, Y. J., Lin, W. L., D'Alton, S., Sheng, H., Casey, M. C., Tong, J., Knight, J., Yu, X., Rademakers, R., Boylan, K., Hutton, M.,

- McGowan, E., Dickson, D. W., Lewis, J. & Petrucelli, L. 2010. Wild-type human TDP-43 expression causes TDP-43 phosphorylation, mitochondrial aggregation, motor deficits, and early mortality in transgenic mice. *J Neurosci*, 30, 10851-9.
- Ye, J., Rawson, R. B., Komuro, R., Chen, X., Davé, U. P., Prywes, R., Brown, M. S. & Goldstein, J. L. 2000. ER stress induces cleavage of membrane-bound ATF6 by the same proteases that process SREBPs. *Mol Cell*, 6, 1355-1364.
- Ye, X., Meeker, H. C., Kozlowski, P. & Carp, R. I. 2004. The occurrence of vacuolation, and periodic acid-Schiff (PAS)-positive granules and plaques in the brains of C57BL/6J, AKR, senescence-prone (SAMP8) and senescence-resistant (SAMR1) mice infected with various scrapie strains. *Brain Res*, 995, 158-66.
- Yeomans, A. M. 2013. *Regulation of RNA translation by Phenethyl Isothiocyanate*. Doctoral, University of Southampton.
- Ylinen, A., Bragin, A., Nadasdy, Z., Jando, G., Szabo, I., Sik, A. & Buzsaki, G. 1995. Sharp wave-associated high-frequency oscillation (200 Hz) in the intact hippocampus: network and intracellular mechanisms. *J Neurosci*, 15, 30-46.
- Yoon, S. O., Park, D. J., Ryu, J. C., Ozer, H. G., Tep, C., Shin, Y. J., Lim, T. H., Pastorino, L., Kunwar, A. J., Walton, J. C., Nagahara, A. H., Lu, K. P., Nelson, R. J., Tuszynski, M. H. & Huang, K. 2012. JNK3 perpetuates metabolic stress induced by Abeta peptides. *Neuron*, 75, 824-37.
- Zhan, Q., Antinore, M. J., Wang, X. W., Carrier, F., Smith, M. L., Harris, C. C. & Fornace, A. J., Jr. 1999. Association with Cdc2 and inhibition of Cdc2/Cyclin B1 kinase activity by the p53-regulated protein Gadd45. *Oncogene*, 18, 2892-900.
- Zhang, J., Zhang, D., McQuade, J. S., Behbehani, M., Tsien, J. Z. & Xu, M. 2002. c-fos regulates neuronal excitability and survival. *Nat Genet*, 30, 416-20.
- Zhang, P., Hirsch, E. C., Damier, P., Duyckaerts, C. & Javoy-Agid, F. 1992. c-fos protein-like immunoreactivity: distribution in the human brain and over-expression in the hippocampus of patients with Alzheimer's disease. *Neuroscience*, 46, 9-21.
- Zhang, S. J., Buchthal, B., Lau, D., Hayer, S., Dick, O., Schwaninger, M., Veltkamp, R., Zou, M., Weiss, U. & Bading, H. 2011. A signaling cascade of nuclear calcium-CREB-ATF3 activated by synaptic NMDA receptors defines a gene repression module that protects against extrasynaptic NMDA receptor-induced neuronal cell death and ischemic brain damage. *J Neurosci*, 31, 4978-90.
- Zhang, S. J., Zou, M., Lu, L., Lau, D., Ditzel, D. A., Delucinge-Vivier, C., Aso, Y., Descombes, P. & Bading, H. 2009. Nuclear calcium signaling controls expression of a large gene pool: identification of a gene program for acquired neuroprotection induced by synaptic activity. *PLoS Genet*, 5, e1000604.
- Zhang, X. M. & Zhu, J. 2011. Kainic Acid-induced neurotoxicity: targeting glial responses and glia-derived cytokines. *Curr Neuropharmacol*, 9, 388-98.
- Zhang, Y. Q. & Chandra, S. S. 2014. Oligomerization of Cysteine String Protein alpha mutants causing adult neuronal ceroid lipofuscinosis. *Biochim Biophys Acta*, 1842, 2136-46.
- Zhang, Y. Q., Henderson, M. X., Colangelo, C. M., Ginsberg, S. D., Bruce, C., Wu, T. & Chandra, S. S. 2012. Identification of CSPalpha clients reveals a role in dynamin 1 regulation. *Neuron*, 74, 136-50.
- Zhao, L. & Ackerman, S. L. 2006. Endoplasmic reticulum stress in health and disease. *Curr Opin Cell Biol*, 18, 444-452.

- Zhao, L., Longo-Guess, C., Harris, B. S., Lee, J. W. & Ackerman, S. L. 2005. Protein accumulation and neurodegeneration in the woozy mutant mouse is caused by disruption of SIL1, a cochaperone of BiP. *Nat Genet*, 37, 974-9.
- Zhao, X., Lein, E. S., He, A., Smith, S. C., Aston, C. & Gage, F. H. 2001. Transcriptional profiling reveals strict boundaries between hippocampal subregions. *J Comp Neurol*, 441, 187-196.
- Zheng, X. Y., Zhang, H. L., Luo, Q. & Zhu, J. 2011. Kainic acid-induced neurodegenerative model: potentials and limitations. *J Biomed Biotechnol*, 2011, 457079.
- Zhu, P. J., Huang, W., Kalikulov, D., Yoo, J. W., Placzek, A. N., Stoica, L., Zhou, H., Bell, J. C., Friedlander, M. J., Krnjevic, K., Noebels, J. L. & Costa-Mattioli, M. 2011. Suppression of PKR promotes network excitability and enhanced cognition by interferon-gamma-mediated disinhibition. *Cell*, 147, 1384-96.
- Zhu, X., Raina, A. K., Rottkamp, C. A., Aliev, G., Perry, G., Bux, H. & Smith, M. A. 2001. Activation and redistribution of c-jun N-terminal kinase/stress activated protein kinase in degenerating neurons in Alzheimer's disease. *J Neurochem*, 76, 435-41.
- Zinsmaier, K. E., Eberle, K. K., Buchner, E., Walter, N. & Benzer, S. 1994. Paralysis and early death in cysteine string protein mutants of *Drosophila*. *Science*, 263, 977-80.
- Zinsmaier, K. E., Hofbauer, A., Heimbeck, G., Pflugfelder, G. O., Buchner, S. & Buchner, E. 1990. A cysteine-string protein is expressed in retina and brain of *Drosophila*. *J Neurogenet*, 7, 15-29.

Appendices

Appendix 1: Transgenic mouse models of chronic neurodegenerative diseases

Mouse model	Line	Mutations	Pathology		
			Gliosis	Synaptic/axonal loss	Neurodegeneration
AD	Tg6799 (Tg-5XFAD)	Human APP (Swedish mutation: K670N, M671L; the Florida mutation: I716V; the London mutation: V717I) and PSEN1 (M146L and L286V mutations)	✓ Oakley et al., 2006	✓ Oakley et al., 2006	✓ Oakley et al., 2006
	TgCRND8	Human APP (Swedish mutation: K670N, M671L and Indiana mutation V717F)	✓ Dudal et al., 2004	✓ Adalbert et al., 2009	✓ Brautigam et al., 2012
	APP ^{swe} /PS1 Δ E9	Chimeric mouse/human APP (Swedish mutation: K670N, M671L) and PSEN1 (Δ E9)	✓ Perez et al., 2009		✓ Perez et al., 2007
	APP/Lo	Human APP (London mutation: V717I)	✓ Heneka et al., 2005	✓ Perez-Cruz et al., 2011	
	APP ^{swe} /PS1M146L	Human APP (Swedish mutation: K670N, M671L) and PSEN1 (M146L)	✓ Gordon et al., 2002		✓ Sadowski et al., 2004
Tauopathy	rTg4510	Human MAPT (P301L)	✓ Ramsden et al., 2005	✓ Rocher et al., 2010	✓ Spires et al., 2006

PD	G2-3	Human SCNA (A53T)	✓ Lee et al., 2002	✓ Martin et al., 2006	✓ Martin et al., 2006
	SYN120	Truncated human SCNA	✓ Tofaris et al., 2006		
ALS	SOD1 G93A	Human SOD1 (G93A)	✓ Fischer et al., 2004	✓ Fischer et al., 2004	✓ Fischer et al., 2004
	SOD1 G85R	Human SOD1 (G85R)	✓ Wang et al., 2009, Wang et al., 2011		✓ Wang et al., 2009, Wang et al., 2011
	TDP-43 A315T	Human TARDBP (A315T)	✓ Węgorzewska et al., 2009	✓ Węgorzewska et al., 2009	✓ Węgorzewska et al., 2009

Appendix 1 Table 1 Transgenic mouse models of AD, PD and ALS referenced in this thesis.

Evidence for gliosis, synaptic/axonal loss and neurodegeneration is highlighted.

Appendix 2: Transgenic mouse models of prion disease

Mouse line	Mutation	Expression levels	Gliosis	Synaptic/axonal loss	Neurodegeneration
Tg(PG14-A3 ^{+/-})	Insertion of 9 extra octapeptide repeats in mouse Prnp gene	~1× ^a	✓ Chiesa et al., 1998		✓ Chiesa et al., 1998
Tg37 inoculated with RML scrapie	Homozygous Hemizygous	~6× ^b ~3× ^b	✓ Moreno et al., 2013, Moreno et al., 2012	✓ Moreno et al., 2013, Moreno et al., 2012	✓ Moreno et al., 2013, Moreno et al., 2012
Tg(WT-E1 ^{+/+})	None	~4× ^a	No Chiesa et al., 1998		No Chiesa et al., 1998
Tg(CJD-A21 ^{+/-})	Mouse Prnp D177N/V128	~1× ^b	✓ Dossena et al., 2008	✓ Dossena et al., 2008	✓ Dossena et al., 2008
Tg(CJD-66 ^{+/-})	Mouse Prnp D177N/V128	~2× ^b	✓ Bouybayoune et al., 2015	✓ Bouybayoune et al., 2015	✓ Bouybayoune et al., 2015
Tg(FFI-26 ^{+/-})	Mouse Prnp D177N/M128	~2× ^b	✓ Bouybayoune et al., 2015		✓ Bouybayoune et al., 2015
Tg388 inoculated with 127S scrapie	Sheep Prnp (136V, 154R, 171Q)	8–10× ^b (Watts and Prusiner, 2014)	✓ Langevin et al., 2011		✓ Langevin et al., 2011

Appendix 2 Table 1 Transgenic mouse models of prion disease referenced in this thesis.

Evidence for gliosis, synaptic/axonal loss and neurodegeneration is highlighted.

^acompared to endogenous hamster PrP, ^brelative to endogenous expression in non-Tg mice.

Appendix 3: Suppliers of reagents

Name	Supplier
1-Bromo-3-chloropropane (BCP)	Sigma-Aldrich
3,3'-Diaminobenzidine (DAB)	Sigma-Aldrich
Acrylamide/Bis-acrylamide	Sigma-Aldrich
Agar	Melford
Agarose	Melford
Ammonium persulphate (APS)	Fischer Scientific
Avidin-biotinylated horseradish peroxidase complex (ABC) kit	Vector Labs
Borate	Fisher Scientific
Bovine serum albumin (BSA)	Fisher Scientific
Bovine serum albumin (BSA) for restriction digest	Promega
Brilliant Blue G-Colloidal	Sigma-Aldrich
Bromophenol Blue	Sigma-Aldrich
Buffer H	Promega
Buffer P1	Qiagen
Buffer P2	Qiagen
Buffer P3	Qiagen
CaCl ₂	Sigma-Aldrich
Citric Acid	Sigma-Aldrich
DC Protein Assay Kit	Bio-Rad
DH5α cells (Library Efficiency)	Invitrogen
DMSO	Sigma-Aldrich
DNA ladder	Bioline
DNA loading buffer	Bioline
Dried skimmed milk	Sainsbury's
Dulbecco's Modified Eagle Medium (D-MEM)	Life Technologies
Dulbecco's PBS (D-PBS)	Life Technologies
EcoRI	Promega
EDTA	Sigma-Aldrich
Ethanol	Fisher Scientific
Fetal Bovine Serum (FBS)	Thermo Scientific HyClone

Formalin	Sigma-Aldrich
GelRed	Biotium
Glacial acetic acid	Fisher Scientific
Glucose	Sigma-Aldrich
Glycerol	Fisher Scientific
Glycine	Fisher Scientific
Halt protease and phosphatase inhibitor cocktail	Thermo Scientific
Harris Haematoxylin	Sigma-Aldrich
Heparin	Southampton General Hospital Pharmacy
HEPES	Fisher Scientific
Histoclear	National Diagnostics
Hoechst	Thermo Scientific
HCl	Fisher Scientific
Hydrogen peroxide (H ₂ O ₂)	Sigma-Aldrich
iQ SYBR Green Supermix	Bio-Rad
iScript Select cDNA Synthesis Kit	Bio-Rad
Isopentane	Fisher Scientific
Isopropanol	Sigma-Aldrich
iTaq Universal SYBR Green Supermix	Bio-Rad
Kainic acid	Sigma-Aldrich
Kanamycin	Sigma-Aldrich
KCl	Sigma-Aldrich
Ketamine	Centaur Services
Lacrilube	Allergan Ltd
Lidocaine	Biorex Laboratories Ltd
Luria broth agar	Media kitchen, Life Sciences building. Prepared by laboratory technicians
Luria broth medium	Media kitchen, Life Sciences building. Prepared by laboratory technicians
Methanol	Fisher Scientific
MgSO ₄	Sigma-Aldrich
Mounting medium	Merck Millipore

Mowiol-488	Sigma-Aldrich
M-PER	Thermo Scientific
Na ₂ HPO ₄	Sigma-Aldrich
NaCl	Sigma-Aldrich
NaH ₂ PO ₄	Sigma-Aldrich
NaHCO ₃	Sigma-Aldrich
NH ₄ Cl	Sigma-Aldrich
Nuclease-free water	Promega
NuGEN Encore SP+ Complete DR Multiplex System 1-8 and 9-16	NuGEN
Optimal cutting temperature (OCT) compound	Thermo Scientific
Page Ruler Plus Prestained Protein Ladder	Thermo Scientific
Paraffin wax	Polywax
Paraformaldehyde (PFA)	Fisher Scientific
Phenethyl isothiocyanate (PEITC)	Sigma-Aldrich
Phenylmethanesulfonyl fluoride (PMSF)	Sigma-Aldrich
Phosphate buffered saline (PBS)	Fisher Scientific
Pierce BCA Protein Assay Kit	Thermo Fisher Scientific
Proteinase K (PK)	Promega
REDTaq ReadyMix PCR Reaction Mix	Sigma-Aldrich
RNAqueous-Micro Kit	Ambion
RNase-free water	Qiagen
RNaseZAP	Sigma-Aldrich
RNeasy Mini Kit	Qiagen
S.O.C medium	Life Technologies
SDS	Fisher
Serum (immunohistochemistry and immunofluorescence)	Vector Labs
Sodium pentobarbital	Centaur Services
Sterile saline (0.9% NaCl w/v)	Fannin
TEMED	Sigma-Aldrich
TOPO TA cloning kit	Invitrogen
Tris	Invitrogen
Tris buffered saline (TBS)	Fisher Scientific
Triton X-100	Sigma-Aldrich
Trizol	Invitrogen

Tunicamycin	Sigma-Aldrich
Tween-20	Sigma-Aldrich
X-gal	Fisher Scientific
Xylazine	Centaur Services
Xylene	Fisher Scientific
β -Mercaptoethanol	Sigma-Aldrich

Appendix 3 Table 1 Suppliers of reagents used in the thesis.

Appendix 4: Example calculation of the number of plasmid copies per μl

Calculation of plasmid copy number per μL , using equations:

- Moles = mass/molecular weight
- Molecular weight = $660 \times \text{no. base pairs}$
- Mass = concentration

Plasmid copy number per μl = moles \times Avogadro's constant (6.022×10^{23})

Example calculation for BiP plasmid:

Size of plasmid and insert = 4134 bp

Concentration = 1654.3 ng/ μl

Molecular weight = $660 \times 4134 = 2.73 \text{ g}/\mu\text{l}$

Moles = $1654.3 \times 10^{-9} / 2.73 = 6.06 \times 10^{-7}$

Plasmid copy per μl = $6.06 \times 10^{-7} \times 6.022 \times 10^{23} = 3.65 \times 10^{17}$ plasmid copies per μl

Plasmids were then diluted to 1×10^{15} plasmids/ μl , followed by 1:10 dilutions to 1×10^8 plasmids/ μl using nuclease-free water.

Appendix 5: Example of plasmid sequence insert

Plasmid containing CHOP insert =

Plasmid sequence with insert:

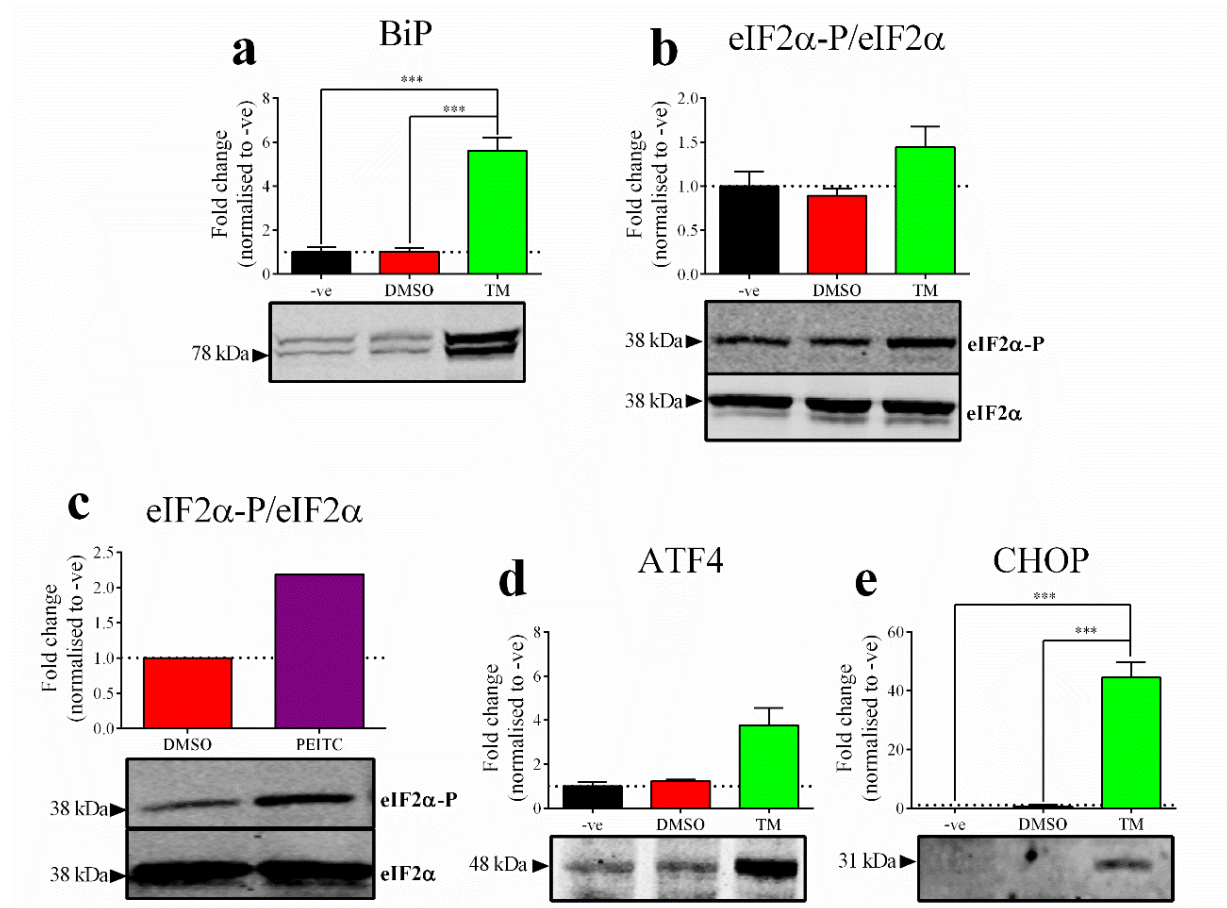
```
CTACGAGCTCGGATCCACTAGTAACGGCCGCCAGTGTGCTGGAATTCGCCCT
TTCATGCGTTGCTTCCCAGGC CGGGCTGGGCACTGACCACTCTGTTTCCGTT
TCCTAGTTCTTCCTTGCTCTTCCTCCTCTTCCTCCTGGGCCATAGAACTCTGA
CTGGAATCTGGAGAGCGAGGGCTTTGGGATGTGCGTGTGACCTCTGTTGGC
CCTGGCTCCTCTGTCAGCCAAGCTAGGGACGCAGGGTCAAGAGTAGTGAAG
GTTTTTGATTCTTCCTCTTCGTTTCCTGGGGA AAGGGCGAATTCTGCAGATAT
CCATCACACTGGCGGCCGCTCGAGCATGCATCTAGAGGGGCCCAATTCGCCC
TATAGTGAGTCGTATTACAATTCAGTGGCCGTCGTTTTACAACGTCGTGACT
GGGAAAACCCTGGCGTTACCCAACTTAATCGCCTTGACGACATCCCCCTTT
CGCCAGCTGGCGTAATAGCGAAGAGGCCCGCACCGATCGCCCTTCCCAACA
GTTGCGCAGCCTGAATGGCGAATGGACGCGCCCTGTAGCGGCGCATTAAAGC
GCGGCGGGTGTGGTGGTTACGCGCAGCGTGACCGCTACACTTGCCAGCGCC
CTAGCGCCCCGCTCCTTTCGCTTTCCTCCCTTCCTTTCTCGCCACGTTTCGCCG
CTTTCCCCGTCAAGCTCTAAATCGGGGGCTCCCTTTAGGGTTCCGATTTAGT
GCTTTACGGCACCTCGACCCCAAAAACTTGATTAGGGTGATGGTTCACGTA
GTGGGCCATCGCCCTGATAGACGGTTTTTCGCCCTTTGACGTTGGAGTCCAC
GTTCTTTAATAGTGGACTCTTGTTCCAACTGGAACAACACTCAACCCTATC
TCGGTCTATTCTTTTGATTTATAAAGGGATTTTGCCGATTTTCGGCCTATTGGT
TTAAAAAATGAGCTGATTTAACAAAAATTTAACGCGAATTTTAACAAAATT
CAGGC
```

cDNA sequence with insert :

```
ATGGCAGCTGAGTCCCTGCCTTTTACCTTGGAGACGGTGTCCAGCTGGGAGC
TGGAAGCCTGGTATGAGGATCTGCAGGAGGTCCTGTCTCAGATGAAATTG
GGGCGACCTATATCTCATCCCCAGGAAACGAAGAGGAAG AATCAAAAACCT
TCACTACTCTTGACCTTGGCTCCCTAGCTTGGCTGACAGAGGAGCCAGGGCC
AACAGAGGTACACGCCACATCCCAAAGCCCTCGCTCTCCAGATTCCAGTCA
GAGTTCTATGGCCAGGAGGAAGAGGAGGAAGAGCAAGGAAGAAGAACTAGGA
AACGGAAACAGAGTGGTCAGTGCCTCAGCCCC GCCTGGGAAGCAACGCATG
AAGGAGAAGGAGCAGGAGAACGAGCGGAAAGTGGCACAGCTAGCTGAAGA
GAACGAGCGGCTCAAGCAGGAAATCGAGCGCCTGACCAGGGAGGTGGAGA
CCACACGGCGGGCTCTGATCGACCGCATGGTCAGCCTGCACCAAGCATGA
```

Yellow represents the sense (forward) primer and purple represents the antisense (reverse primer). Green is the insert sequence

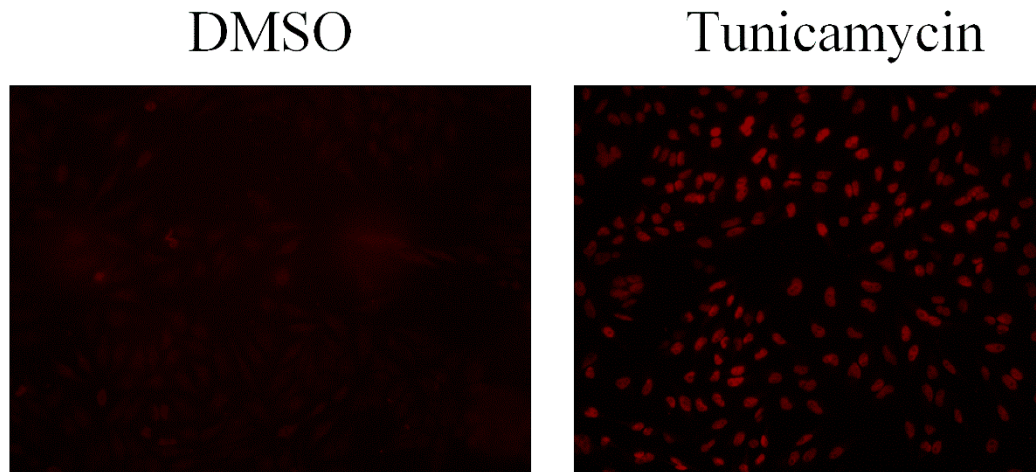
Appendix 6: Quantification of UPR proteins in tunicamycin and PEITC treated HeLa cells



Appendix 6 Figure 1 Quantification of UPR proteins in tunicamycin and PEITC treated HeLa cells.

Representative western blotting and related quantification of BiP (a), eIF2α-P (Ser51) (b-c), ATF4 (d) and CHOP (e) proteins in HeLa cells treated with 2 µg/ml tunicamycin (6 hr) or 20 µM PEITC (1 hr). Data in graphs represents mean ± SEM protein expression values from $n = 3$ HeLa cell preparations, except for (c) $n = 1$ and (d) $n = 2$. Statistical test (a, b and e) = one-way ANOVA with Bonferroni post-analysis. Statistical significance relative to control (-ve or DMSO): *** $P \leq 0.001$ -ve, untreated; hr, hour and TM, tunicamycin.

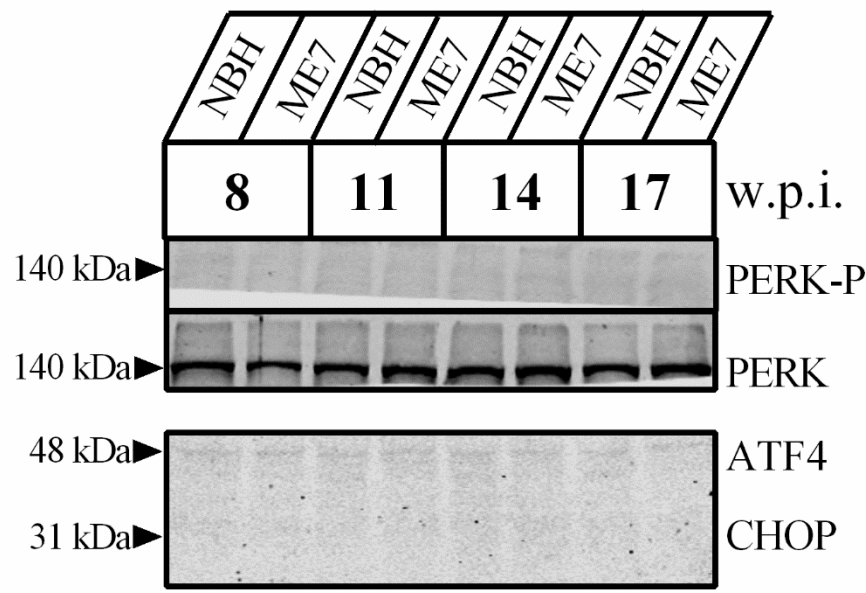
Appendix 7: Immunofluorescence for ATF4 in tunicamycin treated HeLa cells



Appendix 7 Figure 1 Immunofluorescence staining for ATF4 protein in tunicamycin treated HeLa cells.

Immunofluorescence staining for ATF4 in HeLa cells treated with 2 $\mu\text{g/ml}$ tunicamycin compared to DMSO treated HeLa cells. HeLa cells were treated with DMSO or tunicamycin for 6 hr. Red staining reflects positive immunoreactivity for ATF4. Scale bar, 40 μm . hr, hour.

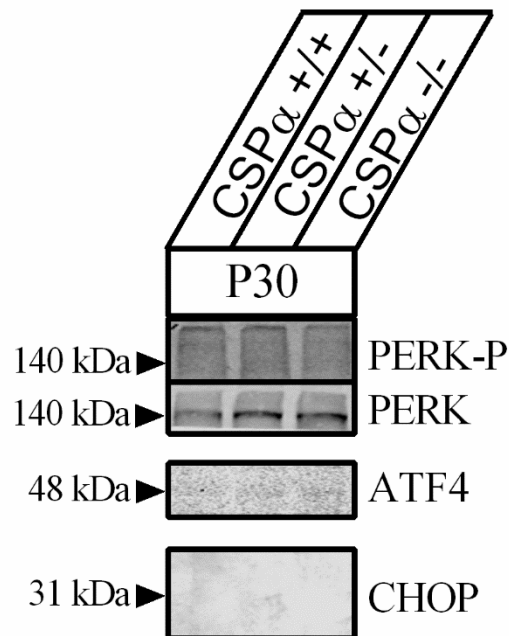
Appendix 8: PERK-P, ATF4 and CHOP protein expression in ME7-animals



Appendix 8 Figure 1 Western blotting of the UPR proteins: PERK-P, ATF4 and CHOP in ME7-animals.

Representative western blotting for PERK-P (Thr980), PERK, ATF4 and CHOP in SDS extracted hippocampi from NBH- and ME7-animals killed at different time-points (8-20 w.p.i.). $n = 3$ animals (PERK-P and PERK) and $n = 4$ animals (ATF4 and CHOP) per condition and time-point. w.p.i., weeks post-inoculation.

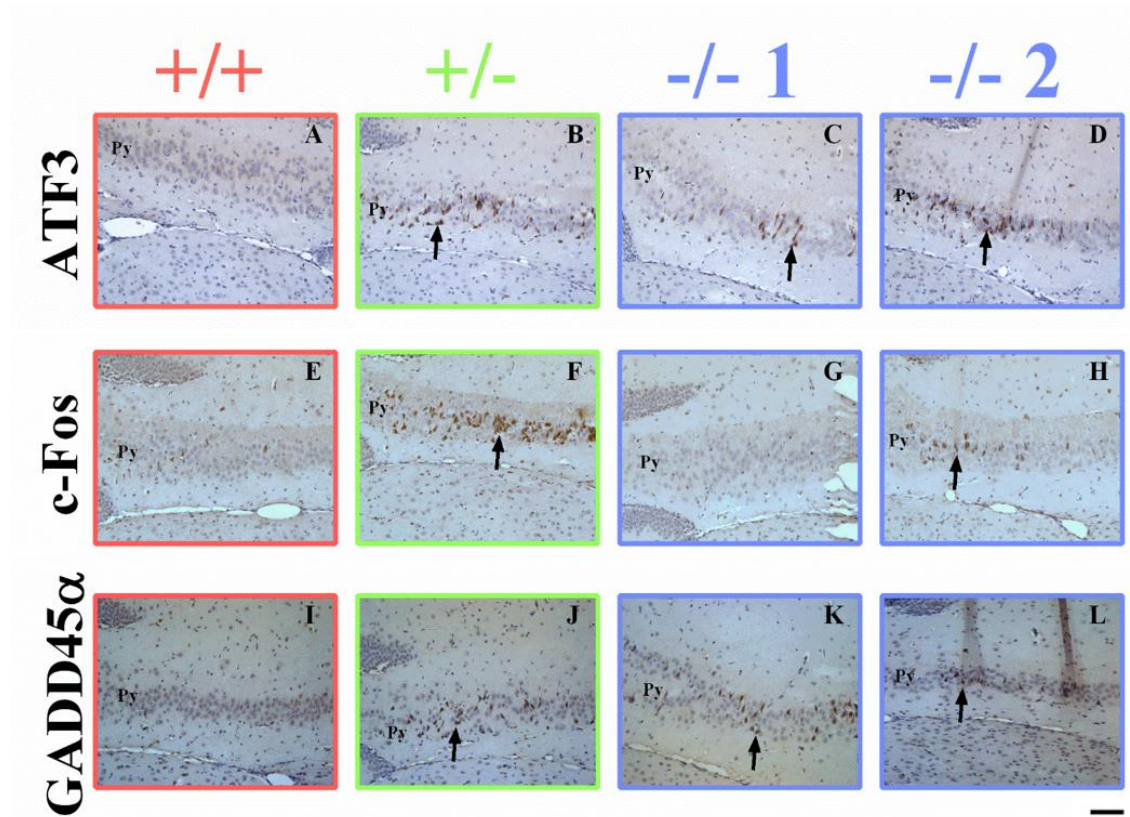
Appendix 9: PERK-P, ATF4 and CHOP protein expression in CSP α $-/-$ animals



Appendix 9 Figure 1 Western blotting of the UPR proteins: PERK-P, ATF4 and CHOP in CSP α $-/-$ animals.

Representative western blotting for PERK-P (Thr980), PERK, ATF4 and CHOP in SDS extracted hippocampi from CSP α $+/+$, $+/-$ and $-/-$ animals killed at P30. $n = 3$ animals for all CSP α genotypes, except for CSP α $-/-$ (PERK-P and PERK), where $n = 4$ animals. $n = 3$ animals per genotype for ATF4 and CHOP. P, postnatal days.

Appendix 10: ATF3, c-Fos and GADD45 α protein expression in the CA3b region of the hippocampus in CSP α animals



Appendix 10 Figure 1 Immunohistochemical staining for ATF3, c-Fos and GADD45 α proteins in the CA3b region of the hippocampus in CSP α animals.

Immunohistochemical staining for ATF3, c-Fos and GADD45 α in the CA3b region of the hippocampus. Immunohistochemical staining was performed on CSP α +/+, +/- and -/- animals killed at P29. $n = 2$ animals per genotype, except for CSP α +/- where $n = 3$. The scale bar for the images is indicated under image L (100 μ m). -/- 1 and -/- 2 refer to two different CSP α -/- animals. Black arrows represent distinct and positive immunostaining. +/+, wildtype; +/-, heterozygous; -/-, knockout; CA3, Cornu Ammonis region 3 and Py, pyramidal layer.

Appendix 11: Publication

Davies, M. J., Cooper, M., Perry, V. H. & O'Connor, V. 2015. Reduced expression of the presynaptic co-chaperone cysteine string protein alpha (CSPalpha) does not exacerbate experimentally-induced ME7 prion disease. *Neurosci Lett*, 589, 138-43.



Research article

Reduced expression of the presynaptic co-chaperone cysteine string protein alpha (CSP α) does not exacerbate experimentally-induced ME7 prion disease



Matthew J. Davies*, Matthew Cooper, V. Hugh Perry, Vincent O'Connor

Centre for Biological Sciences (CfBS), University of Southampton, Southampton SO17 1BJ, United Kingdom

HIGHLIGHTS

- CSP α is reduced in ME7-animals during disease progression.
- CSP α heterozygosity does not accelerate behavioural changes in ME7-animals.
- Prion disease pathology is not altered by reduced CSP α expression.

ARTICLE INFO

Article history:

Received 2 November 2014

Received in revised form

18 December 2014

Accepted 20 January 2015

Available online 23 January 2015

Keywords:

CSP α

Gliosis

ME7

PrP^{Sc}

Synaptic loss

ABSTRACT

Infection of mice with the ME7 prion agent results in well-characterised neuropathological changes, which includes vacuolation, neurodegeneration and synaptic degeneration. Presynaptic dysfunction and degeneration is apparent through the progressive reduction in synaptic vesicle proteins and eventual loss of synapses. Cysteine string protein alpha (CSP α), which regulates refolding pathways at the synapse, exhibits an early decline during chronic neurodegeneration implicating it as a mediator of disease mechanisms. CSP α null mice develop a progressive neuronal dysfunction through disruption of the integrity of presynaptic function. In this study, we investigated whether reduced expression of CSP α would exacerbate ME7 prion disease. Wild type (+/+) and heterozygous (+/−) mice, which express about a ~50% reduction in CSP α , were used as a distinct genetic background on which to impose prion disease. +/+ and +/− mice were inoculated with brain homogenate from either a normal mouse brain (NBH) or from the brain of a mouse which displayed clinical signs of prion disease (ME7). Behavioural tests, western blotting and immunohistochemistry, which resolve key elements of synaptic dysfunction, were used to assess the effect of reduced CSP α on disease. Behavioural tests revealed no change in the progression of disease in ME7–CSP α +/− animals compared to ME7–CSP α +/+ animals. In addition, the accumulation of misfolded PrP^{Sc}, the diseased associated gliosis or synaptic loss were not different. Thus, the misfolding events that generate synaptic dysfunction and lead to synaptic loss are unlikely to be mediated by a disease associated decrease in the refolding pathways associated with CSP α .

© 2015 The Authors. Published by Elsevier Ireland Ltd. This is an open access article under the CC BY license (<http://creativecommons.org/licenses/by/4.0/>).

1. Introduction

Prion diseases, are a group of rare and fatal neurodegenerative diseases of human and animals [1] involving the conversion of the cellular prion protein (PrP^C) into a misfolded form (PrP^{Sc}), which accumulates and deposits as amyloid plaques [2]. Characteristics of these diseases include gliosis, spongiform changes, and synaptic loss which proceeds neuronal death [3–6]. Prion diseases can occur

sporadically, be genetically inherited or transmitted infectiously [7]. This infectious capacity, unique amongst neurodegenerative diseases, was successfully exploited in the development of models of chronic neurodegeneration [8,9]. Pathology in prion-infected mice develops in a well-defined and predictable manner, over a time course dependent on the prion strain used. This well-defined temporal progression renders prion-based models ideal for investigating significant disease events and underlying mechanisms of pathology [5,6,10,11].

One murine model, utilising the ME7 prion agent, involves bilateral injection of ME7-infected brain homogenate into the dorsal hippocampus of C57BL/6J mice [5] and this paradigm leads

* Corresponding author. Tel.: +44 7760668757.

E-mail address: mjd1g08@soton.ac.uk (M.J. Davies).

to hippocampal pathology shared by several strains [12,13]. This sequence of progression includes PrP^{Sc} deposits, hypertrophied astrocytes and activated microglia, followed shortly after by synaptic loss in the stratum radiatum of the hippocampus [5,6]. However, neuronal loss is not seen until late-stage disease [5]. The early synaptic loss appears to selectively involve the presynaptic compartment, with reduced expression of a number of presynaptic proteins [6]. One such synaptic protein which shows an early and progressive reduction in the hippocampus of ME7-animals is CSP α [6] and in view of its role in synaptic re-folding suggests potential for a direct role in disease progression.

CSP α is a synaptic vesicle protein and functions as a molecular chaperone in conjunction with Hsc70 and a small glutamine-rich tetratricopeptide repeat (TRP)-containing protein (SGT) [14] which controls the conformational folding of the SNARE protein, SNAP-25 [15]. CSP α null mice are normal at birth but develop a progressive muscle weakness and sensorimotor deficit between 2 and 4 weeks of age [16]. At about ~P15 these mice stop gaining weight, become lethargic and begin to die in the second postnatal month [16]. There is however, no obvious difference between wildtype (+/+) and heterozygous (+/–) CSP α mice, which suggests that reduced levels (~50%) of CSP α is not sufficient to cause a neurodegenerative phenotype. In contrast, mutations that reduce the human CSP α gene DNAJC5's function cause ceroid-lipofuscinosis that coincides with accelerated age-dependent neurodegeneration [17]. Finally, CSP α and associated chaperone activities are also more widely implicated in proteostasis [18]. This led us to reason that the ME7 prion disease pathology would, via direct synaptic dysfunction or deficient proteostasis, be exacerbated in CSP α +/- mice. To test this we used behavioural assays and molecular changes that act as sensitive measures of disease evolution in cohorts of CSP α +/+ and CSP α +/- animals infected with ME7.

2. Materials and methods

2.1. Animal husbandry

CSP α +/+ and +/- mice were generated as described [16,19,20] and crossed and maintained on a C57BL/6J Charles River background [21]. The cohort of 26 animals (13 CSP α +/+ and 13 CSP α +/-) used in this study were generated from a common set of littermates. All animals were housed according to UK Home office regulations, on a standard 12 h: 12 h light–dark cycle at an ambient room temperature of 21 ± 2 °C, with food and water provided *ad libitum*.

2.2. ME7 prion disease

All procedures were carried out under a UK Home Office licence and in accordance with the United Kingdom Animals (Scientific Procedures) Act, 1986. Surgical procedures were carried out as previously described [5]. CSP α +/+ and +/- female animals 8–13 weeks of age were anaesthetized and bilaterally injected into the dorsal hippocampus with either 1 μ l of NBH or ME7 homogenate, using the stereotaxic co-ordinates anteroposterior +2.0 mm, lateral ±1.7 mm and depth –1.6 mm measured at Bregma. Eleven weeks post-inoculation (w.p.i.) NBH- and ME7-animals were subjected to behavioural tests, widely used to define preclinical and clinical disease. These tests included burrowing, glucose consumption and open field as measure of affective behaviour as previously described [5,10,21]. In addition, muscle strength and co-ordination were measured using an inverted screen as described previously [10,21]. The experiments followed a schedule of inverted screen tests preceding early afternoon open field tests, followed by late afternoon two hour burrowing tests. 24 h burrowing was then

tested overnight in conjunction with glucose consumption. All animals used in the study were killed at a humane endpoint at 21 w.p.i. regardless of treatment or genetic background. At this point all animals were terminally anaesthetized with sodium pentobarbital and perfused transcardially with heparinised saline.

2.3. General tissue processing

For western blotting hippocampal tissue was micro-dissected on dry ice as described [21]. Brain tissue for immunohistochemistry was perfused and post-fixed with 10% neutral buffered formalin and subsequently paraffin-embedded as detailed elsewhere [6].

2.4. Western blotting

The dissected hippocampi from animals sacrificed at 21 w.p.i. were homogenised in 5 volumes (w/v) of RNase-free 1 × PBS supplemented with a protease and phosphatase inhibitor cocktail (Thermo Scientific). Each hippocampal homogenate was combined with an equal volume of lysis buffer (40 mM HEPES pH 7.4, 250 mM NaCl, 4% v/v SDS supplemented with a protease and phosphatase inhibitor cocktail (Thermo Scientific)). Samples were heated at 95 °C and subsequently centrifuged. The supernatant was collected and the protein concentration determined using the Bio-Rad Dc protein assay (Bio-Rad). Hippocampal homogenates were then diluted equivalently. Equal amounts of protein were resolved by SDS-PAGE and subjected to fluorescent-based western blotting or stained with colloidal Coomassie Blue [6]. Following blocking in 5% w/v non-fat milk, nitrocellulose membranes were incubated in 5% w/v bovine serum albumin (BSA) containing 0.1% v/v Tween-20 and one of the following primary antibodies: anti-CSP α (1:1,000; Abcam); anti-GFAP (1:5,000; Dako); anti-PrP (1:5,000; 6H4 Prionics); anti-Synapsin (1:1,000; Chemicon); anti-Synaptophysin (1:1,000; Abcam) and anti-VAMP-2 (1:1,000; Synaptic Systems). Membranes were then probed with the appropriate fluorescent-coupled goat anti-mouse or anti-rabbit secondary antibody (Licor). Immunoreactivity of protein bands was determined using a Licor Odyssey infrared detection system (Licor). The signal obtained for each antigen was normalised to total protein, as measured by the signal obtained from scanning individual lanes of colloidal Coomassie stained gels.

2.5. Immunohistochemistry

10 μ m paraffin-embedded coronal hippocampal sections were cut on a microtome, and subsequently dewaxed in xylene and rehydrated through a decreasing series of ethanol concentrations. Non-specific endogenous peroxidase activity was eliminated by incubation with 1% H₂O₂ and antigen retrieval was performed using citrate buffer (pH 6) and microwaving, or autoclaving-formic acid treatment for PrP^{Sc} [5,6]. Non-specific antibody binding was blocked by incubation with the appropriate serum. Subsequently, sections were incubated in a humid chamber with one of the following primary antibodies: anti-GFAP (1:1000; Dako), anti-IBA1 (1:500; Abcam); anti-PrP (1:4000; 6H4 Prionics) and anti-Synaptophysin (1:100; Abcam). Specific binding was detected using a biotinylated secondary antibody (Vector Laboratories), followed by incubation in ABC (Vector Laboratories) and visualisation using DAB. Nuclei were counterstained with Harris hematoxylin.

2.6. Statistical analysis

For behavioural tests, repeated measures two-way ANOVA was used with Bonferroni post-analysis. Unpaired *t*-test was used for biochemical data. The statistical analysis was performed using

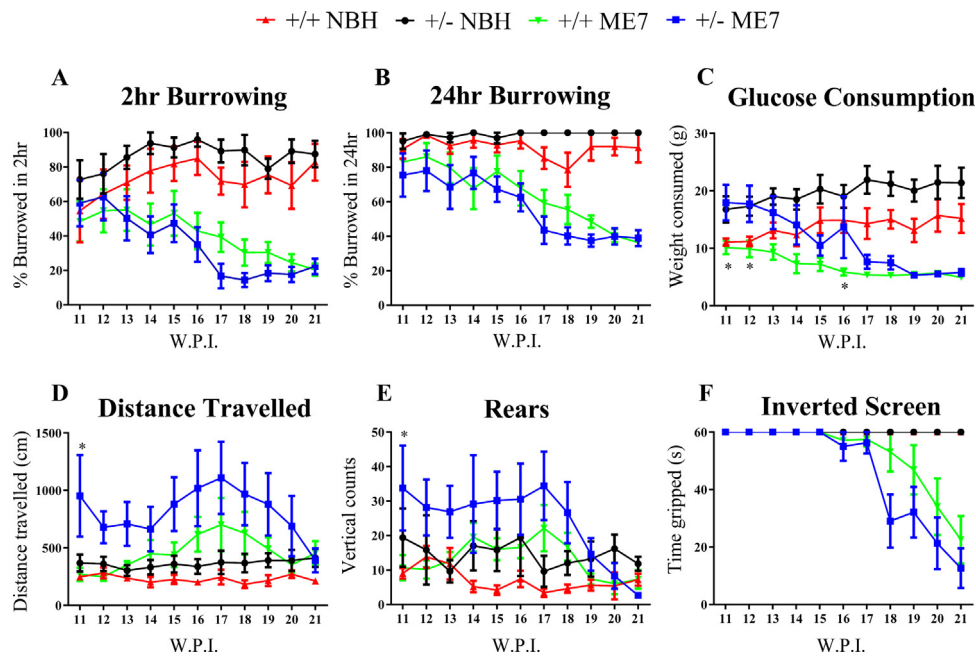


Fig. 1. Behavioural changes in CSP α +/+ and +/- NBH- and ME7-animals.

Burrowing behaviour (A and B), glucose consumption (C), distance travelled (D), rears (E) and inverted screen strength (F) were tested. There were no significant differences in the behaviours between CSP α +/+ or +/- animals infected with ME7. The baseline levels for CSP α +/- animals are higher for burrowing, glucose consumption, distance travelled and rears compared to CSP α +/+ animals. Data in graphs represents mean \pm SEM from $n=4$ animals (NBH) and $n=8$ animals (ME7). * $P \leq 0.05$, repeated measures two-way ANOVA with Bonferroni post-analysis. +/+, wildtype; +/-, heterozygous.

Graph Pad Prism (version 6, Graph Pad Software Inc.). Quantification values were expressed as the mean \pm standard error of the mean (S.E.M.), with a p value of ≤ 0.05 considered as statistically significant. Behavioural tests, $n=4$ (NBH) and $n=8$ (ME7); western blotting, $n=3$ (NBH) and $n=4$ (ME7) and immunohistochemistry, $n=2$ (NBH and ME7).

3. Results

3.1. Reduced expression of CSP α does not exacerbate behavioural changes in ME7-animals

Previous behavioural studies in ME7-animals show a progressive decrease from 12 w.p.i. onwards in the number of pellets burrowed compared to NBH-animals, concurrent with a decrease in glucose consumption and an increase in distance travelled and rears [5,10,21]. Additionally, at 18 w.p.i., motor deficits become apparent, as evidenced by declining performance in the inverted screen test [10,21]. This decline in behavioural performance as a consequence of prion disease is apparent in the behavioural tests performed as part of this study, with both ME7–CSP α +/+ and +/- animals showing progressively decreasing burrowing behaviour (Fig. 1A and B) and glucose consumption (Fig. 1C), increased distance travelled (Fig. 1D) and rears (Fig. 1E) and reduced strength (Fig. 1F) compared to NBH-animals. Although CSP α +/- animals have a higher baseline level in the number of pellets burrowed in 2 h (Fig. 1A) and overnight (Fig. 1B), the amount of glucose consumed (Fig. 1C), distance travelled (Fig. 1D) and rears (Fig. 1E), there was no difference in the progression of the behavioural decline in ME7-animals between CSP α genotypes (Fig. 1A–F).

Protein expression of markers of prion pathology reveals no difference between CSP α +/+ and +/- animals infected with ME7.

Hippocampi taken from brains extracted at 21 w.p.i. were homogenised and used for western blotting to study expression levels of CSP α (Fig. 2A), total PrP (Fig. 2B), the astrocyte marker GFAP (Fig. 2C) and the presynaptic proteins Synaptophysin

(Fig. 2D), Synapsin (Fig. 2E) and VAMP-2 (Fig. 2F). Western blots for CSP α showed that CSP α +/- animals (Fig. 2A) displayed a ~50% reduction in protein as a consequence of their heterozygous genetic background. In contrast, there are no differences in the expression of any of the other three presynaptic proteins (Fig. 2D–F) between CSP α +/+ and +/- NBH animals. This indicates that the reduced level of CSP α is not due to a decrease in the number of synaptic vesicles but rather a fall in the complement of CSP α molecules per vesicle.

As shown in previous work there was a decrease in CSP α levels during disease [6]. This is seen when comparing relative levels of the CSP α in ME7-animals compared to CSP α +/+ and CSP α +/- NBH-animals. In the latter case a decrease from an already reduced level of CSP α . Similar measurements of the presynaptic proteins Synaptophysin (Fig. 2D), Synapsin (Fig. 2E) and VAMP-2 (Fig. 2F) showed the reduced levels in ME7-animals compared to NBH-animals in both CSP α genotypes. Consistent with previous observations, the robustness of the presynaptic protein reduction due to ME7 was more marked for Synapsin and VAMP-2 [6,22].

Total PrP immunoreactivity (Fig. 2B) acts to indicate ME7 infection and prion disease development. There was a significant increase in PrP expression of un-, mono- and diglycosylated forms in both CSP α +/+ and +/- animals infected with ME7- compared to NBH-animals (Fig. 2B). However, there is no significant difference seen in its expression between ME7- and CSP α +/+ and +/- animals (Fig. 2B). Our previous data indicates that ME7 related increase in total prion immunoreactivity is a good correlate of misfolded protein [6]. Western blotting of GFAP showed an increase in its levels in ME7-animals compared to NBH-animals (Fig. 2C). However, like PrP, there was no significant difference in levels of its expression between ME7–CSP α +/+ and +/- animals (Fig. 2C).

We then performed immunohistochemistry to determine if there were any discernible changes in protein expression of some of these markers in different regions of the hippocampus. Coronal sections containing the hippocampus were taken from NBH- and ME7-animals at 21 w.p.i. The sections were immunostained for PrP^{Sc}, GFAP, the microglia marker IBA1 and Synaptophysin

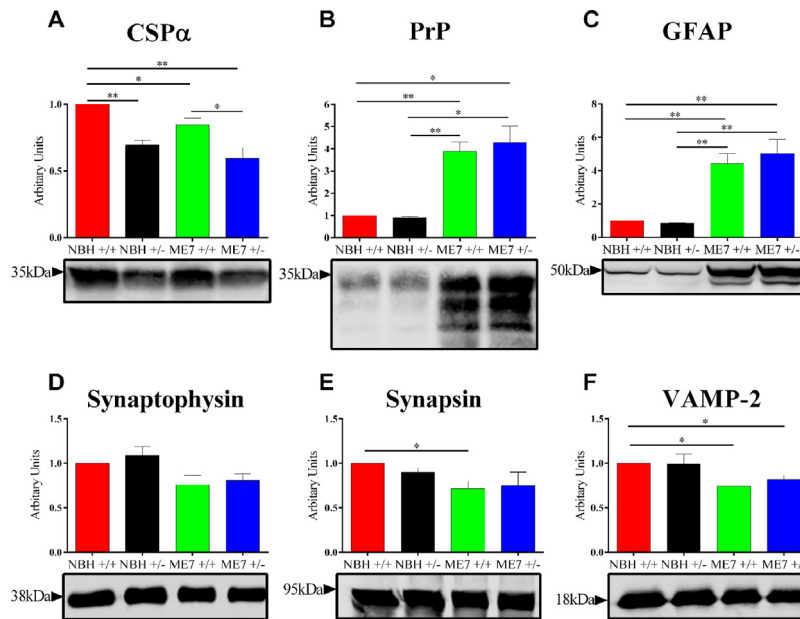


Fig. 2. Analysis of prion pathology in ME7-CSPα +/+ and +/- animals.

Quantitative western blotting of CSPα (A), total PrP (B), GFAP (C), Synaptophysin (D), Synapsin (E) and VAMP-2 (F) in hippocampal homogenates from CSPα +/+ and +/- mice inoculated with either NBH or ME7. Representative western blots are shown. (A) A decrease in CSPα expression is seen in +/- animals compared to +/+. CSPα expression is further reduced in ME7-animals compared to NBH-animals. (B) Significant differences in total PrP immunoreactivity were seen between NBH- and ME7-animals, but no difference was seen between CSPα +/+ and +/- animals injected with ME7. (C) ME7 infection causes increased expression of the astrocyte marker GFAP. However, there is no difference in expression between ME7-CSPα +/+ and +/- animals. (D-F) The levels of the three presynaptic proteins Synaptophysin (D), Synapsin (E) and VAMP-2 (F) are reduced in ME7-animals compared to NBH-animals. There is no change in the expression of these three proteins between ME7-CSPα +/+ and +/- animals. Data in bar charts represents mean \pm SEM from $n=3$ animals (NBH) and $n=4$ animals (ME7). * $P<0.05$ and ** $P<0.01$, unpaired t -test. +/+, wildtype; +/-, heterozygous.

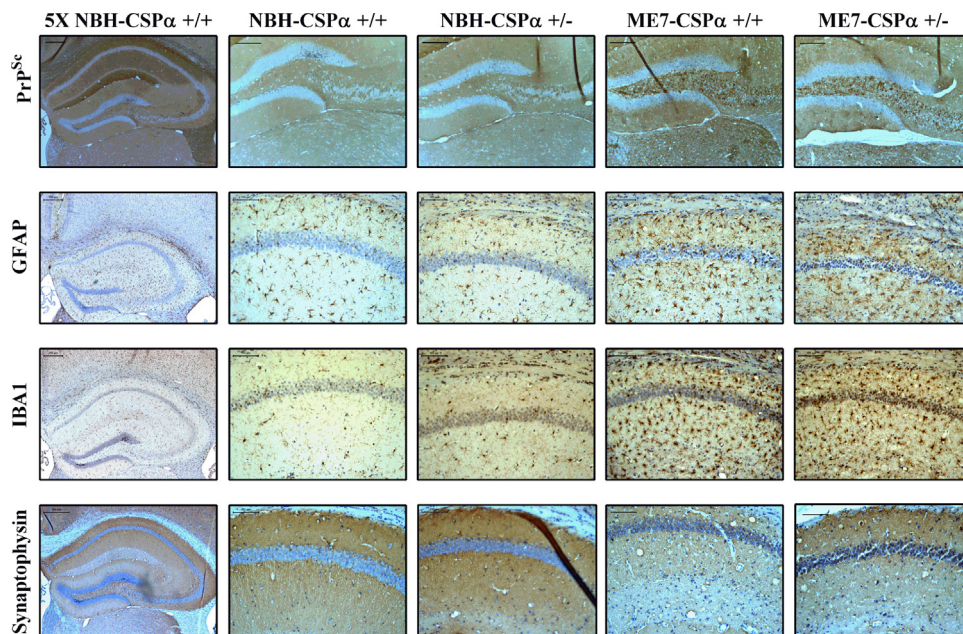


Fig. 3. Immunostaining of hippocampal coronal sections from NBH- and ME7-injected CSPα +/+ and +/- animals.

ME7 animals show PrP^{Sc} deposition in the hilus of the dentate gyrus extending to the CA3 region, increased number and size of both astrocytes and microglia and loss of synapses in the stratum radiatum of the hippocampus compared to NBH-animals. However, there are no visible differences in any of these pathologies between ME7-CSPα +/- animals compared to ME7-CSPα +/+. $n=2$ animals per genotype and condition. Scale bars, 100 μ m except for Synaptophysin images where scale bars are 200 μ m and 5 \times images where scale bars are 300 μ m. +/+, wildtype; +/-, heterozygous; CA3, Cornu Ammonis region 3.

(Fig. 3). Whilst there is no PrP^{Sc} deposition in the hippocampus of NBH-animals, we observe the appearance of these formic acid resistant deposits of PrP^{Sc}, in both ME7-CSPα +/+ and +/- animals (Fig. 3). However, there is no visible difference in the number or pattern of deposition of PrP^{Sc} between CSPα +/+ and +/- animals. In ME7 hippocampi, GFAP+ astrocytes are generally larger

in number, with more developed processes than in NBH-animals and often show infiltration of the neuronal layers (Fig. 3). Similarly, we observe a large increase in the number of visible microglia in ME7-animals compared to NBH-animals (Fig. 3). In addition, like astrocytes we also note the increased infiltration of microglia into the neuronal layers of the hippocampus in ME7-animals (Fig. 3).

Despite this there is no clear difference in the number or appearance of astrocytes or microglia between ME7–CSP α +/+ and +/- animals. Previous studies, staining for the synaptic protein Synaptophysin revealed disorganized and a relative reduced intensity of staining in the stratum radiatum of the hippocampus as ME7 pathology progresses [5,6]. In keeping with these findings, our work revealed reduced and disorganised Synaptophysin staining in the stratum radiatum in ME7-infected brains 21 w.p.i. (Fig. 3). However, once again, there was no clear difference between ME7 and CSP α +/- animals compared to ME7–CSP α +/+ animals (Fig. 3).

4. Discussion

Experimentally induced ME7 prion disease presents a predictable and well-defined neuropathology enabling the correlation of cellular and molecular findings with important pathological events [5]. For example, the loss of synapses in the stratum radiatum of the hippocampus coincides with the onset of subtle behavioural changes in animals injected with ME7. In this study, we have used an established battery of behavioural tests [5,10,21] that resolve underlying pathological mechanisms at the level of the whole organism. In particular, we have investigated if the behavioural decline that marks synaptic dysfunction and mid-stage disease (burrowing, glucose consumption and open field) or late stage disease (inverted screen) differs in genetic backgrounds with different levels of CSP α .

As synaptic degeneration may be a potentially reversible event in neurodegenerative diseases, significant research has gone into discovering molecular pathways related to synaptic pathology. We have previously reported the decreased expression of a number of presynaptic proteins in ME7-animals including the synaptic chaperone CSP α [6]. CSP α knockout mice undergo premature death, however, animals with only a ~50% reduction in CSP α levels appear comparatively normal compared to +/+ animals [16]. This indicates that a ~50% reduction in CSP α is sufficient to largely preserve synaptic integrity. However, it is unclear at what point reduced CSP α expression becomes pathological as the complete knock out of the gene is post-embryonic lethal [16]. The focus of our study was to determine whether a genetic background of low CSP α expression would exacerbate experimentally-induced ME7 prion disease. To achieve this, we injected CSP α +/+ and +/- mice with either NBH or ME7-infected brain homogenate, and evaluated the genetic impact upon prion disease progression via behavioural tests and protein expression using western blotting and immunohistochemistry.

Given the role of CSP α in preserving synaptic function, it was hypothesized that the reduced levels of CSP α in CSP α +/- mice may increase synaptic susceptibility to degeneration and in doing so amplify the behavioural changes associated with disease. There are reports of small changes in measures of spontaneous locomotion associated with the reduction in CSP α expression in the heterozygous mice, however, this is not due to any synaptic loss [16]. This may underlie the shifted baseline behaviour we noted that was particularly clear in the glucose consumption test. However, the clear observation is that the decreased expression of CSP α did not have a significant effect in the behaviours tested between ME7 and CSP α +/+ and +/- animals (Fig. 1). These results indicate that reduced CSP α levels in +/- animals are not sufficient to accelerate disease progression.

Western blots revealed reduced levels of CSP α in CSP α +/- animals compared to +/+, with a further reduction in ME7-animals (Fig. 2A). There are estimated to be around ~2 copies of CSP α per synaptic vesicle [23]. This would suggest that in the CSP α +/- animals where there is a ~50% reduction of CSP α , there would only be around ~1 copy of CSP α per synaptic vesicle, as there is no evidence for a reduced synaptic vesicle number in the CSP α +/- mice

[16]. The further reduction of CSP α seen in ME7–CSP α +/- animals is likely to be due to the synaptic loss which occurs in ME7 [5,6,24]. Overt loss of synapses would reduce the content of synaptic vesicle proteins as we see in the current study. However, the previously reported differential loss of presynaptic proteins and the accumulating dysmorphic nature of synaptic vesicle profiles identified in disease could imply routes to reduced synaptic vesicle content prior to a more overt synaptic loss.

Although ME7-animals had high levels of total PrP (Fig. 2B) and deposits of PrP^{Sc} (Fig. 3) there were no significant differences in the levels of PrP or the number or distribution of PrP^{Sc} deposits between ME7 and CSP α +/+ and ME7 and CSP α +/- animals. In addition, there was no difference between the expression of GFAP (Fig. 2C), the number of astrocytes and microglia and their appearance (Fig. 3) between ME7 and CSP α +/+ and ME7–CSP α +/- animals. Despite this the most likely detrimental effect of reduced CSP α levels in ME7-animals is reduced synaptic number, given the protein's role in chaperoning SNAP-25 and promoting vesicle exocytosis [25]. The levels of the presynaptic proteins Synaptophysin (Fig. 2D), Synapsin (Fig. 2E) and VAMP-2 (Fig. 2F) were reduced in ME7-animals compared to NBH-animals, however, there was no difference in their expression between ME7–CSP α +/+ and +/- animals. Additionally, staining for Synaptophysin (Fig. 3) failed to reveal a difference between ME7-animals of both CSP α genotypes. This indicates that whatever mechanisms are contributing to synaptic loss seen in ME7-animals, reduction in CSP α levels is not a critical dose limiting step. Therefore, whilst a complete absence of the protein is detrimental to synaptic health, a compound reduction resulting from a heterozygous genetic background is insufficient to exacerbate ME7 prion disease.

One explanation for the apparent lack of effect of CSP α reduction on ME7 prion disease progression may be the neuronal type undergoing synaptic degeneration. In CSP α null mice, the synapses most strongly affected are those with high activity, necessitating superior SNARE function [16,26,27]. Previous prion studies proposed that highly active GABAergic synapses may undergo degeneration, as there is evidence for severe, selective GABAergic cell loss in human and experimental Creutzfeldt–Jakob disease [28,29]. However, studies in ME7 prion disease revealed no significant loss of parvalbumin (PV)-positive GABAergic inhibitory neurons in the hippocampus of ME7-animals [30]. In ME7 prion disease synaptic loss in the hippocampus occurs along the Schaffer Collateral axons of CA3 pyramidal neurons, which have lower activity and hence demand for proper SNARE chaperoning. As such, these synapses may be less susceptible to low CSP α levels than others.

5. Conclusion

Protein expression studies and behavioural assays of disease progression both failed to provide evidence for an effect of a CSP α -deficient genetic background on the protein misfolding or subsequent progression of prion pathology resulting from ME7 infection. This is despite the previously reported detrimental neurological consequences of CSP α absence and reports of reduced CSP α expression in ME7-infected animals. These results suggest that reducing CSP α expression to about ~50% is not sufficient to enhance synaptic loss and prion disease pathology.

Author contributions

M.J.D. and M.C. did most of the experimental work. V.H.P. and V.O.C. directed and supervised the project. All authors contributed to the writing of the paper.

Acknowledgements

Matthew Davies is supported by the Medical Research Council (MRC) and Gerald Kerkut Charitable Trust (Southampton, UK). Vincent O'Connor and V. Hugh Perry are supported by MRC grant (G800134). Matthew Cooper contribution to this study was during his participation on the CfBS MBiolMed undergraduate programme. The authors declare no competing financial interests. We are grateful to Rafael Fernández-Chacón (University of Seville, Spain) for providing the original CSP α breeding pairs.

References

- [1] S.B. Prusiner, Molecular biology of prion diseases, *Science* 252 (1991) 1515–1522.
- [2] K.M. Pan, M. Baldwin, J. Nguyen, M. Gasset, A. Serban, D. Groth, I. Mehlhorn, Z. Huang, R.J. Fletterick, F.E. Cohen, Conversion of alpha-helices into beta-sheets features in the formation of the scrapie prion proteins, *Proc. Natl. Acad. Sci. U. S. A.* 90 (1993) 10962–10966.
- [3] H. Fraser, Diversity in the neuropathology of scrapie-like diseases in animals, *Br. Med. Bull.* 49 (1993) 792–809.
- [4] M. Jeffrey, W.G. Halliday, J. Bell, A.R. Johnston, N.K. MacLeod, C. Ingham, A.R. Sayers, D.A. Brown, J.R. Fraser, Synapse loss associated with abnormal PrP precedes neuronal degeneration in the scrapie-induced murine hippocampus, *Neuropathol. Appl. Neurobiol.* 26 (2000) 41–54.
- [5] C. Cunningham, R. Deacon, H. Wells, D. Boche, S. Waters, C.P. Diniz, H. Scott, J.N. Rawlins, V.H. Perry, Synaptic changes characterize early behavioural signs in the ME7 model of murine prion disease, *Eur. J. Neurosci.* 17 (2003) 2147–2155.
- [6] B.C. Gray, Z. Siskova, V.H. Perry, V. O'Connor, Selective presynaptic degeneration in the synaptopathy associated with ME7-induced hippocampal pathology, *Neurobiol. Dis.* 35 (2009) 63–74.
- [7] S.B. Prusiner, Molecular biology and pathogenesis of prion diseases, *Trends Biochem. Sci.* 21 (1996) 482–487.
- [8] J. Cuille, P. Chelle, Experimental transmission of trembling to goat, *C.R. Seances Acad. Sci.* 208 (1939) 1058–1060.
- [9] R.L. Chandler, Encephalopathy in mice produced by inoculation with scrapie brain material, *Lancet* 1 (1961) 1378–1379.
- [10] K. Guenther, R. Deacon, V.H. Perry, J.N.P. Rawlins, Early behavioural changes in scrapie-affected mice and the influence of dapsone, *Eur. J. Neurosci.* 14 (2001) 401–409.
- [11] R. Atarashi, V.L. Sim, N. Nishida, B. Caughey, S. Katamine, Prion strain-dependent differences in conversion of mutant prion proteins in cell culture, *J. Virol.* 80 (2006) 7854–7862.
- [12] C. Cunningham, R.M.J. Deacon, K. Chan, D. Boche, J.N.P. Rawlins, V.H. Perry, Neuropathologically distinct prion strains give rise to similar temporal profiles of behavioural deficits, *Neurobiol. Dis.* 18 (2005) 258–269.
- [13] K.J. Hilton, C. Cunningham, R.A. Reynolds, V.H. Perry, Early hippocampal synaptic loss precedes neuronal loss and associated with early behavioural deficits in three distinct strains of prion disease, *PLoS One* 8 (2013) e68062.
- [14] S. Tobaben, P. Thakur, R. Fernández-Chacón, T.C. Südhof, J. Rettig, B. Stahl, A trimeric protein complex functions as a synaptic chaperone machine, *Neuron* 31 (2001) 987–999.
- [15] M. Sharma, J. Burré, T.C. Südhof, CSP α promotes SNARE-complex assembly by chaperoning SNAP-25 during synaptic activity, *Nat. Cell Bio.* 13 (2010) 30–39.
- [16] R. Fernández-Chacón, M. Wölfel, H. Nishimune, L. Tabares, F. Schmitz, M. Castellano-Muñoz, C. Rosenmund, M.L. Montesinos, J.R. Sanes, R. Schneggenburger, T.C. Südhof, The synaptic vesicle protein CSP α prevents presynaptic dysfunction, *Neuron* 42 (2004) 237–251.
- [17] L. Nosková, V. Stránecký, H. Hartmannová, A. Přistoupilová, V. Barešová, R. Ivánek, H. Hůlková, H. Jahnová, J. van der Zee, J.F. Staropoli, K.B. Sims, J. Tyynelä, C. Van Broeckhoven, P.C. Nijssen, S.E. Mole, M. Elleder, S. Knoch, Mutations in DNAJC5, encoding cysteine-string protein alpha, cause autosomal-dominant adult-onset neuronal ceroid lipofuscinosis, *Am. J. Hum. Genet.* 89 (2011) 241–252.
- [18] B.Z. Schmidt, R.J. Watts, M. Aridor, R.A. Frizzell, Cysteine string protein promotes proteasomal degradation of the cystic fibrosis transmembrane conductance regulator (CFTR) by increasing its interaction with the C terminus of Hsp70-interacting protein and promoting CFTR ubiquitylation, *J. Biol. Chem.* 284 (2009) 168–178.
- [19] T.W. Rosahl, D. Spillane, M. Missler, J. Herz, D.K. Selig, J.R. Wolff, R.E. Hammer, R.C. Malenka, T.C. Südhof, Essential functions of synapsins I and II in synaptic vesicle regulation, *Nature* 375 (1995) 488–493.
- [20] R. Janz, Y. Goda, M. Geppert, M. Missler, T.C. Südhof, SV2A and SV2B function as redundant Ca²⁺ regulators in neurotransmitter release, *Neuron* 24 (1999) 1003–1016.
- [21] A.A. Asuni, K. Hilton, Z. Siskova, K. Lunnon, R. Reynolds, V.H. Perry, V. O'Connor, Alpha-synuclein deficiency in the C57BL/6J OlaHsd strain does not modify disease progression in the ME7-model of prion disease, *Neuroscience* 165 (2009) 662–674.
- [22] B.C. Gray, Evidence for Synaptic Dysfunction in Prion Disease, Ph.D. Thesis, School of Biological Sciences, University of Southampton, Southampton, UK, 2006.
- [23] B.G. Wilhelm, S. Mandad, S. Truckenbrodt, K. Kröhnert, C. Schäfer, B. Rammner, S.J. Koo, G.A. Claßen, M. Krauss, V. Haucke, H. Urlaub, S.O. Rizzoli, Composition of isolated synaptic boutons reveals the amounts of vesicle trafficking proteins, *Science* 344 (2014) 1023–1028.
- [24] Z. Sisková, A. Page, V. O'Connor, V.H. Perry, Degenerating synaptic boutons in prion disease: microglia activation without synaptic stripping, *Am. J. Pathol.* 175 (2009) 1610–1621.
- [25] M. Sharma, J. Burré, P. Bronk, Y.S. Zhang, W. Xu, T.C. Südhof, CSP alpha knockout causes neurodegeneration by impairing SNAP-25 function, *EMBO J.* 31 (2012) 829–841.
- [26] P. García-Junco-Clemente, G. Cantero, L. Gómez-Sánchez, P. Linares-Clemente, J.A. Martínez-López, R. Luján, R. Fernández-Chacón, Cysteine string protein-alpha prevents activity-dependent degeneration in GABAergic synapses, *J. Neurosci.* 30 (2010) 7377–7391.
- [27] F. Schmitz, L. Tabares, D. Khimich, N. Strenzke, P. de la Villa-Polo, M. Castellano-Muñoz, A. Bulankina, T. Moser, R. Fernández-Chacón, T.C. Südhof, CSP α -deficiency causes massive and rapid photoreceptor degeneration, *Proc. Natl. Acad. Sci. U. S. A.* 103 (2006) 2926–2931.
- [28] M. Guentchev, M.H. Groschup, R. Kordek, P.P. Liberski, H. Budka, Severe, early and selective loss of a subpopulation of GABAergic inhibitory neurons in experimental transmissible spongiform encephalopathies, *Brain Pathol.* 8 (1998) 615–623.
- [29] M. Guentchev, J. Wanschitz, T. Voigtländer, H. Flicker, H. Budka, Selective neuronal vulnerability in human prion diseases: fatal familial insomnia differs from other types prion disease, *Am. J. Pathol.* 155 (1999) 1453–1457.
- [30] S.L. Franklin, S. Love, J.R. Greene, S. Betmouni, Loss of perineuronal net in ME7 prion disease, *J. Neuropathol. Exp. Neurol.* 67 (2008) 189–199.